



## Specific Ion Effects in Thermo-Responsive Polymer Solutions

Moghaddam, Saeed Zajforoushan

*Publication date:*  
2017

*Document Version*  
Publisher's PDF, also known as Version of record

[Link back to DTU Orbit](#)

*Citation (APA):*  
Moghaddam, S. Z. (2017). *Specific Ion Effects in Thermo-Responsive Polymer Solutions*. DTU Chemistry.

---

### General rights

Copyright and moral rights for the publications made accessible in the public portal are retained by the authors and/or other copyright owners and it is a condition of accessing publications that users recognise and abide by the legal requirements associated with these rights.

- Users may download and print one copy of any publication from the public portal for the purpose of private study or research.
- You may not further distribute the material or use it for any profit-making activity or commercial gain
- You may freely distribute the URL identifying the publication in the public portal

If you believe that this document breaches copyright please contact us providing details, and we will remove access to the work immediately and investigate your claim.

# **Specific Ion Effects in Thermo-Responsive Polymer Solutions**

Saeed Zajforoushan Moghaddam

PhD Thesis



Technical University of Denmark

May 2017

Technical University of Denmark

Department of Chemistry

Kemitorvet, Building 206

2800 Kgs. Lyngby, Denmark

## **Acknowledgements**

I would like to thank my supervisor Associate Professor Esben Thormann for his massive help, support, advice and guidance during my studies, as well as introducing me to the fascinating field of colloids and surface science and helping me to improve my background knowledge in physical chemistry of polymers. Our regular discussions regarding the progress in the experiments, interpretation of the findings and preparation of the papers have been an enormous support and encouragement during my PhD studies.



## Abstract

Stimuli-responsive polymers are macromolecules that undergo a significant change in conformation and interactions in response to an external stimulus such as temperature and addition of salts. The applications of these materials are numerous ranging from biomedical applications to fabrication of smart surfaces. The present PhD thesis deals with understanding the fundamentals and mechanisms, which control the physiochemical properties of stimuli-responsive polymers in aqueous saline solutions. The whole study can be divided into two sections: (i) polymers in bulk solution and (ii) polymers adsorbed/grafted to a solid/aqueous interface. The first research approach comprises of three subprojects mainly concerned with understanding the mechanisms through which the salts can affect the polymer stability in solution, an effect that is widely known as the *Hofmeister effect*. The second research approach includes two subprojects that address adsorption and behavior of homo- and copolymers at solid/aqueous interfaces. Besides understanding the fundamentals of polymer properties at the interfaces, this part aims to indicate how changing the structure of the polymers or addition of salts can affect the structure of the polymer layer. The experimental methods that have been used in this project can also be divided into bulk-related and surface-related measurements. Differential scanning calorimetry was used in order to obtain the phase transition temperature of the polymer solutions, as well as thermodynamics of the transition. Dynamic light scattering was employed to assess the hydrodynamic size of the polymer coils and interchain aggregates. To study adsorption, hydration and conformation of the polymers at the solid/aqueous interfaces, quartz crystal microbalance with dissipation monitoring was used. Ultimately, atomic force microscopy imaging and colloidal probe measurements were conducted to study the topography of the polymer layers and the interactions between the polymer-coated surfaces.

## Abstrakt

Stimuli-responsive polymerer er makromolekyler, der undergår en signifikant ændring i struktur og interaktioner som response på et eksternt stimulus, såsom temperatur og tilsætning af salte. Anvendelserne af disse materialer er talrige og rækker lige fra biomedicinske applikationer til fremstilling af ”smarte” overflader. Denne ph.d.-afhandling beskæftiger sig med de grundlæggende mekanismer, der styrer de fysiokemiske egenskaber ved stimuli-responsive polymerer i vandige saltopløsninger. Undersøgelsen kan opdeles i to sektioner: (i) polymerer i opløsning og (ii) polymerer adsorberet eller vedhæftet til en fast overflade. Den første sektion består af tre delprojekter, der hovedsageligt omhandler forståelsen af de mekanismer, hvormed saltene kan påvirke polymerstabiliteten i opløsning, en effekt, der bredt er kendt som Hofmeister-effekten. Den anden sektion omfatter to delprojekter, der adresserer adsorption og opførsel af homo- og copolymerer som er vedhæftet en fast overflade. Ud over at undersøge de grundlæggende polymeregenskaber ved grænseflader, sigter denne del på at angive, hvordan ændring af den kemiske struktur af polymererne eller tilsætning af salte kan påvirke den fysiske struktur af et polymerlag. De eksperimentelle metoder, der er blevet anvendt i dette projekt, kan også opdeles i ”bulk”-relaterede og overfladerelaterede metoder. Differential scanningkalorimetri blev anvendt til bestemmelse af faseovergangstemperaturen af polymeropløsningerne såvel som bestemmelse af andre termodynamiske parametre for faseadskillelsen. Dynamisk lysspredning blev anvendt til at bestemme den hydrodynamiske størrelse af polymerskæderne og eventuel aggregering af polymererne. For at studere adsorption, hydrering og struktur af polymererne ved de faste overflader blev en resonansteknik kaldet QCM-D anvendt. Atomkraftmikroskopi blev anvendt for at studere topografien af polymerlag samt interaktionerne mellem polymeroverflader.

## List of Papers

My thesis is based on the following papers, which in the context are referred to by their roman numbers.

- I. Hofmeister effect of salt mixtures on thermo-responsive poly(propylene oxide)**  
S.Z. Moghaddam and E. Thormann.  
Physical Chemistry Chemical Physics 17.9 (2015): 6359-6366.
- II. Hofmeister effect on thermo-responsive poly(propylene oxide): role of polymer molecular weight and concentration**  
S.Z. Moghaddam and E. Thormann.  
Journal of colloid and interface science 465 (2016): 67-75.
- III. Hofmeister effect on thermo-responsive poly(propylene oxide) in H<sub>2</sub>O And D<sub>2</sub>O**  
S.Z. Moghaddam and E. Thormann.  
RSC Advances 6.33 (2016): 27969-27973.
- IV. Hofmeister effect on PNIPAM in bulk and at an interface: surface partitioning of weakly hydrated anions**  
S.Z. Moghaddam and E. Thormann.  
Langmuir 33.19 (2017): 4806-4815 (2017).
- V. Thermo-responsive diblock and triblock cationic copolymers at the silica/aqueous interface: a QCM-D and AFM study**  
S. Z. Moghaddam, K. Zhu, B. Nyström, E. Thormann  
Submitted for publication.
- VI. The Hofmeister effect in aqueous polymer solutions: where we are and where we should go**  
S.Z. Moghaddam and E. Thormann.  
Manuscript

## List of Abbreviations

AFM	Atomic force microscopy
ASA	Accessible surface area
DLS	Dynamic light scattering
DLVO	Derjaguin-Landau-Verwey-Overbeek
DSC	Differential scanning calorimetry
FJC	Freely jointed chain
LCST	Lower critical solution temperature
LMWA	Law of matching water affinities
PEO	Poly(ethylene oxide)
PNIPAM	Poly(N-isopropylacrylamide)
PPO	Poly(propylene oxide)
QCM-D	Quartz crystal microbalance with dissipation monitoring
SPM	Solute partitioning model
UCST	Upper critical solution temperature
VdW	Van der Waals

## List of Symbols

A	Hamaker constant (J)
B	Jones-Dole viscosity coefficient
b	monomer length (m) or average hydration number ( $\text{H}_2\text{O}/\text{\AA}^2$ )
$B_{\text{max}}$	Saturation constant ( $^{\circ}\text{C}$ )
c	Molarity ( $\text{mol dm}^{-3}$ )
$C_{\infty}$	Characteristic ratio
D	Surface separation distance (m), dissipation factor ( $10^{-6}$ )
$D_{\text{h}}$	Hydrodynamic diameter (m)
F	Force (N)

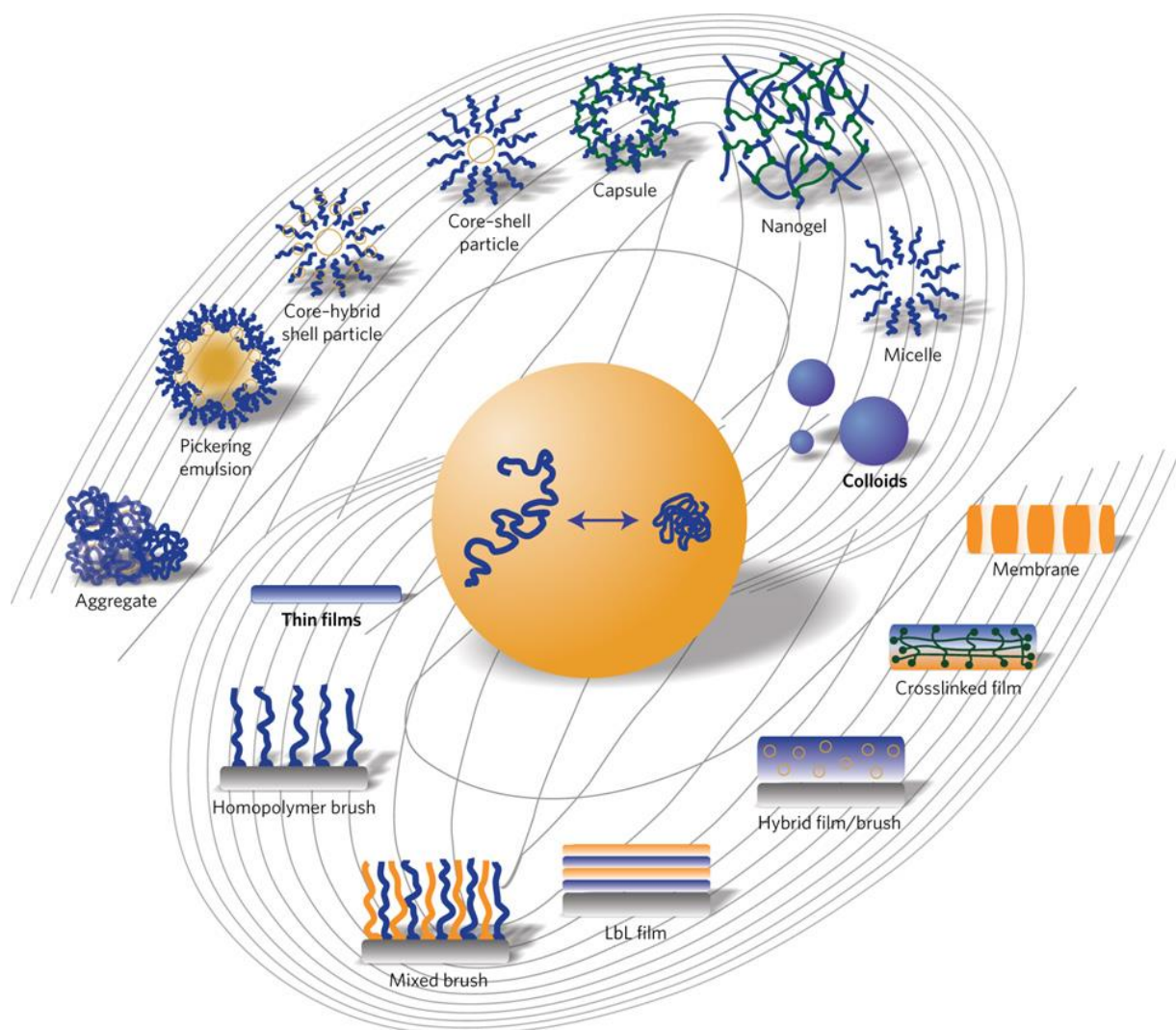
$f$	Oscillation frequency (Hz)
$k$	Spring constant ( $\text{N m}^{-1}$ )
$K_A$	Binding constant ( $\text{M}^{-1}$ )
$k_B$	Boltzmann's constant ( $1.381\text{e}^{-23} \text{ J K}^{-1}$ )
$K_p$	Partition coefficient
$M_n$	Number-average molecular weight ( $\text{g mol}^{-1}$ )
$M_w$	Weight-average molecular weight ( $\text{g mol}^{-1}$ )
$n$	Refractive index or overtone number
PDI	Polydispersity index
$R$	Radius (m) or molar gas constant ( $8.314 \text{ J K}^{-1} \text{ mol}^{-1}$ )
$r_f$	End-to-end distance (m)
$R_g$	Radius of gyration (m)
$T$	Temperature ( $^{\circ}\text{C}$ or $\text{K}$ )
$W$	Interaction free energy (J)
$z$	Ion valency
$\alpha$	Polarizability ( $\text{C m}^2 \text{ V}^{-1}$ )
$\gamma$	Surface tension ( $\text{N m}^{-1}$ )
$\varepsilon$	Permittivity
$\eta$	Viscosity ( $\text{Pa s}$ )
$\theta$	Bond angle ( $^{\circ}$ )
$\kappa^{-1}$	Debye length (m)
$\mu_i$	Dipole moment (C m), chemical potential (J/mol)
$\rho$	Density ( $\text{kg m}^{-3}$ )
$\sigma$	Grafting density ( $\text{chains/nm}^2$ )
$\nu$	Ionization frequency
$\varphi$	Conformation angle ( $^{\circ}$ )
$\chi$	Flory Huggins interaction parameter
$\Omega$	Number of possible arrangements

# Table of Contents

Abstract .....	i
Abstrakt .....	ii
List of Papers.....	iii
List of Abbreviations.....	iv
List of Symbols .....	iv
<b>1. INTRODUCTION .....</b>	<b>1</b>
<b>2. BACKGROUND.....</b>	<b>6</b>
2.1. Physical polymer science .....	7
2.1.1. Molecular weight and conformation.....	8
2.1.2. Thermodynamics of polymer solutions .....	12
2.1.3. Phase equilibrium .....	17
2.1.4. Concentration regimes .....	19
2.2. Phase separation from molecular perspective .....	21
2.3. Polymers at solid/aqueous interfaces .....	26
2.4. Ions in aqueous solution .....	33
2.5. The Hofmeister effect.....	38
2.5.1. Triple effects: polarization, surface tension and direct binding.....	41
2.5.2. The solute partitioning model.....	42
2.5.3. The law of matching water affinities .....	45
2.5.4. Ion dispersion interactions.....	46
2.6. Surface forces in aqueous media .....	49
2.6.1. Electrostatic double layer force .....	50
2.6.2. Van der Waals forces.....	51
2.6.3. Solvation (hydration) forces .....	53
2.6.4. Interaction between hydrophobic surfaces in water .....	54
2.6.5. Polymer-mediated forces.....	55
<b>3. METHODS.....</b>	<b>60</b>
3.1. Differential scanning calorimetry (DCS) .....	61
3.2. Dynamic light scattering (DLS) .....	64
3.3. Quartz crystal microbalance with dissipation monitoring (QCM-D).....	67
3.4. Atomic force microscopy (AFM).....	71
3.4.1. Determination of the cantilever spring constant.....	73

3.4.2. Attaching the particle to the AFM cantilever .....	74
3.4.3. Force measurements .....	76
3.4.4. Construction of force vs distance curves .....	77
<b>4. SUMMARY OF THE PAPERS .....</b>	<b>79</b>
<b>5. REFERENCES .....</b>	<b>89</b>

# 1. INTRODUCTION



\* The schematic illustration describes the various types of materials that are related to the phase behavior of macromolecules in bulk solution and at aqueous interfaces.[1]



This thesis aims to present and discuss some fundamental aspects of stimuli-responsive polymers stability in the aqueous saline solutions, which I have investigated during my PhD studies. The provided knowledge can be of great importance, both from a fundamental and a practical point of view. Understanding the underlying mechanisms that control the macromolecular stability in the aqueous solution can shed light on the role of these entities in various biological systems, as well as enabling us to control their properties more effectively for multiple applications such as drug delivery or fabrication of smart surfaces. The major part of my studies were dedicated to investigating the behavior of thermo-responsive polymers in saline solutions, in order to understand how different ions affect the polymer solubility and properties in water, an effect that is widely recognized as the *Hofmeister effect*. My research objective was to assess how each existing component in the solution can contribute to the Hofmeister effect, as well as testing the validity of the previously reported mechanisms. As another part of my investigations, though in the same line with the first part, I inspected the properties of polymers at gold/aqueous and silica/aqueous interfaces, in terms of the polymer conformation and interactions in saline and salt-free solutions. The work conducted during my PhD studies has resulted in six papers, which form the backbone of this thesis.

In the *first* paper, I investigated the Hofmeister effect of salt mixtures on the stability and phase separation of poly(propylene oxide) (PPO). The main objective of this study was to understand the *specific-ion effects* when a mixture of two different salts is present. There were two primary reasons behind this study. First, to assess the previously reported mechanisms for the Hofmeister effect of weakly- and strongly-hydrated anions, which could successfully explain the effects of single salts in solution. In addition, I wanted to investigate the Hofmeister effect under a condition that is more similar to the physiological and biological systems. For instance, various diseases and disorders in human body have been attributed to the ions present in the body fluids and their corresponding

Hofmeister effects on the biomacromolecules such as proteins. Nevertheless, in body fluids, one could always find a mixture of different ions not just a single entity. With this in mind, I systematically investigated the behavior of three basic salt mixtures, i.e., mixture of two salts with a *salting-out effect* (destabilizer), two salts with a *salting-in effect* (stabilizer), and one salt with a salting-out and the other with a salting-in effect.

In the *second* paper, I inquired the role of polymer properties on the Hofmeister effect. For a given polymer, various parameters such as the molecular weight can affect the phase separation of the polymer solution. Interestingly, in almost all the previously reported studies on the Hofmeister effect in polymer solutions, the effect of varying salt type or salt concentration have been studied on a particular polymer. My experimental approach was to fix the salt type, then see how the corresponding Hofmeister effect can be affected by changing the polymer molecular weight and concentration in the solution. In this case, the Hofmeister effect of two salts (one salting-in and one salting-out) was studied on PPO with four different molecular weights and at two different polymer concentrations.

By this point, I examined the role of ions and polymer properties in the Hofmeister effect. In the *third* paper, I aimed to study how changing the solvent properties can affect the Hofmeister effect. Therefore, the polymer and the salt entities were fixed and the Hofmeister effect was assessed in light ( $\text{H}_2\text{O}$ ) and heavy ( $\text{D}_2\text{O}$ ) water in parallel. Due to the more restricted atomic vibrations, the hydrogen bonding strength in heavy water is roughly 5% stronger compared to in light water; hence, one can investigate the effect of solvent perturbation on the ions hydration, as well the polymer hydration.

In the *fourth* paper, I investigated the Hofmeister effect of three different salts on Poly(N-isopropylacrylamide) (PNIPAM) in bulk solution and at the gold/aqueous interface. This extensive

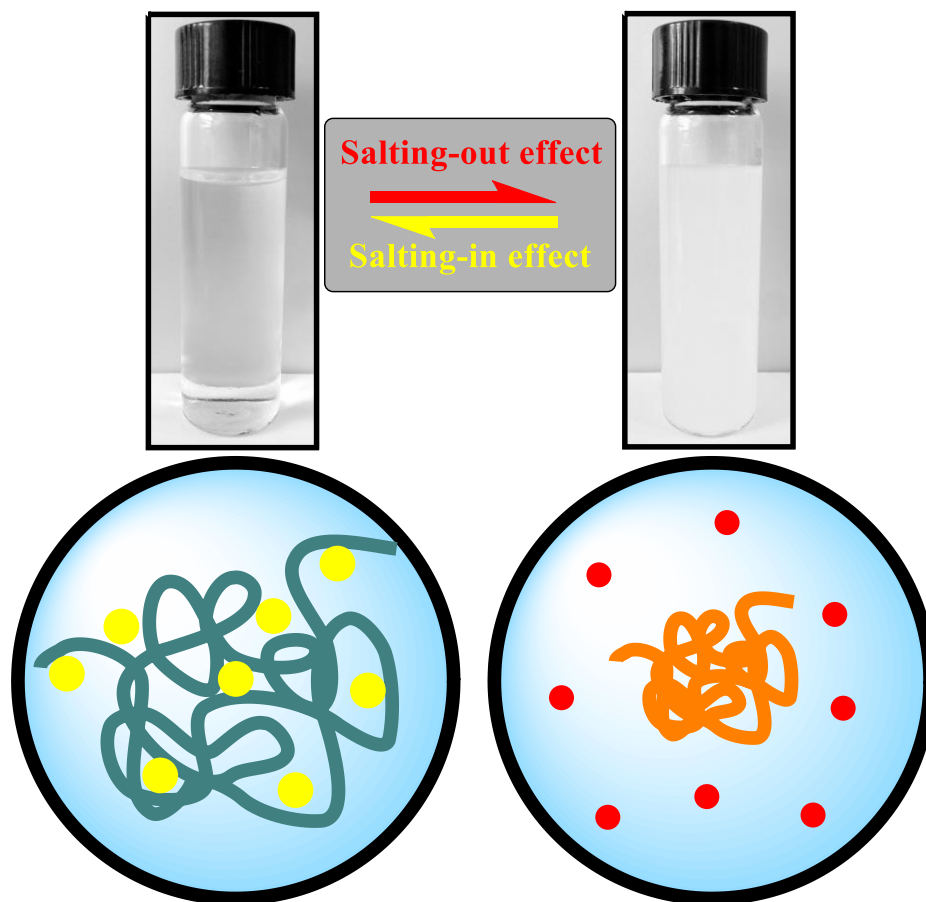
study helped me to perceive how different salts can affect the conformation of PNIPAM, as well as the interactions between PNIPAM-covered gold surfaces. In particular, I wanted to better understand the ion-specific effects by weakly hydrated anions. As reported in the literature, such anions preferentially accumulate at the polymer surface; nevertheless, it has been less discussed how the accumulated anions give rise to polymer stabilization. Herein, I closely characterized the following effects by a strongly hydrated anion, i.e. fluoride ( $F^-$ ) and two weakly hydrated anions, i.e., thiocyanate ( $SCN^-$ ) and trichloroacetate ( $TCA^-$ ) on PNIPAM conformation and interactions.

In the *fifth* paper, I scrutinized the properties of two cationic block copolymers at the silica/aqueous interface. The story behind this research work was to more closely examine the adsorption of polymers at the solid/aqueous interfaces, which was partly addressed in my fourth paper. The only difference between the two copolymers was that one included an additional hydrophilic PEG block, which indeed affirmed to have significant effects on the copolymer adsorption, structure and interactions at the surface. Therefore, the results were directed towards suggesting how one can tune the properties at the interface and obtain more homogenous polymer layers through modification of the copolymer structure.

At last, my *sixth* paper is devoted to review what I have learned and what I have investigated during my PhD studies. The first part of the review paper deals with the essential mechanisms that have been formerly suggested to explain the Hofmeister effect in polymer solutions. This indeed covers different models and theories ranging from molecular descriptions to macroscopic thermodynamic explanations that I have perused in the literature. The second part of the review paper includes my personal opinions and suggestions about the future research on the Hofmeister effect in polymer solutions, which indeed are the topics that I have partly addressed during my PhD studies, but surely require further excavation and scrutiny.

After concisely introducing the outline and outcome of my PhD studies, I will discuss the theoretical and experimental facets of my work in the coming sections. In section two, I will provide the background knowledge about physicochemical aspects of thermo-responsive polymers in salt-free and saline solutions, both in bulk state and at solid/aqueous interfaces. This section encompasses the underlying knowledge about polymer physics, phase separation mechanisms, polymers at solid interfaces, specific ion effects in water, Hofmeister effect in polymer solutions, and finally surface forces between polymer-covered substrates. These topics are not illustrated in details in the attached papers, thus the following section can be served as a basis for understanding the findings and discussions provided in my papers. The third section is dedicated to the experimental methods that I have employed during my PhD projects. This section presents a basic introduction to each method and then describes how the experiments were performed and analyzed. In addition, some experimental procedures, e.g. preparation of colloidal probes for the AFM measurements, are not explained in details in the papers, thus are elucidated here. In section four, I will discuss the most notable findings and conclusions of each of my papers. Combination of all these results together can surely provide a better understanding of the obtained knowledge and the relation between my studies.

## 2. BACKGROUND



In this background section, I will provide the essential knowledge and principles of the investigated systems. Although most of the topics are briefly highlighted in the attached papers, a concise recapitulation is necessary for a better grasp and interpretation of my results. The section begins with a rather basic description of the behavior and properties of polymers, from physical and thermodynamical viewpoints. This will be useful to perceive better the principles of polymer mixing and phase transition. Next, I will discuss the hydration, thermo-responsivity, and phase separation of polymers in aqueous solution in terms of the molecular interactions. Together with the polymer physics approach, this can render a deeper insight into different aspects of polymer solutions, before digging into the more complex systems that contain ions as well. I will then bring up some important facets of polymers behavior at the solid/aqueous interfaces, which can be useful for interpretation of my fourth and fifth papers. After being acquainted with the behavior of polymers in water, I will propound the *specific-ion* effects on polymers solution stability. In this case, a succinct but essential description of the hydration of ions is first provided; afterwards, the most important mechanisms through which the ions can affect the polymer stability are illustrated. I will complete this section with some essential discussion about surface forces existing between polymer-covered surfaces, which are relevant to my studies on polymers behavior at the solid/aqueous interfaces.

## **2.1. Physical polymer science**

Several terms such as polymer chain conformation, phase separation, miscibility, phase boundary, lower critical solution temperature, radius of gyration, random coil conformation, etc., are repeatedly used in this thesis to describe different aspects of polymers behavior and properties. Since these terms indeed form the basis of my research, I first provide some relevant basic knowledge that mostly comes from a branch of polymer science known as *polymer physics*. For a

more detailed description of the enclosed topics, I would like to refer you to “*Introduction to Polymer Physics*” by L. H. Sperling, which indeed is one of the most interesting sources for digging into general physical polymer science. For a deeper understanding of the physical behavior of polymers at interfaces, I strongly encourage you to have a look at “*Polymers at Interfaces*” by G. J. Fleer et al.

### 2.1.1. Molecular weight and conformation

Polymers are large chain-like molecules of varying molecular weights ranging from a few thousands to millions; hence, they are generally referred to as the *macromolecules*.<sup>[2-4]</sup> An individual polymer chain is composed of numerous repeating subunits, which are recognized as the *monomers* or *building blocks*. Unlike small molecules, all common synthetic polymers as well as most natural polymers possess a distribution in their molecular weight, meaning that one can find polymer chains of different length and sizes in the same sample. Accordingly, the average molecular weights and the molecular weight distribution were introduced. The number-average molecular weight ( $M_n$ ) and the weight-average molecular weight ( $M_w$ ) are defined as:

$$M_n = \frac{\sum_i N_i M_i}{\sum_i N_i}$$

$$M_w = \frac{\sum_i N_i M_i^2}{\sum_i N_i M_i}$$

Herein,  $N_i$  is the number of the polymer chains with the molecular weight of  $M_i$ . The molecular weight characterization is actually the first consideration before any investigation on any polymer. The typical molecular weight distribution of a copolymer, which was partly studied during one of my PhD studies, is depicted in Figure 2.1.

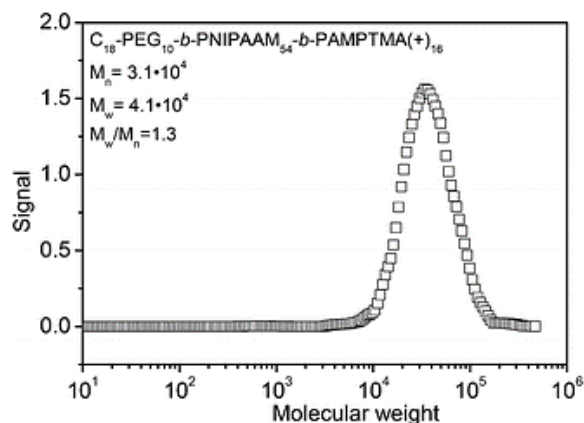


**Figure 2.1** The molecular weight distribution of a synthesized copolymer partly investigated during my PhD studies, which is obtained from the asymmetric flow field-flow fractionation (AFFFF) measurements.[5]

The molecular weight distribution can be assessed by different techniques such as gel permeation chromatography (GPC) and asymmetric flow field-flow fractionation (AFFFF). As shown in Figure 2.1,  $M_n$  is usually found to be near the distribution peak maximum, while  $M_w$  is always larger than  $M_n$ . The ratio of these two ( $M_w / M_n$ ) indicates the molecular weight distribution and is considered as the polydispersity index ( $PDI$ ), which strongly depends on the employed polymerization method and conditions. For my investigations, a narrow molecular weight distribution or in other words a  $PDI$  value close to unity was always desired, since the presence of extremely short or long polymer chains could have additional effects on the overall polymer properties and solubility.[6, 7]



**Figure 2.2** Some examples of random coil conformation. The random coil term merely refers to spatial arrangement of the polymer segments with no preferred orientation.



The other fundamental property of a polymer chain is its *conformation* in space, which represents different spatial arrangements that the polymer chain can adopt through rotations about its single bonds.[8-10] There are many possible conformations for a polymer chain, e.g. *stretched zigzag*, *helical*, *globular*, and *random coil*. I should underline that these are just the principal types of polymer conformations, which differ significantly in their spatial arrangement and properties, while almost none of them refer to a specific conformational structure. The *random coil conformation*, which is typically considered for the neutral hydrophilic polymers in my studies, is a general term to describe the polymer chain conformation when the monomer subunits are randomly oriented; hence, the random coil indeed represents many different conformations (Figure 2.2).

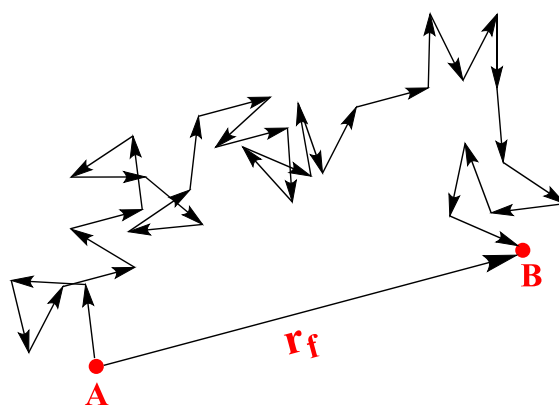


**Figure 2.3** A freely jointed polymer chain (linear homopolymer) made of  $n$  randomly oriented vectors of length  $l$ . Each vector represents a single carbon-carbon bond and the angle between two vectors is arbitrary.

A helpful visualization of polymer chain conformation is provided in Figure 2.3, where we start from point  $A$  aiming to reach point  $B$ , through drawing  $n$  consecutive randomly oriented vectors of the same size ( $l$ ). The obtained sketch represents a randomly oriented polymer chain, which is known as the *freely jointed chain (FJC)*, because the angles between all the vectors are arbitrary and random. Propagation of the end point of such a polymer chain reminisces the Brownian motion; accordingly, the distance between  $A$  and  $B$  points, or in other words the *mean square end-to-end distance* of the sketched polymer chain can be calculated as:

$$\langle r_f^2 \rangle = n \times l^2$$

In the formula,  $r_f$  is the end-to-end distance of the freely jointed polymer chain (the distance between the  $A$  and  $B$  points), while  $n$  and  $l$  are the number and length of the single carbon-carbon bonds (vectors), respectively. To obtain a more realistic picture of the polymer chain conformation, now we have to consider two additional constraints for the chemical bonds.

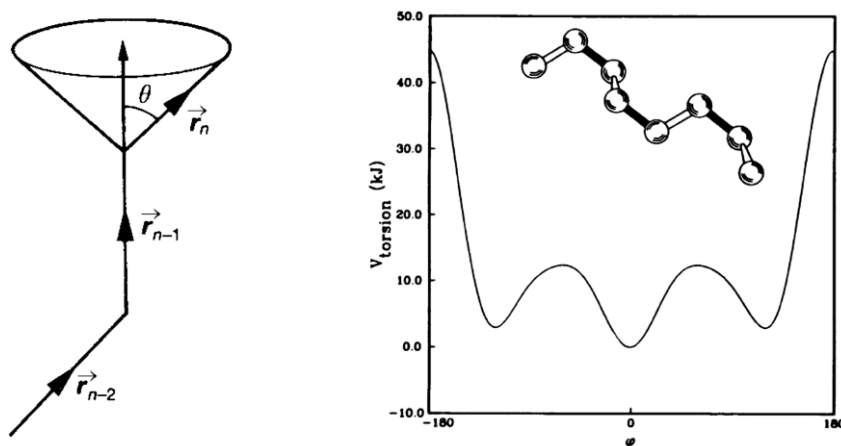


**Figure 2.4** (Left) Torsional angle of a single bond with respect to the plane delineated by the previous two bonds. The third bond can be located on the surface of the cone. (Right) The rotational energy diagram for C-C single bonds in a linear hydrocarbon polymer. The energy wells of *gauche minus* ( $\phi = -120^\circ$ ), *trans* ( $\phi = 0^\circ$ ) and *gauche plus* ( $\phi = +120^\circ$ ) conformations are shown.[2]

**First**, the angle between two C-C bonds (recognized as the bond angle) ( $\theta$ ) is fixed at  $109^\circ 28'$ , which expands the chain mean square end-to-end distance by a factor of  $[(1-\cos\theta)/(1+\cos\theta)]$ . Besides that, each bond can only adopt specific angles with respect to the plane delineated by the previous two bonds, referred to as the conformation angles ( $\phi$ ) (Figure 2.4). For a linear homopolymer made of single C-C bonds, three stable conformation angles are possible for each bond, i.e., the *trans* ( $\phi = 0^\circ$ ), the *gauche plus* ( $\phi = +120^\circ$ ), and the *gauche minus* ( $\phi = -120^\circ$ ). We can see these stable conformations from the rotational potential energy diagram shown in Figure 2.4. The higher the population of the *trans* conformation would be, the more elongated and planar

the polymer chain conformation will be. The energy difference between the *gauche* and *trans* states determines the thermodynamic flexibility of the chain. If the energy difference is smaller than the thermal energy ( $kT$ ) then flexibility is infinite, while if the energy difference is much larger than  $kT$ , the *trans* conformation will be more likely and the polymer chain will be stiff. If we consider the constraints, the mean square end-to-end distance of the polymer chain is corrected to be:

$$\langle r_f^2 \rangle = n \times l^2 \times \frac{1 - \cos \theta}{1 + \cos \theta} \times \frac{1 + \cos \phi}{1 - \cos \phi} = n \times l^2 \times C_\infty$$

The term  $C_\infty$ , known as the characteristic ratio, is a measure of polymer chain stiffness or softness. Relatively speaking, the higher this value is, the polymer chain is more extended and stiffer. For instance, poly(ethylene oxide) has a  $C_\infty$  of around 4, which is considered to be a flexible polymer chain due to the presence of ether bonds in the backbone and no side groups.[11] On the other hand, poly(N-isopropylacrylamide) has a  $C_\infty$  of around 10 and is relatively more stiff than poly(ethylene oxide), due to the presence of side groups that can restrict the free rotations.[12]

This equation is still quite simplified, as it underestimates the end-to-end distance of the real polymer chain by neglecting some essential factors such as the excluded volume effect and the short-ranged interactions between the monomers. However, it can provide a sensible picture of the polymer chain conformation, which I will frequently refer to in the coming sections.

### 2.1.2. Thermodynamics of polymer solutions

Knowing the preliminary information about the polymer chain conformation, the next step is to address how a polymer chain is dissolved in the aqueous solution, which was the first step for each of my experiments. I would like to commence with the thermodynamic perspective, since it can highlight the entropic and enthalpic aspects of the polymers solubility and phase behavior. Several advanced models and equations of states, e.g. Sanchez-Lacombe (SL) equation of state or Flory-

Orwall-Vrij equation of state, have been suggested in this case, which are beyond the scope of this study. Herein, I present the basic but essential thermodynamic description of polymer mixing proposed by Flory and Huggins, which indeed serves as the basis for the more elaborated theories. It renders a simple description of polymer mixing process in terms of enthalpy and entropy changes of the system; moreover, it can distinguish between some basic differences between the mixing of small molecules and macromolecules with water.[13-17]

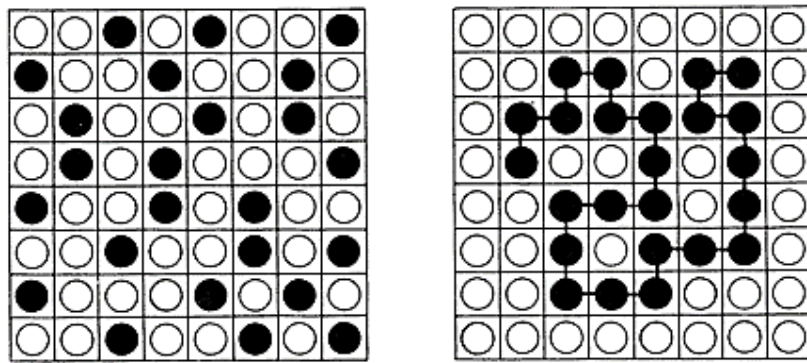


**Figure 2.5** Placement of solute molecules on a lattice. (Left)  $N_2$  small molecules. (Right) A polymer chain occupying  $N_2$  cells. The number of possible ways to put a single polymer chain on the lattice is relatively less, because the occupied cells by the chain should be necessarily connected with each other.

From the thermodynamic point of view, dissolving a polymer in water is plainly accompanied with an entropic and an enthalpic change, just like any other phenomenon. According to the statistical thermodynamics, the entropy of mixing is determined by counting the number of possible arrangements in space ( $\Omega$ ) that the molecules can adopt, which can be converted into the entropy of mixing, according to the Boltzmann's relation:

$$\Delta S = k \ln \Omega$$

Now consider the solvent (water) as component 1 and the solute (small molecule) as component 2. Using the lattice system (Figure 2.5), we can approximate the number of possible ways to put  $N_2$

solute molecules (small molecules of the same size of solvent molecules) on a lattice including  $N_0=N_1+N_2$  empty cells. This provides us the following equation for the entropy of mixing:

$$\Delta S_{mix} = -k(N_1 \ln n_1 + N_2 \ln n_2)$$

Where  $n_i$  represents the mole fraction of component  $i$ . Now, for a polymer chain composed of  $x$  segments, and by considering that each segment occupies a cell (same size of the solvent molecule), the above equation is rearranged:

$$\Delta S_{mix} = -k(N_1 \ln v_1 + N_2 \ln v_2)$$

In this case,  $v_i$  is the mole fraction of the component  $i$ , which can be defined as:

$$v_1 = \frac{N_1}{N_1 + xN_2}$$

$$v_2 = \frac{xN_2}{N_1 + xN_2}$$

This equation tells us that the number of the ways that the system can be rearranged in space is reduced when one of the species exists as long chains. This can plainly explain why the monomer of a polymer is always more soluble in the solvent rather than the polymer chain itself.

For the same polymer-solvent system, the enthalpic term of mixing is taken into account using the *Flory-Huggins interaction parameter* ( $\chi$ ) given as:

$$\chi = \frac{(\epsilon_{11} + \epsilon_{22} - 2\epsilon_{12})}{kT} = \frac{\Delta H_{mix}}{kTN_1v_2}$$

The interaction parameter is defined as the difference between the mixed interaction energy  $\epsilon_{12}$  and sum of the pure component energies ( $\epsilon_{11}$  and  $\epsilon_{22}$ ). Therefore, it describes how favorable polymer-

solvent interactions are in comparison to polymer-polymer and solvent-solvent interactions. Combining the provided entropic and enthalpic terms gives us the statistical free energy of mixing:

$$\Delta G_{mix} = kT(N_1 \ln v_1 + N_2 \ln v_2 + \chi N_1 v_2)$$

The first two terms on the left represent the entropic role and the last term indicates the enthalpic contribution. The derived equation suggests two major features that distinguish the thermodynamics of polymer mixtures in comparison with their small molecules analogous. First, the considerably reduced combinatorial entropy contribution typically results in immiscibility in absence of favorable enthalpic interactions. Second and more interestingly, unlike most of the small molecules mixtures, macromolecular mixtures can undergo phase separation upon heating through a lower critical solution transition (LCST), which I will discuss more in the coming sections.

As mentioned, the Flory-Huggins interaction parameter determines if the interaction between the polymer segments and the solvent molecules is favorable or not. This brings up some new terms, which are repeatedly used in this thesis to describe the behavior of stimuli-responsive polymers at different temperatures. Accordingly, when  $\chi$  is smaller than 0.5, the polymer-solvent interactions are considered to be more favorable than the polymer-polymer interactions, known as the *good solvent condition*. The favorable interaction between the polymer and solvent gives rise to swelling of the polymer chain in solution. When  $\chi$  is larger than 0.5, the polymer-polymer interactions are more favorable than the polymer-solvent interactions, referred to as the *bad solvent condition*, where the polymer chain tends to shrink and minimize its *solvent-accessible surface area*. The interaction parameter of 0.5 is considered as the *Flory  $\theta$ -solvent condition*, meaning that the polymer-solvent interactions are identical to the polymer-polymer interactions, thus the repulsive and attractive contributions to the chain excluded volume cancel out each other. Under such

condition, the polymer chain is considered to be in the *unperturbed state*, adopting a random coil conformation. To quantify the size of the random coil, the *radius of gyration* ( $R_g$ ) is defined as:

$$R_g^2 = \left(\frac{1}{N}\right) \sum_{i=1}^N r_i^2$$

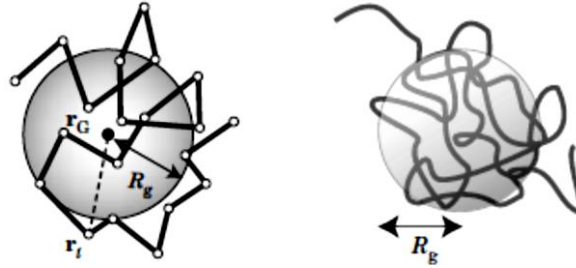


**Figure 2.6** Center of mass and radius of gyration of a polymer chain with random coil conformation.[2] It is a more meaningful parameter to address the polymer coil size rather than the end-to-end distance. More importantly, it can be experimentally determined using scattering techniques.

The radius gyration of a polymer coil can be mathematically interpreted as the mean square distance of all the segments of the polymer coil from its center of mass (Figure 2.6). Hence, the polymer chain with random coil conformation is approximated with a sphere with the radius of  $R_g$ . Several scaling laws between the properties of a random coil polymer and its radius of gyration have been suggested, including the must-know relation between the radius of gyration and number of monomers:

$$R_g = bN^{\nu}$$

I have frequently used this equation during my studies, whenever I required a rough but realistic estimation of the polymer coil size. It solely requires the estimated monomer length ( $b$ ) that is typically in the range of 0.2-0.3 nm, and the degree of polymerization ( $N$ ) that can be estimated from the average molecular weight. Depending on solvent condition, the exponent ( $\nu$ ) roughly varies from 0.3 to 0.6 (Figure 2.7).

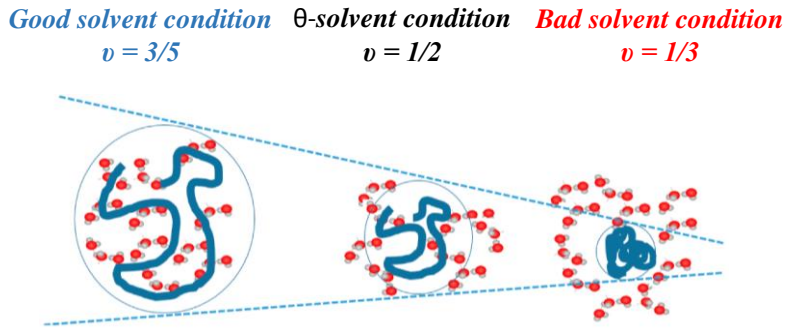


**Figure 2.7** General scaling law between the radius of gyration and the degree of polymerization for a random coil.

### 2.1.3. Phase equilibrium

Based on the described statistical free energy change of mixing, now we can examine the phase diagrams of the polymer solutions. This is of great importance for understanding the phase behavior of thermo-responsive polymers in aqueous solution, which indeed was the primary phenomenon that I investigated in saline solutions during my studies.

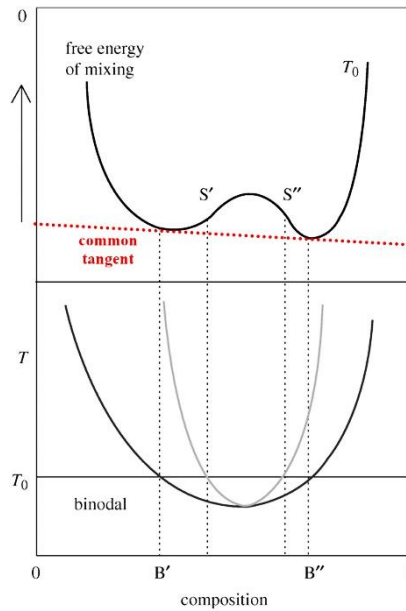


**Figure 2.8**  $\Delta G_{mix}$  as a function of polymer composition in the biphasic regime. For each temperature, the first order derivative of the free energy function provides the corresponding binodal boundary concentrations, so the whole phase boundary can be provided.



According to basic thermodynamics, equilibrium between two phases is obtained only if the partial chemical potential of the components (1 as the solvent and 2 as the solute) in the two phases (solvent-rich (I) and polymer-rich (II)) are equal:

$$\mu_1^I = \mu_1^{II} \text{ and } \mu_2^I = \mu_2^{II}$$

To meet these criteria, free energy of mixing plotted as a function of polymer composition should have a common tangent. In Figure 2.8, the  $B'$  and  $B''$  represent the points at which the common tangent criterion is met, meaning that  $\mu_1$  and  $\mu_2$  between the phases are equal and an equilibrium state is obtained. Accordingly, all the compositions between  $B'$  and  $B''$  are unstable and will phase separate into  $B'$  and  $B''$  compositions, which form the so-called *binodal* phase boundary. The inflection points ( $S'$  and  $S''$ ) are obtained from the second order derivative of the free energy, indicating the *spinodal* phase boundary. Discussion on binodal and spinodal phase boundaries is beyond the scope of this thesis; however, I should highlight that phase separation through the binodal phase boundary differs from the spinodal boundary, in terms of the kinetics of transition and the final morphology. Finally, the *critical point* is calculated by solving the first order and second order derivatives of the chemical potential function:

$$v_c = \frac{1}{1 + \chi^{0.5}} \quad \text{and} \quad \chi_c \cong \frac{1}{2} + \frac{1}{n^{0.5}}$$

Now if we repeat the same procedure for other temperatures, the binodal and spinodal phase boundaries will be found as a function of temperature. The obtained phase boundary may show either an upper critical solution temperature (UCST) or a lower critical solution temperature (LCST). The LCST behavior –characteristic of the polymers studied in my projects- in general is related to systems where mixing is accompanied with a negative entropy change and release of heat (exothermic).[18, 19] It can be also reasoned based on the effect of temperature on the Flory-

Huggins interaction parameter; where with increasing the temperature, an increment in the interaction parameter is observed (Figure 2.9).

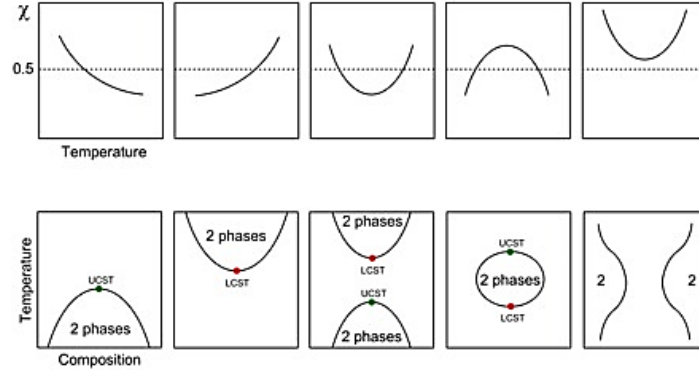


**Figure 2.9** Different types of polymer solution phase diagrams resulting from temperature-dependence of the Flory Huggins interaction parameter.[20]

#### 2.1.4. Concentration regimes

The next background topic I want to highlight is different concentration regimes in a polymer solution, which is a significantly important parameter of a polymer solution. The importance of this parameter is addressed in one of my studies (paper II), in which it is demonstrated how changing the polymer solution can affect the polymer stability in certain salt solutions.

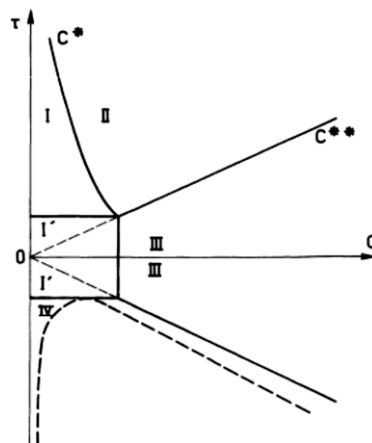


**Figure 2.10** Typical phase diagram of a polymer solution, suggested by Daoud and Jannink.  $\tau$  is the reduced temperature defined as  $\frac{T-\theta}{\theta}$ . [21]

Depending on the concentration of the polymer, solutions of different properties can be obtained, which differ greatly in microscopic and macroscopic characteristics. In a renowned work by Daoud and Jannink [21, 22], the polymer-solvent phase diagram was divided into four distinct regions, each possessing specific characteristics and scaling laws (Figure 2.10). The first region (I) is considered as the *dilute regime*, which is constrained by  $\tau$  and  $C^*$ . This region corresponds to a solution in which the polymer coils are well separated and no overlapping and entanglement is found between the chains (Figure 2.11). In all of my investigations, the polymer solutions were prepared in the dilute regime, to be able to study the single chain behavior. The  $C^*$  indicates the critical polymer concentration at which the chains start overlapping, which can be approximated using the following equation:

$$C^* = \frac{3M}{4\pi R_g^3 N_A}$$

Where  $M$  and  $R_g$  are the molecular weight and radius of gyration of the polymer chain, respectively. This is another essential equation, which I frequently used during my studies to estimate the dilute concentration range. It solely requires the average molecular weight, and the radius of gyration of the polymer that can be estimated from the introduced scaling law.

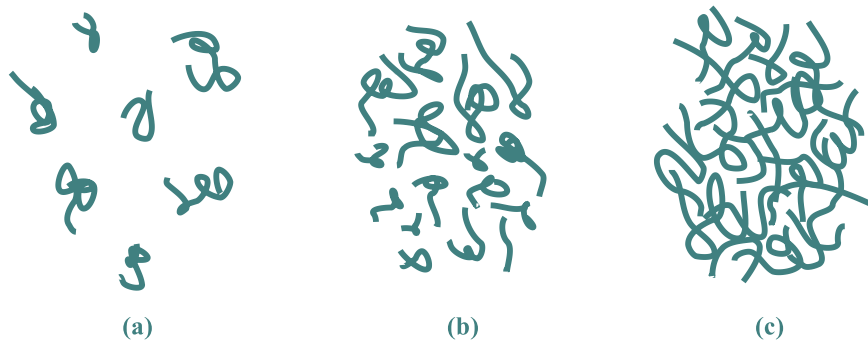


**Figure 2.11** Polymer solution concentration regimes: (a) Separated chains, (b) Overlapping chains, (c) Overlapping comparable to bulk polymer state.

## 2.2. Phase separation from molecular perspective

In the former section, I briefly discussed the phase behavior of polymer solutions in terms of general thermodynamics of polymer mixing. In this section, I will look over the same system but from the molecular interactions perspective, which is the prerequisite to understand my studies on the effect of salts on the polymers miscibility with water.

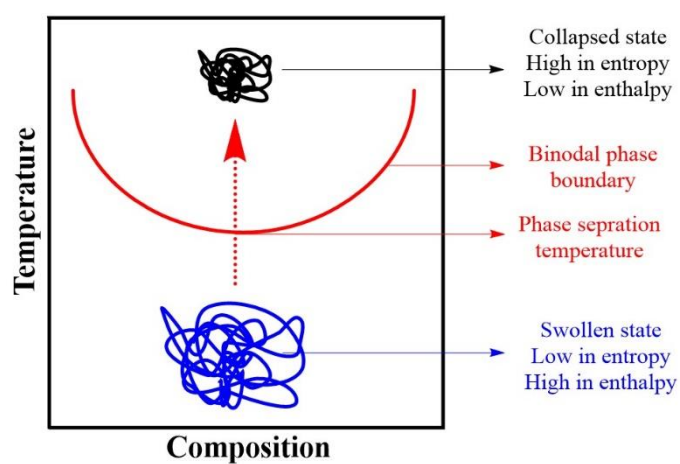


**Figure 2.12** Typical phase diagram of a polymer solution with a LCST behavior. Below the phase transition temperature, the polymer chain is found in a swollen random coil conformation (good solvent condition) and is considered to be hydrophilic. Above the phase separation temperature, the polymer chain turns into a collapsed globule considered to be hydrophobic. Accordingly, mixing of polymers with a LCST behavior is accompanied with a decrement in entropy but an increment in enthalpy. The former is related to the hydrophobic effect and the latter refers to specific interactions with water.

With respect to molecular interactions point of view, the solubility and phase behavior of polymers in water can be argued based on the interplay between the segment-segment (either short-ranged or long-ranged) and segment-solvent interactions.[23-25] In case of uncharged thermo-responsive polymers studied in my project, the most decisive interactions are the hydrophobic attractions and the hydrogen bonding. The strength of these interactions is closely related to the temperature of the

system, and that is the reason that changing the temperature can affect the polymer-solvent miscibility and phase separation occurs.

As shown in Figure 2.12, The LCST phase separation of stimuli-responsive polymers is generally envisaged as a transition from a swollen random coil conformation to a dehydrated collapsed (globular) state. With respect to the hydration and interaction, the polymer chain below the phase separation temperature is considered to be in the hydrophilic state (good solvent condition), while it becomes hydrophobic (or more accurately less hydrophilic!) above the phase separation temperature (bad solvent condition). Such a single molecular transition is only probable under an extremely dilute solution condition (considerably below the  $C^*$ ). [26-28] At relatively higher polymer concentrations, the collapsed globules also tend to form aggregates due to attractive interchain interactions.

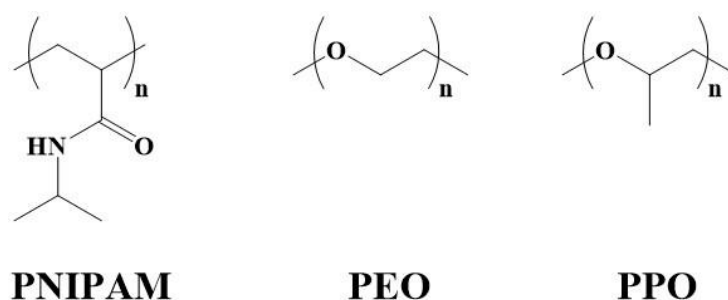


**Figure 2.13** Chemical structure of the thermo-responsive polymers studied in my projects. (Left) Poly(N-isopropylacrylamide) with hydrophobic backbone and isopropyl side groups and hydrophilic amide groups. (Middle) Poly(ethylene oxide) with hydrophobic backbone and hydrophilic ether groups. (Right) Poly(propylene oxide) with hydrophobic backbone and methylene side groups and hydrophilic ether groups. For PEO and PPO, at sufficiently low molecular weights, the hydroxyl end groups can also contribute to polymer hydrophilicity.

Herein, I exclusively discuss the thermo-responsive polymers, which I have investigated during my studies (Figure 2.13), i.e., Poly(N-isopropylacrylamide) (PNIPAM) as member of the family of Poly(N-acrylamide)s [29-31], Poly(ethylene oxide) (PEO) and Poly(propylene oxide) (PPO)

representing the poly(alkaline oxide)s [32-34]. With respect the chemical structure, all these polymers render a delicate balance between the hydrophilic (polar) and hydrophobic (apolar) parts in their repeating units. The former is responsible for the enthalpically favorable specific interactions with the water molecules, i.e. hydrogen bonding, while the latter is associated with the entropically unfavorable *hydrophobic effect* of water.[35-37] It has been widely discussed that inserting a purely hydrophobic solute in water changes the structure and hydrogen bonds network of the adjacent water molecules.[38-40] Compared to the bulk solution, the water molecules surrounding the hydrophobic solute are believed to interact more strongly with each other (favorable enthalpic term); nevertheless, they possess a smaller degree of freedom and thus a lower entropy. This indeed is referred to as the water hydrophobic effect, which strongly contributes to various physiochemical aqueous phenomena, including phase transition of the polymers that I investigated.

Accordingly, with respect to hydration structure, water molecules around a polymer chain (with hydrophilic and hydrophobic surfaces) can be divided into two groups: (i) the water molecules that are hydrogen bonded to the hydrophilic groups of the polymer (ii) the hydration layer adjacent to the hydrophobic surfaces of the polymer. The LCST phase behavior of polymers then originates from the temperature-dependent balance of these two hydration effects.[41, 42] Below the phase separation temperature, the favorable enthalpic term (specific interactions) dominates, thus the polymer chains are miscible with water. On the other hand, above the LCST, the unfavorable entropic term (hydrophobic dehydration) prevails and the polymer becomes immiscible with water. As a result, the polymer chain contracts and minimizes its solvent-accessible hydrophobic surface, which allows the water molecules in the hydrophobic hydration shell transfer to the bulk solution. Such a transition (phase separation) is then accompanied with a gain in entropy (due to the release of water molecules) and a drop in enthalpy (due to the breakage of relatively strong interactions),

which is in accordance with the thermodynamics of the phase separation that I provided in the former section.

Regarding the water molecules in the hydrophilic hydration shell, different mechanisms are likely depending on the type of the polar groups and polymer structure. In case of PEO and PPO (Figure 2.14), it has been suggested that the hydrogen bonds between ether groups and water molecules become gradually weaker with an increase in temperature, meaning that the number of bonded water molecules per segment monotonically decreases, giving rise to a relatively broad phase separation.[43-46] In contrast, it has been demonstrated that PNIPAM never becomes hydrophobic even above the LCST, as the collapsed coil still contains around 60% water, suggesting that the hydrogen bonded water molecules (to the amide groups) are not significantly affected during the phase separation, causing an abrupt phase separation.[47-51]

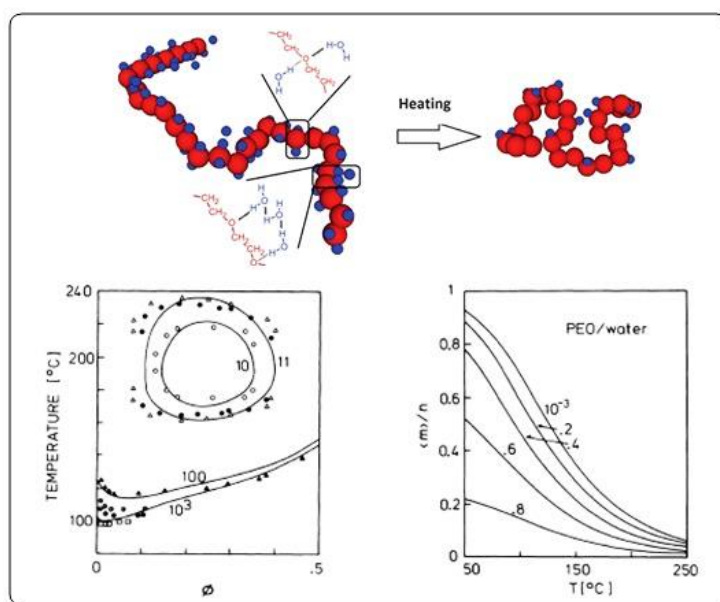


**Figure 2.14** (Top) Schematic illustration of PEO chain conformation and hydration below and above the LCST point.[35] (Bottom) Phase diagram and number of water molecules per segment for different PEO/water systems of different segment numbers. As shown, by decreasing the molecular weight of PEO the phase diagram turns into a closed loop (UCST and LCST), and increasing the temperature leads to gradual dehydration of the polymer.[43]

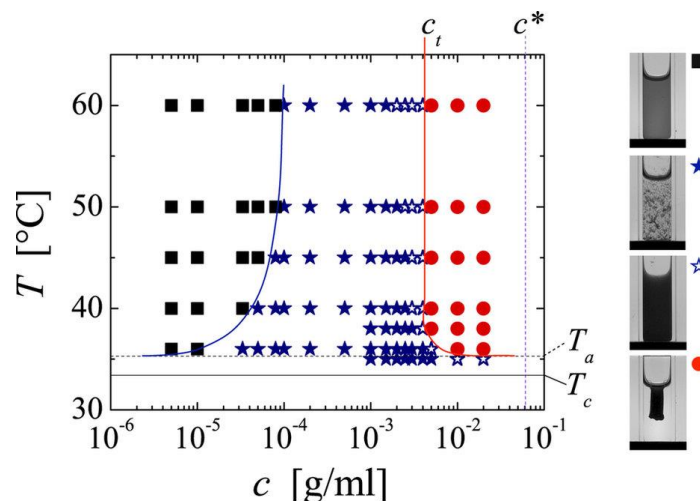


**Figure 2.15** Phase separation of PNIPAM can produce stable mesoglobules (black squares), flocks (blue filled stars), space-filling aggregates (blue open stars) or shrinking gels (red circles).[30]

There are various factors can affect the phase separation and LCST of the polymers. In general, any parameter that favors polymer-solvent interaction will give rise to stabilization, or in other words increases the phase separation temperature. In contrast, the factors that promote segment-segment interaction destabilize the polymer and thus a drop in LCST is predicted. The chemical structure or in other words the balance between hydrophilic/hydrophobic parts of the polymer segment is the first parameter that governs the polymer stability. For instance, PEO typically has a phase separation temperature above 100 °C in the salt-free aqueous solution; however, (PPO) typically phase separates at temperatures below 20 °C that drastically decreases with increasing its molecular weight.[52, 53] The only difference in the structure of the two polymers is the methylene side group present in PPO chain, which besides making the polymer more hydrophobic can affect packing of the polymer chains in solution. Nevertheless, it should be noticed that the situation is not always this simple. In other words, the ratio of carbon to oxygen atoms cannot readily determine the polymer solubility and phase separation temperature. For instance, poly(methylene oxide) (PMO) has a similar linear structure as PEO with one less carbon atom per segment, so it is relatively more hydrophilic than PEG and expectedly must have a higher LCST. Now the fact is that PMO is nearly



insoluble in water, most probably due to the strong packing and strong polymer-polymer interactions in the pure crystalline state, so water cannot dissociate the chains and dissolve them.[35, 54]

For a given polymer, increasing the molecular weight decreases the LCST because of the larger entropic loss for a longer polymer chain.[55, 56] This can be even seen for PNIPAM, which is actually believed to have an almost molecular-weight independent LCST; however, by going to relatively low molecular weights one can observe a clear increment in LCST.[57, 58] Such an effect is more pronounced for PEO (and PPO), where for relatively low molecular weights the LCST is found to be around 170 °C, while for relatively large molecular weights it is around 100 °C.[59] Confinement of the polymers at the interfaces has been also suggested to affect the LCST compared to the unperturbed state in the bulk solution. I will further discuss this effect in the next section, in which the behavior of polymers at aqueous/solid interfaces is addressed.

## **2.3. Polymers at solid/aqueous interfaces**

Polymer chains can spontaneously adsorb from the bulk solution to the solid surfaces through different mechanisms. Before going any further, I would like emphasize that the properties of the surface, e.g., roughness, curvature, and local chemical heterogeneity, can significantly affect the adsorption process.[60-62] What I discuss herein describes the adsorption of polymers on a flat, atomically smooth and chemically homogenous solid surface, which is impenetrable by the polymer chains. Regarding adsorption of polymers on spherical particles (employed in the conducted AFM colloidal probe measurements); the particle surface can be assumed as a flat substrate, regarding the considerably larger diameter of the particle compared to the polymer chains size.[63-65]

Three different approaches of preparing polymers layers at the solid/aqueous interfaces were employed and studied during my PhD studies, which I will illustrate and compare them in terms of

the layer formation and conformation. In one of my accomplished studies (paper IV), the physical (segmental) adsorption of a high molecular weight PNIPAM homopolymer on the gold surface was investigated. With respect to a neutral polymer, the polymer chains spontaneously adsorb on the surface in case of having a relatively strong segmental affinity for the surface.[66-70] The other important factor that must be taken into account is the segment-segment attraction compared relatively with the segment-surface interaction.[70-73] Besides the already-discussed effects of temperature on the interactions of the polymer with solvent and surface, one has to consider that the thermal energy of the polymer chain favors desorption from the surface.[67, 68] With respect to a polymer chain adsorbed on a solid surface, three typical conformations can be present throughout the polymer chain backbone. [74-76] The polymer segments that are bound to the surface (*trains*), the sections that form the *loops* between the *trains*, and finally the dangling *tails* of the polymer chain in the solution (Figure 2.16).

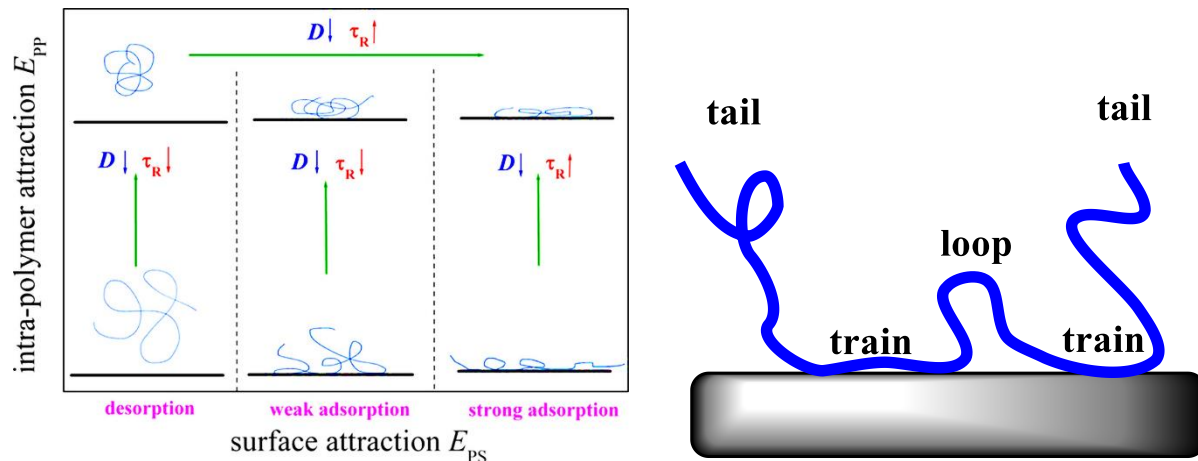


**Figure 2.16** Segmental adsorption of a polymer chain on a solid surface. (Left) The interplay between segment-segment attraction and segment-surface attraction controls adsorption and conformation of the adsorbed chain.[70] (Right) Conformation of a strongly adsorbed polymer chain on the surface. The segment-segment and segment-surface affinity affect the polymer adsorption in opposite directions. While relatively stronger segment-segment interaction tend to withdraw the polymer chain from the surface, the relatively stronger segment-surface interaction promotes adsorption and formation of *trains* on the surface.

Besides the favorable polymer-surface attraction (the enthalpic term), adsorption of a neutral polymer chain on an impenetrable solid surface is associated with an unfavorable entropic restriction, imposed by the surface.[77-79] In other terms, the number of the conformations that the polymer chain can adopt at the surface is smaller compared to in bulk solution. In this case, the polymer chain is typically broken up into the so-called *blobs*, where the polymer structure and conformation within each blob is considered as an unperturbed polymer chain (Gaussian chain) far from the surface.[80, 81] This provides the opportunity to employ the relevant scaling laws for an unperturbed coil, in order to calculate the entropic repulsion resulting from adsorption of a polymer chain at a specific temperature. The interaction potential of segment-surface attraction should be summed up with this entropic repulsive force. The compromise of these two opposite effects thus governs the segmental adsorption of a neutral polymer chain on a solid surface.

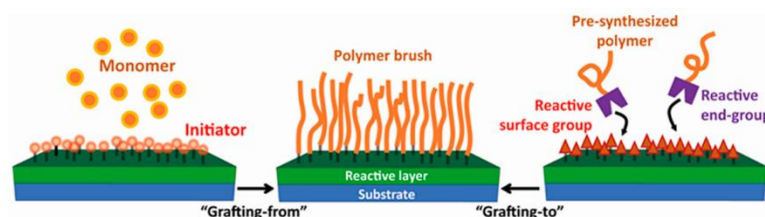


**Figure 2.17** Schematic illustration of grafting-from and grafting-to methods.[82]

In another part of my studies (paper IV), grafting of a mono thiol-terminated PNIPAM sample to the gold surface was assessed. In general, grafting the polymer on the surface at one end can be carried out via two different approaches.[83, 84] (i) The *grafting-from* method, in which the monomers are polymerized from the surface sites, so the polymer chains grow from the surface. (ii) The *grafting-to* method where the polymer chains are end-functionalized with specific chemical groups that can establish strong bonding with the surface[85-88], e.g., thiol-gold chemistry[89, 90] that I employed in my studies.

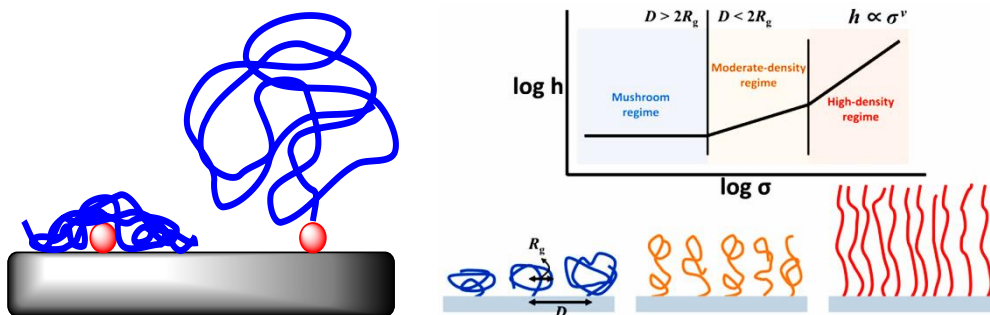


**Figure 2.18** End-tethered polymer chains. (Left) pancake (low grafting density, bad solvent condition, strong segmental affinity) and mushroom (low grafting density, good solvent condition, weak segmental affinity for the surface) conformations. (Right) mushroom-to-brush conformation transition resulting from increment in the grafting density.[82]

For a polymer grafted to the surface, besides the segment-surface affinity and the solvent quality, the other essential parameter is the grafting density  $\sigma$ , which is defined as the number of anchored polymer chains per unit area of the surface. To quantify this parameter, the overlap grafting density is defined as  $\sigma^*$  that scales with segment length and number of segments according to  $a^{-2}N^{-6/5}$  under good solvent condition.[91] For grafting densities smaller than  $\sigma^*$ , the polymer chains are well separated on the surface, in other words the distance between the grafting points are larger than the polymer coil size, where depending on segment-surface affinity and solvent condition two possible conformations are possible.[92-94] In case of relatively strong segment-surface interaction and (or) bad solvent condition, the polymer chains are expected to flatten on the surface, giving a so-called *pancake* conformation. In case of weak segment-surface affinity and (or) good solvent condition, the polymer chains are found in the swollen random coil conformation, providing a *mushroom* conformation. Polymer layers prepared using the grafting-to method usually give rise to these two structures, since the diffusion barrier typically prevents formation of densely grafted structures. For grafting densities larger than  $\sigma^*$  (the distance between the grafted points is smaller than the unperturbed coil size), the polymer chains overlap and interact. Considering the solvent quality to be good, the polymer segments will repel each other. Nevertheless, since the lateral

distance between the anchored chains is fixed by the grafting density, the polymer chains inevitably extend away from the surface to avoid each other as much as it is possible. Under such a condition, the layer thickness is considerably larger than the unperturbed polymer coil size, and is known as the *brush* conformation.[95-97] Such a dense layer structure is usually obtained using the grafting-from method.

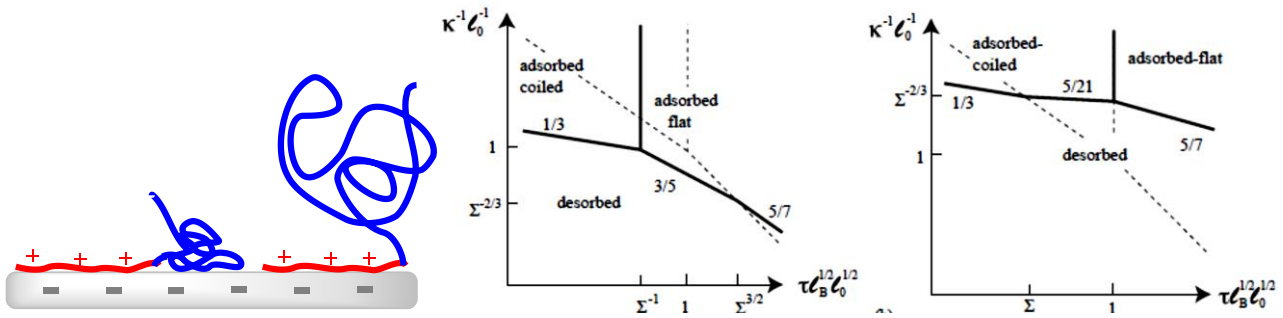


**Figure 2.19** Adsorption of a cationic copolymer on a negatively charged surface. (Left) Depending on segment-surface affinity, the uncharged block can form pancake or mushroom conformations. (Middle) Adsorption scaling diagram for strongly charged surfaces. (Right) Adsorption scaling diagram for weakly charged surfaces. A fully charged polyelectrolyte chain is expected to adsorb as a flat layer, whereas charge-diluted polyelectrolytes can form coiled layers with loops and dangling ends or even desorb from the surface.[98]

In another part of my investigations (paper V), the adsorption of synthesized cationic diblock and triblock copolymers on the negatively charged silica surface was assessed. The dominant driving force for adsorption of a polyelectrolyte chain on an oppositely charged surface is considered to be the electrostatic attraction, and other interaction contributions such as segmental affinity are typically neglected.[99-104] Nevertheless, it should be considered that a polyelectrolyte chain adsorbing on the surface gives rise to desorption of counter ions existing on the surface, which is accompanied with a favorable entropic term.[105, 106] Adsorption of a polyelectrolyte on an oppositely charged surface then should be studied in terms of the electrostatic repulsions between the polymer segments, and the electrostatic attraction between segment and surface. The amount of

the electrostatic charge on the polyelectrolyte chain and the surface as well as the salt concentration strongly affect the adsorption and conformation of the adsorbed chain on the surface (Figure 2.19).[98] With respect to the cationic copolymers examined in my project, the uncharged blocks can possibly adopt different conformations depending on the segment-surface interactions. If the uncharged block has a relatively weak affinity for the surface, then a mushroom conformation will be expected. This can be the case for adsorption of the cationic copolymer with a neutral PEG block on silica surface, where PEG was shown to have a weak affinity for the silica surface. On the other hand, if the uncharged block has a strong segmental tendency for the surface, a pancake conformation is likely, e.g., adsorption of the cationic copolymer with neutral PNIPAM block on the silica, where PNIPAM was affirmed to have a relatively strong affinity for the silica.

At last, I shortly bring up some aspects of thermo-responsive behavior of polymers at the solid surfaces. For a polymer adsorbed or grafted at a solid/aqueous interface, the phase separation (either the phase separation temperature or the phase separation width) can be different from that in bulk solution, which has been confirmed by both theoretical and experimental studies.[107-114]

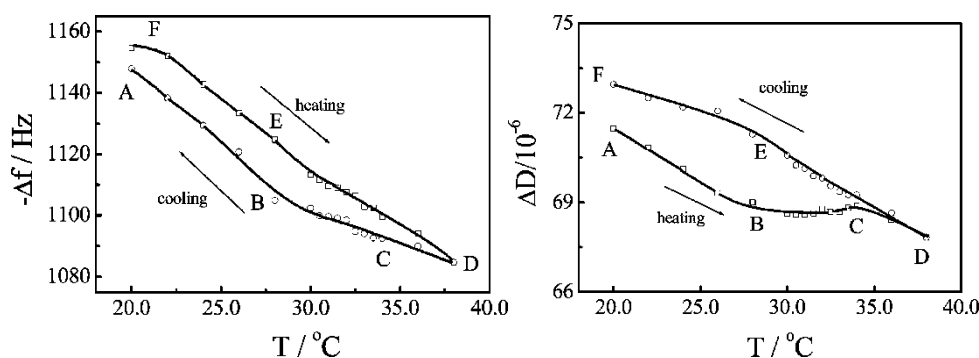


**Figure 2.20** Phase transition of a PNIPAM brush studied with QCM-D.[109] (Left) Positive frequency shift with heating suggests dehydration of the brush. (Right) Negative dissipation shift with heating indicates conformational collapse of the layer. Unlike the abrupt single chain collapse of PNIPAM in bulk, the coil-globule transition at the surface occurs over a broad temperature range.

There are two important considerations regarding the coil-globule collapse of the polymers at the surface. First, the polymer layers of low grafting density not only indicate a vertical collapse, i.e. decrement in the layer thickness, but also can undergo a lateral phase separation through which the collapsed chains can form clusters on the bare substrate. Such a lateral phase separation becomes less likely for polymer layers of high grafting density, which exhibit a large enough degree of chain stretching. Second and more importantly, unlike the sharp coil-globule transition for isolated chains in bulk solution, the polymer chains confined at a solid surface usually render a gradual and broad collapse. This can be seen from Figure 2.20, where the thermo-responsive behavior of a PNIPAM brush layer is assessed using quartz crystal microbalance with dissipation (QCM-D). In brief, the frequency data refers to dehydration of the brush and the dissipation data indicates conformational collapse and shrinkage of the layer. As can be seen, both sets of data suggest broadening of PNIPAM phase transition, which can be attributed to the lower solvent strength caused by the repulsive interactions between the grafted chains, as well as the entropic constraint cause by confinement at the solid surface and the excluded volume repulsion between the chains.

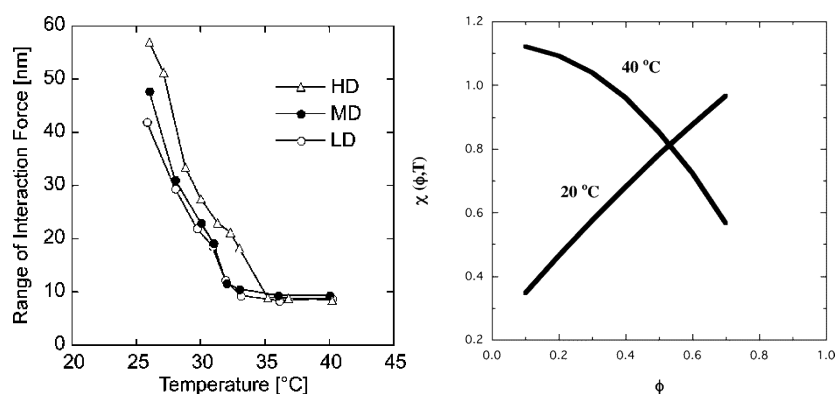


**Figure 2.21** (Left) Vertical collapse with heating for a grafted PNIPAM at three different grafting densities, studied by atomic force microscopy colloidal probe measurements.[115] (Right) The effective Flory-Huggins interaction parameter as a function of polymer local density below and above the collapse temperature.[116]

In addition, the phase separation of polymer layers has been demonstrated to strongly depend on several factors such as the molecular weight of the polymer and the grafting density.[115-120] Such an effect can also be reasoned based on the concentration-dependence of the Flory-Huggins interaction parameter together with the well-known chain stretching effect caused by increasing the grafting density under good solvent condition (Figure 2.21).

## 2.4. Ions in aqueous solution

In the previous sections, I provided the prerequisite knowledge for understanding the polymer hydration and phase transition behavior. From now, I switch the topic to the behavior and properties of polymers in aqueous saline solution. I start with a concise introduction to *specific ion effects* in pure water, and then I will discuss how ions can affect polymer stability in water. For a more detailed discussion on these topics, I strongly suggest the “*specific ion effects*” book by W. Kunz.

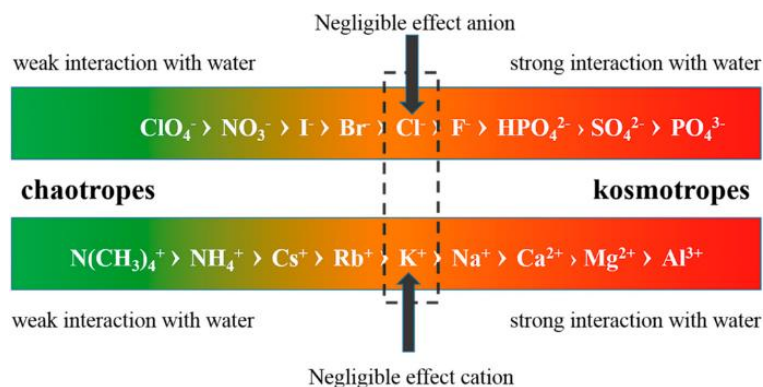


**Figure 2.22** Schematic of relative intensity of interactions of anions and cations with the surrounding water molecules. Ions to the right strongly interact with water and make the adjacent water molecules more ordered, thus are called kosmotropes. In contrast, ions to left are poorly hydrated and promote disorderness in the water network, thus are recognized as chaotropes. Chloride and potassium are considered as the *borderline* ions, since they have negligible effects on the water structure.[121]

Water is a highly structured liquid with an extensive network of hydrogen bonds; whereas, the exact structure of the network and the extent of hydrogen bonding is still under debate.[122-124]



Electrolytes in water dissociate into hydrated ions, which can affect the structure of hydrogen bonds network. The electric field around the ions can cause the water molecules to rearrange their orientation around the ion, suggesting that the structure of the water molecules in the ionic hydration shell differs from the bulk network. The continuum electrostatic models, e.g. Debye and Huckel model, assume all the interactions to be purely electrostatic and consider the ions as simple point charges; hence, the electric charge is the only decisive parameter.[125, 126] This means that such models cannot distinguish between ions of the same charge but different size or shapes, e.g. the halide anions. This indeed makes these classic models unable to describe the *ion-specific* phenomena.[125-129] The examples of *ion-specificity* in aqueous solution are numerous, e.g., the differences in ion pairing tendency, e.g., fluoride has a considerably stronger tendency to pair with lithium rather than iodide does.[130, 131] As another example, according to the classic electrostatic models, all the ions are strongly hydrated and a repulsion between all the ions and non-polar surfaces is predicted due to the image forces. Nevertheless, it has been confirmed that bulky ions with a low surface charge density preferentially accumulate at the non-polar surfaces and interfaces, an ion-specific phenomenon that is attributed to the polarizability of the ions and the contribution of dispersion forces, which are indeed neglected in the classic electrostatic models.[132, 133] In addition, it has been also shown that anions and cations interact differently with the water molecules; hence, their hydration characteristics and the following effects on the water structure are entirely different.[134, 135]

Further attempts in order to distinguish the effect of different ions on the water structure led to the introduction of *water structure maker* and *water structure breaker* terms.[135, 136] The former – also known as *kosmotropic*- describes the behavior of relatively small ions with a strong hydration capacity, suggesting that such ions make their adjacent water molecules more ordered than bulk water. One way to quantify these effects is through the *Jones-Dole viscosity coefficients*. [137]

$$\frac{\eta}{\eta_0} = A\sqrt{c} + Bc$$

In the formula,  $A$  is an *electrostatic* parameter, and  $B$  is an *ion-specific* parameter that is known as the *Jones Dole Viscosity coefficient* (Table 2.1). Accordingly, kosmotropic ions have a positive Jones-Dole viscosity coefficient, meaning that their corresponding saline solution has a higher viscosity than pure water. On the other hand, structure breakers or *chaotropic* ions are relatively large and bulky ions with poor hydration power, which can disrupt the water network structure and decrease the viscosity of water (have a negative Jones-Dole viscosity coefficient). Classification of ions into water structure maker and structure breakers has been fairly accepted by now; nonetheless, the question regarding the distances through which the ions can influence the structure of water has not been clarified exactly yet.[138-140]

**Table 2.1** Electrochemical mobility, Jones-Dole viscosity coefficient, enthalpy of hydration, crystal radii, and polarizability of some important anions and cations.[127]

Ion	$\mu_i$ ( $\text{cm}^2 \text{V}^{-1} \text{s}^{-1} \times 10^4$ )	$B$	$\Delta H_{\text{hydration}}$ ( $\text{kJ mol}^{-1}$ )	$a$ (Å)	$\alpha_0$ (Å <sup>3</sup> )
$\text{CH}_3\text{COO}^-$	4.23	0.236	-425	—	—
$\text{F}^-$	5.70	—	-515	1.12	1.218
$\text{Cl}^-$	7.91	-0.007	-381	1.86	4.220
$\text{Br}^-$	8.13	-0.032	-347	2.16	6.028
$\text{NO}_3^-$	7.40	-0.046	-314	2.21	4.008
$\text{I}^-$	7.95	-0.080	-305	2.33	8.967
$\text{SCN}^-$	—	-0.103	-310	2.39	7.428
$\text{Li}^+$	4.01	0.147	-519	0.42	0.028
$\text{Na}^+$	5.19	0.086	-409	0.67	0.131
$\text{K}^+$	7.62	-0.007	-322	1.06	0.795
$\text{NH}_4^+$	7.60	-0.007	-307	—	—
$\text{Rb}^+$	7.92	-0.029	-293	1.23	1.348
$\text{Cs}^+$	7.96	-0.045	-264	1.62	2.354

The first hydration shell is found for most of the ions, even the large monovalent species.[141, 142] This can be seen from Figure 2.23 in which the radial distribution of the water molecules around lithium, sodium and potassium cations are compared with that in pure water. Accordingly, the distance between lithium and sodium with the nearest water oxygen atom is shorter than the oxygen-oxygen distance in pure water, which represents a relatively strong hydration power. On the

other hand, potassium indicates a relatively larger distance, suggesting a weak hydration. Presence of the second hydration shell is common for small and highly charged ions.[142, 143]

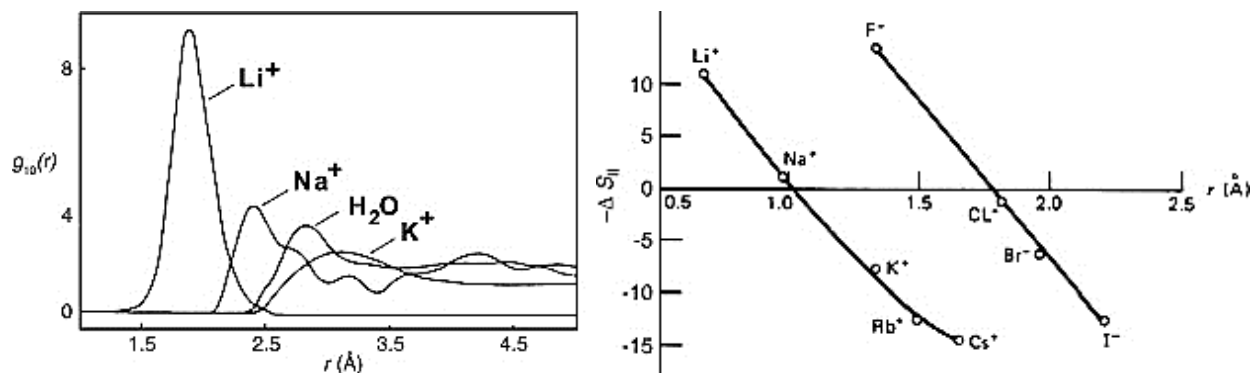


**Figure 2.23** (Left) The radial distribution functions for  $\text{Li}^+$ ,  $\text{Na}^+$ , water, and  $\text{K}^+$  in liquid water, showing the distance between the cations to the nearest solvent oxygen, while the water curve measures the oxygen–oxygen distance in pure water.[141] (Right) The entropy of water near an ion minus the entropy of bulk water. Kosmotropes are in the upper portion of the figure and the chaotropes are in the lower portion.[144]

It should be considered that presence of these hydration shells changes the *effective radii* of the ions in solution, which has been confirmed by different methods such as conductivity measurements of different salt solutions.[127, 145] In this experiment, the cations migrate towards the negative electrode and the anions move toward the positive electrode. At the first glance, one would expect higher mobility for the small ions and lower for the large entities; nevertheless, in reality the order is reversed (Table 2.1). Observations like this have confirmed that the effective size of the ions in water is very different from that in a crystal state, i.e., small and strongly hydrated ions carry several water molecules with them. Another way of addressing ion-specificity on water structure is illustrated in Figure 2.23, which compares the effect of different ions on the entropy of their adjacent water molecules. Accordingly, small ions of high charge density such as fluoride immobilize their neighboring water molecules (decrease the entropy); while large ions of low charge density such as iodide actually *free up* the nearby water molecules (increase the entropy).

**Table 2.2** Entropy of hydration of different ions.[135]

ion	Krestov <sup>106</sup>	Abraham <sup>153</sup>	Marcus <sup>205</sup>	
	$\Delta S_{\text{struct}}$	$\Delta S_{\text{struct}}$	$\Delta S_{\text{struct}}$	$\Delta C_{p \text{ struct}}$
Li <sup>+</sup>	-69	-81	-52	147
Na <sup>+</sup>	-19	-27	-14	83
K <sup>+</sup>	21	40	47	0
Rb <sup>+</sup>	39	50	52	-38
Cs <sup>+</sup>	46	76	68	-83
Ag <sup>+</sup>	-13	-20	-15	47
NH <sub>4</sub> <sup>+</sup>	-8 <sup>a</sup>		5	28
Me <sub>4</sub> N <sup>+</sup>			41	-30
Ca <sup>2+</sup>	-159		-59	215
La <sup>3+</sup>	-300		-113	355
F <sup>-</sup>	-57	-87	-27	20
Cl <sup>-</sup>	20	-2	58	-62
Br <sup>-</sup>	41	21	81	-88
I <sup>-</sup>	68	52	117	-113
NO <sub>3</sub> <sup>-</sup>	23		66	-59
SCN <sup>-</sup>			83	-33
ClO <sub>4</sub> <sup>-</sup>	44 <sup>a</sup>	68	107	-87
CO <sub>3</sub> <sup>2-</sup>	-160 <sup>a</sup>		-52	68
SO <sub>4</sub> <sup>2-</sup>	-100 <sup>a</sup>		8	-14
PO <sub>4</sub> <sup>3-</sup>	-319 <sup>a</sup>		-131	103

This can also reveal the difference between the hydration of anions and cations, i.e., fluoride and potassium ions are comparable in size and charge, but the anion is strongly hydrated while the cation is weakly hydrated, which suggests difference in the ways anions and cations interact with water.[134] The electronegative oxygen atom of water can accept negative charge from anions, while charge transfer from cations to water is difficult. In addition, since anions interact with the hydrogen atom of water, they allow intra-shell hydrogen bonding within the hydration shell, which is not possible for cations that interact with the oxygen atom.[146-148]

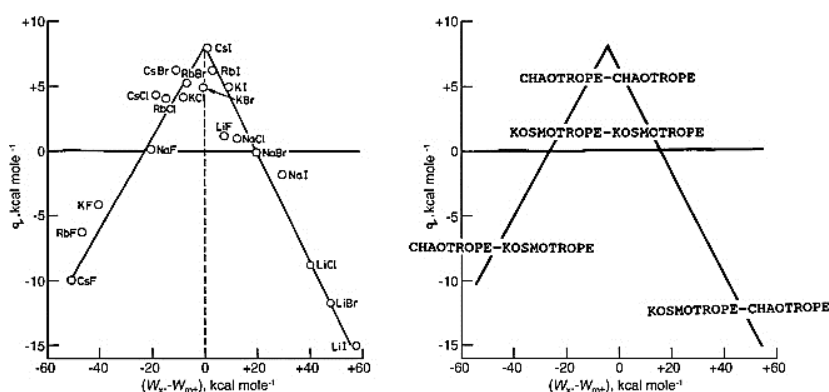


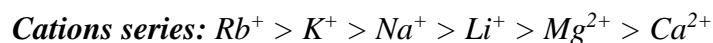
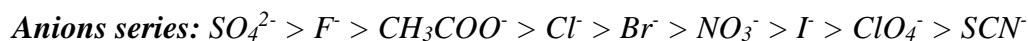
**Figure 2.24** The Volcano plot. (Left) The standard heat of solution of salts (at infinite dilution) vs the difference between the absolute heats of hydration of the corresponding gaseous anion and cation. (Right) The enthalpy of solution of chaotrope–chaotrope and kosmotrope–kosmotrope salts is positive; nevertheless, for a negative enthalpy, the salt must have a kosmotropic and a chaotropic ion.[144]

As I mentioned before, ion pairing is another important ion-specific phenomenon, which can be quantified based on the so-called *volcano plot* (Figure 2.24).[144] Accordingly, a negative standard heat of solution is obtained only if we have a chaotrope and a kosmotrope in the salt. In other terms, neutral salts of a kosmotrope plus a chaotrope favorably dissociate into hydrated ions, since the kosmotropic ion forms relatively stronger interactions with water in solution than it has with the chaotrope in the crystal (release of heat upon dissolution). In contrast, a kosmotrope plus a kosmotrope tend to stay together as ion pair, thus heat is required for breaking the strong kosmotrope–kosmotrope interactions. Moreover, the relatively stronger water–water interactions will keep the chaotrope plus chaotrope ion pairs together, and heat is required to break the strong water-water interactions. Considering that all the salts in the volcano plot are monovalent, thus the long-ranged electric fields generated must be quite similar. Therefore, the striking differences in the salts behavior refers to difference in the strength of short-ranged chemical interactions with water. These arguments form the basis of the well-known *Law of Matching Water Affinities*, which I will discuss in more details in the coming section about ion-specificity in polymer solutions.

## 2.5. The Hofmeister effect

*Hofmeister* or *lyotropic* effect is a ubiquitous term referring to the ion-specific phenomena, which cannot be explained by the classic electrolyte theories.[149-153] Examples of these phenomena are numerous, e.g. bubble coalescence, enzymatic activities, proteins stabilization, bacterial growth and many others.[154-162] Back to 1888, Franz Hofmeister reported the effect of different salts on precipitation of the egg yolk protein.[163, 164] For that salts with same cation, he sorted the anions in a series with respect to their power in precipitating the protein, while by fixing the anion, a ranking for the cations was obtained, which together establish the framework of the *Hofmeister*

*series*. This ranking of ions was later affirmed to describe the effect of salts on the solubility of polymers in water, as well.[165-167]



Accordingly for neutral polymers, anions to the right are the most stabilizers known to have a *salting-in* effect, meaning that they can increase the phase separation temperature. On the other hand, the anions to the left are strong destabilizers that have a so-called *salting-out* effect and decrease the phase separation temperature. For decades, there has been an extensive debate on whether these effects should be attributed to bulk water or the surface-related effects. In the beginning, the Hofmeister effect was argued with respect to the specific interactions of ions with water molecules. As discussed in the previous section, ion-specificity on the water properties has been addressed in various terms such as Jones-Dole viscosity coefficients, electrochemical mobility of ions and ion pairing. This classification of ions into kosmotropes and chaotropes could provide a rather general explanation for the observed Hofmeister series in polymer solutions; nevertheless, various observations remained unexplained. One of the most important observations was the Hofmeister effect of cations, where the strongly hydrated cations have a salting-in effect and the weakly hydrated cations destabilize the polymer.[168, 169] This indicates that the hydration capacity and *water withdrawing power* is not the only decisive factor. As another important observation, in some systems a *reversed* Hofmeister series has been obtained.[170-173] For instance, with respect to proteins aggregation, the *direct* Hofmeister series is usually observed at pH values above the protein isoelectric point (IEP). The series however reverses by decreasing the pH below the IEP, while again at a pH below IEP the series changes from *inversed* to *direct* order. Such examples suggest that both specific ion-surface and ion–water interactions are involved in the

Hofmeister effect. In addition, the water-polymer interactions should be taken into account. It has been recently shown that the direct and reversed series can be obtained depending on the nature of the surface, e.g. hydrophobic or hydrophilic, charged or uncharged; nonetheless, the idea that there is a fixed universal Hofmeister series persists. According to the current opinion, reversal of the Hofmeister series or similar discrepancies from the early-suggested ranking should be considered as “*a rule rather than an exception*”.[174, 175] For decades, it was thought that Hofmeister effects were associated merely with phenomena occurring at high salt concentrations, but later, ion specificity was found at low salt concentrations as well.[176-178] It has been also discussed that ions do not influence hydrogen bonding of water beyond their first or second solvation shells, which indeed rule out the speculated long-ranged effects of ions on the water structure.[179] All these together highlight the importance of considering specific ion effects to explain the Hofmeister series. I will introduce and discuss the previously reported mechanisms that have gained attention during recent years, in which ion-specificity in polymer solutions has been addressed. The explanations in the previous sections regarding polymer phase behavior and ionic hydration will be used together with the ion-specific effects on the polymer hydration layer and polymer surface to scrutinize the Hofmeister effect in polymer solutions, which form the basis of papers I to IV.

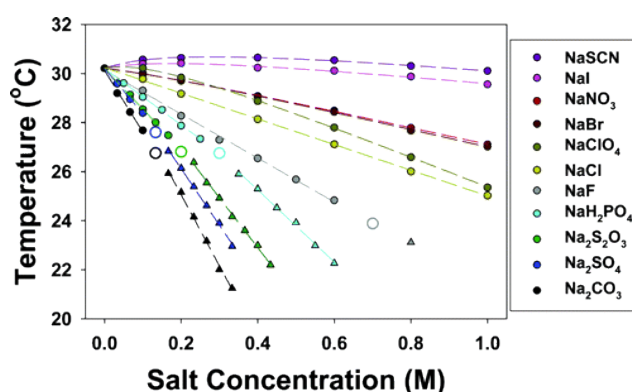


**Figure 2.25** The Hofmeister series of sodium salts on the phase separation temperature of PNIPAM.[180] Weakly hydrated anions such as thiocyanate have a non-linear salting-in effect, while strongly hydrated anions such as fluoride cause a linear salting-out effect.

### 2.5.1. Triple effects: polarization, surface tension and direct binding

Cremer and coworkers have published a series of publications going back to 2004, in which they extensively investigated the specific ion effects on PNIPAM and proteins stability.[180-192] They have suggested three principal mechanisms through which different anions can affect the stability of polymers and proteins, which are summarized in Figure 2.26.

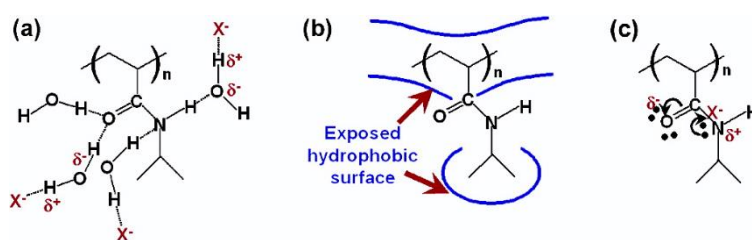


**Figure 2.26** Interactions of anions with PNIPAM surface and its hydration water. (a) Polarization effect on the hydration shell of the amide bonds (b) The surface tension effect at the hydrophobic surfaces of polymer (c) Direct binding to the amide.[180]

The first suggested mechanism is the polarization of the water molecules that are hydrogen bonded to the amide groups of PNIPAM, through which the anions affect the hydration shell of the polymer, which in turn can facilitate dehydration of the amide groups. As argued by the authors, such a destabilizing effect is possible for the strongly hydrated anions, and the extent of the effect is in direct correlation with the entropy of hydration of the anions or the hydration power. As the second mechanism, anions could interfere with the hydrophobic hydration of PNIPAM by increasing the surface tension of the cavity surrounding the backbone and the isopropyl side chains, and thus making the hydrophobic hydration more entropically costly and thus the polymer becomes destabilized. Such a mechanism was considered to be possible for all the anions; however, in their later publications the authors claimed that depending on the polymer surface chemistry, some weakly hydrated anions can indeed decrease the surface tension causing a stabilizing effect. Finally, the poorly hydrated anions can directly bind to the amide bond, and cause stabilization of the



polymer. The authors further discussed this mechanism in their later publications, in which suggested other possible binding sites on the polymer backbone, i.e., atoms with a partial positive charge. To quantify these effects together, the authors suggested the following empirical equation:

$$T = T_0 + c[M] + \frac{B_{max}K_A[M]}{1 + K_A[M]}$$

In this equation,  $T$  is the phase separation temperature of the saline solution,  $T_0$  is the phase separation temperature of PNIPAM in pure water and  $[M]$  is the molarity of the salt. By fitting the measured phase separation temperatures to this equation, three parameters can be determined.  $c$  is the slope of the linear part of the figure (Figure 2.25) indicating the strength of the first and second mechanisms,  $K_A$  is the binding constant of the anion to the polymer and  $B_{max}$  is the maximum increase in the phase separation temperature or the saturation value. Therefore, the  $c$  value represents the destabilization effects and the last term on the right hand, which is reminiscent of the Langmuir isotherm binding, indicates the third mechanism.

**Table 2.3** Fitted values obtained for  $c$ ,  $K_A$ ,  $B_{max}$  and the water surface tension increment and hydration entropy.[180]

anion	$\sigma^a$ (mN L/m mol)	$\Delta S_{hyd}^b$ (J/K mol)	$B_{max}$ (°C)	$K_A$ (M <sup>-1</sup> )	$c$ (°C/mol)		
					initial	first step	second step
CO <sub>3</sub> <sup>2-</sup>	2.6	-245	—	—	-25.1	-29.0	-9.7
SO <sub>4</sub> <sup>2-</sup>	2.7	-200	—	—	-18.3	-23.1	-10.0
S <sub>2</sub> O <sub>3</sub> <sup>2-</sup>	2.9	-180	—	—	-16.3	-20.3	-10.9
H <sub>2</sub> PO <sub>4</sub> <sup>-</sup>	2.3	-166	—	—	-11.5	-14.7	-8.3
F <sup>-</sup>	2.0	-137	—	—	-9.0		
Cl <sup>-</sup>	1.6	-75	—	—	-5.3		
Br <sup>-</sup>	1.3	-59	0.7	2.7	-3.7		
NO <sub>3</sub> <sup>-</sup>	1.1	-76	0.6	2.9	-3.5		
I <sup>-</sup>	1.0	-36	1.1	4.3	-1.5		
ClO <sub>4</sub> <sup>-</sup>	1.4	-57	1.8	5.1	-6.4		
SCN <sup>-</sup>	0.5	-66	1.6	4.3	-1.4		

## 2.5.2. The solute partitioning model

Pegram and Record have discussed the Hofmeister series and the effect of different salts on the polymers and proteins stability, in terms of the partition coefficient of the ions at the polymer surface and the change in the solvent-accessible surface area of the polymer.[193-200] The authors

initially discussed the effect of different salts on the surface tension of water in terms of the preferential accumulation or exclusion of the ion at or from the air/water interfacial region, confirming that the effect of salts on the surface tension follows the Hofmeister series. In order to explain the effect of the salts on the polymers stability, the authors introduced the *Solute Partitioning Model (SPM)* to examine the Hofmeister effect in terms of the surface hydration ( $\text{H}_2\text{O}/\text{\AA}^2$ ) and the solute partition coefficient  $K_p$ . The partition coefficient is defined as the ratio of the ion concentration at the surface to the bulk solution, which then indicates the extent of surface accumulation/exclusion. A  $K_p$  larger than unity indicates surface accumulation, while a  $K_p$  smaller than unity describes surface exclusion. According to this model, the effect of salts on aqueous phenomena can be characterized by the m-values given as:

$$m = \frac{d\Delta G}{dm_3} = -RT \frac{d\ln K}{dm_3} = RT \Delta \frac{d\ln f_2}{dm_3} = \Delta \frac{d\mu_2}{dm_3} = \Delta\mu_{23}$$

Where  $m_3$  is the salt concentration,  $K$  is the equilibrium constant of the process in terms of equilibrium concentrations of the products and reactants and  $G$  is the free energy change.[201, 202] Accordingly, interaction of the salt (3) with the polymer (2) affects the activity coefficient of the polymer ( $f_2$ ) in solution, and thus leads to a change in the chemical potential ( $\mu_2$ ) of the polymer.

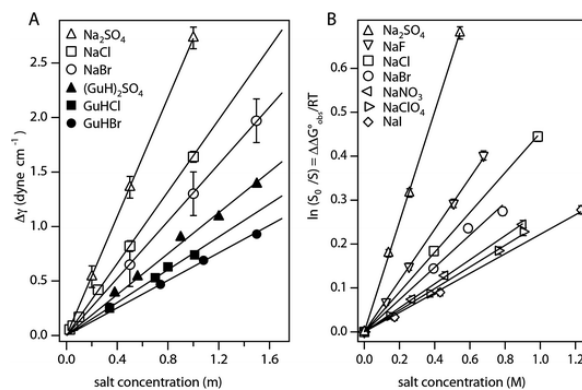


**Figure 2.27** Hofmeister effect on model processes involving nonpolar surfaces exposed to water.[199] (Left) Increase in surface tension of water as a function salt concentration. (Right) Effect of salts on the relative solubility of benzene.

A typical usage of this model is shown in Figure 2.27, in terms of the effect of different salts on surface tension of water, and solubility of a non-polar solute in water, where the m-value can be extracted from the slope of the lines. Accordingly, it has been shown that the effect of salts on the surface tension and solubility of the hydrophobic solute follows the same order. The obtained chemical potential derivative is proportional to the accessible surface area (ASA) of the macromolecules through the proportionality constant  $\alpha$ , which includes an average hydration ( $b_1$ ) term average solute partitioning coefficient ( $K_p$ ):

$$\frac{m - value}{RT} = \Delta \frac{\mu_{23}}{RT} = \alpha_{3,2} \Delta ASA = \frac{-(v_+ K_{p,+} + v_- K_{p,-} - v) b_1 (1 + \varepsilon_{\pm})}{55.5} \Delta ASA$$

Where  $\varepsilon$  is salt-salt non-ideality correction term, i.e., derivatives of activity coefficient of the salt with respect to its concentration. The interaction potential ( $\alpha$ ) quantifies the strength and direction of preferential interaction of salt with polymer surface, which is almost independent of the change in accessible surface area, salt concentration and non-ideality correction parameter. Based on this equation, the partition coefficients of various ions for non-polar surfaces and polar groups such as amide and hydroxyl groups were calculated (Figure 2.28).

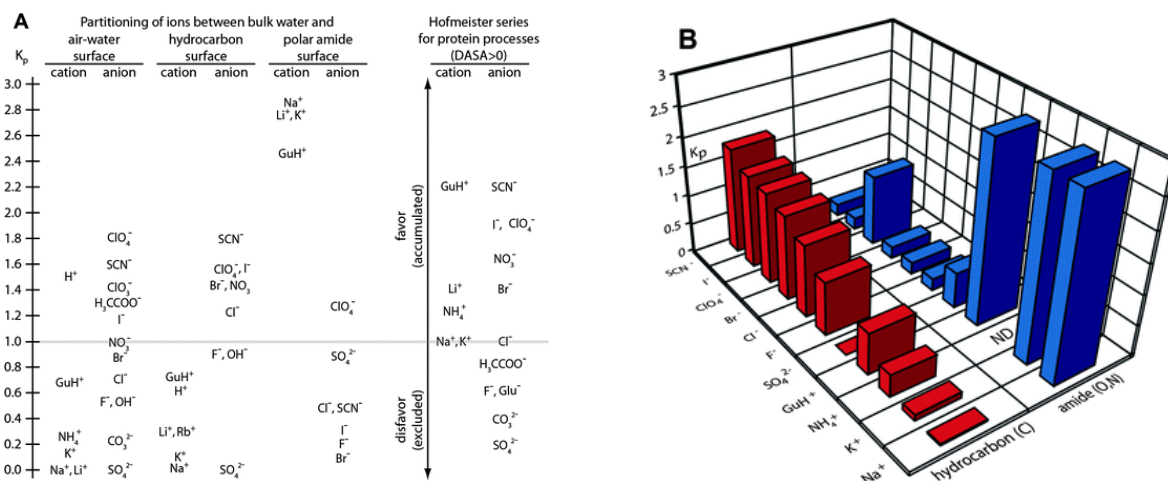


**Figure 2.28** Partition coefficients for the cations and anions at nonpolar and polar surfaces.[199]

### 2.5.3. The law of matching water affinities

As explained in the section about hydration of ions, the law of matching water affinities (*LMWA*) was formulated by Collins to address specificity in the ion-ion and ion-charged site interactions.[125, 136, 141, 144, 203-206] First, the ions are classified as being kosmotropic or chaotropic to distinguish their hydration power and resulting effects on the water structure. Then, the association of anions and cations to form ion pairs is discussed with respect to the Volcano plot, which can be interpreted as cations and anions form stable ion pairs if their corresponding hydration enthalpies match. In other words, a kosmotropic cation likes a kosmotropic anion, and a chaotropic cation likes a chaotropic anion (Figure 2.29).

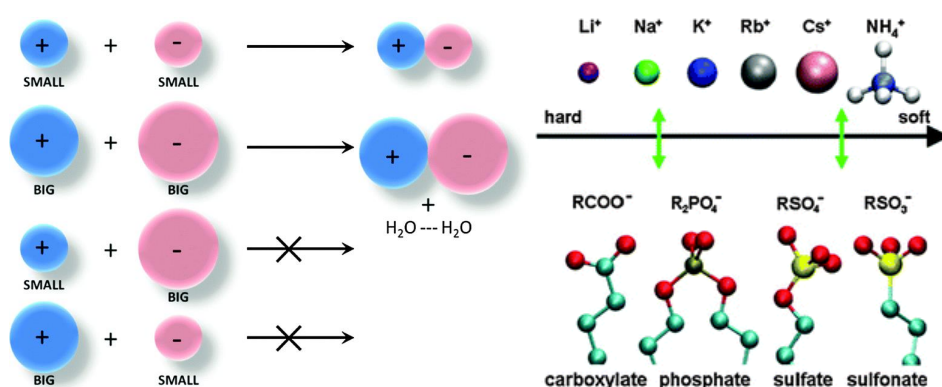


**Figure 2.29** (Left) Schematic illustration of ion pairing based on the LMWA. As shown, when both anion and cation are kosmotropic or chaotropic, they form stable ion pairs. While if one ion is kosmotropic and the other is chaotropic, they tend to dissociate in solution.[141] (Right) LMWA schematic illustration of ion-headgroup binding. Small and strongly hydrated ions are referred to as *hard* ions, while bulky and weakly hydrated ions are called *soft* ions. [207]

Using the same framework, Kunz provided a qualitative explanation for the affinity of the charged functional groups for different counter ions (Figure 2.29).[207] In a similar argument, for a chaotropic head group, the binding tendency of the chaotropic counter ions is larger and vice versa, which can be used to justify the observed series for counter ion binding to the charged residues of the proteins, as well.

This speculation has been used to explain many biological observations. For instance, the fact that the strongly hydrated  $Ca^{2+}$  and  $Na^+$  ions are pumped out of the living cells, whereas the weakly hydrated  $K^+$  is pumped in. This is because  $Ca^{2+}$  and  $Na^+$  are well matched to the strongly hydrated intracellular anions (phosphate, the carboxylate, and carbonate), and tend to form contact ions pairs with them (and then come out of solution).[127] However, it is worth mentioning that the LMWA is not actually a theory, but rather an empirical rule based on the observed Hofmeister series for ion-ion and ion-site interactions. It does not clearly explain why the hydration properties of the ions at infinite dilution should determine ion pairing and ion-site binding. More importantly, it merely addresses the interaction of the ions with the charged groups of polymers and proteins; nevertheless, as mentioned before, ions can interact with the hydrophobic surfaces and uncharged polar groups.

#### 2.5.4. Ion dispersion interactions

While electrostatic and hydration forces have been typically considered to explain the Hofmeister effect, Ninham and coworkers have suggested dispersion interactions as another source of ion-specificity.[126, 132, 152, 175, 206, 208-212] As explained before, electrostatic interactions solely cannot elucidate the ion-specific phenomena, because ions of the same charge can have different size and shapes. Therefore, one has to consider the dispersion forces to account ion-specificity.

Accordingly, at any aqueous interface, ions experience a dispersion potential given by the Lifshitz theory. Therefore, for a colloidal particle in the solution, an additional mean field term ( $U_x^{dispersion}$ ) related to the dispersion potential should be included in the mean field Poisson-Boltzmann equation, to address the image forces, many body dipole-dipole, dipole-induced dipole, and induced dipole-induced dipole forces, as interactions that strongly depend on the nature of the species:

$$\rho_x = \rho_0 e^{-(ze\psi_x + U_x^{dispersion})/kT}$$

The dispersion potential itself is given as:

$$U_{\pm}(x) = \frac{1}{x^3} \int_0^{\infty} \frac{\alpha(i\omega)}{\varepsilon_w(i\omega)} \left( \frac{\varepsilon_w(i\omega) - \varepsilon_s(i\omega)}{\varepsilon_w(i\omega) + \varepsilon_s(i\omega)} \right) d\omega$$

Where  $\alpha$  represents the polarizability and  $\varepsilon$  refers to the dielectric constants of water and surface. This equation demonstrates that frequency dependence of the dielectric function of the substrate determines the sign of the dispersion potential, meaning any ion experiences an additional dispersion potential, which can either enhance or decrease the electrostatic potential. (Figure 2.30)

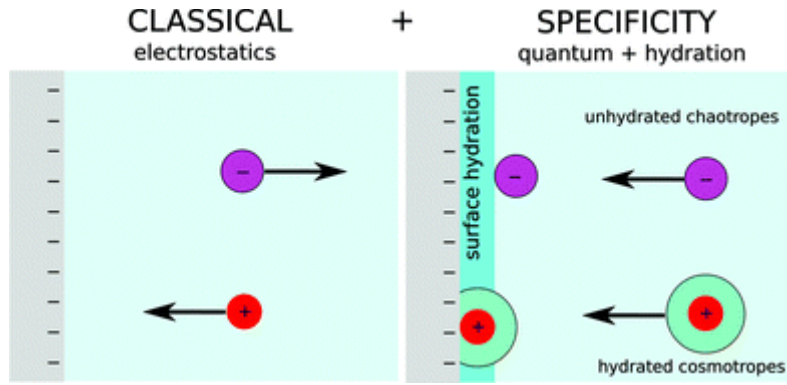


**Figure 2.30** Schematic representation of the classic Poisson-Boltzmann theory and the modified version with the dispersion and hydration forces included.[152]

The dispersion potential can be estimated from the static polarizability of the ions and single adsorption frequency, providing:

$$U_x^{dispersion} = \frac{B}{x^3}$$

$$B = \frac{\alpha^*(0)h\omega}{16\pi} (n_w^2 - n_s^2)$$

Where  $n$  represents the refractive index,  $h\omega$  indicates the ionization potential of the ions, and  $\alpha^*(0)$  is the static polarizability of the ion. Based on this equation, we can evidently find out that the difference between the refractive index of water and the substrate determines the sign of the

dispersion potential, i.e., if the refractive index of the substrate is larger the dispersion potential will be positive and vice versa. Moreover, the higher the polarizability of the ion is, the stronger the dispersion force contribution will be. In order to include the ion hydration role into the dispersion potential, Parsons and coworkers[152, 212] calculated the frequency dependent dynamic polarizability of the ions, giving the dispersion potential as:

$$U_x^{dispersion} = \frac{B}{x^3} f(x)$$

$$B = \frac{kT}{2} \sum_n \frac{\alpha^*(i\omega_n)}{\varepsilon_w(i\omega_n)} \left( \frac{\varepsilon_w(i\omega) - \varepsilon_s(i\omega)}{\varepsilon_w(i\omega) + \varepsilon_s(i\omega)} \right)$$

In this equation,  $f(x)$  is called the form factor and accounts for the finite size of the ion and hydration, and  $\alpha^*(i\omega)$  is the excess dynamic polarizability.

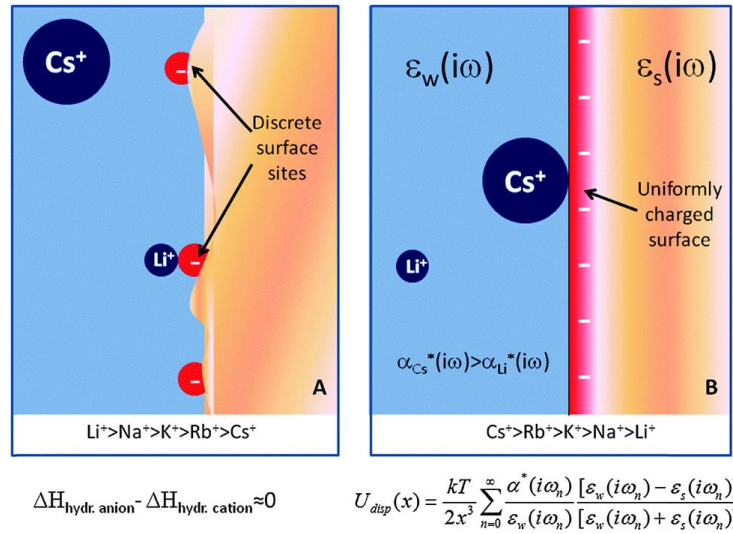


**Figure 2.31** Schematic comparison between (A) LMWA and (B) the theory of dispersion forces, to explain the specific interactions of weakly- and strongly hydrated ions with an oppositely charged surface. Depending on the nature of the surface, the two approaches may predict opposite Hofmeister series.[127]

This theory indicates that the ionic size and polarizability have opposite effects on the dispersion potential. Polarizability increases with size, thus enhancing the dispersion forces. On the other hand,

the increased size weakens the dispersion forces. In addition, hydrated ions have a different effective size, which can also affect the dispersion interactions. The outcome is thus a balance between all these effects, which can address the ion-specificity in the ion-ion and ion-surface interactions. This indeed reveals the differences between the LMWA and the quantum approach (Figure 2.31). While the former merely concerns with binding of ions to the charged binding sites on the surface, the latter examines ion-surface interaction by considering a uniformly charged substrate with a dielectric constant.

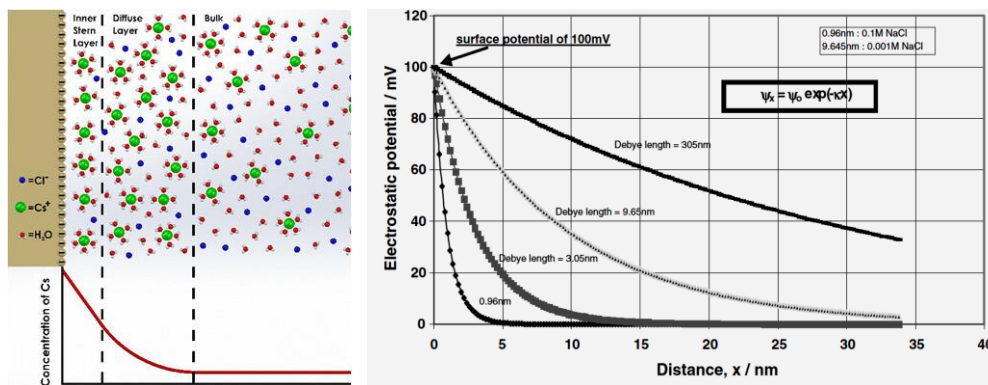


**Figure 2.32** (Left) Parts of the electrostatic double layer for a gold surface in CsCl aqueous solution.[213] (Right) Electrostatic potential decay in different NaCl concentrations.[214]

## 2.6. Surface forces in aqueous media

In this section, I will describe the general principles of the colloidal stability and surfaces forces between the polymer-covered surfaces, which can be useful for understanding and analysis of my AFM colloidal probe results (paper IV and V). The main forces that had to be considered during my work are electrostatic double layer forces, Van der Waals forces, hydration forces, and more importantly polymer-related steric and bridging interactions. I will go through the nature and origins of each of these interactions to provide a framework for interpretation of the AFM force profiles. For a deeper understanding of these concepts, I would like to refer you to “*Intermolecular and*



*Surface Forces*” by Jacob N. Israelachvili, which is definitely one of the best sources on this topic. For a more exclusive knowledge on the polymer-mediated interactions, “*Polymers at Interfaces*” by G. J. Fleer et al. is definitely a useful book.

### 2.6.1. Electrostatic double layer force

Surfaces in the aqueous medium can be charged through different mechanisms such as ionization or dissociation of surface groups, e.g. deprotonation of surface carboxylic groups, or adsorption of ionic species from the solution to the surface, e.g., adsorption of the hydroxide anion to water/hydrophobic interfaces.[215] The formed surface charge is compensated with a distribution of the counter- and co-ions, which was described by the Gouy and Chapman diffusive double layer.[216, 217] Afterwards, Stern introduced the concept of the adsorbed counter ions in the fixed first layer from the surface, known as the Stern plane.[218, 219] Accordingly, the potential at the surface  $\psi_0$  linearly decreases to a value of  $\psi_d$  located at the Stern plane, and then exponentially decreases to zero value in the bulk solution (Figure 2.32).[220] The double layer thickness is accordingly formulated as:

$$\kappa^{-1} = \left( \frac{\varepsilon_r \varepsilon_0 kT}{e^2 \sum_i c_{mi} Z_i^2} \right)^{0.5}$$

Where  $\varepsilon_r$  is the relative permittivity,  $\varepsilon_0$  is the permittivity of vacuum,  $k$  is the Boltzmann constant,  $T$  is the absolute temperature,  $C_m$  is the molarity of the ions,  $Z_i$  is the valiancy of the ions, and  $e$  is the electric charge. For 1:1 electrolytes, the equation is reformulated to:

$$\kappa^{-1} = \frac{0.304}{\sqrt{C}}$$

In this equation,  $C$  should be inserted in  $\text{mol.dm}^{-3}$  and the Debye length then comes out in nm. Accordingly, by increasing the electrolyte concentration, the double layer thickness decreases. For

instance, in the 0.01 mM NaCl solution, the double layer thickness is found to be around 100 nm, and in a 100 mM solution, it is roughly 1 nm (Figure 2.32). Therefore, the double layer thickness is determined by the salt concentration and indicates how extensive the double layer repulsion will be. When the surfaces get too close such that their electrostatic double layers overlap, a repulsion force will be produced, because the limited space between the surfaces does not allow complete potential decay for each double layer. The produced electrostatic repulsive potential energy is formulated in the following form [215, 220]:

$$W_R(D) = Ce^{-\kappa D}$$

Accordingly, the electrostatic potential energy exponentially decays with an increase in the distance, and becomes zero at large separations. The rate of the decay is determined by the double layer thickness, i.e., the larger the double layer thickness is the slower the decay will be and vice versa.[221-223] The parameter  $C$  is a constant that accounts for the geometry of the interacting surfaces and their surface charge density. In my AFM colloidal probe measurements, I typically used 10 mM NaCl solution (Debye length of around 3 nm) as the buffer, in order to screen the long-ranged electrostatic repulsions so the polymer-related interactions could be studied.

### 2.6.2. Van der Waals forces

Atoms and molecules can attract each other at relatively short distances due to the Van der Waals (VdW) forces, which has three components.[224-226] **First**, the attractive interaction between two molecules with permanent dipoles (dipole moment of  $\mu_i$ ), which for freely rotating dipoles provides an interaction energy (*Keesom orientation force*) of:

$$W(D) = -\frac{\mu_1^2 \mu_2^2}{3(4\pi\epsilon\epsilon_0)^2 kTD^6}$$

**Second**, a molecule with permanent dipole can induce a dipole to another molecule (with polarizability of  $\alpha_2$ ), which produces an attractive interaction potential (*Debye induction force*) of:

$$W(D) = -\frac{\mu_1^2 \alpha_2}{(4\pi\epsilon_0)^2 D^6}$$

**Third**, the dispersion (*London*) forces that exist between all atoms and molecules, even between the non-polar species. Displacement in the electron clouds of the atoms can produce an instantaneous dipole moment, which can thus affect the surrounding molecules through attractive or repulsive interaction potential, given by:

$$W(D) = -\frac{3\alpha_1\alpha_2}{2(4\pi\epsilon\epsilon_0)^2 D^6} \frac{h\nu_1\nu_2}{(\nu_1 + \nu_2)}$$

To account the VdW forces between two identical macroscopic bodies (1) interacting in a medium (3) such as water, the Lifshitz expression for the Hamaker constant needs to be considered:

$$A = \frac{3kT}{4} \left( \frac{\epsilon_1 - \epsilon_3}{\epsilon_1 + \epsilon_3} \right)^2 + \frac{3v_e(n_1^2 - n_3^2)^2}{16\sqrt{2}(n_1^2 + n_3^2)^{3/2}}$$

In this formula, the atomic structure is ignored and the large bodies are treated as continuous media; accordingly, the forces between the surfaces are derived in terms of the bulk properties as their dielectric constant  $\epsilon_i$  and refractive index  $n_i$ . [227, 228] By having the Hamaker constant between two surfaces in a medium one can calculate the VdW interaction force for different geometries, such as between a flat surface and a spherical particle, which can represent the AFM colloidal probe-flat surface geometry:

$$\frac{F_{VdW}}{R} = -\frac{A_{123}}{6D^2}$$

This equation is obtained by assuming that the particle radius is considerably larger than the separation distance between the surfaces. [220] I should emphasize that roughness of the surface or

presence of a polymer layer on the surface can significantly affect the VdW interactions between the substrates[229, 230], which is why in my results the contribution of VdW forces can be considered to be of minor importance.

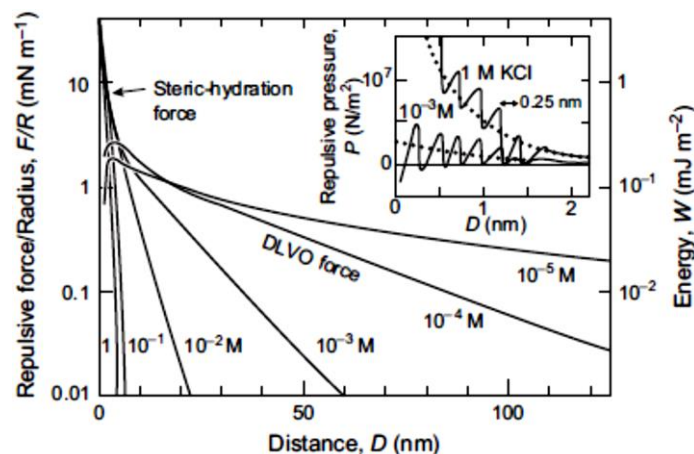


**Figure 2.33** Forces between mica surfaces in 1:1 salt solutions. The right-hand axis gives the theoretical interaction energy between two flat surfaces from the Derjaguin approximation. For low salt concentrations, the theoretical DLVO theory works, while at high concentrations an additional short-ranged hydration repulsion is produced due to the presence of adsorbed cations.[220]

### 2.6.3. Solvation (hydration) forces

The primitive form of the DLVO theory based on the repulsive double layer forces and the attractive Van der Waals forces cannot address all the existing interactions in systems that are more complex, e.g., polymer-covered surfaces. It has been demonstrated that when two surfaces approach closer than a few nanometers, the continuum theories of DLVO forces often fail to describe the net interactions.[231] This has led to the introduction of a new class of surface forces known as the non-DLVO interactions.

One of these interactions is the presence of a monotonically repulsive force at very short distances (typically  $< 5$  nm), which has been attributed to the hydration (solvation) forces (Figure 1.33).[232-234] This can occur for hydrophilic surfaces where polar or ionic head groups are effectively

hydrated, or when the hydrated counter ions are accumulated at the surface.[235-237] For instance, the repulsive hydration force between two silica surfaces in presence of different salts solutions indicated a ranking for the dehydration repulsion by cations  $Mg^{+2} > Ca^{+2} > Li^+ \sim Na^+ > K^+ > Cs^+$ , suggesting that the hydration capacity and number of the ions is a decisive factor in the observed solvation forces.[220] In both cases, when the surfaces are sufficiently close, the disjoining pressure corresponding to dehydration of the species is likely and thus a short-ranged repulsion is found.

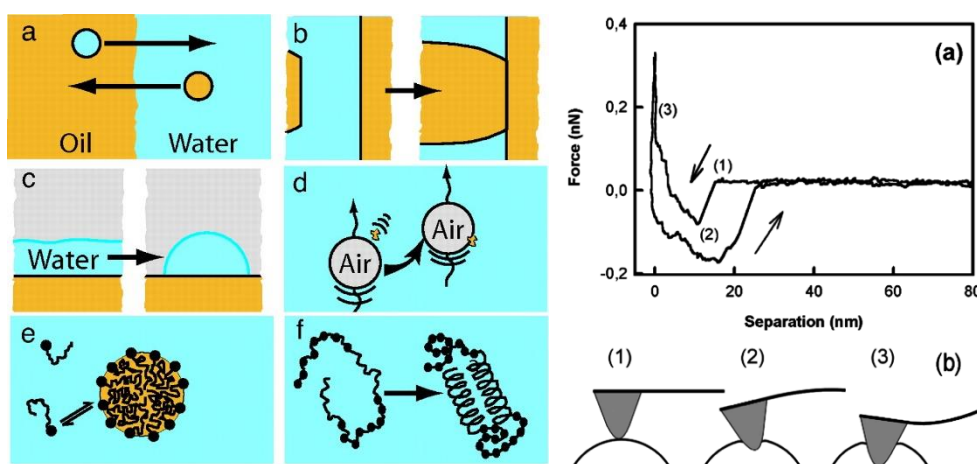


**Figure 2.34** (Left) Several systems that are driven by the hydrophobic interaction and the hydrophobic effect.[238] (a) Low solubility of nonpolar solutes in water and vice versa, (b) The strong attraction between solid hydrophobic surfaces, (c) Dewetting, (d) Bubble coalescence and adsorption of hydrophobic entities to the air/water interface, (e) Micellization, (f) Protein folding. (Right) Typical force curve in an area containing nanobubbles (a). The force curve represents the interaction between a single nanobubble and the AFM probe tip.[239]

#### 2.6.4. Interaction between hydrophobic surfaces in water

As explained before, the theory of *hydrophobic effect* has been postulated to address the behavior of non-polar solutes and molecular surfaces in water (such as low solubility of nonpolar solutes in water, micellization and proteins folding (Figure 2.34)), an effect that has been suggested to be of entropic origin.[240-242] The theory of *ice-berg* water structures was one of the initial attempts to explain this phenomenon[243, 244], while later the presence of a *hydrophobic bond* between

nonpolar molecules was also speculated.[245, 246] Such an effect has been considered as the source of the unusually strong attraction between nonpolar groups and surfaces in water, which is considerably larger than that of the classic *Lifshitz theory* of VdW interactions. One critical consideration regarding the hydrophobic effect is the fact that such attractions are due to not only the properties of the particles themselves, but also the suspending aqueous medium.

During recent years, there has been an extensive research on direct measurement of forces between macroscopic hydrophobic surfaces using various techniques such as AFM [247-251]; however, there is no single theory that can elucidate all the experimental results and a deep understanding of the exact origins is still missing. One of the intriguing observations is the long range of the attractive interactions between the macroscopic surfaces, which can go up to hundreds of nanometers. In this case, it should be considered that although a depletion layer of water molecules exists at the hydrophobic surfaces, the thickness of this layer is expected to be in the range of one or two water molecules, which can only justify the short-ranged attractions. Accordingly, several speculations have been proposed to illustrate the extremely long-ranged attractions, e.g., coalescence of the nanobubbles existing on the hydrophobic surfaces.[252-254]

### **2.6.5. Polymer-mediated forces**

In section 2.3, I discussed the mechanisms through which the polymer chains can adsorb or anchored to the surfaces in aqueous solution. Presence of an adsorbed or grafted polymer layer at solid surfaces can give rise to either repulsive or attractive interactions between the surfaces, which again cannot be elucidated based on the DLVO theory.[255, 256] For a specific type of polymer, there are various factors such as the molecular weight of the polymer, the thickness of the layer, grafting density (or the amount of adsorbed polymer), conformation of the polymer chains, solvent

quality, segment-surface affinity, etc., that can considerably contribute to these interactions (Figure 2.34).[257-261]

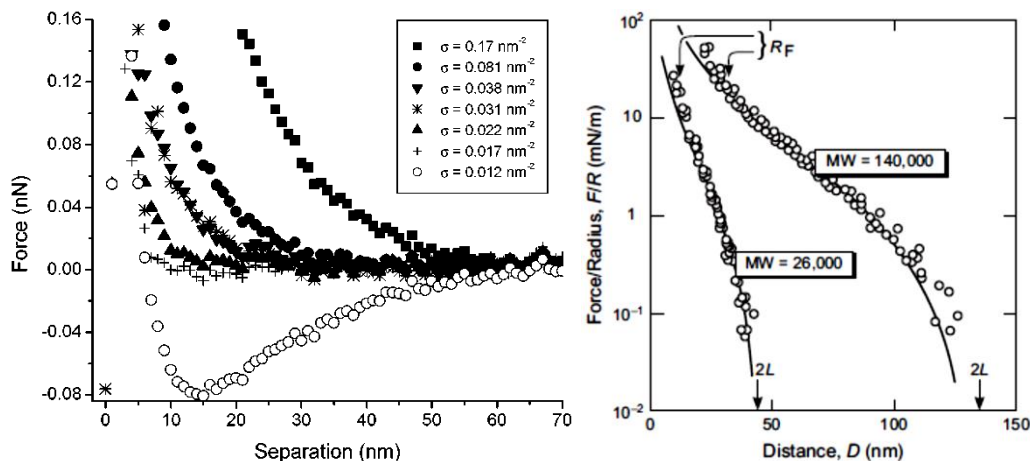


**Figure 2.34** Steric repulsive forces between polymer-covered surfaces. (Left) Effect of grafting density on the repulsive steric force of a polymer.[259] (Right) Effect of polymer molecular weight on the steric repulsion.[220]

One possible interaction is the repulsive *steric* or *overlap* forces between the polymer-covered surfaces. Consider two flat surfaces each covered with a polymer layer with a uniform thickness of  $\delta$ . When the surfaces get close in a way that the separation distance ( $h$ ) becomes smaller than  $2\delta$ , the local segment density in the interaction region enhances. Considering that the polymer chains are effectively hydrated, such an increment in the local segment density produces a strong repulsion, resulting from two factors.[262-265] First, the overlap of the chains (higher local segment density) increases the osmotic pressure within the layers due to the unfavorable mixing of the polymer chains under the good solvent condition. Second, compression of the polymer chains indeed reduces the configuration entropy and number of possible conformations of the chains, due to the restriction in the available volume for the chains. The former is then related to the free energy of mixing of the polymers, while the latter refers to the entropic or elastic free energy of the polymer chains.

With respect to the first contribution, I refer to the section 2.1.2, in which I discussed the free energy of mixing of polymers. As I explained in more details there, the free energy of mixing depends on the solvent quality or in other words the polymer-solvent Flory Huggins interaction parameter. In simple terms, if the polymer-polymer interaction is stronger than polymer-solvent (bad solvent condition); the free energy contribution is negative. On the other hand, if the polymer-solvent interaction is stronger than polymer-polymer (good solvent condition) the free energy contribution is positive. Therefore, depending on the solvent quality, the free energy contribution to the steric forces can be either attractive or repulsive. I observed this effect in some of my AFM measurements on PNIPAM-covered surfaces below and above the phase separation temperature (Paper IV). Unlike the mixing term, the entropic contribution always produces a repulsive force due to the unfavorable restriction in polymer configurational entropy by compression, even under bad solvent condition.

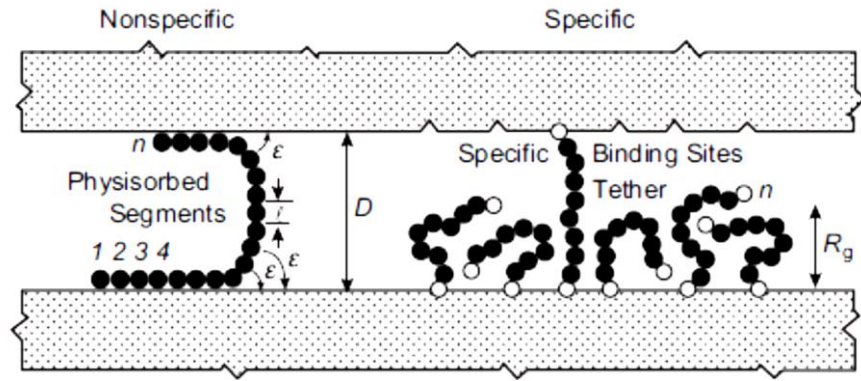


**Figure 2.35** Polymer-substrate bridging.[220] (Left) Non-specific segmental adsorption to the opposite surface. (Right) Specific binding to the opposite surface.

Besides the steric force, one can also observe attractive polymer-mediated forces between polymer-coated surfaces, known as *bridging forces*. [266-268] It can originate from attractive interactions between the polymer chains from one surface, with the chains on the other surface. In addition,



polymer chains can also bridge to the opposite bare surface, on condition of having strong segment-surface affinity and relatively low surface coverage (Figure 2.35).

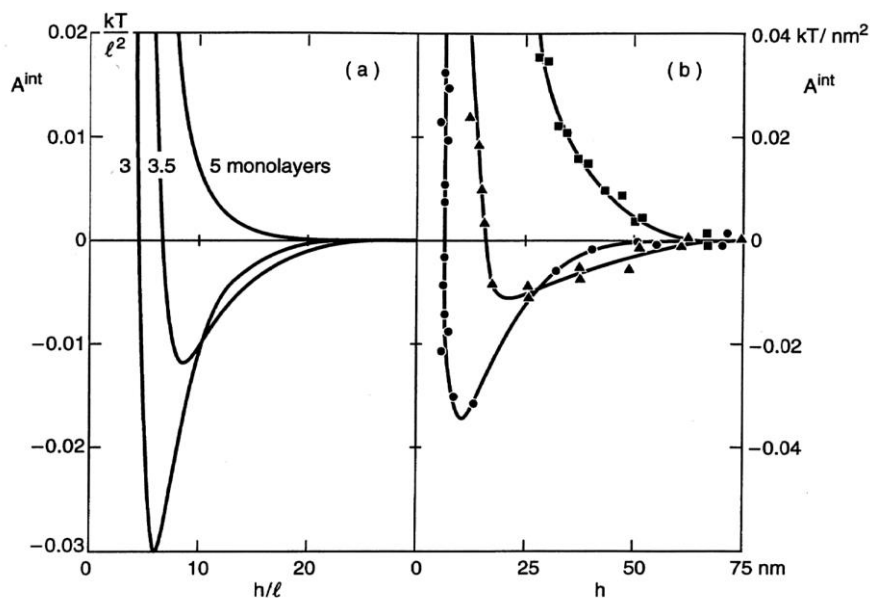
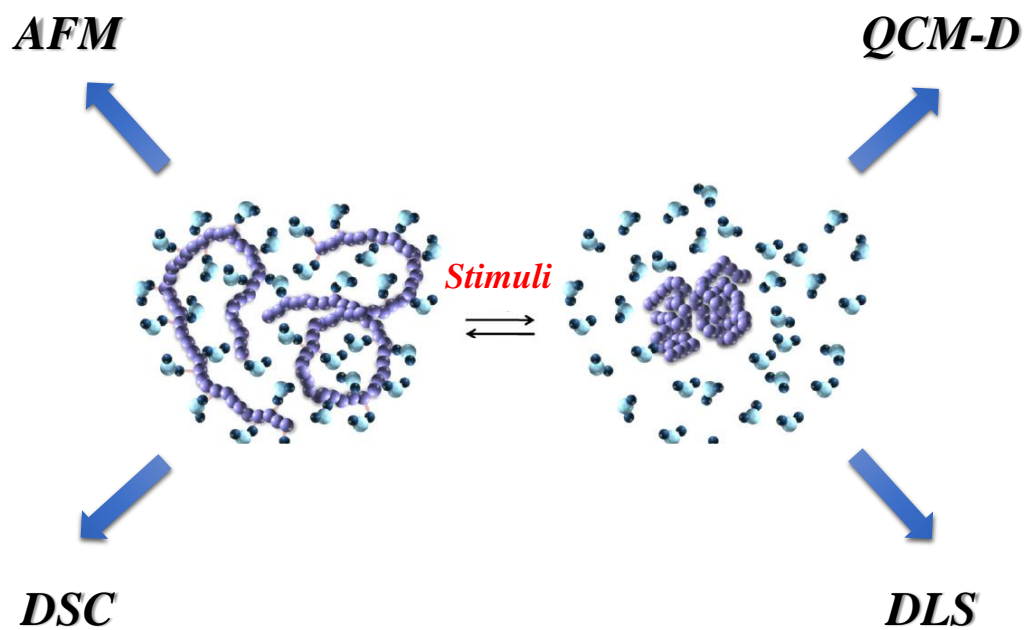


**Figure 2.36** (a) Theoretical and (b) experimental force-distance curves between two flat substrates covered with different amounts of polymer under  $\Theta$ -solvent condition.[64] At relatively low surface coverage, the bridging dominates. By increasing the surface coverage, the repulsive steric forces dominate.

The polymer-polymer bridging is possible under the bad solvent condition where polymer-polymer interactions are more favorable than polymer-solvent interactions. The attractive interactions can be due to VdW or solvent-mediated forces, or can be more specific interactions such as hydrogen bonding between the polymer chains, e.g. in case of PNIPAM. The polymer-substrate bridging depends on various parameters such as solvent quality, layer thickness and conformation, surface coverage by the polymer chains, and segmental affinity for the surface.[257-259] The polymer-substrate can also be non-specific physical interactions (observed between PNIPAM and gold in my AFM measurements) or specific binding interactions, e.g., if the polymer bears a specific end group such as thiol that can bound to the opposite surface.[269] The combination of steric repulsions and attractive bridging can be attractive or repulsive depending on several parameters such as the

polymer surface coverage. This can be seen from Figure 2.36 in which the effect of surface coverage on the force-distance profile between polymer-coated surfaces is depicted. At relatively low surface coverages, the overall interaction close to the surface is attractive (bridging dominates); while by increasing the surface coverage the overall interaction becomes purely repulsive (steric forces dominate).

### 3. METHODS



In this section, the experimental methods that were employed during my PhD studies are described in details. Each method is briefly introduced in terms of its fundamentals, and then the typical experimental procedure of the measurements and analysis of the data are explained. Regarding the chemicals that were used for the projects, I would like to refer you to the attached papers, in which the characteristics of all the supplied polymers are provided. The employed experimental methods can be divided into two categories: (i) characterization of the properties of polymers in bulk solution state, i.e., differential scanning calorimetry and dynamic light scattering, (ii) characterization of the polymer properties at a solid/aqueous interface, i.e., quartz crystal microbalance with dissipation monitoring and atomic force microscopy.

### **3.1. Differential scanning calorimetry (DSC)**

Often as the first experiment, I performed DSC measurements on the polymer solution samples. It can provide the accurate phase separation temperature of the polymer solutions. This information is of great importance, since the phase separation temperature of the polymer was the basic information required for all the conducted projects. In some studies (papers I-III), the effect of different salts of various concentrations was assessed on the stability of the polymers, while for the other studies (papers IV and V) the polymer properties were investigated at temperatures below and above the collapse temperature.

In addition to the phase separation temperature, DSC can provide information on thermodynamics of the phase transition, i.e., the enthalpy change of transition, the entropy change of transition, and the change in the heat capacity upon transition.[270, 271] Based on the discussions I provided in the background section, such thermodynamic data can be attributed to the energy change upon dehydration of the polymer; accordingly, could be helpful in case of understanding the underlying mechanisms of the phase transition.

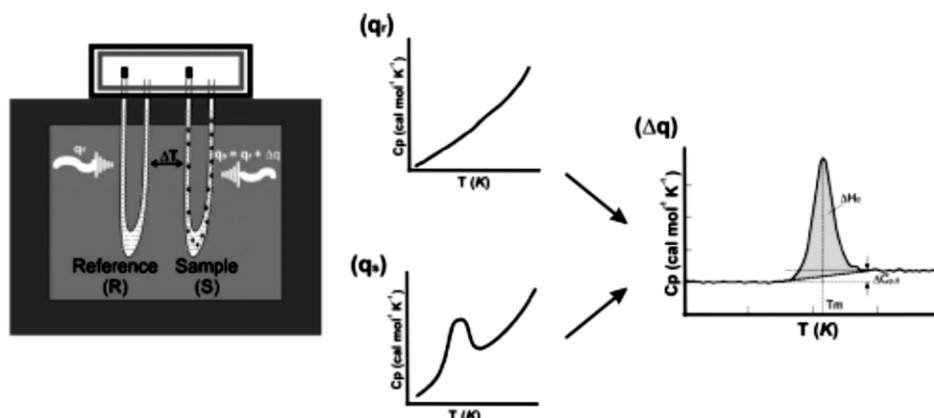


**Figure 3.1** Typical DSC setup. The instrument consists of two parallel U-shaped cells, one for the reference (buffer) solution, and the other for the sample (polymer) solution. The temperature of both cells is increased with a specific heating rate. Any exothermic or endothermic phenomenon that occurs in the sample cell will be compensated with an equal amount of heat so the temperatures of the cells remain identical.[270]

Briefly about the technique, DCS is a thermoanalytical method that measures the amount of the heat required to increase the temperature of a sample and a reference cell as a function of temperature (Figure 3.1).[270] The instrument consists of two U-shaped cells for the reference and the sample solutions. For my measurements, the reference (buffer) was the solution without the polymer, which could be pure water or saline solutions. The sample solution was the buffer plus the dissolved polymer. After loading the buffer and polymer solutions in their corresponding cells and instrumental thermal stabilization, the temperature of the cells is increased with a constant heating rate ( $^{\circ}\text{C}/\text{min}$ ). As long as no thermal phenomenon occurs in the sample solution, a stable baseline is recorded by the instrument, which means that both the solutions require constant amounts of heat to increase their temperatures. When a thermal phenomenon such as polymer phase separation occurs in the sample solution, the amount of heat required to increase the temperature of the sample cell (with the same heating rate) changes. If the phase transition absorbs heat, the instrument heater will transfer the same amount of heat to the sample cell and vice versa; so the temperatures of the

reference and sample cells remain identical. The additional exchanged heat with the sample cell is then recorded as a function of temperature, which produces the DSC thermogram.

The appeared peak in the thermogram represents the phase separation of polymer solution and thermodynamic data of the process can be extracted from it (Figure 3.2). The temperature of the peak maxima (point 3 on the figure) can be considered as the phase separation temperature of polymer. However, the more accurate phase separation temperature can be the onset of the peak (point 2), i.e., the temperature at which the peak appears. The area under the peak (region 4) corresponds to the total additional heat exchanged with the sample cell, which after normalization to the amount of the polymer in solution (in gram or mole) provides the enthalpy change associated with the phase separation ( $\Delta H$ ). Considering that at the phase separation point,  $\Delta G$  of transition equals to zero, then the entropy change of the phase separation can be obtained from  $\Delta S = -\Delta H/T$ . The change in the heat capacity ( $\Delta C_p$ ) can also provide additional information on changes in the solvent-accessible surface area of the polymer.

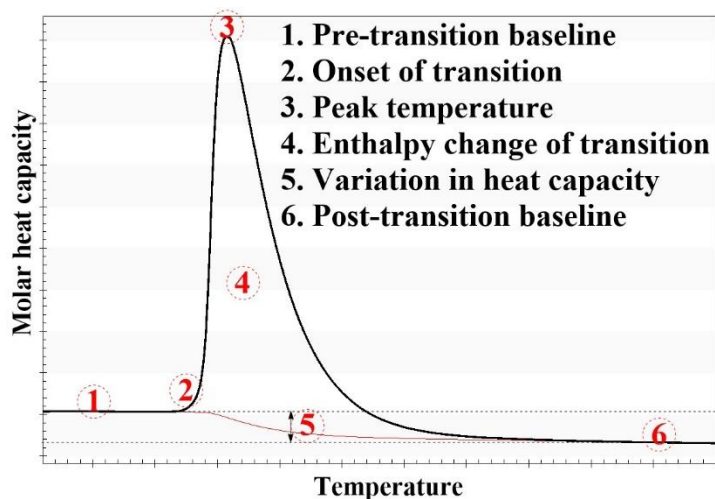


**Figure 3.2** Typical DSC thermogram of a polymer solution. The pre-transition baseline refers to the temperatures at which the polymer is fully soluble in water. The peak area corresponds to the temperature range at which the phase separation occurs. The post-transition baseline indicates the temperatures where the phase separation is terminated.

As mentioned, to be able to calculate the enthalpy change of transition, the raw heat data must be normalized to the amount of the polymer in the sample cell, to obtain the molar heat capacity data (MHC) that can be used for analysis and comparison[272]:

$$c_p \left( \frac{kJ}{mol.K} \right) = C_p \left( \frac{kJ}{K} \right) \times \frac{M_{polymer}}{V_{cell} \times w_{polymer} \times \rho_{solution}}$$

In this equation,  $c_p$  is the molar heat capacity,  $C_p$  is the raw measured heat data,  $M_{polymer}$  is the molecular weight of the polymer,  $V_{cell}$  is the volume of the instrument sample cell,  $w_{polymer}$  is the weight concentration of polymer in solution, and  $\rho_{solution}$  is the density of the solution. After converting the raw data to the molar heat capacity values, the area under the peak can be integrated, using a first order fitting for pre- and post-transition baselines.

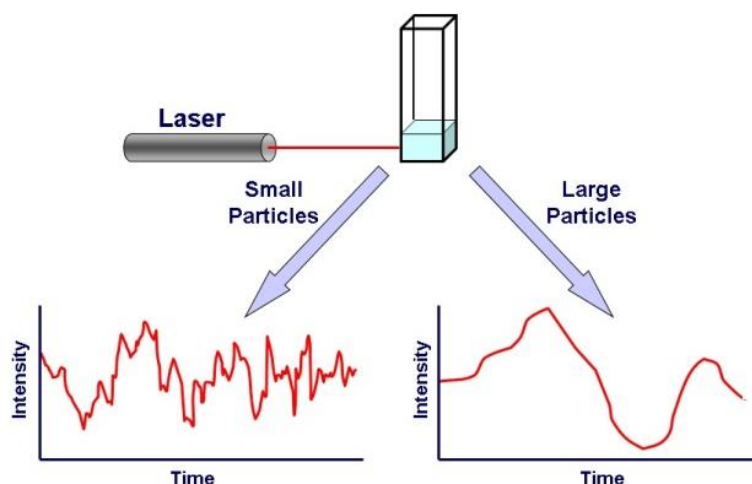


**Figure 3.3** Schematic illustration of DSL. As shown, the laser beam is scattered from the particles in the solution, while the Brownian motion of the entities gives rise to time-dependent fluctuations in the scattered light intensity.

## 3.2. Dynamic light scattering (DLS)

For some projects (papers IV and V), I conducted DLS measurements to provide information on the hydrodynamic diameter ( $D_h$ ) distribution of the polymers in solution. By doing the measurements at various temperatures, it was also possible to study the polymer solution in terms of the aggregation

temperature and to assess the aggregation type, i.e., macroscopic phase separation, micellization, or formation of mesoglobules.

In a dilute polymer solution (below the overlapping concentration) where inter-chain interactions are negligible, the individual polymer coils can be considered to have random Brownian motions, which originates from the strikes from the water molecules and the thermal energy of polymer chains. These motions give rise to randomness in the phase of the scattered beam from a spatially limited volume of the solution, which causes time-dependent fluctuations in the scattered light (Figure 3.3). This time-dependence in the scattering intensity is recorded, which can be related to the diffusion constant of the polymer coils and then using the Stokes-Einstein equation can provide the hydrodynamic size distribution.[273] The fluctuation are assessed using the second order correlation function, as follows:

$$g^{(2)}(\tau) = \frac{\langle I(t)I(t + \tau) \rangle}{\langle I(t) \rangle^2}$$

Where  $I(t)$  is the scattering intensity at the time  $t$  and  $\tau$  is the delay time. The obtained correlation data (also known as the *correlogram*) can be analyzed through different methods and algorithms, to obtain the diffusion coefficient and size distribution profile. For a mono-dispersed sample, the *Cumulants* approach, which is based on the moment analysis of the linear form of the correlogram, can be employed to calculate the mean or *Z-average* size and the *polydispersity index (PdI)*. In brief, the first cumulant is used to calculate the intensity weighted Z-average mean size, which is related to the initial slope of the linear form of the correlation function. The second moment provides the PdI value, which is related to the inflection point at which the correlogram (in semi-log scale) deviates from linearity. The Cumulants analysis considers merely the initial (i.e., small delay time values) parts of the correlation function to stabilize the analysis and fitting, because using more data points will produce fitting errors.



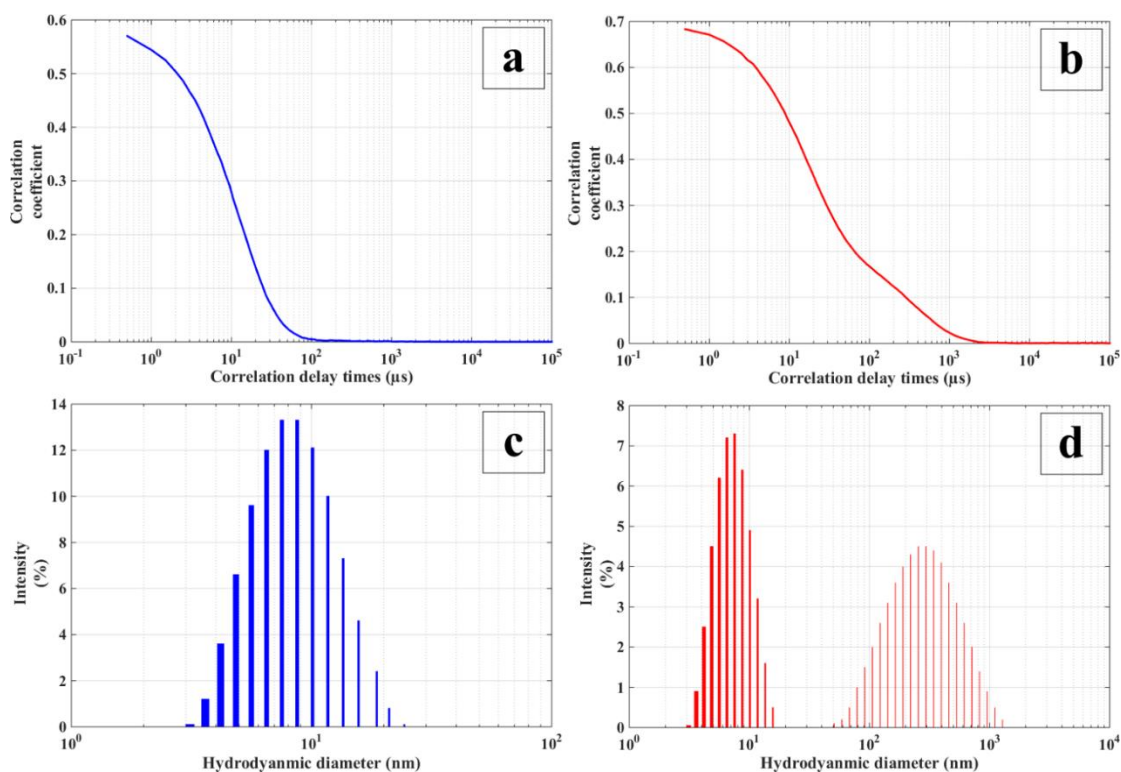


**Figure 3.4** Typical DLS data of two copolymer solutions used in my studies; (Left) A monodispersed size distribution where the Cumulants fit can provide reliable data, (Right) a bimodal size distribution that is not suitable for the Cumulants fit, and distribution fit can be used to assess the size distribution of different entities in the solution. For instance, having single polymer chains and intermicellar complexes together in the solution.

Accordingly, for polydisperse samples, the Cumulants analysis can be rather misleading as only a limited portion of the correlation data is analyzed and a single average size is reported for a multimodal size distribution. Under such condition, the *CONTIN* algorithm can be used to extract a more accurate data, and model the correlation data as an intensity contribution for each of a number of size bands. These intensities will be represented in the displayed size distribution as peaks, each with a characteristic width. As a note, I should emphasize that for a hydrated polymer coil the measured hydrodynamic radius is larger than the radius of gyration of the polymer.[274] Nevertheless, it can provide an approximate information about the polymer size in solution and its aggregation behavior, which was useful for my studies.

### 3.3. Quartz crystal microbalance with dissipation monitoring (QCM-D)

I conducted QCM-D measurements (paper IV and V) in order to investigate the adsorption/grafting of polymers to the solid/aqueous interfaces (gold/aqueous and silica/aqueous), as well as assessing the changes in hydration state and conformation of the prepared polymer layers.

A QCM-D sensor chip consists of a thin quartz disc, which is sandwiched between a pair of electrodes. By applying an alternating voltage, the sensor is excited to oscillate at its fundamental resonance frequency. The resonance frequency ( $f$ ) inversely depends on the total oscillating mass of the sensor and the adhering layers on the sensor surface, which herein includes the adsorbed polymer chains plus their water content. In the salt solutions, the ions adsorbed or trapped within the polymer layer as well as the ions adsorbed to the sensor surface can contribute to the resonance frequency value. Accordingly, adsorption of any species such as polymer chains to the sensor surface is accompanied with a negative shift in the frequency.

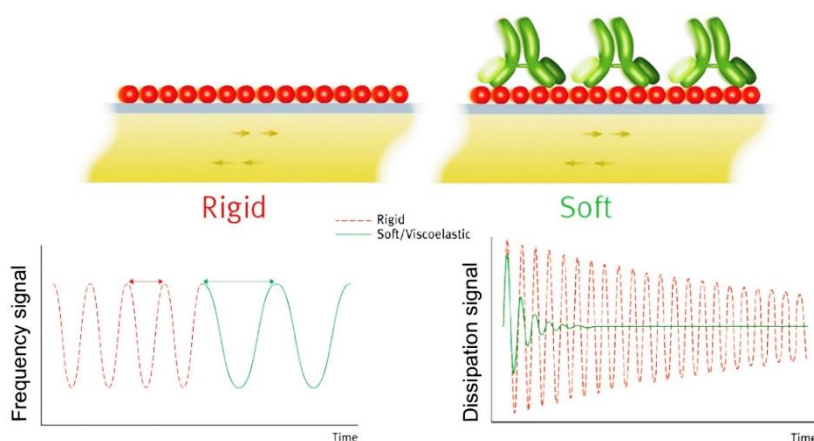


**Figure 3.5** QCM-D response in presence of a rigid and soft adhered layer.

On condition that the adsorbed film is thin and rigid, the decrement in the frequency is linearly proportional to the amount of the added mass to the sensor. Assuming the layer to be of a uniform thickness and density, the calculated layer mass can be converted into layer thickness by having the

density of the layer. The mass of a rigid adhering layer is calculated using the Sauerbrey relation[275]:

$$\Delta m = -C \frac{\Delta f}{n}$$

Where  $C$  is a proportional constant that depends on fundamental frequency, thickness and density of the quartz crystal ( $17.7 \text{ ng.Hz}^{-1}.\text{cm}^{-2}$  for a 5 MHz quartz crystal) and  $n$  (1, 3, 5, 7, 9, 11, 13) is the overtone number. Nevertheless, in most cases including adsorbed/grafted polymer layers, the Sauerbrey relation is not valid. As mentioned, the Sauerbrey estimation assumes that the added mass is small compared to the crystal mass, rigidly adsorbed with no slip or deformation during the oscillation and evenly distributed.

During a QCM-D measurement, the drive generator output repeatedly ceases and the subsequent decay of the sensor oscillation is also monitored. Accordingly, the dissipation (damping) factor ( $D$ ) is calculated as the energy dissipated per oscillation divided by the total energy stored in the system:

$$D = \frac{E_{lost}}{2\pi E_{stored}}$$

Herein,  $E_{lost}$  is the dissipated energy during one oscillation cycle, and  $E_{stored}$  is the total energy stored in the oscillator. A rigid adhered layer follows the oscillation with no significant deformation and thus has a small damping factor. On the other hand, a soft adhered film is deformed during the oscillation; hence, gives rise to a high dissipation value. Therefore, for polymer layers, the dissipation value can provide semi-quantitative structural and conformational information about the swelling and collapse of the polymer film. The Sauerbrey estimation can be employed when there are no significant dissipation shifts ( $\Delta D < 1$ ) and the frequency shifts do not spread between the harmonics, or in other words, the frequency curves are not overtone-dependent.

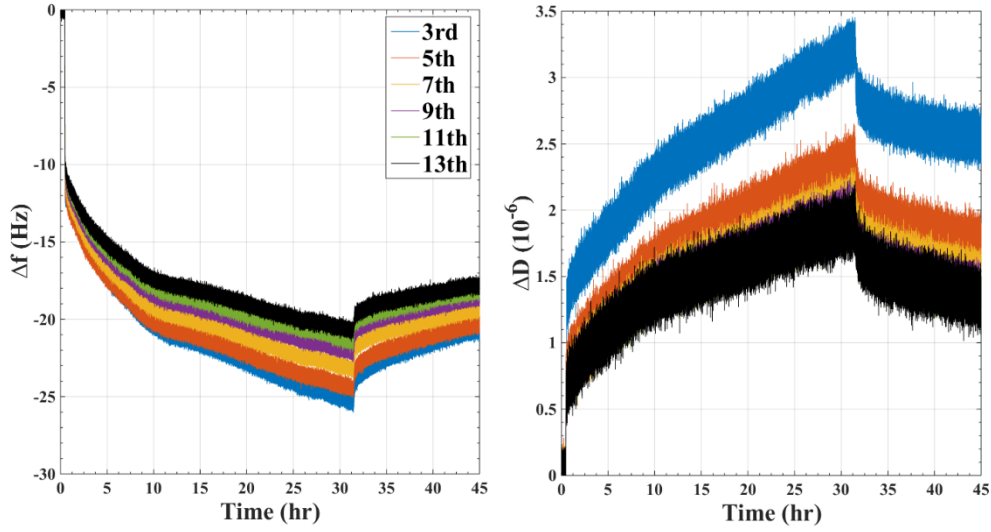


**Figure 3.6** Typical adsorption curve of a polymer on the QCM-D sensor. (Left) Frequency shifts. (Right) Dissipation shifts. The negative frequency shift corresponds to attaching the hydrated polymer chains to the sensor surface. The clear overtone-dependence of the frequency shift curves suggests viscoelasticity of the adsorbed layer. The positive dissipation shift suggests formation of a dissipative layer on the sensor that can damp the sensor decaying oscillation.

For a soft and viscoelastic polymer layer the Sauerbrey relation will underestimate the mass at the surface. This is the case when the adsorption curves indicate significant dissipation shifts ( $\Delta D > 1$ ) and well-separated frequency shifts for the different harmonics (overtone-dependence). This provides the opportunity to consider different fundamental frequencies and overtone numbers, which can render additional information about the layer viscoelasticity and thickness, by applying a viscoelastic model, e.g. the Voigt model, in order to approximate properties of the film.[276, 277] In the viscoelastic Voigt modeling, the adhered film is represented by a layer of homogenous thickness and density, with elastic and viscous components. The frequency and dissipation shifts for such a layer can be calculated from the imaginary and real parts of the  $\beta$  function:

$$\Delta f = \frac{Im(\beta)}{2\pi t\rho}$$

$$\Delta D = \frac{Re(\beta)}{\pi f t\rho}$$

Where  $t$  and  $\rho$  are thickness and density of the quartz crystal, respectively. The  $\beta$  function represents shear viscosity  $\eta$  and shear elasticity  $\mu$  of the adhered layer, which in the case of a single viscoelastic film (1) covered with a Newtonian liquid (2) can be obtained from the following equation:

$$\beta = \frac{\xi_1 \omega \eta_1 - i \mu_1}{\omega} \frac{1 - \alpha^2 \xi_1 h_1}{1 + \alpha^2 \xi_1 h_1}$$

$$\omega = 2\pi f$$

$$\alpha = \frac{\frac{\xi_1 \omega \eta_1 - i \mu_1}{\xi_2 \omega \eta_2} + 1}{\frac{\xi_1 \omega \eta_1 - i \mu_1}{\xi_2 \omega \eta_2} - 1}$$

$$\xi_1 = \sqrt{-\frac{\omega^2 \rho_1}{\mu_1 + i \omega \eta_1}}$$

$$\xi_2 = \sqrt{i \frac{\omega \rho_2}{\eta_2}}$$

By fitting the Voigt model to the measured  $\Delta f$  and  $\Delta D$  data of different overtones, one can estimate the density ( $\rho_1$ ), thickness ( $h_1$ ), shear viscosity ( $\eta_1$ ) and shear elasticity ( $\mu_1$ ) of the adhered layer. The film viscosity and density cannot be obtained together; hence, usually the density of the polymer layer is independently determined or assumed.

In my studies, I used the instrument software for viscoelastic Voigt modeling of the data. It provides two solutions from the fitting, where one would be a thin and rigid layer, and the other is a thicker and soft layer. One of the solutions usually has a much better fit quality than the other has and is therefore used. Density and viscosity of the solvent together with the density of hydrated polymer layer are required for fitting, which can be estimated from the values in the literature.

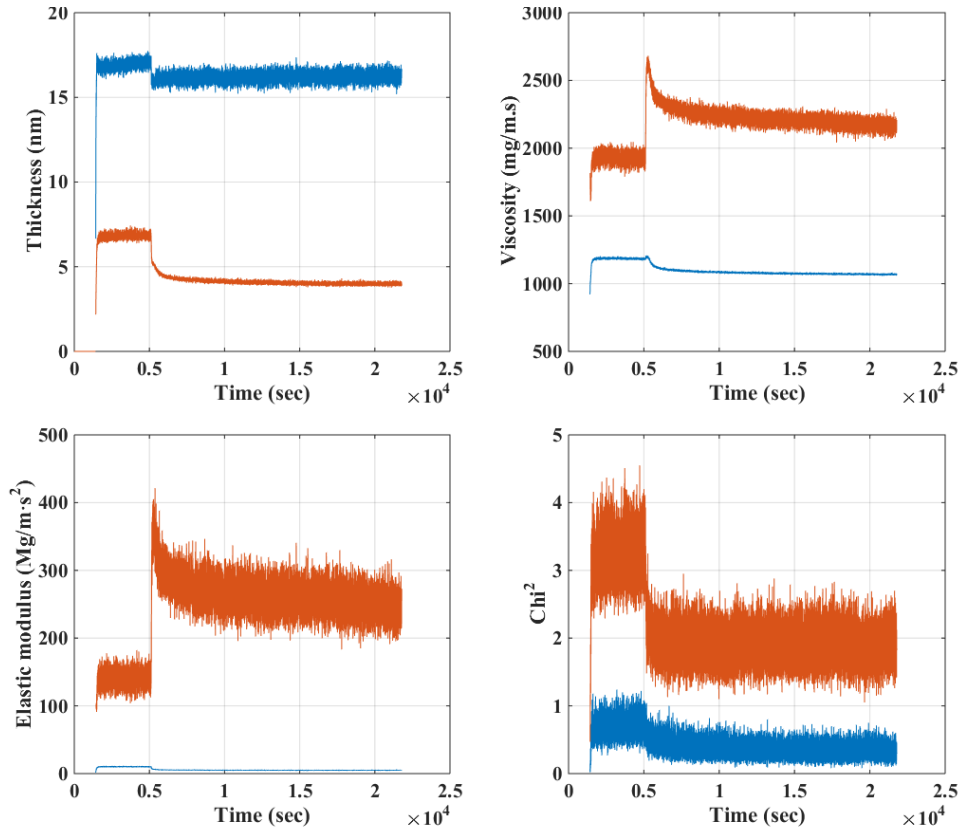


**Figure 3.7** Typical viscoelastic Voigt modeling of the QCM-D data of a polymer layer by the instrument software.

### 3.4. Atomic force microscopy (AFM)

AFM is a member of the *scanning probe microscopes* that is working based on the interaction between the sample surface and a so-called *probe*.<sup>[278]</sup> It constitutes of a cantilever with a probe, a piezoelectric scanner, a laser beam, and a photodiode detector. The piezoelectric scanner provides the ability to scan over the sample surface in three directions at sub-nanometer scale. The tip that is mounted to the cantilever is thus scanned over the sample surface, and the forces between the tip and the sample are measured by detecting the deflection of the cantilever, and can be used to obtain topographical images. The resolution of the imaging is determined by the tip geometry and size. The local attractive or repulsive interactions between the sample surface and the tip give rise to bending of the cantilever. To monitor the deflection of the cantilever, a laser beam is employed that

is reflected from the backside of the cantilever onto a detector. When the cantilever is bent, the angle of the reflected laser beam changes and the laser spot falls on a new spot of the quadrant photodetector, which can be converted into the vertical and lateral deflection of the cantilever (Figure 3.8). The cantilever itself can be considered as a spring, meaning that deflection of the cantilever can be converted into force by knowing the accurate spring constant of the cantilever. Depending on the type of measurement, various cantilevers with different tip shapes and spring constants can be used.

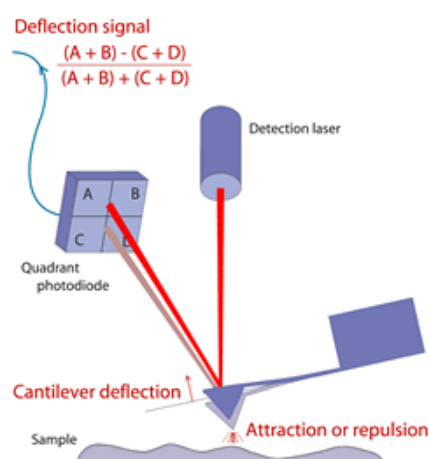


**Figure 3.8** Schematic illustration of AFM

The most basic mode of operation of AFM is the *contact mode*, where the cantilever is deflected on the surface. During contact imaging, the deflection or in other words the amount of applied force is kept at a constant setpoint, through adjusting the z-position of the piezo element controlled by a PI controller. However, for some cases such as molecular layers and polymer films, this mode can be quite vigorous and can change or even destroy the structure. Alternatively, the *tapping mode* imaging is employed, where the cantilever is forced to oscillate vertically near its resonance frequency. When the sample-tip distance decreases the frequency and amplitude of the oscillation changes, thus the piezo withdraws the tip from the surface, and vice versa.

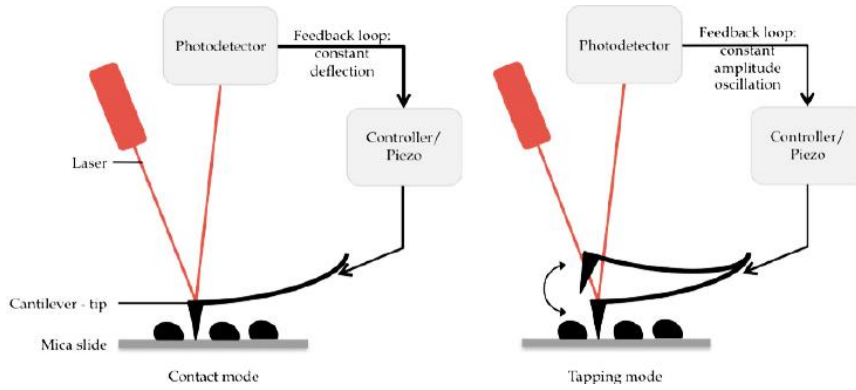


**Figure 3.9** Contact and tapping modes.[279]

Besides imaging the surfaces, AFM can be used as an accurate tool to measure the interactions between surfaces of different chemistries and structures.[280] In the initial studies, the forces between the AFM tip and flat substrates were measured.[281, 282] Nevertheless, since the exact shape and size of the AFM tip was unknown, quantitative comparison of such measurements and the obtained force profiles with theories such as DLVO was not possible. Later, Ducker and coworkers[283] solved this problem by attaching a spherical silica particle to the end of the cantilever, then measuring the forces between the silica particle and a flat silica surface. Accordingly, the measured forces can be compared with the theoretical data. Furthermore, the measured forces between a micron-sized particle and substrate are considerably larger than between the nano-meter sized AFM tip and substrate, which can make the measurements more accurate. In addition, this technique can be used to attach particles of different chemistries, as well as preparing polymer-covered particles and measure the interactions between the polymer layers.

### 3.4.1. Determination of the cantilever spring constant

In the AFM measurements, the forces are simply calculated using the Hooke's law:

$$F = -kz$$



Where  $F$  is the force,  $z$  is the deflection of the cantilever, and  $k$  is the cantilever spring constant. The purchased cantilevers often render approximate spring constant (which is enough for AFM imaging); nevertheless, for accurate colloidal probe measurements, these numbers are not precise enough. The width, length, thickness, back-coating thickness and material, etc., differ from one cantilever to another, which indeed can significantly affect the spring constant value. Therefore, it is required to calibrate the cantilever's spring constant prior to performing the force measurements. Several methods have been proposed to calculate the spring constant of the cantilevers.[284] Herein, I used the *thermal noise* method suggested by Sader and coworkers[285, 286], which calculates the spring constant from the resonance frequency of the unloaded cantilever. To do so, the accurate length and width of the cantilever are required, as well as the medium properties (air) such as density. For a tipless rectangular cantilever, the spring constant is given by:

$$k = 0.1906\rho_f b^2 L Q_f \Gamma_i(\omega_f) \omega_f^2, \quad \frac{L}{b} > 5$$

Where  $\omega$  is the fundamental resonance frequency,  $b$  is the width,  $L$  is the length,  $\rho$  is the density of the fluid (air),  $Q_f$  is the quality factor, and  $\Gamma_i$  is the imaginary component of the hydrodynamic function. Accordingly, the first step is to obtain the precise plan view dimensions of the cantilever, using an optical microscope. After that, the resonance frequency and quality factor of the cantilever is measured in air at room temperature using the AFM instrument and analyzed by the software.

### 3.4.2. Attaching the particle to the AFM cantilever

To prepare the colloidal probe, one requires a sharp wire for handling the glue and the particle, an optical microscope, a micromanipulator, and a water-resistant epoxy glue. Using the wire, a small amount of the glue is first put on the tipless cantilever end, and then a particle is put right on the glue. For the first step, the tungsten wire is etched by immersing one end of it in a 1 M KOH

solution, and applying a voltage of around 30 Volts between the wire and the electrode placed in the solution.

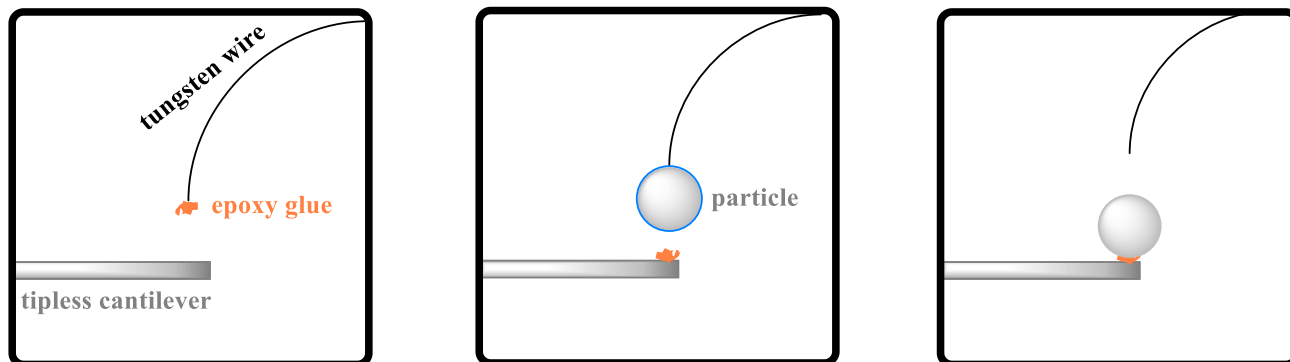


**Figure 3.10** Schematic illustration of colloidal probe preparation

The etching is continued until the end of the wire has a relatively smaller size than the particles diameter. Then the wire is washed, dried, and then mounted on the micromanipulator. A small amount of the two-component epoxy adhesive is prepared on the glass slide. Using the micromanipulator, the end of the wire is dipped in the glue to pick up a small amount of glue. The amount of glue can be controlled to some extent. For instance, if too much glue is picked up, one can decrease the amount of glue by touching the glass slide for a few times until a tiny amount of glue is remained on the wire. The wire is then moved on the cantilever and the glue is placed on the very end of the cantilever. It should be considered that a very small amount of glue is enough for attaching a micron-sized particle (excess glue can make serious problems such a coverage of the particle with glue). The next step is to place the particle on the glue before it hardens, so this step must be performed rather quickly. Using a new sharpened tungsten wire, a single particle is picked up from the particles on a glass slide. There is always a thin water layer on the surfaces under ambient condition, which can cause capillary attractive forces and adhesion between the wire and the particle, which is enough for handling the particle. The particle is then maneuvered over the cantilever, and placed exactly on the glue, and in the center of the cantilever. The fabricated

colloidal probe should be kept for around one day (depending on the glue) in room temperature to let the glue cure and set.

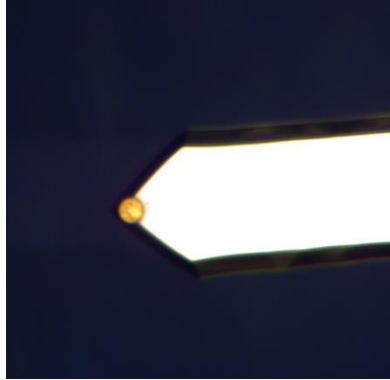


**Figure 3.11** 7  $\mu\text{m}$  silica particle attached to the tipless cantilever using the described method.

### 3.4.3. Force measurements

The prepared colloidal probe can be used for performing the AFM force measurements. During AFM force measurements, the tip (colloidal probe) is repeatedly brought into contact with the flat substrate (approach step), and separated again (retract step), while the piezo element moves only in the Z-direction. Forces between the probe and the substrate will cause the cantilever to deflect, which is monitored and then plotted as cantilever deflection vs piezo movement (Figure 3.12).

As seen, at large separation distances where there is no interaction between the probe and the substrate, a stable baseline corresponding to zero force is found. Close to the surface, the attractive or repulsive interactions between the probe and the substrate give rise to a downward or upward bending of the cantilever. When the surfaces come into contact (no indentation), the probe movement complies with the movement of the piezo. This renders a linear region, known as the *constant compliance* region or the *hard wall compression*. When retracting the probe from the surface, usually an adhesion between the surfaces is found. Finally, after separation of the surfaces, the piezo is moved to the initial separation distance where no interaction exist between the surfaces.

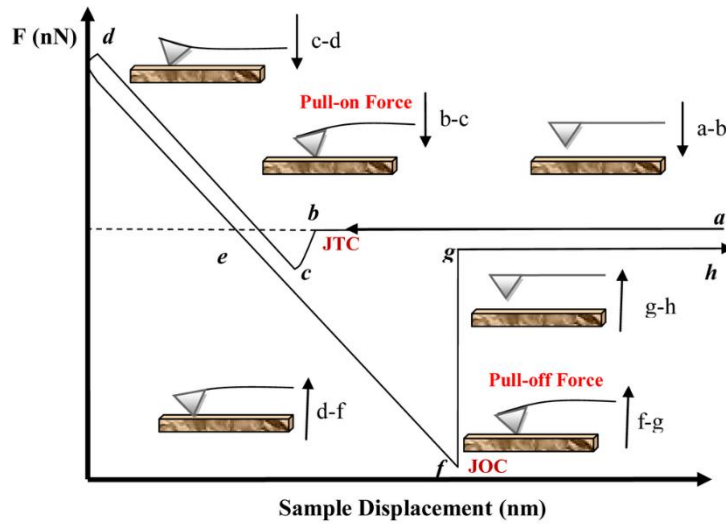


**Figure 3.12** Typical AFM force-distance profile.[287] (a-b) at far separation distance where no interaction between the probe and surface is found. (b-c) close to the surface, an attractive interaction causes *jump-in*. (c-d) the cantilever is pressed on the surface. (d-f) the cantilever is retracted from the surface. (f-g) the tip leaves the surface. (g-h) far separations where no interaction is found. This procedure provides the force-distance profile at one point of surface. To obtain statistically reliable data, the force measurements are performed on various points over a surface area.

#### 3.4.4. Construction of force vs distance curves

The deflection vs piezo movement graph should be converted into the force vs distance curve, in which the force in Newton is plotted as a function of actual separation distance between the probe and the substrate. This is done through multiple consecutive steps. First, by using the calculated cantilever spring constant (using the thermal noise method), the deflection in mV is converted into force in Newton. Next, the separation distance baseline at which no force is found between the surfaces should be shifted to zero force value. Afterwards, the point of zero separation should be found from the constant compliance region. The onset of the hard wall compression is considered as the zero separation distance. This can be a tricky step specifically in case of having a soft polymer layer on the surface, where there is always a finite distance between the surfaces.

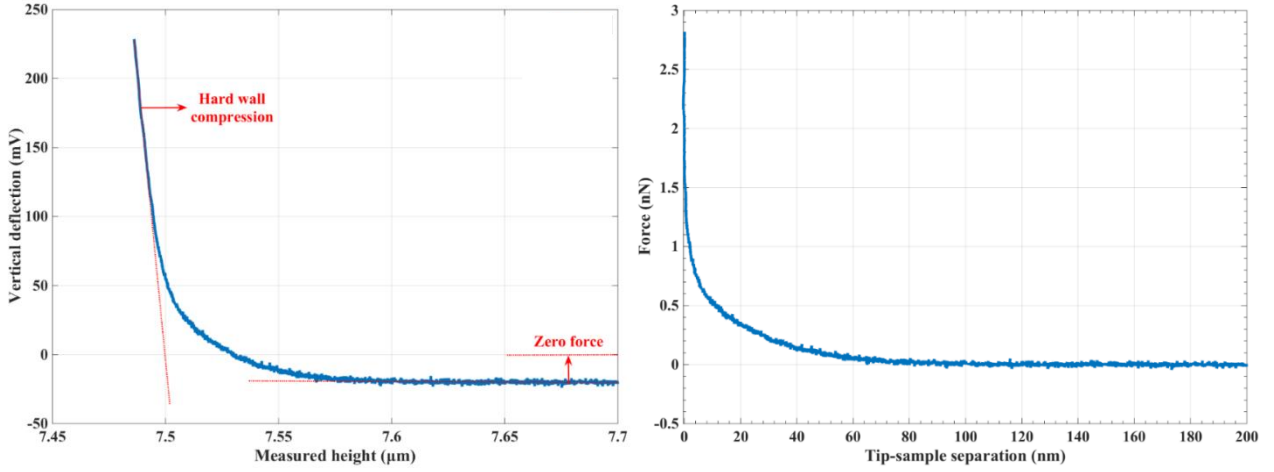


**Figure 3.13** Construction of the force vs tip-sample separation distance curve. (Left) cantilever deflection vs piezo displacement. (Right) force vs tip-sample separation distance

Once the zero separation distance is found, the separation is calculated from the distance travelled by the piezo and the change in cantilever deflection relative to the onset of the constant compliance region. Moreover, as explained, the output of the photodiode is in Volt. To convert the change in Volt into deflection in nanometer, the linear part is again used, since in this region the movement of the piezo and the probe are the same. Thus, the slope provides the relation between the photodiode output and the cantilever deflection, which is known as the cantilever *sensitivity*. For my studies, I usually performed an initial force measurement between the colloidal probe and solid substrate (before grafting or adsorbing the polymers), in order to obtain the correct sensitivity from the hard wall compression. By subtracting this Voltage-output from the raw data for each point, the final force vs tip-sample separation distance curves is obtained. Usually the force curve is presented in terms of force per probe diameter, which is related to interaction energy per unit of area according to the Derjaguin approximation[288]:

$$\frac{F(D)}{R} = 2\pi W(D)$$

## **4. SUMMARY OF THE PAPERS**

In this section, I will discuss the main findings of my papers and provide the relation between them. The *first* paper is about the Hofmeister effect of salt mixtures on the phase separation of PPO. The objective of this study is twofold. First, to study the Hofmeister effect in systems that are more similar to biological systems, where a mixture of ions can be found. Second, to assess the previously reported mechanisms for the salting-out and salting-in effects in such a complex system. The effect of four single salts, i.e., NaCl, NaBr, NaI and NaSCN was firstly studied on the phase separation temperature of PPO. NaCl and NaBr both showed a linear salting-out effect, while the former had a stronger destabilizing effect. NaI and NaSCN both showed a non-linear salting-in effect, while the latter demonstrated a stronger stabilizing effect. With respect to the mixtures, I investigated NaCl + NaBr (mixture of two destabilizer salts), NaCl + NaSCN (mixture of one destabilizer salt and one stabilizer salt) and NaI + NaSCN (mixture of two stabilizer salts). In order to follow the effect of having two different salts in the solution, I systematically varied the concentration of one salt while keeping the concentration of the other salt constant at 0.1 M. In other words, the effect of adding a second type of salt to the solutions only containing different concentrations of the first type of salt was investigated. The effects of the salt mixtures and their single salt solutions on the phase separation temperature of PPO are compared in Figure 4.1.

The results in general indicated that the Hofmeister effect of salt mixtures strongly depends on the type of the salts, as well as the absolute and relative concentration of each salt. Accordingly, the behavior of the salt mixtures was divided into *additive* and *non-additive* Hofmeister effects. The mixtures of one salting-in and one salting-out demonstrated *additivity* in the Hofmeister effects. This observation can support the idea of *anion-polymer surface interaction* for the weakly hydrated anions together with *anion-polymer hydration shell* for the strongly hydrated anions. In other terms, since the two anions affect the polymer through different mechanisms, they do not have to compete with each other for the polymer surface or for the polymer hydration water.

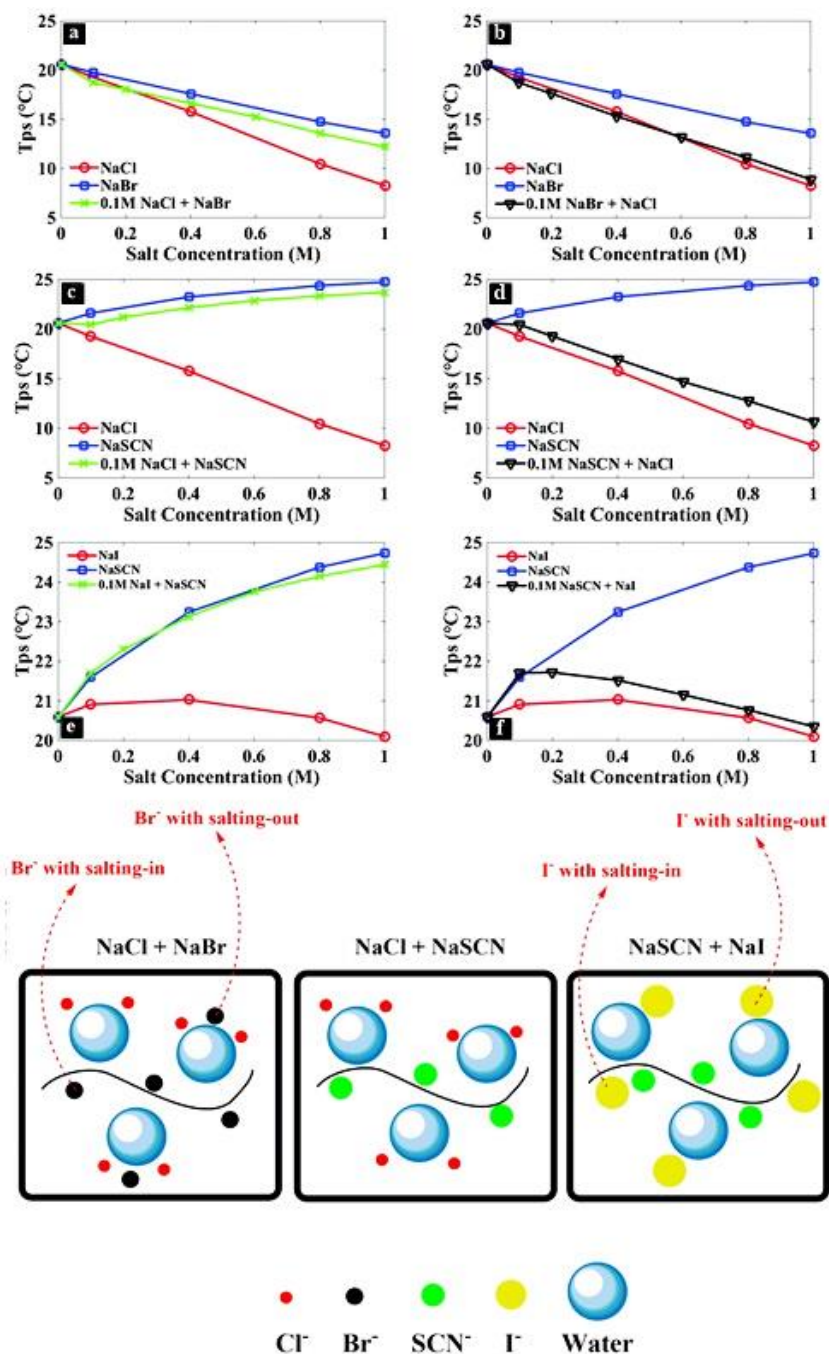


**Figure 4.1** Hofmeister effect of salts mixtures: (a, b) mixtures of NaCl and NaBr, (c, d) mixtures of NaCl and NaSCN, (e, f) mixtures of NaI and NaSCN.

On the other hand, mixtures of two salts with similar Hofmeister effects indicated *non-additivity*. With respect to the mixture of two salts with salting-in effects, the stronger stabilizer was shown to govern the overall salting-in behavior of the mixture, while the weaker stabilizer has a *relative*



*salting-out* effect. This can indicate the competition of two weakly hydrated anions for the polymer surface. For the mixture of two salts with salting-out effects, the stronger destabilizer was demonstrated to dominate the overall salting-out behavior, while the weaker one should have a *relative salting-in* effect. This suggests the competition of two strongly hydrated anions for the polymer hydration water.

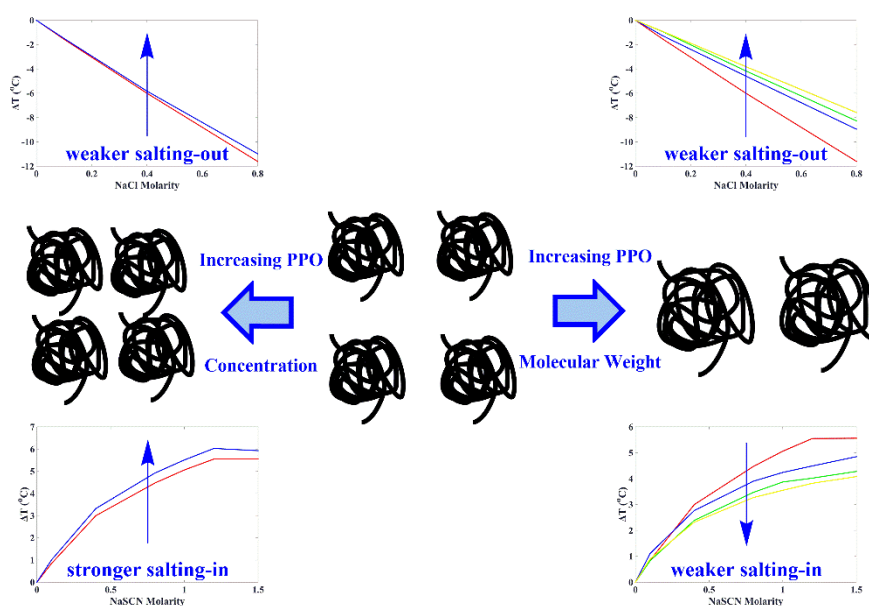


**Figure 4.2** Effect of PPO molecular weight and concentration. Increasing the PPO molecular weight weakens both the salting-out and salting-in effects. Increasing the polymer concentration weakens the salting-out effect, but intensifies the salting-in effect.

My *second* paper examines the effect of PPO molecular weight and concentration on the Hofmeister effect of salts. NaCl was chosen to represent the salting-out effect and NaSCN the salting-in effect. The objective of this study was to understand the contribution of polymer in the Hofmeister effect. We already observed that the Hofmeister effect of certain salts could be different on various polymers. Since comparison between two different polymers can be more complicated (many parameters are changed), investigation of how changing the molecular weight and concentration for a certain polymer can affect the Hofmeister effect can be a reasonable approach

towards studying the polymer role. In other words, fixing the chemical structure while changing the solvent-accessible surface area of the polymer. Four different molecular weights between 1000 to 4000 g/mol and two concentrations 0.5 and 2 wt% were studied. Regarding the salting-out effect, it was shown that increasing the molecular weight of PPO leads to a considerable decrement in the salting-out effect, while increasing the PPO concentration has a similar but weaker effect. It was considered that  $\text{Cl}^-$  is effectively repelled from the PPO interface and that it can destabilize the partially hydrophobic surface of the PPO coils. Since increasing either the molecular weight or the concentration decreases the accessible surface area of PPO in solution, the unfavorable interplay between ion and polymer is decreased and the magnitude of the salting-out is then attenuated. With respect to NaSCN, increasing the molecular weight of PPO resulted in a pronounced decrease in the magnitude of the salting-in effect, while increasing the PPO concentration amplified the salting-in effect, specifically in the case of PPO1000. It was suggested that  $\text{SCN}^-$  preferentially accumulates around and within the PPO coils, and stabilizes partially hydrophobic surface of the coils. Since increasing the molecular weight leads to a decrease in the accessible surface area of PPO in solution, the magnitude of the salting-in effect becomes weaker. The larger salting-in effect on PPO1000 and to some extent PPO2000 and PPO2700 upon increasing the PPO concentration was explained by the stronger effect of electrostatic repulsions between closely-packed coils compared to more isolated coils.

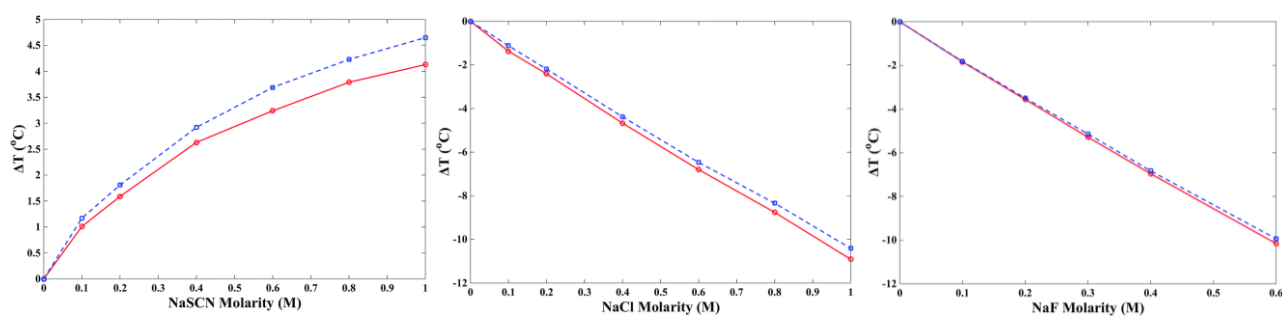


**Figure 4.3** Effect of solvent perturbation (red in  $\text{H}_2\text{O}$  and blue in  $\text{D}_2\text{O}$ ) on the Hofmeister effect of salts.

In the *third* paper, I discussed the effect of solvent perturbation on the Hofmeister effect. The idea behind the project was to investigate the role of solvent properties on the Hofmeister effect. The Hofmeister effect of three salts, i.e., NaSCN, NaCl and NaF on PPO was assessed. The idea behind choosing these salts was: (i) NaSCN has a salting-in effect, while thiocyanate becomes more weakly hydrated in heavy water. (ii) NaCl has a salting-out effect, while chloride becomes more weakly hydrated in heavy water. (iii) NaF has a salting-out effect, but fluoride is one of the fewest anions that becomes more strongly hydrated in heavy water. Besides the information that I obtained from the literature on ions hydration in heavy water, we observed that PPO in salt-free D<sub>2</sub>O is less stable than in salt-free H<sub>2</sub>O. Putting these two effects together, I tried to reason the following observations.

With respect to the effect of NaSCN, the salting-in effect was found to be considerably stronger in D<sub>2</sub>O. Due to the relatively weaker hydration of thiocyanate in D<sub>2</sub>O, It was suggested that the thiocyanate anions are more strongly attracted to the PPO interface in D<sub>2</sub>O. With respect to the effect of NaCl, the salting-out effect was found to be weaker in heavy water. In D<sub>2</sub>O, the hydration of chloride becomes slightly weaker and the polymer accessible surface area diminishes as well. These two effects can both give rise to a weaker salting-out effect in heavy water. With respect to the effect of NaF, no significant difference between the salting-out effects in light and heavy water was observed. I reasoned this observation based on the opposite solvent isotope effects on the ion hydration and the polymer accessible surface area, which in this case apparently are nearly cancelling each other.

In the *fourth* paper, I assessed the Hofmeister effect of three sodium salts on PNIPAM both in bulk and at the gold/aqueous interface. Two important objectives were considered for this work. First, to understand the effect of weakly hydrated anions on the properties of the polymer in terms of conformation and interaction. Second, to understand the behavior of weakly hydrated salts that

show a salting-in to salting-out transition. NaF was studied as the destabilizer and NaSCN was considered as the weakly hydrated salt with a salting-in effect. NaTCA was chosen as the third salt, as a weakly hydrated salt that has a salting-out effect. The thought behind working with these salts was to compare the behavior of NaTCA with the two other salts, so the similarities and differences in behavior could be assessed.

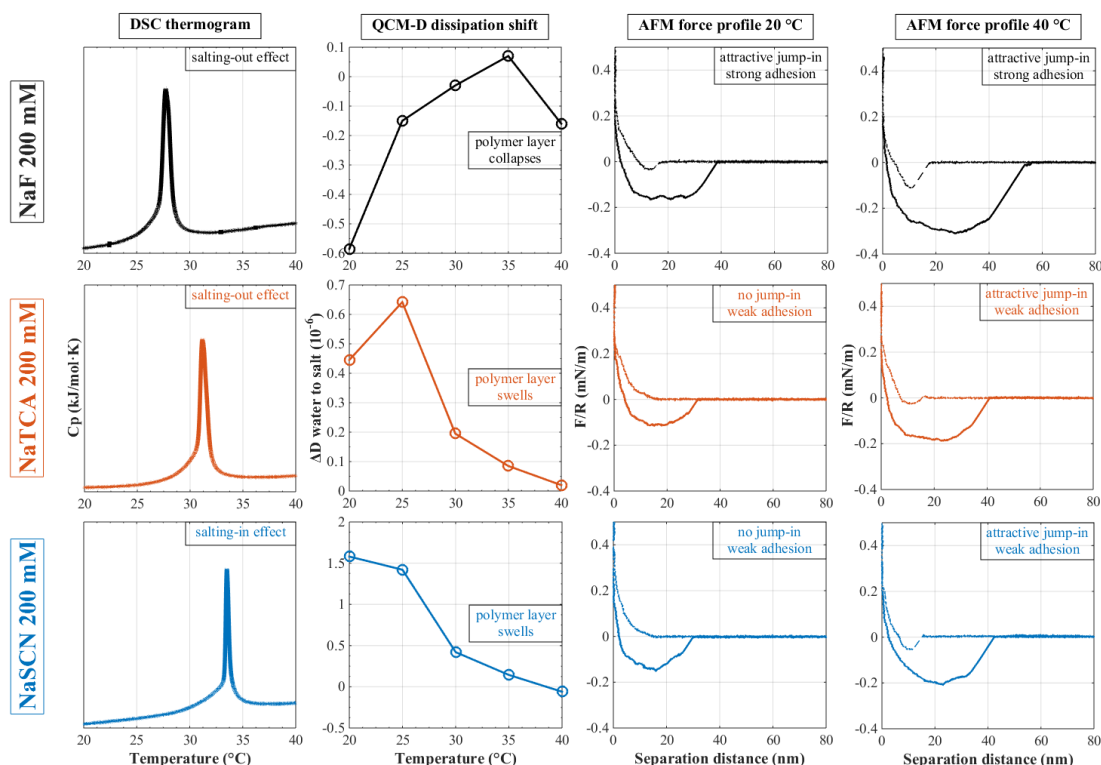


**Figure 4.4** Hofmeister effect of NaF, NaTCA and NaSCN salts on PNIPAM. (First column) DSC thermograms, (Second column) QCM-D dissipation shifts for a PNIPAM layer adsorbed to the gold surface when changing the solvent from water to saline solutions, (Third and fourth column) AFM force-distance curves between two PNIPAM-covered gold surfaces in the salt solutions at 20 and 40 °C.

The phase separation of PNIPAM in bulk solution was firstly studied. Then the effect of the salts on PNIPAM at the gold/aqueous interface was investigated. Addition of NaF led to a large decline in the phase separation temperature, conformational collapse and shrinkage of the polymer layer, and considerably strong PNIPAM–gold and PNIPAM–PNIPAM attractive interactions were detected.

Addition of NaSCN increased the phase separation temperature, caused swelling of the PNIPAM film, and showed relatively weak attractive forces. At last, addition of NaTCA revealed features of both a stabilizing and a destabilizing salt, as a decrement in the phase separation temperature was found, whereas a swollen film conformation and relatively weak chain–substrate and chain–chain interactions were detected, which was discussed in terms of previously reported mechanisms.

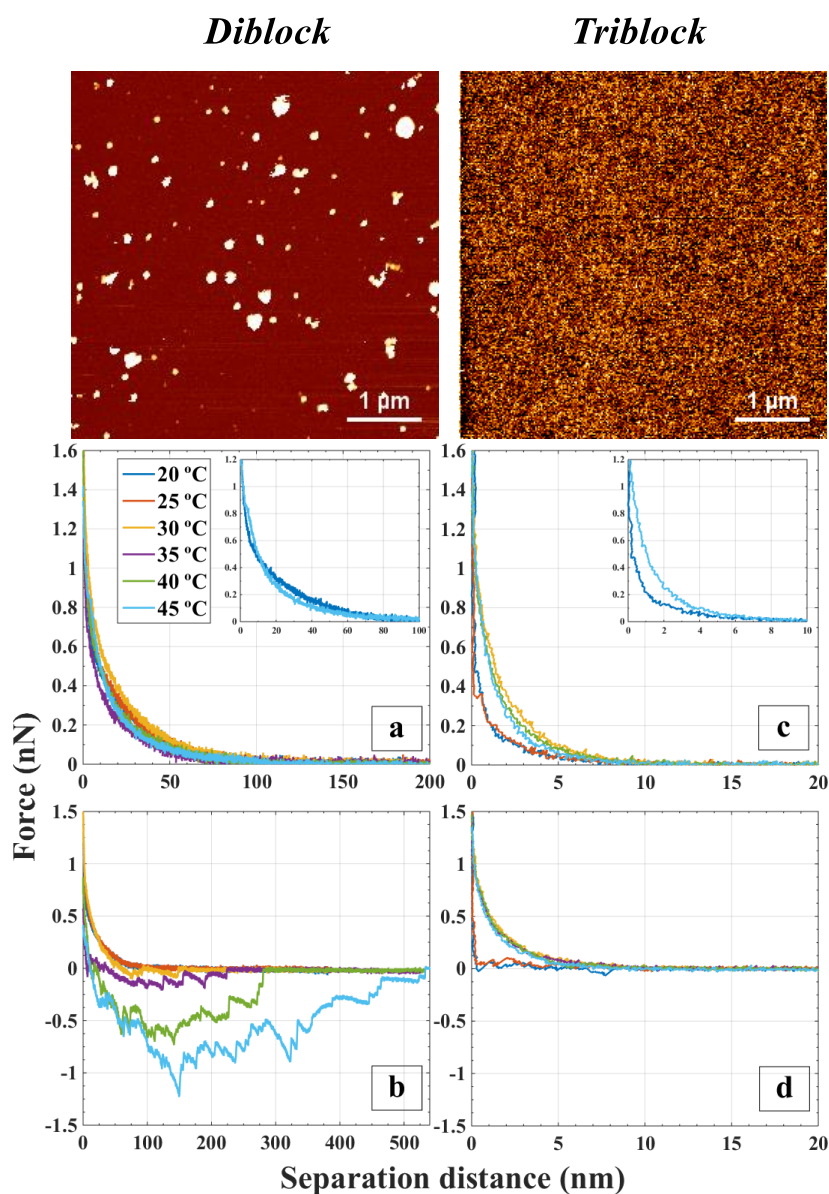


**Figure 4.5** AFM images (at 20  $^{\circ}\text{C}$ ), approach (a, c) and retrace (b, d) force-distance curves (at 20–45  $^{\circ}\text{C}$ ) of the copolymers adsorbed on the silica surface.

In my *fifth* paper, I compared the adsorption of two copolymers at the silica surface and their corresponding films. Both the copolymers bear a cationic block that enables them to adsorb electrostatically on the negatively charged silica surface. The diblock copolymer has a PNIPAM block and the triblock copolymer has the same PNIPAM block plus a PEG block. The bulk solution of the copolymers was firstly studied using dynamic light scattering. Then, the polymers were adsorbed on the silica surface and the film thickness of each was estimated using QCM-D data and corresponding viscoelastic Voigt modeling, which indeed suggested quite similar film characteristics. Then, the topography of the films was studied by AFM imaging and surprisingly it was shown that the diblock forms large clusters on the surface, while the triblock produces a uniform and homogenous layer. To support this observation, I performed AFM colloidal probe measurements on the copolymer-coated surfaces. Similar conclusions could be made from the results, i.e., the layer thickness for the diblock was found to be around 50 nm (As a note, average thickness is not meaningful for such a heterogeneous layer.); while for the triblock the average thickness was around 5 nm. Thermo-responsive behavior of the layers was also studied to see how the interactions are affected. In case of the diblock copolymer, it was shown that the adhesion between the copolymer-coated surfaces progressively increases, while for the triblock no adhesion was found even at temperatures up to 45 °C. I should mention that although this study was not focused on the Hofmeister effect, it was interesting to perceive how variations in the polymer structure can significantly affect the adsorption behavior and following film properties.

Finally yet importantly, my *sixth* paper recapitulates everything I have learned and explored during my PhD studies. This review paper constitutes of two sections. First, a summary of the Hofmeister effect in polymer solutions and more importantly a compilation of the essential mechanisms. The second part is devoted to my rather personal opinions and suggestions regarding the future research on the Hofmeister effect in polymer solutions, which indeed are the ideas that I have partly

investigated during my PhD studies; however, further experimentation and research is necessary on these important topics for a progression in ion-specificity research.

## **5. REFERENCES**



1. Stuart, M.A.C., et al., *Emerging applications of stimuli-responsive polymer materials*. Nature materials, 2010. **9**(2): p. 101-113.
2. Sperling, L.H., *Introduction to physical polymer science*. 2005: John Wiley & Sons.
3. Gedde, U., *Polymer physics*. 2013: Springer Science & Business Media.
4. Doi, M., *Introduction to polymer physics*. 1996: Oxford university press.
5. Wang, W., et al., *Complex coacervate micelles formed by a C18-capped cationic triblock thermoresponsive copolymer interacting with SDS*. Soft Matter, 2012. **8**(45): p. 11514-11525.
6. Cooke, D.M. and A.-C. Shi, *Effects of polydispersity on phase behavior of diblock copolymers*. Macromolecules, 2006. **39**(19): p. 6661-6671.
7. Lietor-Santos, J., et al., *The Role of Polymer Polydispersity in Phase Separation and Gelation in Colloid– Polymer Mixtures*. Langmuir, 2009. **26**(5): p. 3174-3178.
8. De Gennes, P.-G., *Some conformation problems for long macromolecules*. Reports on Progress in Physics, 1969. **32**(1): p. 187.
9. de Gennes, P.-G., *Reptation of a polymer chain in the presence of fixed obstacles*. The Journal of chemical physics, 1971. **55**(2): p. 572-579.
10. Gō, N. and H.A. Scheraga, *On the use of classical statistical mechanics in the treatment of polymer chain conformation*. Macromolecules, 1976. **9**(4): p. 535-542.
11. Mark, J. and P. Flory, *The configuration of the polyoxyethylene chain*. Journal of the American Chemical Society, 1965. **87**(7): p. 1415-1423.
12. HAMANO, K.K.K., et al., *Characterization of poly (N-isopropylmethacrylamide) in water*. Polymer journal, 1990. **22**(12): p. 1051-1057.
13. Flory, P.J., *Thermodynamics of high polymer solutions*. The Journal of chemical physics, 1942. **10**(1): p. 51-61.
14. Flory, P.-J. *Statistical thermodynamics of semi-flexible chain molecules*. in *Proceedings of the Royal Society of London A: Mathematical, Physical and Engineering Sciences*. 1956. The Royal Society.
15. Flory, P.J., *Fifteenth Spiers memorial lecture. Thermodynamics of polymer solutions*. Discussions of the Faraday Society, 1970. **49**: p. 7-29.
16. Utracki, L.A. and C.A. Wilkie, *Polymer blends handbook*. Vol. 1. 2002: Springer.
17. Huggins, M.L., *Solutions of long chain compounds*. The Journal of chemical physics, 1941. **9**(5): p. 440-440.
18. Sanchez, I.C. and R.H. Lacombe, *Statistical thermodynamics of polymer solutions*. Macromolecules, 1978. **11**(6): p. 1145-1156.
19. BATES, F., *Polymer-polymer phase behavior*. Science, 1991. **251**(4996): p. 898-905.
20. Koningsveld, R., W.H. Stockmayer, and E. Nies, *Polymer phase diagrams: a textbook*. 2001: Oxford University Press, USA.
21. Daoud, M. and G. Jannink, *Temperature-concentration diagram of polymer solutions*. Journal de physique, 1976. **37**(7-8): p. 973-979.
22. Farnoux, B., et al., *Cross-over in polymer solutions*. Journal de physique, 1978. **39**(1): p. 77-86.
23. Roy, D., W.L. Brooks, and B.S. Sumerlin, *New directions in thermoresponsive polymers*. Chemical Society Reviews, 2013. **42**(17): p. 7214-7243.
24. Zhuang, J., et al., *Multi-stimuli responsive macromolecules and their assemblies*. Chemical Society Reviews, 2013. **42**(17): p. 7421-7435.
25. Zhang, Q., et al., *Thermoresponsive polymers with lower critical solution temperature: from fundamental aspects and measuring techniques to recommended turbidimetry conditions*. Materials Horizons, 2017. **4**(2): p. 109-116.
26. Grosberg, A.Y. and D.V. Kuznetsov, *Single-chain collapse or precipitation? Kinetic diagram of the states of a polymer solution*. Macromolecules, 1993. **26**(16): p. 4249-4251.
27. Wu, C. and S. Zhou, *Laser light scattering study of the phase transition of poly (N-isopropylacrylamide) in water. 1. Single chain*. Macromolecules, 1995. **28**(24): p. 8381-8387.
28. Wu, C. and S. Zhou, *Thermodynamically stable globule state of a single poly (N-isopropylacrylamide) chain in water*. Macromolecules, 1995. **28**(15): p. 5388-5390.
29. Halperin, A., M. Kröger, and F.M. Winnik, *Poly (N-isopropylacrylamide) Phase Diagrams: Fifty Years of Research*. Angewandte Chemie International Edition, 2015. **54**(51): p. 15342-15367.

30. Bischofberger, I. and V. Trappe, *New aspects in the phase behaviour of poly-N-isopropyl acrylamide: systematic temperature dependent shrinking of PNIPAM assemblies well beyond the LCST*. Scientific reports, 2015. **5**: p. 15520.
31. Mao, H., et al., *High-throughput studies of the effects of polymer structure and solution components on the phase separation of thermoresponsive polymers*. Macromolecules, 2004. **37**(3): p. 1031-1036.
32. Bekiranov, S., R. Bruinsma, and P. Pincus, *Solution behavior of polyethylene oxide in water as a function of temperature and pressure*. Physical Review E, 1997. **55**(1): p. 577.
33. Saeki, S., et al., *Upper and lower critical solution temperatures in poly (ethylene glycol) solutions*. Polymer, 1976. **17**(8): p. 685-689.
34. Alexandridis, P., *Poly (ethylene oxide)/poly (propylene oxide) block copolymer surfactants*. Current opinion in colloid & interface science, 1997. **2**(5): p. 478-489.
35. Hocine, S. and M.-H. Li, *Thermoresponsive self-assembled polymer colloids in water*. Soft Matter, 2013. **9**(25): p. 5839-5861.
36. Pace, C.N., *Contribution of the hydrophobic effect to globular protein stability*. Journal of molecular biology, 1992. **226**(1): p. 29-35.
37. Spolar, R.S., J.-H. Ha, and M.T. Record, *Hydrophobic effect in protein folding and other noncovalent processes involving proteins*. Proceedings of the National Academy of Sciences, 1989. **86**(21): p. 8382-8385.
38. Pratt, L.R. and D. Chandler, *Theory of the hydrophobic effect*. The Journal of chemical physics, 1977. **67**(8): p. 3683-3704.
39. Southall, N.T., K.A. Dill, and A. Haymet, *A view of the hydrophobic effect*, 2002, ACS Publications.
40. Dill, K.A., et al., *Modeling water, the hydrophobic effect, and ion solvation*. Annu. Rev. Biophys. Biomol. Struct., 2005. **34**: p. 173-199.
41. Tanford, C., *The hydrophobic effect and the organization of living matter*. Science, 1978. **200**(4345): p. 1012-1018.
42. Huang, D.M. and D. Chandler, *Temperature and length scale dependence of hydrophobic effects and their possible implications for protein folding*. Proceedings of the National Academy of Sciences, 2000. **97**(15): p. 8324-8327.
43. Matsuyama, A. and F. Tanaka, *Theory of solvation-induced reentrant phase separation in polymer solutions*. Physical Review Letters, 1990. **65**(3): p. 341.
44. Shikata, T., M. Okuzono, and N. Sugimoto, *Temperature-dependent hydration/dehydration behavior of poly (ethylene oxide) s in aqueous solution*. Macromolecules, 2013. **46**(5): p. 1956-1961.
45. Shikata, T., R. Takahashi, and A. Sakamoto, *Hydration of poly (ethylene oxide) s in aqueous solution as studied by dielectric relaxation measurements*. The Journal of Physical Chemistry B, 2006. **110**(18): p. 8941-8945.
46. Grinberg, V.Y., et al., *Energetics of LCST transition of poly (ethylene oxide) in aqueous solutions*. Polymer, 2015. **73**: p. 86-90.
47. Okada, Y. and F. Tanaka, *Cooperative hydration, chain collapse, and flat LCST behavior in aqueous poly (N-isopropylacrylamide) solutions*. Macromolecules, 2005. **38**(10): p. 4465-4471.
48. Bischofberger, I., et al., *Hydrophobic hydration of poly-N-isopropyl acrylamide: a matter of the mean energetic state of water*. Scientific reports, 2014. **4**: p. 4377.
49. Ono, Y. and T. Shikata, *Hydration and dynamic behavior of poly (N-isopropylacrylamide) s in aqueous solution: A sharp phase transition at the lower critical solution temperature*. Journal of the American Chemical Society, 2006. **128**(31): p. 10030-10031.
50. Pelton, R., *Poly (N-isopropylacrylamide)(PNIPAM) is never hydrophobic*. Journal of colloid and interface science, 2010. **348**(2): p. 673-674.
51. Winnik, F.M., H. Ringsdorf, and J. Venzmer, *Methanol-water as a co-nonsolvent system for poly (N-isopropylacrylamide)*. Macromolecules, 1990. **23**(8): p. 2415-2416.
52. Alexandridis, P., J.F. Holzwarth, and T.A. Hatton, *Micellization of poly (ethylene oxide)-poly (propylene oxide)-poly (ethylene oxide) triblock copolymers in aqueous solutions: thermodynamics of copolymer association*. Macromolecules, 1994. **27**(9): p. 2414-2425.

53. Brown, W., et al., *Micelle and gel formation in a poly (ethylene oxide)/poly (propylene oxide)/poly (ethylene oxide) triblock copolymer in water solution: dynamic and static light scattering and oscillatory shear measurements*. The Journal of Physical Chemistry, 1991. **95**(4): p. 1850-1858.
54. Weber, C., R. Hoogenboom, and U.S. Schubert, *Temperature responsive bio-compatible polymers based on poly (ethylene oxide) and poly (2-oxazoline) s*. Progress in Polymer Science, 2012. **37**(5): p. 686-714.
55. Jeong, N.S., et al., *Polymers with molecular weight dependent LCSTs are essential for cooperative behaviour*. Polymer Chemistry, 2012. **3**(3): p. 794-799.
56. Lessard, D., M. Ousaleh, and X. Zhu, *Effect of the molecular weight on the lower critical solution temperature of poly (N, N-diethylacrylamide) in aqueous solutions*. Canadian journal of chemistry, 2001. **79**(12): p. 1870-1874.
57. Furyk, S., et al., *Effects of end group polarity and molecular weight on the lower critical solution temperature of poly (N-isopropylacrylamide)*. Journal of Polymer Science Part A: Polymer Chemistry, 2006. **44**(4): p. 1492-1501.
58. Tong, Z., et al., *Inverse molecular weight dependence of cloud points for aqueous poly (N-isopropylacrylamide) solutions*. Macromolecules, 1999. **32**(13): p. 4488-4490.
59. Bailey, F. and R. Callard, *Some properties of poly (ethylene oxide) 1 in aqueous solution*. Journal of applied polymer science, 1959. **1**(1): p. 56-62.
60. van der Linden, C.C., et al., *Adsorption of polymers on heterogeneous surfaces*. Macromolecules, 1994. **27**(7): p. 1915-1921.
61. Biver, C., et al., *Neutral and charged polymer brushes: a model unifying curvature effects from micelles to flat surfaces*. Macromolecules, 1997. **30**(6): p. 1787-1792.
62. Baumgärtner, A. and M. Muthukumar, *Effects of surface roughness on adsorbed polymers*. The Journal of chemical physics, 1991. **94**(5): p. 4062-4070.
63. Giesbers, M., et al., *Forces between polymer-covered surfaces: a colloidal probe study*. Colloids and Surfaces A: Physicochemical and Engineering Aspects, 1998. **142**(2): p. 343-353.
64. Fleer, G., et al., *Polymers at interfaces*. 1993: Springer Science & Business Media.
65. Binder, K. and A. Milchev, *Polymer brushes on flat and curved surfaces: How computer simulations can help to test theories and to interpret experiments*. Journal of Polymer Science Part B: Polymer Physics, 2012. **50**(22): p. 1515-1555.
66. Plunkett, M.A., et al., *Adsorption of pNIPAM layers on hydrophobic gold surfaces, measured in situ by QCM and SPR*. Langmuir, 2003. **19**(17): p. 6837-6844.
67. Wu, B., et al., *Adsorption kinetics and adsorption isotherm of poly (N-isopropylacrylamide) on gold surfaces studied using QCM-D*. The Journal of Physical Chemistry C, 2007. **111**(3): p. 1131-1135.
68. Netz, R.R. and D. Andelman, *Neutral and charged polymers at interfaces*. Physics reports, 2003. **380**(1): p. 1-95.
69. Wu, K., et al., *Adsorption isotherms and dissipation of adsorbed poly (N-isopropylacrylamide) in its swelling and collapsed states*. The Journal of Physical Chemistry B, 2007. **111**(30): p. 8723-8727.
70. Yang, Q.-H. and M.-B. Luo, *Dynamics of adsorbed polymers on attractive homogeneous surfaces*. Scientific reports, 2016. **6**.
71. Linse, P. and N. Kallrot, *Polymer adsorption from bulk solution onto planar surfaces: effect of polymer flexibility and surface attraction in good solvent*. Macromolecules, 2010. **43**(4): p. 2054-2068.
72. De Gennes, P., *Polymers at an interface; a simplified view*. Advances in colloid and interface science, 1987. **27**(3-4): p. 189-209.
73. Zhu, D.-M., et al., *Physisorption of poly (N-isopropylacrylamide) in its swollen and collapsed states: effects of molecular conformation and substrate interaction*. The Journal of Physical Chemistry C, 2007. **111**(50): p. 18679-18686.
74. O'Shaughnessy, B. and D. Vavylonis, *Non-equilibrium in adsorbed polymer layers*. Journal of Physics: Condensed Matter, 2004. **17**(2): p. R63.
75. Kleshchanok, D., R. Tuinier, and P.R. Lang, *Direct measurements of polymer-induced forces*. Journal of Physics: Condensed Matter, 2008. **20**(7): p. 073101.

76. De Gennes, P.G., *Scaling theory of polymer adsorption*. Journal de physique, 1976. **37**(12): p. 1445-1452.
77. Daoud, M. and P. De Gennes, *Statistics of macromolecular solutions trapped in small pores*. Journal de physique, 1977. **38**(1): p. 85-93.
78. Smyda, M.R. and S.C. Harvey, *The entropic cost of polymer confinement*. The Journal of Physical Chemistry B, 2012. **116**(35): p. 10928-10934.
79. Alexander, S., *Polymer adsorption on small spheres. A scaling approach*. Journal de physique, 1977. **38**(8): p. 977-981.
80. de Gennes, P., *Conformations of polymers attached to an interface*. Macromolecules, 1980. **13**(5): p. 1069-1075.
81. Aubouy, M. and E. Raphael, *Scaling description of a colloidal particle clothed with polymers*. Macromolecules, 1998. **31**(13): p. 4357-4363.
82. Kim, M., et al., *From self-assembled monolayers to coatings: advances in the synthesis and nanobio applications of polymer brushes*. Polymers, 2015. **7**(7): p. 1346-1378.
83. Zhao, B. and W.J. Brittain, *Polymer brushes: surface-immobilized macromolecules*. Progress in Polymer Science, 2000. **25**(5): p. 677-710.
84. Kato, K., et al., *Polymer surface with graft chains*. Progress in Polymer Science, 2003. **28**(2): p. 209-259.
85. Zhang, G. and C. Wu, *Quartz crystal microbalance studies on conformational change of polymer chains at interface*. Macromolecular rapid communications, 2009. **30**(4-5): p. 328-335.
86. Ishida, N. and S. Biggs, *Direct Observation of the Phase Transition for a Poly (N-isopropylacrylamide) Layer Grafted onto a Solid Surface by AFM and QCM-D*. Langmuir, 2007. **23**(22): p. 11083-11088.
87. Nordgren, N., et al., *Top-down grafting of xyloglucan to gold monitored by QCM-D and AFM: enzymatic activity and interactions with cellulose*. Biomacromolecules, 2008. **9**(3): p. 942-948.
88. Liu, G., et al., *Study of the Kinetics of the Pancake-to-Brush Transition of Poly (N-isopropylacrylamide) Chains*. The Journal of Physical Chemistry B, 2005. **109**(47): p. 22603-22607.
89. Pensa, E., et al., *The chemistry of the sulfur-gold interface: in search of a unified model*. Accounts of chemical research, 2012. **45**(8): p. 1183-1192.
90. Häkkinen, H., *The gold-sulfur interface at the nanoscale*. Nature chemistry, 2012. **4**(6): p. 443-455.
91. Alexander, S., *Adsorption of chain molecules with a polar head a scaling description*. Journal de physique, 1977. **38**(8): p. 983-987.
92. Liu, G. and G. Zhang, *QCM-D studies on polymer behavior at interfaces*. 2013: Springer.
93. Koutsos, V., E. Van der Vegte, and G. Hadzioannou, *Direct view of structural regimes of end-grafted polymer monolayers: A scanning force microscopy study*. Macromolecules, 1999. **32**(4): p. 1233-1236.
94. Currie, E., W. Norde, and M.C. Stuart, *Tethered polymer chains: surface chemistry and their impact on colloidal and surface properties*. Advances in colloid and interface science, 2003. **100**: p. 205-265.
95. Milner, S.T., T. Witten, and M. Cates, *Theory of the grafted polymer brush*. Macromolecules, 1988. **21**(8): p. 2610-2619.
96. Edwards, S.F., *The statistical mechanics of polymers with excluded volume*. Proceedings of the Physical Society, 1965. **85**(4): p. 613.
97. Brittain, W.J. and S. Minko, *A structural definition of polymer brushes*. Journal of Polymer Science Part A: Polymer Chemistry, 2007. **45**(16): p. 3505-3512.
98. Netz, R.R. and D. Andelman, *Polyelectrolytes in solution and at surfaces*. Encyclopedia of electrochemistry, 2002.
99. Van de Steeg, H.G., et al., *Polyelectrolyte adsorption: a subtle balance of forces*. Langmuir, 1992. **8**(10): p. 2538-2546.
100. Papenhuijzen, J., H. Van der Schee, and G. Fleer, *Polyelectrolyte adsorption: I. A new lattice theory*. Journal of colloid and interface science, 1985. **104**(2): p. 540-552.
101. Sukhishvili, S.A. and S. Granick, *Polyelectrolyte adsorption onto an initially-bare solid surface of opposite electrical charge*. The Journal of chemical physics, 1998. **109**(16): p. 6861-6868.

102. Hesselink, F.T., *On the theory of polyelectrolyte adsorption: The effect on adsorption behavior of the electrostatic contribution to the adsorption free energy*. Journal of colloid and interface science, 1977. **60**(3): p. 448-466.
103. Baba, A., F. Kaneko, and R.C. Advincula, *Polyelectrolyte adsorption processes characterized in situ using the quartz crystal microbalance technique: alternate adsorption properties in ultrathin polymer films*. Colloids and Surfaces A: Physicochemical and Engineering Aspects, 2000. **173**(1): p. 39-49.
104. Shafir, A., D. Andelman, and R.R. Netz, *Adsorption and depletion of polyelectrolytes from charged surfaces*. The Journal of chemical physics, 2003. **119**(4): p. 2355-2362.
105. Sens, P. and J.-F. Joanny, *Counterion release and electrostatic adsorption*. Physical Review Letters, 2000. **84**(21): p. 4862.
106. Henzler, K., et al., *Adsorption of  $\beta$ -lactoglobulin on spherical polyelectrolyte brushes: direct proof of counterion release by isothermal titration calorimetry*. Journal of the American Chemical Society, 2010. **132**(9): p. 3159-3163.
107. Zhulina, E., et al., *Coil-globule type transitions in polymers. 1. Collapse of layers of grafted polymer chains*. Macromolecules, 1991. **24**(1): p. 140-149.
108. Annaka, M., et al., *Real-time observation of coil-to-globule transition in thermosensitive poly (N-isopropylacrylamide) brushes by quartz crystal microbalance*. Polymer, 2007. **48**(19): p. 5713-5720.
109. Liu, G. and G. Zhang, *Collapse and swelling of thermally sensitive poly (N-isopropylacrylamide) brushes monitored with a quartz crystal microbalance*. The Journal of Physical Chemistry B, 2005. **109**(2): p. 743-747.
110. Grest, G.S. and M. Murat, *Structure of grafted polymeric brushes in solvents of varying quality: a molecular dynamics study*. Macromolecules, 1993. **26**(12): p. 3108-3117.
111. Tang, H. and I. Szleifer, *Phase behavior of grafted polymers in poor solvents*. EPL (Europhysics Letters), 1994. **28**(1): p. 19.
112. Laloyaux, X., et al., *Surface and bulk collapse transitions of thermoresponsive polymer brushes*. Langmuir, 2009. **26**(2): p. 838-847.
113. Jonas, A.M., et al., *Effect of nanoconfinement on the collapse transition of responsive polymer brushes*. Nano letters, 2008. **8**(11): p. 3819-3824.
114. Lai, P.Y. and K. Binder, *Structure and dynamics of polymer brushes near the  $\Theta$  point: a Monte Carlo simulation*. The Journal of chemical physics, 1992. **97**(1): p. 586-595.
115. Ishida, N. and S. Biggs, *Effect of grafting density on phase transition behavior for poly (N-isopropylacrylamide) brushes in aqueous solutions studied by AFM and QCM-D*. Macromolecules, 2010. **43**(17): p. 7269-7276.
116. Yim, H., et al., *Effects of grafting density and molecular weight on the temperature-dependent conformational change of poly (N-isopropylacrylamide) grafted chains in water*. Macromolecules, 2006. **39**(9): p. 3420-3426.
117. Kidoaki, S., et al., *Thermoresponsive structural change of a poly (N-isopropylacrylamide) graft layer measured with an atomic force microscope*. Langmuir, 2001. **17**(8): p. 2402-2407.
118. Malham, I.B. and L. Bureau, *Density effects on collapse, compression, and adhesion of thermoresponsive polymer brushes*. Langmuir, 2009. **26**(7): p. 4762-4768.
119. Zhu, X., et al., *End-grafted low-molecular-weight PNIPAM does not collapse above the LCST*. Langmuir, 2007. **23**(1): p. 162-169.
120. Plunkett, K.N., et al., *PNIPAM chain collapse depends on the molecular weight and grafting density*. Langmuir, 2006. **22**(9): p. 4259-4266.
121. Zhao, L., K. Ma, and Z. Yang, *Changes of water hydrogen bond network with different externalities*. International journal of molecular sciences, 2015. **16**(4): p. 8454-8489.
122. Frank, H.S. and W.-Y. Wen, *Ion-solvent interaction. Structural aspects of ion-solvent interaction in aqueous solutions: a suggested picture of water structure*. Discussions of the Faraday Society, 1957. **24**: p. 133-140.
123. Chen, B., et al., *Hydrogen bonding in water*. Physical Review Letters, 2003. **91**(21): p. 215503.
124. Jorgensen, W.L., et al., *Comparison of simple potential functions for simulating liquid water*. The Journal of chemical physics, 1983. **79**(2): p. 926-935.

125. Collins, K.D., *Why continuum electrostatics theories cannot explain biological structure, polyelectrolytes or ionic strength effects in ion–protein interactions*. Biophysical chemistry, 2012. **167**: p. 43-59.
126. Boström, M., D. Williams, and B. Ninham, *Specific ion effects: why DLVO theory fails for biology and colloid systems*. Physical Review Letters, 2001. **87**(16): p. 168103.
127. Salis, A. and B.W. Ninham, *Models and mechanisms of Hofmeister effects in electrolyte solutions, and colloid and protein systems revisited*. Chemical Society Reviews, 2014. **43**(21): p. 7358-7377.
128. Baer, M.D. and C.J. Mundy, *Toward an understanding of the specific ion effect using density functional theory*. The Journal of Physical Chemistry Letters, 2011. **2**(9): p. 1088-1093.
129. Ball, P. and J.E. Hallsworth, *Water structure and chaotropicity: their uses, abuses and biological implications*. Physical Chemistry Chemical Physics, 2015. **17**(13): p. 8297-8305.
130. Marcus, Y. and G. Hefter, *Ion pairing*. Chemical reviews, 2006. **106**(11): p. 4585-4621.
131. Van Der Vegt, N.F., et al., *Water-mediated ion pairing: Occurrence and relevance*. Chemical reviews, 2016. **116**(13): p. 7626-7641.
132. Ninham, B.W. and V. Yaminsky, *Ion binding and ion specificity: the Hofmeister effect and Onsager and Lifshitz theories*. Langmuir, 1997. **13**(7): p. 2097-2108.
133. Edwards, S. and D. Williams, *Hofmeister effects in colloid science and biology explained by dispersion forces: analytic results for the double layer interaction*. Current opinion in colloid & interface science, 2004. **9**(1): p. 139-144.
134. Yang, L., Y. Fan, and Y.Q. Gao, *Differences of cations and anions: Their hydration, surface adsorption, and impact on water dynamics*. The Journal of Physical Chemistry B, 2011. **115**(43): p. 12456-12465.
135. Marcus, Y., *Effect of ions on the structure of water: structure making and breaking*. Chemical reviews, 2009. **109**(3): p. 1346-1370.
136. Collins, K.D. and M.W. Washabaugh, *The Hofmeister effect and the behaviour of water at interfaces*. Quarterly reviews of biophysics, 1985. **18**(04): p. 323-422.
137. Jones, G. and M. Dole, *The viscosity of aqueous solutions of strong electrolytes with special reference to barium chloride*. Journal of the American Chemical Society, 1929. **51**(10): p. 2950-2964.
138. Soper, A.K. and K. Weckström, *Ion solvation and water structure in potassium halide aqueous solutions*. Biophysical chemistry, 2006. **124**(3): p. 180-191.
139. Tielrooij, K., et al., *Cooperativity in ion hydration*. Science, 2010. **328**(5981): p. 1006-1009.
140. Paschek, D. and R. Ludwig, *Specific ion effects on water structure and dynamics beyond the first hydration shell*. Angewandte Chemie International Edition, 2011. **50**(2): p. 352-353.
141. Collins, K.D., G.W. Neilson, and J.E. Enderby, *Ions in water: characterizing the forces that control chemical processes and biological structure*. Biophysical chemistry, 2007. **128**(2): p. 95-104.
142. Kiriukhin, M.Y. and K.D. Collins, *Dynamic hydration numbers for biologically important ions*. Biophysical chemistry, 2002. **99**(2): p. 155-168.
143. Ohtaki, H. and T. Radnai, *Structure and dynamics of hydrated ions*. Chemical reviews, 1993. **93**(3): p. 1157-1204.
144. Collins, K.D., *Charge density-dependent strength of hydration and biological structure*. Biophysical journal, 1997. **72**(1): p. 65-76.
145. Nightingale Jr, E., *Phenomenological theory of ion solvation. Effective radii of hydrated ions*. The Journal of Physical Chemistry, 1959. **63**(9): p. 1381-1387.
146. Hribar, B., et al., *How ions affect the structure of water*. Journal of the American Chemical Society, 2002. **124**(41): p. 12302-12311.
147. Fujisawa, K., et al., *Anion– $\pi$  and Cation– $\pi$  Interactions on the Same Surface*. Angewandte Chemie, 2014. **126**(42): p. 11448-11451.
148. Schmid, R., A.M. Miah, and V.N. Sapunov, *A new table of the thermodynamic quantities of ionic hydration: values and some applications (enthalpy–entropy compensation and Born radii)*. Physical Chemistry Chemical Physics, 2000. **2**(1): p. 97-102.
149. Okur, H.I., et al., *Beyond the Hofmeister Series: Ion-Specific Effects on Proteins and Their Biological Functions*. The Journal of Physical Chemistry B, 2017. **121**(9): p. 1997-2014.

150. Boström, M., W. Kunz, and B. Ninham, *Hofmeister effects*. Water Encyclopedia, 2005.
151. Nostro, P.L., et al., *Hofmeister effects in supramolecular and biological systems*. Biophysical chemistry, 2006. **124**(3): p. 208-213.
152. Parsons, D.F., et al., *Hofmeister effects: interplay of hydration, nonelectrostatic potentials, and ion size*. Physical Chemistry Chemical Physics, 2011. **13**(27): p. 12352-12367.
153. Lo Nostro, P. and B.W. Ninham, *Hofmeister phenomena: an update on ion specificity in biology*. Chemical reviews, 2012. **112**(4): p. 2286-2322.
154. Craig, V.S., *Bubble coalescence and specific-ion effects*. Current opinion in colloid & interface science, 2004. **9**(1): p. 178-184.
155. Henry, C.L., et al., *Ion-specific coalescence of bubbles in mixed electrolyte solutions*. The Journal of Physical Chemistry C, 2007. **111**(2): p. 1015-1023.
156. Bauduin, P., et al., *Hofmeister effect on enzymatic catalysis and colloidal structures*. Current opinion in colloid & interface science, 2004. **9**(1): p. 43-47.
157. Salis, A., et al., *Hofmeister effects in enzymatic activity: weak and strong electrolyte influences on the activity of Candida rugosa lipase*. The Journal of Physical Chemistry B, 2007. **111**(5): p. 1149-1156.
158. Bilanicová, D., et al., *Specific anion effects on enzymatic activity in nonaqueous media*. The Journal of Physical Chemistry B, 2008. **112**(38): p. 12066-12072.
159. Yang, Z., *Hofmeister effects: an explanation for the impact of ionic liquids on biocatalysis*. Journal of biotechnology, 2009. **144**(1): p. 12-22.
160. Shahriari, S., et al., *Role of the Hofmeister series in the formation of ionic-liquid-based aqueous biphasic systems*. The Journal of Physical Chemistry B, 2012. **116**(24): p. 7252-7258.
161. Kowacz, M., et al., *Hofmeister effects of ionic liquids in protein crystallization: Direct and water-mediated interactions*. CrystEngComm, 2012. **14**(15): p. 4912-4921.
162. Holm, G.E. and J.M. Sherman, *Salt effects in bacterial growth: I. Preliminary paper*. Journal of bacteriology, 1921. **6**(6): p. 511.
163. Hofmeister, F., *Zur lehre von der wirkung der salze*. Naunyn-Schmiedeberg's Archives of Pharmacology, 1888. **25**(1): p. 1-30.
164. Kunz, W., J. Henle, and B.W. Ninham, *'Zur Lehre von der Wirkung der Salze'(about the science of the effect of salts): Franz Hofmeister's historical papers*. Current opinion in colloid & interface science, 2004. **9**(1): p. 19-37.
165. Saito, S., *Salt effect on polymer solutions*. Journal of Polymer Science Part A-1: Polymer Chemistry, 1969. **7**(7): p. 1789-1802.
166. Lundberg, R., F. Bailey, and R. Callard, *Interactions of inorganic salts with poly (ethylene oxide)*. Journal of Polymer Science Part A-1: Polymer Chemistry, 1966. **4**(6): p. 1563-1577.
167. Ataman, M., *Properties of aqueous salt solutions of poly (ethylene oxide). Cloud points,  $\theta$  temperatures*. Colloid & polymer science, 1987. **265**(1): p. 19-25.
168. Lo Nostro, P., et al., *Effect of cations and anions on the formation of polypseudorotaxanes*. The Journal of Physical Chemistry B, 2002. **106**(9): p. 2166-2174.
169. Schwierz, N., D. Horinek, and R.R. Netz, *Anionic and cationic Hofmeister effects on hydrophobic and hydrophilic surfaces*. Langmuir, 2013. **29**(8): p. 2602-2614.
170. Schwierz, N., D. Horinek, and R.R. Netz, *Reversed anionic Hofmeister series: the interplay of surface charge and surface polarity*. Langmuir, 2010. **26**(10): p. 7370-7379.
171. Boström, M., et al., *Possible origin of the inverse and direct Hofmeister series for lysozyme at low and high salt concentrations*. Langmuir, 2011. **27**(15): p. 9504-9511.
172. Lund, M. and P. Jungwirth, *Patchy proteins, anions and the Hofmeister series*. Journal of Physics: Condensed Matter, 2008. **20**(49): p. 494218.
173. Peula-García, J.M., J.L. Ortega-Vinuesa, and D. Bastos-González, *Inversion of Hofmeister series by changing the surface of colloidal particles from hydrophobic to hydrophilic*. The Journal of Physical Chemistry C, 2010. **114**(25): p. 11133-11139.
174. Schwierz, N., et al., *Reversed Hofmeister series—The rule rather than the exception*. Current opinion in colloid & interface science, 2016. **23**: p. 10-18.

175. Parsons, D., et al., *Why direct or reversed Hofmeister series? Interplay of hydration, non-electrostatic potentials, and ion size*. Langmuir, 2009. **26**(5): p. 3323-3328.
176. BORAH, J., et al., *Specific ion effects in adsorption at the solid/electrolyte interface: A probe into the concentration limit*. Langmuir, 2011. **47**: p. 8710-8717.
177. Pashley, R., *DLVO and hydration forces between mica surfaces in Li<sup>+</sup>, Na<sup>+</sup>, K<sup>+</sup>, and Cs<sup>+</sup> electrolyte solutions: A correlation of double-layer and hydration forces with surface cation exchange properties*. Journal of colloid and interface science, 1981. **83**(2): p. 531-546.
178. Parsons, D.F. and A. Salis, *Hofmeister effects at low salt concentration due to surface charge transfer*. Current opinion in colloid & interface science, 2016. **23**: p. 41-49.
179. Omta, A.W., et al., *Negligible effect of ions on the hydrogen-bond structure in liquid water*. Science, 2003. **301**(5631): p. 347-349.
180. Zhang, Y., et al., *Specific ion effects on the water solubility of macromolecules: PNIPAM and the Hofmeister series*. Journal of the American Chemical Society, 2005. **127**(41): p. 14505-14510.
181. Zhang, Y. and P.S. Cremer, *Interactions between macromolecules and ions: the Hofmeister series*. Current opinion in chemical biology, 2006. **10**(6): p. 658-663.
182. Zhang, Y., et al., *Effects of Hofmeister anions on the LCST of PNIPAM as a function of molecular weight*. The journal of physical chemistry. C, Nanomaterials and interfaces, 2007. **111**(25): p. 8916.
183. Chen, X., et al., *Specific ion effects on interfacial water structure near macromolecules*. Journal of the American Chemical Society, 2007. **129**(40): p. 12272-12279.
184. Cho, Y., et al., *Effects of Hofmeister anions on the phase transition temperature of elastin-like polypeptides*. The journal of physical chemistry. B, 2008. **112**(44): p. 13765.
185. Zhang, Y. and P.S. Cremer, *The inverse and direct Hofmeister series for lysozyme*. Proceedings of the National Academy of Sciences, 2009. **106**(36): p. 15249-15253.
186. Zhang, Y. and P.S. Cremer, *Chemistry of Hofmeister anions and osmolytes*. Annual review of physical chemistry, 2010. **61**: p. 63-83.
187. Chen, X., et al., *Specific anion effects on water structure adjacent to protein monolayers*. Langmuir, 2010. **26**(21): p. 16447-16454.
188. Kherb, J., S.C. Flores, and P.S. Cremer, *Role of carboxylate side chains in the cation Hofmeister series*. The Journal of Physical Chemistry B, 2012. **116**(25): p. 7389-7397.
189. Rembert, K.B., et al., *Molecular mechanisms of ion-specific effects on proteins*. Journal of the American Chemical Society, 2012. **134**(24): p. 10039-10046.
190. Paterová, J., et al., *Reversal of the Hofmeister series: specific ion effects on peptides*. The Journal of Physical Chemistry B, 2013. **117**(27): p. 8150-8158.
191. Okur, H.I., J. Kherb, and P.S. Cremer, *Cations bind only weakly to amides in aqueous solutions*. Journal of the American Chemical Society, 2013. **135**(13): p. 5062-5067.
192. Rembert, K.B., et al., *An NH moiety is not required for anion binding to amides in aqueous solution*. Langmuir, 2015. **31**(11): p. 3459-3464.
193. Pegram, L.M. and M.T. Record, *Hofmeister salt effects on surface tension arise from partitioning of anions and cations between bulk water and the air– water interface*. The Journal of Physical Chemistry B, 2007. **111**(19): p. 5411-5417.
194. Pegram, L.M. and M.T. Record Jr, *The thermodynamic origin of hofmeister ion effects*. The journal of physical chemistry. B, 2008. **112**(31): p. 9428.
195. Pegram, L. and M. Record, *Quantifying accumulation or exclusion of H<sup>+</sup>, HO<sup>−</sup>, and Hofmeister salt ions near interfaces*. Chemical physics letters, 2008. **467**(1): p. 1-8.
196. Pegram, L.M. and M.T. Record, *Quantifying the roles of water and solutes (denaturants, osmolytes, and Hofmeister salts) in protein and model processes using the solute partitioning model*. Protein Structure, Stability, and Interactions, 2009: p. 179-193.
197. Pegram, L.M., et al., *Why Hofmeister effects of many salts favor protein folding but not DNA helix formation*. Proceedings of the National Academy of Sciences, 2010. **107**(17): p. 7716-7721.
198. Guinn, E.J., et al., *Quantifying why urea is a protein denaturant, whereas glycine betaine is a protein stabilizer*. Proceedings of the National Academy of Sciences, 2011. **108**(41): p. 16932-16937.



199. Record, M.T., et al., *Introductory lecture: Interpreting and predicting Hofmeister salt ion and solute effects on biopolymer and model processes using the solute partitioning model*. Faraday discussions, 2013. **160**: p. 9-44.
200. Record Jr, M.T., et al., *Faraday Discussion 160 Introductory Lecture: Interpreting and Predicting Hofmeister Salt Ion and Solute Effects on Biopolymer and Model Processes Using the Solute Partitioning Model*. Faraday discussions, 2013. **160**: p. 9.
201. Myers, J.K., C. Nick Pace, and J. Martin Scholtz, *Denaturant  $m$  values and heat capacity changes: relation to changes in accessible surface areas of protein unfolding*. Protein Science, 1995. **4**(10): p. 2138-2148.
202. Plaxco, K.W., K.T. Simons, and D. Baker, *Contact order, transition state placement and the refolding rates of single domain proteins*. Journal of molecular biology, 1998. **277**(4): p. 985-994.
203. Collins, K.D., *Sticky ions in biological systems*. Proceedings of the National Academy of Sciences, 1995. **92**(12): p. 5553-5557.
204. Collins, K.D., *Ions from the Hofmeister series and osmolytes: effects on proteins in solution and in the crystallization process*. Methods, 2004. **34**(3): p. 300-311.
205. Collins, K.D., *Ion hydration: Implications for cellular function, polyelectrolytes, and protein crystallization*. Biophysical chemistry, 2006. **119**(3): p. 271-281.
206. Duignan, T.T., D.F. Parsons, and B.W. Ninham, *Collins's rule, Hofmeister effects and ionic dispersion interactions*. Chemical physics letters, 2014. **608**: p. 55-59.
207. Vlachy, N., et al., *Hofmeister series and specific interactions of charged headgroups with aqueous ions*. Advances in colloid and interface science, 2009. **146**(1): p. 42-47.
208. Boström, M., D.R. Williams, and B.W. Ninham, *Ion specificity of micelles explained by ionic dispersion forces*. Langmuir, 2002. **18**(16): p. 6010-6014.
209. Bostrom, M. and B. Ninham, *Dispersion self-free energies and interaction free energies of finite-sized ions in salt solutions*. Langmuir, 2004. **20**(18): p. 7569-7574.
210. Boström, M., W. Kunz, and B.W. Ninham, *Hofmeister effects in surface tension of aqueous electrolyte solution*. Langmuir, 2005. **21**(6): p. 2619-2623.
211. Parsons, D.F. and B.W. Ninham, *Importance of accurate dynamic polarizabilities for the ionic dispersion interactions of alkali halides*. Langmuir, 2009. **26**(3): p. 1816-1823.
212. Parsons, D.F. and B.W. Ninham, *Surface charge reversal and hydration forces explained by ionic dispersion forces and surface hydration*. Colloids and Surfaces A: Physicochemical and Engineering Aspects, 2011. **383**(1): p. 2-9.
213. Welch, D.A., et al., *Using molecular dynamics to quantify the electrical double layer and examine the potential for its direct observation in the in-situ TEM*. Advanced Structural and Chemical Imaging, 2015. **1**(1): p. 1.
214. Pashley, R.M. and M.E. Karaman, *Surfactants and Self-Assembly*. Applied colloid and surface chemistry, 2004: p. 61-77.
215. Kontogeorgis, G.M. and S. Kiil, *Introduction to applied colloid and surface chemistry*. 2016: John Wiley & Sons.
216. Bolt, G., *Analysis of the validity of the Gouy-Chapman theory of the electric double layer*. Journal of Colloid Science, 1955. **10**(2): p. 206-218.
217. Torrie, G. and J. Valleau, *Electrical double layers. 4. Limitations of the Gouy-Chapman theory*. The Journal of Physical Chemistry, 1982. **86**(16): p. 3251-3257.
218. Zukoski, C. and D. Saville, *The interpretation of electrokinetic measurements using a dynamic model of the stern layer: I. The dynamic model*. Journal of colloid and interface science, 1986. **114**(1): p. 32-44.
219. Zukoski, C. and D. Saville, *The interpretation of electrokinetic measurements using a dynamic model of the stern layer: II. Comparisons between theory and experiment*. Journal of colloid and interface science, 1986. **114**(1): p. 45-53.
220. Israelachvili, J.N., *Intermolecular and surface forces*. 2011: Academic press.
221. Barten, D., et al., *Double layer of a gold electrode probed by AFM force measurements*. Langmuir, 2003. **19**(4): p. 1133-1139.

222. Butt, H.-J., *Electrostatic interaction in atomic force microscopy*. Biophysical journal, 1991. **60**(4): p. 777-785.
223. Grabbe, A. and R.G. Horn, *Double-layer and hydration forces measured between silica sheets subjected to various surface treatments*. Journal of colloid and interface science, 1993. **157**(2): p. 375-383.
224. Van Oss, C.J., M.K. Chaudhury, and R.J. Good, *Interfacial Lifshitz-van der Waals and polar interactions in macroscopic systems*. Chemical reviews, 1988. **88**(6): p. 927-941.
225. Tabor, D. and R. Winterton. *The direct measurement of normal and retarded van der Waals forces*. in *Proceedings of the Royal Society of London A: Mathematical, Physical and Engineering Sciences*. 1969. The Royal Society.
226. Margenau, H., *Van der Waals forces*. Reviews of Modern Physics, 1939. **11**(1): p. 1.
227. Hamaker, H., *The London—van der Waals attraction between spherical particles*. physica, 1937. **4**(10): p. 1058-1072.
228. Visser, J., *On Hamaker constants: A comparison between Hamaker constants and Lifshitz-van der Waals constants*. Advances in colloid and interface science, 1972. **3**(4): p. 331-363.
229. Thormann, E., *Surface forces between rough and topographically structured interfaces*. Current opinion in colloid & interface science, 2017. **27**: p. 18-24.
230. Dagastine, R.R., et al., *Calculation of van der Waals forces with diffuse coatings: applications to roughness and adsorbed polymers*. The Journal of Adhesion, 2004. **80**(5): p. 365-394.
231. Grasso, D., et al., *A review of non-DLVO interactions in environmental colloidal systems*. Reviews in Environmental Science and Biotechnology, 2002. **1**(1): p. 17-38.
232. Morag, J., M. Dishon, and U. Sivan, *The governing role of surface hydration in ion specific adsorption to silica: An AFM-based account of the Hofmeister universality and its reversal*. Langmuir, 2013. **29**(21): p. 6317-6322.
233. Donose, B.C., I.U. Vakarelski, and K. Higashitani, *Silica surfaces lubrication by hydrated cations adsorption from electrolyte solutions*. Langmuir, 2005. **21**(5): p. 1834-1839.
234. Pashley, R., *Hydration forces between mica surfaces in aqueous electrolyte solutions*. Journal of colloid and interface science, 1981. **80**(1): p. 153-162.
235. Dishon, M., O. Zohar, and U. Sivan, *From repulsion to attraction and back to repulsion: the effect of NaCl, KCl, and CsCl on the force between silica surfaces in aqueous solution*. Langmuir, 2009. **25**(5): p. 2831-2836.
236. Valle-Delgado, J., et al., *Hydration forces between silica surfaces: Experimental data and predictions from different theories*. The Journal of chemical physics, 2005. **123**(3): p. 034708.
237. Dishon, M., O. Zohar, and U. Sivan, *Effect of cation size and charge on the interaction between silica surfaces in 1: 1, 2: 1, and 3: 1 aqueous electrolytes*. Langmuir, 2011. **27**(21): p. 12977-12984.
238. Meyer, E.E., K.J. Rosenberg, and J. Israelachvili, *Recent progress in understanding hydrophobic interactions*. Proceedings of the National Academy of Sciences, 2006. **103**(43): p. 15739-15746.
239. Holmberg, M., et al., *Nanobubble trouble on gold surfaces*. Langmuir, 2003. **19**(25): p. 10510-10513.
240. Widom, B., P. Bhimalapuram, and K. Koga, *The hydrophobic effect*. Physical Chemistry Chemical Physics, 2003. **5**(15): p. 3085-3093.
241. Perry, J., B. Tiemann, and D. Dougherty, *Reconciling the magnitude of the microscopic and macroscopic hydrophobic effects*. Phys. Lett, 1974. **24**: p. 445.
242. Chandler, D., *Interfaces and the driving force of hydrophobic assembly*. Nature, 2005. **437**(7059): p. 640-647.
243. Frank, H.S. and M.W. Evans, *Free volume and entropy in condensed systems III. Entropy in binary liquid mixtures; partial molal entropy in dilute solutions; structure and thermodynamics in aqueous electrolytes*. The Journal of chemical physics, 1945. **13**(11): p. 507-532.
244. Galamba, N., *Water's structure around hydrophobic solutes and the iceberg model*. The Journal of Physical Chemistry B, 2013. **117**(7): p. 2153-2159.
245. Klotz, I.M., *Protein hydration and behavior*. Science, 1958. **128**(3328): p. 815-822.
246. Kauzmann, W., *Some factors in the interpretation of protein denaturation*. Advances in protein chemistry, 1959. **14**: p. 1-63.

247. Ishida, N., et al., *Nano bubbles on a hydrophobic surface in water observed by tapping-mode atomic force microscopy*. Langmuir, 2000. **16**(16): p. 6377-6380.
248. Tsao, Y.-H., D.F. Evans, and H. Wennerström, *Long-range attractive force between hydrophobic surfaces observed by atomic force microscopy*. SCIENCE-NEW YORK THEN WASHINGTON-, 1993. **262**: p. 547-547.
249. Tsao, Y.H., et al., *Interactions between hydrophobic surfaces. Dependence on temperature and alkyl chain length*. Langmuir, 1991. **7**(12): p. 3154-3159.
250. Ducker, W.A., Z. Xu, and J.N. Israelachvili, *Measurements of hydrophobic and DLVO forces in bubble-surface interactions in aqueous solutions*. Langmuir, 1994. **10**(9): p. 3279-3289.
251. Yoon, R.-H., D.H. Flinn, and Y.I. Rabinovich, *Hydrophobic interactions between dissimilar surfaces*. Journal of colloid and interface science, 1997. **185**(2): p. 363-370.
252. Parker, J.L., P.M. Claesson, and P. Attard, *Bubbles, cavities, and the long-ranged attraction between hydrophobic surfaces*. The Journal of Physical Chemistry, 1994. **98**(34): p. 8468-8480.
253. Attard, P., *Nanobubbles and the hydrophobic attraction*. Advances in colloid and interface science, 2003. **104**(1): p. 75-91.
254. Nguyen, A.V., et al., *Attraction between hydrophobic surfaces studied by atomic force microscopy*. International Journal of Mineral Processing, 2003. **72**(1): p. 215-225.
255. Klein, J., *Surface interactions with adsorbed macromolecules*. Journal of colloid and interface science, 1986. **111**(2): p. 305-313.
256. Milner, S., *Polymer brushes*. Science, 1991. **251**(4996): p. 905-914.
257. Yamamoto, S., et al., *Surface interaction forces of well-defined, high-density polymer brushes studied by atomic force microscopy. 1. Effect of chain length*. Macromolecules, 2000. **33**(15): p. 5602-5607.
258. Yamamoto, S., et al., *Surface interaction forces of well-defined, high-density polymer brushes studied by atomic force microscopy. 2. Effect of graft density*. Macromolecules, 2000. **33**(15): p. 5608-5612.
259. Goodman, D., J.N. Kizhakkedathu, and D.E. Brooks, *Attractive bridging interactions in dense polymer brushes in good solvent measured by atomic force microscopy*. Langmuir, 2004. **20**(6): p. 2333-2340.
260. Biggs, S., *Steric and bridging forces between surfaces bearing adsorbed polymer: an atomic force microscopy study*. Langmuir, 1995. **11**(1): p. 156-162.
261. Kessel, S., et al., *Thermoresponsive PEG-based polymer layers: surface characterization with AFM force measurements*. Langmuir, 2009. **26**(5): p. 3462-3467.
262. Zhulina, E.B., O.V. Borisov, and V.A. Priamitsyn, *Theory of steric stabilization of colloid dispersions by grafted polymers*. Journal of colloid and interface science, 1990. **137**(2): p. 495-511.
263. Gast, A.P. and L. Leibler, *Interactions of sterically stabilized particles suspended in a polymer solution*. Macromolecules, 1986. **19**(3): p. 686-691.
264. Manor, O., et al., *Polymeric stabilized emulsions: Steric effects and deformation in soft systems*. Langmuir, 2012. **28**(10): p. 4599-4604.
265. Napper, D.H., *Steric stabilization*. Journal of colloid and interface science, 1977. **58**(2): p. 390-407.
266. Hooper, J.B. and K.S. Schweizer, *Contact aggregation, bridging, and steric stabilization in dense polymer-particle mixtures*. Macromolecules, 2005. **38**(21): p. 8858-8869.
267. Swenson, J., M. Smalley, and H. Hatharasinghe, *Mechanism and strength of polymer bridging flocculation*. Physical Review Letters, 1998. **81**(26): p. 5840.
268. Ortiz, C. and G. Hadziioannou, *Entropic elasticity of single polymer chains of poly (methacrylic acid) measured by atomic force microscopy*. Macromolecules, 1999. **32**(3): p. 780-787.
269. Xue, Y., et al., *Quantifying thiol-gold interactions towards the efficient strength control*. Nature communications, 2014. **5**.
270. Gill, P., T.T. Moghadam, and B. Ranjbar, *Differential scanning calorimetry techniques: applications in biology and nanoscience*. J Biomol Tech, 2010. **21**(4): p. 167-193.
271. Schild, H.G. and D.A. Tirrell, *Microcalorimetric detection of lower critical solution temperatures in aqueous polymer solutions*. Journal of Physical Chemistry, 1990. **94**(10): p. 4352-4356.

272. Thormann, E., *On understanding of the Hofmeister effect: how addition of salt alters the stability of temperature responsive polymers in aqueous solutions*. Rsc Advances, 2012. **2**(22): p. 8297-8305.
273. Meurant, G., *Introduction to dynamic light scattering by macromolecules*. 2012: Elsevier.
274. Wu, C. and X. Wang, *Globule-to-coil transition of a single homopolymer chain in solution*. Physical Review Letters, 1998. **80**(18): p. 4092.
275. Sauerbrey, G., *Verwendung von Schwingquarzen zur Wägung dünner Schichten und zur Mikrowägung*. Zeitschrift für Physik A Hadrons and Nuclei, 1959. **155**(2): p. 206-222.
276. McNamara, T.P. and C.F. Blanford, *A sensitivity metric and software to guide the analysis of soft films measured by a quartz crystal microbalance*. Analyst, 2016. **141**(10): p. 2911-2919.
277. Reviakine, I., D. Johannsmann, and R.P. Richter, *Hearing what you cannot see and visualizing what you hear: interpreting quartz crystal microbalance data from solvated interfaces*, 2011, ACS Publications.
278. Jalili, N. and K. Laxminarayana, *A review of atomic force microscopy imaging systems: application to molecular metrology and biological sciences*. Mechatronics, 2004. **14**(8): p. 907-945.
279. Quénet, D., E.K. Dimitriadis, and Y. Dalal, *Atomic force microscopy of chromatin*. 2012: INTECH Open Access Publisher.
280. Butt, H.-J., B. Cappella, and M. Kappl, *Force measurements with the atomic force microscope: Technique, interpretation and applications*. Surface science reports, 2005. **59**(1): p. 1-152.
281. Martin, Y., C.C. Williams, and H.K. Wickramasinghe, *Atomic force microscope-force mapping and profiling on a sub 100-Å scale*. Journal of Applied Physics, 1987. **61**(10): p. 4723-4729.
282. Meyer, G. and N.M. Amer, *Simultaneous measurement of lateral and normal forces with an optical-beam-deflection atomic force microscope*. Applied physics letters, 1990. **57**(20): p. 2089-2091.
283. Ducker, W.A., T.J. Senden, and R.M. Pashley, *Direct measurement of colloidal forces using an atomic force microscope*. Nature, 1991. **353**(6341): p. 239.
284. Burnham, N., et al., *Comparison of calibration methods for atomic-force microscopy cantilevers*. Nanotechnology, 2002. **14**(1): p. 1.
285. Sader, J.E., et al., *Method for the calibration of atomic force microscope cantilevers*. Review of Scientific Instruments, 1995. **66**(7): p. 3789-3798.
286. Sader, J.E., J.W. Chon, and P. Mulvaney, *Calibration of rectangular atomic force microscope cantilevers*. Review of Scientific Instruments, 1999. **70**(10): p. 3967-3969.
287. Leite, F.L., et al., *Theoretical models for surface forces and adhesion and their measurement using atomic force microscopy*. International journal of molecular sciences, 2012. **13**(10): p. 12773-12856.
288. Derjaguin, B.V., *Untersuchungen über die Reibung und Adhäsion, IV*. Colloid & polymer science, 1934. **69**(2): p. 155-164.

**PAPER I**



Cite this: *Phys. Chem. Chem. Phys.*,  
2015, 17, 6359

Received 5th December 2014,  
Accepted 28th January 2015

DOI: 10.1039/c4cp05677a

www.rsc.org/pccp

## Hofmeister effect of salt mixtures on thermo-responsive poly(propylene oxide)

Saeed Zajforoushan Moghaddam and Esben Thormann\*

The Hofmeister series is a classification of ions regarding their ability to stabilize or destabilize aqueous solutions of proteins, polymers and other molecules which are partly miscible with water. In this study, we employ differential scanning calorimetry to investigate how the stability of aqueous solutions of poly(propylene oxide) is affected by mixtures of ions with different location in the Hofmeister series. Our results show that the Hofmeister effects of pure salt species are not always linearly additive and that the relative effect of some ions can be reversed depending on the composition of the salt mixture as well as by the absolute and relative concentration of the different species. We suggest that these results can lead to a better understanding of the potential role of the Hofmeister effect in regulation of biological processes, which does always take place in salt mixtures rather than solutions containing just single salt species.

### 1. Introduction

For more than 100 years, it has been known that the presence of different ions affects the solubility of macromolecules in aqueous solutions.<sup>1–8</sup> In the first systematic study, Franz Hofmeister demonstrated that the coil conformation of proteins in solution could be stabilized by some ions and destabilized by others and that the effect on the protein stability always followed a specific trend with respect to the types of ions.<sup>1</sup> The order of the different ions according to their stabilizing or destabilizing effect is today known as the Hofmeister series.<sup>8–13</sup> Later it has been shown that this observation is a more universal phenomenon and that the Hofmeister series can be used to predict how the presence of different ions affects the physicochemical properties of many aqueous phenomena like swelling/deswelling of hydrogels,<sup>14</sup> proteins crystallization,<sup>15</sup> enzymatic activity,<sup>16</sup> micellization and emulsions stability<sup>17</sup> etc.<sup>12,13,18</sup> It has also been demonstrated that anions have a more pronounced effect than cations.<sup>3–5</sup> The Hofmeister series for some common monovalent anions is:



Here, ions to the left show a salting-out effect on macromolecules, *i.e.* favoring a compact globular conformation, while ions to the right have a salting-in effect on macromolecules, *i.e.* supporting an extended conformation and solution stability.

In spite of the numerous investigations on the Hofmeister effect, it is still obscure to what extent the effect has a role in

nature, *e.g.* in regulation of biological processes. Firstly, it is noticeable that the Hofmeister effect starts to become significant at around physiological salt concentrations where long-ranged electrostatic interactions are screened and ion hydration becomes increasingly important.<sup>12,13</sup> Secondly, biological systems contain a mixture of different ions, which potentially should have a large Hofmeister effect.<sup>13,19</sup> Keeping all this in mind, peculiarly almost all research on the Hofmeister effect on solutions of polymers, proteins and enzymes are focused on the effect of single salt species. This is in contrast to almost all natural systems ranging from body fluids to sea water, where one will find a mixture of different salts. Accordingly, understanding the Hofmeister effect originating from salt mixtures will be the first step towards understanding the relevance of the Hofmeister effect in biological systems. Furthermore, comparing the effect of salt mixtures with their constituent's solutions can be utilized to develop our understanding of the molecular mechanisms behind the Hofmeister effect.

In this paper, the stability of dilute aqueous solutions of poly(propylene oxide) (PPO) in presence of single salt species and salt mixtures is investigated. PPO in aqueous solution undergoes hydrophobic dehydration and phase separation upon heating with a phase separation temperature which depends on both polymer concentration and molecular weight.<sup>20,21</sup> As a model system used to mimic the Hofmeister effect on hydrophobic collapse of macromolecules, PPO has some advantages compared to other well-known thermo-responsive polymers. Compared to for example poly(ethylene oxide) (PEO), PPO has a relatively low phase separation temperature, which can be easily tuned to a biologically relevant range.<sup>10,22,23</sup>

However at the same salt concentrations, it renders more pronounced changes in phase separation temperature compared

Department of Chemistry, Technical University of Denmark, Building 206, Kemitorvet, 2800 Lyngby, Denmark. E-mail: esth@kemi.dtu.dk; Tel: +45 4525 2439



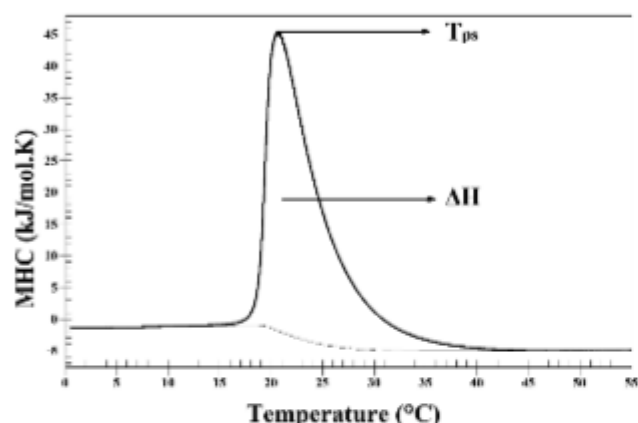


Fig. 1 DSC thermogram of PPO 0.5 wt% aqueous solution. The approximate phase separation temperature ( $T_{ps}$ ) and enthalpy change of dehydration ( $\Delta H$ ) are obtainable as the peak temperature and the integral of the peak, respectively.

to for example poly(*N*-isopropylacrylamide) PNIPAM, which thereby allows fine details to be observed.<sup>4,10,20,22</sup> Hence, it is a suitable system for studies of the Hofmeister effect of salt mixtures. For these investigations, differential scanning calorimetry (DSC) is employed to compare phase separation parameters of the solutions with different salt species and different salt concentrations. Besides measuring precise and reproducible values of phase separation temperatures, this technique provides helpful information on thermodynamical parameters of phase separation phenomenon, such as the enthalpy change upon dehydration (Fig. 1). Hereon, we first explore the effect of four different pure salts on the solubility of PPO, and then obtain the corresponding results for salt mixtures, with a systematic change in the types of anions and in salt concentration.

## 2. Experimental section

### 2.1. Materials

Poly(propylene oxide) with a number average molar mass ( $M_n$ ) of 2000 g mol<sup>-1</sup> and analytical grades of salts were all purchased from Sigma-Aldrich. Aqueous solutions of 0.5 wt% of PPO and different concentrations of salts were prepared using a nutating mixer at 5 °C for 24 hours.

### 2.2. Differential scanning calorimetry (DSC)

Thermograms were obtained using a differential scanning calorimeter (Nano DSC, TA Instruments), with a constant heating rate of 0.2 °C min<sup>-1</sup> and under a pressure of 3 atm. All solutions were sufficiently degassed before measurements in order to avoid bubble formation during heating. The obtained raw heat data directly depends on the mass of solute, why all thermograms were transformed to molar heat capacity, using the values of calorimeter cell volume, solutions density, PPO molecular weight and concentration.<sup>7</sup> Measurements were repeated 3 times for the pure aqueous solution of PPO, which showed desirable reproducibility (standard deviation of  $\pm 0.09$  °C in  $T_{ps}$  and  $\pm 3.5$  kJ mol<sup>-1</sup> in  $\Delta H$ ).

## 3. Results and discussion

### 3.1. Effect of pure salts

In the first series of experiments, the phase separation of PPO in pure water and in 0.1, 0.4, 0.8 and 1.0 M solutions of NaSCN, NaI, NaBr and NaCl is investigated. Fig. 2 depicts DSC data of these solutions in terms of phase separation temperatures (Fig. 2a) and phase separation enthalpies (Fig. 2b). It is observed that addition of NaBr and NaCl both lower the phase separation temperature. For these two salts, the dependency on the salt concentration is approximately linear, and with NaCl showing the strongest salting-out effect. In contrast, addition of NaSCN increases the phase separation temperature but with a declining slope with increasing salt concentration. Addition of NaI has a limited effect on the phase separation temperature and changes from a weak salting-in effect at low salt concentrations to a weak salting-out effect at high salt concentrations. The observed order of salting-in and salting-out effects of the salts is in accordance with the Hofmeister series of the anions. Although the phase separation enthalpies (Fig. 2b) seem to follow the same order, with addition of NaCl given rise the largest increase and addition of NaSCN leads to the largest decrease, the dependency of the concentrations of added salt is less clear. One exception is NaSCN which appears to give rise to a decrease in phase separation enthalpy, which scales almost linearly with the salt concentration. For the three other salts the effect of changes in phase separation enthalpies are relatively small.

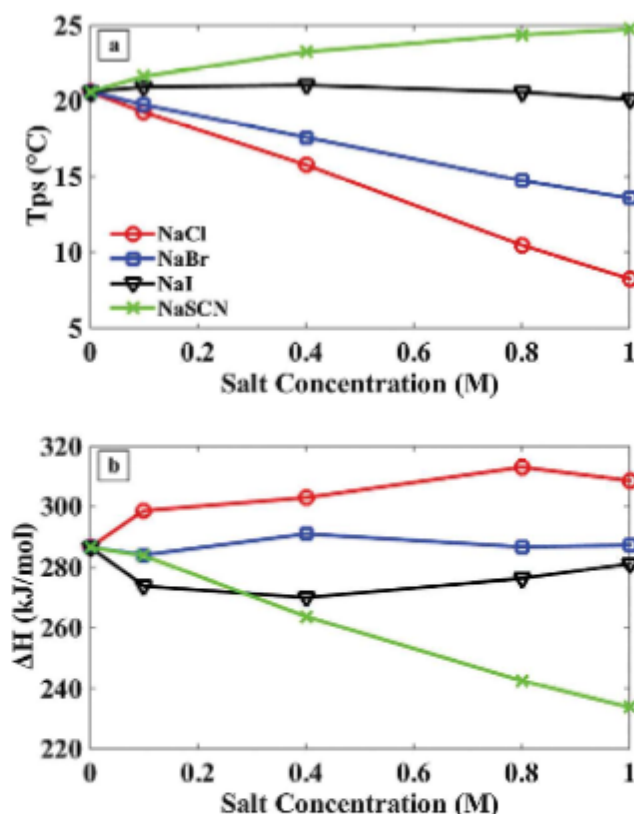


Fig. 2 DSC data of 0.5 wt% PPO in different salt solutions. (a) Phase separation temperature and (b) enthalpy change of dehydration.

In the early studies, the Hofmeister effect was often discussed in terms of different water structure breaking or water structure making abilities of ions.<sup>2,24,25</sup> However, from data of the ion hydration enthalpies and entropies it became clear that the Hofmeister effect cannot solely be explained on the basis of interaction between the ions and water molecules.<sup>26–29</sup> Instead, one must look at both ion and polymer hydrations and how the simultaneous presence of ions and polymer affect the hydration of both components. This was first suggested in a work by Florin *et al.* where relative salting-in and salting-out effect of different ions on PEO aqueous solutions was explained by the effect of an overlap in hydrations zones of the ions and polymer chains.<sup>23</sup> Basically, an overlap in the hydration zones, and thereby partial dehydration of an ion and a hydrophobic polymer consists of a repulsive and an attractive component, *i.e.* unfavourable dehydration of the ion will lead to a salting-out effect, while favourable dehydration of the hydrophobic polymer will lead to a salting-in effect. The magnitudes of the salting-out and salting-in effect will however depend on the type of ions and the type of polymer, which thus both explain the nature of the order of ions in the Hofmeister series and why the Hofmeister ions have a different absolute effect on different polymer systems. Later, Zhang *et al.* has used a similar model to explain the Hofmeister effect on aqueous solutions of PNIPAM.<sup>4–6,30</sup> However, in their works, a third component related to dehydration of the polar amide groups of PNIPAM due to competition with strongly hydrated ions was included.<sup>30,31</sup> This rather simple explanation of the Hofmeister effect is in agreement with a more recent study by Pegram and Record Jr. where it was found that ions with a typical salting-out effect are depleted from air–water interface, while ions with a typical salting-in are more favourably adsorbed.<sup>32,33</sup>

Seen in relation to the present study of the Hofmeister effect of PPO, the above described mechanisms suggest that  $\text{SCN}^-$  and to some extent  $\text{I}^-$  should be attracted to the PPO/water interface, while  $\text{Br}^-$  and  $\text{Cl}^-$  should be depleted from the polymer. This interpretation is also in agreement with two other observations from the DSC experiments. Firstly, the declining increase in the salting-out effect with increasing NaSCN concentration can be explained by the finite surface region of the PPO chains, meaning that the last added  $\text{SCN}^-$  will contribute relatively less to the salting-in effect. This is even more pronounced with  $\text{I}^-$ , which is less attracted to the hydrophobic interface and a large amount of added salt thus contribute more to the salting-out effect than the salting-in effect. The second observation is the significant decrease in phase separation enthalpy by addition of NaSCN, which suggests that association of  $\text{SCN}^-$  at the PPO/water interface lowers the degree of hydrophobic hydration of the polymer.

In contrast, addition of NaBr and NaCl does not show any significant effect of salt concentration, because the ions are depleted from the PPO interface independently of the salt concentration. This qualitative correlation between different ions polarizability and their tendency to accumulate at the polymer interface is in accordance with a more quantitative

model for ions specific dispersion forces as previously described by Ninham and co-workers.<sup>12,18</sup>

### 3.2. Effect of salt mixtures

In the following section, we examine the Hofmeister effect on phase separation of PPO solutions, in the case where two salts in different concentrations are mixed. In order to follow the effect of having two different salts in the solution, our approach is to systematically vary the concentration of one salt while keeping the concentration of the other salt constant at 0.1 M. By doing so it becomes easy to investigate the effect of adding a second type of salt to the solutions only containing different concentrations of the first type of salt.

**3.2.1. Mixtures of two salts with salting-out effect.** As discussed in relation to Fig. 2, NaBr and NaCl both show a salting-out effect with a linear dependency on the salt concentration and with NaCl showing a stronger salting-out effect. In the first case with respect to mixtures of the salts, we kept the concentration of NaCl constant at 0.1 M while systematically varying the concentration of NaBr to investigate how the small amount of added NaCl affects the system compared to the solutions where only NaBr is added. As seen in Fig. 3a, addition of 0.1 M NaCl leads to a nearly constant decrement in the phase separation temperature of approximately 1 °C, at all concentrations of NaBr. The relative decrease in phase separation temperatures corresponds to the effect of adding 0.1 M NaCl to the pure PPO system, which means that the combined effect of NaCl and NaBr in this case appears to be linearly additive. Although the change in the phase separation enthalpies by addition of both pure NaCl and NaBr are small, it is observed from Fig. 3b that the values of the mixtures are found in between the values of pure salts.

In the second case, we kept the concentration of NaBr constant at 0.1 M while systematically varying the concentration of NaCl in order to study how a small amount of added NaBr affects the system compared to the system where only NaCl is added. As seen in Fig. 3c, addition of a small amount of NaBr has a more complex effect, which depends on NaCl concentration. At low NaCl concentrations, addition of 0.1 M NaBr is given rise to a relative salting-out effect similar to what is discussed above. However, as the concentration of NaCl is increased, the relative salting-out effect of NaBr declines and at a NaCl concentration higher than 0.6 M, NaBr is given rise to a relative salting-in effect. With respect to the phase separation enthalpies, the changes are still small and the values are between the values of pure salts.

In the case of the Hofmeister effect of the pure salts, we discussed how the salting-out effect of both NaBr and NaCl salts could be explained by unfavourable overlaps in the hydration zones of the ions and PPO, which leads to effective repulsive interactions between the ions and the polymer chains. Further, the difference between the effect of NaBr and NaCl can be explained by the different hydration strength of  $\text{Br}^-$  and  $\text{Cl}^-$ .

The results presented in Fig. 3 can be interpreted by the same mechanism. But it is further demonstrated that in the case of salt mixtures, one not only has competition between



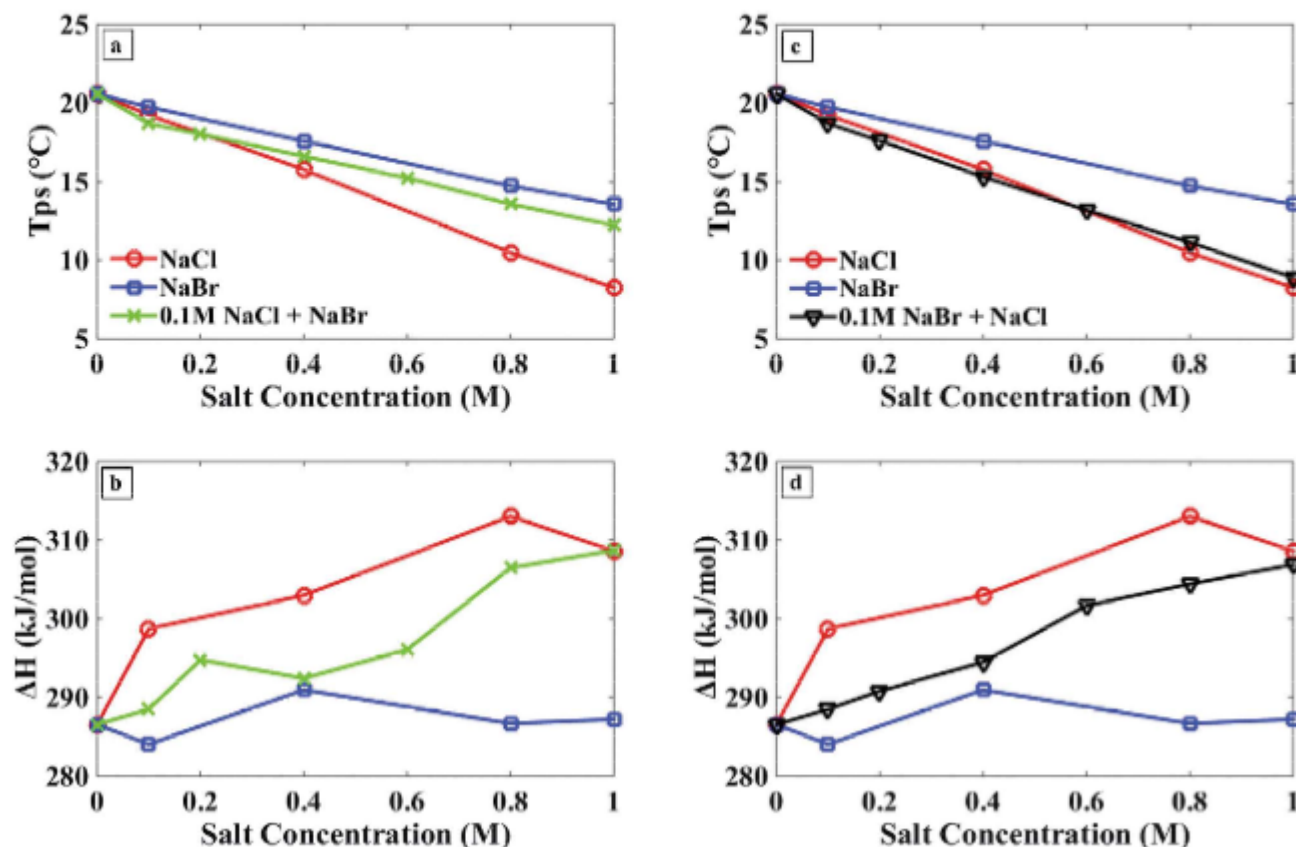


Fig. 3 DSC data of PPO 0.5 wt% in presence of NaCl and NaBr mixtures. (a, b) Addition of 0.1 M of NaCl to solutions of PPO and NaBr. (c, d) Addition of 0.1 M of NaBr to solutions of PPO and NaCl. In the case of the salt mixtures, the salt concentration refer to the concentration of the component which is varied.

hydration of ions and polymers but also between the ions of different hydration strengths. This means that we can observe an additive or non-additive Hofmeister effect depending on the total salt concentration and the ratio of added species. The linear additive increment in total salting out effect seen when a small amount of NaCl is mixed with various concentrations of NaBr (Fig. 3a) can thus simply be explained by the fact that both hydrated anions have unfavourable interaction with the PPO chains. The additivity of the effect is therefore rationalized by the same argument as why the salting-out effect of pure NaBr or NaCl scales linearly with the salt concentration. With the same argumentation, we can explain the complex effect of mixing a small amount of NaBr with different concentrations of NaCl (Fig. 3c). At low concentrations of NaCl, there are enough water molecules available for both types of anions to get fully hydrated, which thus collaterally interact with the hydration zone of PPO in order to show an additive salting-out effect. At higher amounts of  $\text{Cl}^-$ , the two types of anions start to compete for the limited number of water molecules and the salting-out effect of  $\text{Br}^-$  thus becomes less and less pronounced. After a certain concentration (0.6 M NaCl in this case)  $\text{Br}^-$  seems to preferably accumulate at the polymer/water interfacial area, where it does not directly compete with  $\text{Cl}^-$  for the water molecules and at the same time directly associates with polymer backbone. This competition for limited number of water

molecules can be understood more quantitatively according to the hydration number of the anions. Considering 1 M solution of a monovalent salt, roughly 50 water molecules are available per cation-anion pair. In the case of sodium halides, one will expect approximately 5–6 water molecules in the primary hydration zone of  $\text{Na}^+$  and 6–8 water molecules for  $\text{Cl}^-$  and  $\text{Br}^-$  primary hydration zones.<sup>34,35</sup> Regarding also the values of secondary ion hydration zone, it is indicated that roughly one third of all the water molecules are instantly involved in ion hydration, which can support the idea of competition between anions for limited number of water molecules. Such a competitive effect of  $\text{Cl}^-$  and  $\text{Br}^-$  can successfully elucidate the relative salting-in effect of NaBr in the mentioned concentration regime.

**3.2.2. Mixtures of two salts with salting-out and salting-in effect.** Next, we will address the effect of mixing a salt with a salting-in effect and a salt with a salting-out effect. In the first case, we kept the concentration of NaCl constant at 0.1 M while systematically varying the concentration of NaSCN in order to investigate how a small amount of NaCl (the salt with a salting-out effect) affects the system compared to the systems where only NaSCN (the salt with a salting-in effect) is added. Fig. 4a illustrates that adding 0.1 M NaCl to solutions of PPO and NaSCN leads to a constant decline in the phase transition temperature. The relative salting-out effect of NaCl directly corresponds to the salting-out effect of 0.1 M NaCl on PPO

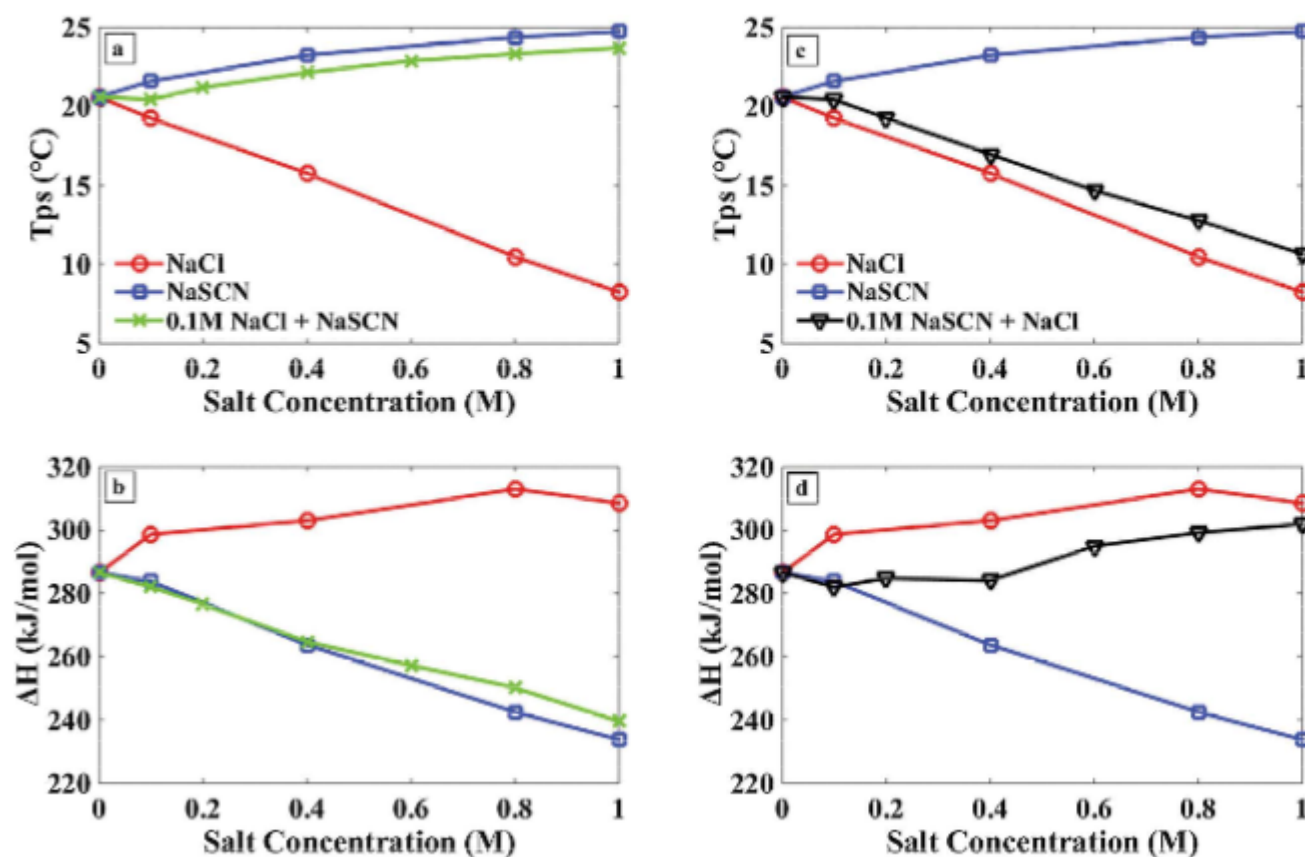


Fig. 4 DSC data of PPO 0.5 wt% in presence of NaCl and NaSCN mixtures. (a, b) Addition of 0.1 M of NaCl to solutions of PPO and NaSCN. (c, d) Addition of 0.1 M of NaSCN to solutions of PPO and NaCl. In the case of the salt mixtures, the salt concentration refer to the concentration of the component which is varied.

solution, which shows that the effects of NaCl and NaSCN in this case are linearly additive. Interestingly, the phase separation enthalpies (Fig. 4b) lie close to the values of pure NaSCN, suggesting the enthalpy change of PPO dehydration to be almost unaffected by the presence of NaCl.

In the second case, we kept the concentration of NaSCN constant at 0.1 M while systematically varied the concentration of NaCl, in order to investigate how a small amount of NaSCN (the salt with a salting-in effect) affects the system compared to the system including only NaCl (the salt with a salting-out effect). As seen in Fig. 4c, the effect appears to be linearly additive at all concentrations of NaCl, as it was also seen in the reversed case in Fig. 4a. The relative salting-in effect of NaSCN is also nearly identical to the salting-in effect of 0.1 M NaSCN added to pure PPO solution. The hydration enthalpies only increase slightly with increasing NaCl concentration and compared to the system containing PPO and NaCl, the values are lowered by an almost constant amount corresponding to the effect of adding 0.1 M NaSCN to the pure PPO solution. This means the hydration enthalpies are dominated by NaSCN rather than NaCl.

The linear additive Hofmeister effect of mixtures of NaCl and NaSCN supports the interpretation that salting-in and salting-out anions modify macromolecular coil-globule transition through two different mechanisms with little interference,

*i.e.*  $\text{SCN}^-$  are preferentially associated with the PPO chains and given rise to a salting-in effect, while  $\text{Cl}^-$  effectively repel the PPO chains and give rise to a salting-out effect. Accordingly, the Hofmeister effect of NaCl and NaSCN are additive with respect to phase separation temperatures, while the change in dehydration enthalpies are dominated by NaSCN.

**3.2.3. Mixtures of two salts with salting-in effect.** As a final situation, we investigate the effect of mixing NaSCN and NaI which are two salts both showing a salting-in effect. In the first case, we kept the concentration of NaI constant at 0.1 M while systematically varied the concentration of NaSCN with the purpose of investigating how a small amount of a salt with a weaker salting-out effect (NaI) affects the system compared to the system where only the salt with a stronger salting-in effect (NaSCN) is added. As seen in Fig. 5a, addition of a small amount of NaI to solutions of PPO and NaSCN seems to have a negligible effect on the phase separation temperature, however with a weak tendency towards a small relative salting-in effect at low NaSCN concentration and a small relative salting-out effect at high NaSCN concentrations. With respect to the phase separation enthalpies, it is evident that the effect is dominated by the salt species leading to the largest decrease. This means that at low NaSCN concentrations the values seem to be dominated by the effect of NaI while at higher NaSCN concentrations the effect is dominated by the effect of NaSCN.

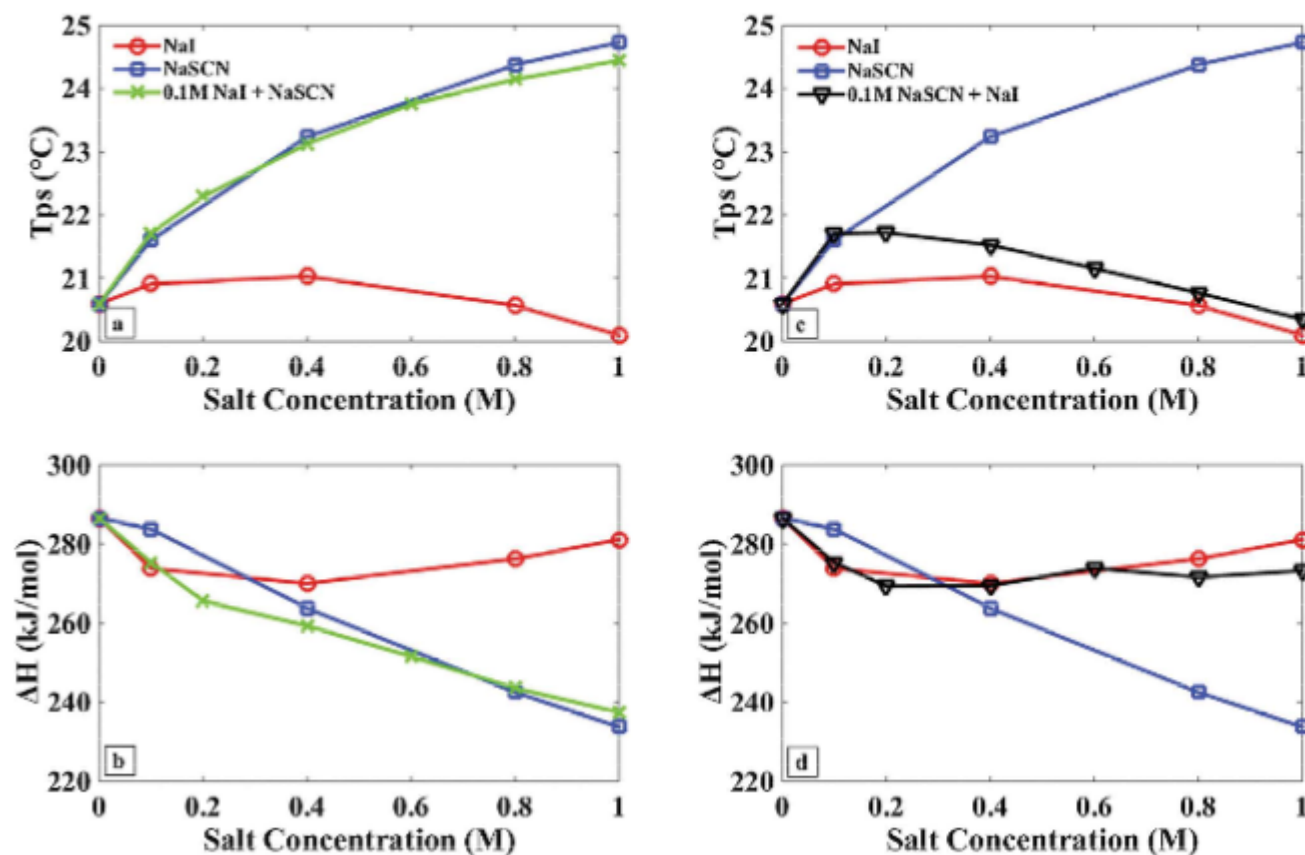


Fig. 5 DSC data of PPO 0.5 wt% in presence of NaSCN and NaI mixtures. (a, b) Addition of 0.1 M of NaI to solutions of PPO and NaSCN. (c, d) Addition of 0.1 M of NaSCN to solutions of PPO and NaI. In the case of the salt mixtures, the salt concentration refer to the concentration of the component which is varied.

In the other case, we kept the concentration of NaSCN constant at 0.1 M while systematically varied the concentration of NaI (Fig. 4c). For a relative low NaI concentration (up to around 0.4 M), the salting-in effect is completely dominated by the 0.1 M added NaSCN. At higher NaI concentrations, the salting-in effect of NaSCN becomes less and less pronounced and at the highest NaI concentration the combined effect is leading to a salting-out effect. It should however be noted that the effect of pure NaI also have a turning point at 0.4 M and that pure NaI at concentrations higher than 0.8 M has an effective salting-out effect. Regarding the phase transition enthalpies, addition of 0.1 M NaSCN has apparently no considerable effect compared to systems containing different concentrations of pure NaI. Nevertheless, regarding the overall trends, it seems that a slight decrement in enthalpy is associated with addition of 0.1 M NaSCN. This minor effect is in agreement with negligible decline in enthalpy with addition of 0.1 M NaSCN to pure PPO solution.

Regarding the propensity of both  $\text{SCN}^-$  and  $\text{I}^-$  to accumulate at the polymer/water interface together with the borderline nature of  $\text{I}^-$ , we can explain the observed trends. At low concentrations of both anions, where there exist vast polymer surface region, the mixture given rise to an increase in the total salting-in effect. Noteworthy, these salting-in effects are however not linearly additive, which suggests more favourable

adsorption of  $\text{SCN}^-$  compared to  $\text{I}^-$ . This is however in line with the fact that the salting-in effect of pure NaSCN and NaI also show a non-linear dependency of the salt concentration. At higher concentrations of NaSCN, direct association of  $\text{I}^-$  with polymer backbone becomes more and more unlikely and NaI thus starts to give rise to a relative salting-out effect.

## 4. Summary and conclusions

The presented results clearly demonstrate that mixture of different salts generally has a more complicated Hofmeister effect on solubility and conformational stability of macromolecules compared to the effect of pure salts. The overall effect strongly depends on the nature of the ion species, the absolute concentration and the relative ratio of the salts. In this study, we tried to obtain a basic understanding of three main salt mixture systems, using a systematic change in the three factors mentioned above. As the most rudimentary system, mixture of two salts with considerable differences in nature (one salting-in and other salting-out) results in linear additive Hofmeister effects. Each ionic element applies its own specific effect on macromolecule stability, regardless of presence or absence of the other ion. This important feature lets us to predict the Hofmeister effect of such mixtures, only by having corresponding



data of each pure salt. Mixtures of two salts with relatively closer natures however show a more complicated trend. In the case of mixing two salts with a salting-in effect, the stronger component (the one with higher propensity toward accumulating at the polymer/water interface) dominates the overall salting-in behavior of the mixture, while the other component is less favored to accumulate at the polymer/water interface. In this case, we observe a reversed effect of NaI, changing from a salting-in effect (when added together with low concentrations of NaSCN) to a relative salting-out effect (when added together with high concentrations of NaSCN). Analogously with respect to mixing two salts with a salting-out effect, the overall salting-out behavior of the mixture is also surmounted by the stronger component (the one with higher hydration capacity), while the other component may tend to directly associate with the polymer backbone. In this case it meant that we observe a reversed effect of NaBr, changing from a salting-out effect when added alone to a relative salting-in effect when added together with high concentrations of NaCl.

These basic explanations can be the first step towards understanding the important role of Hofmeister effect in biological systems. In this case, several reports are available on biological systems where a combination of ions exists. Enzymatic activity and stability have been shown to be strongly sensitive to the nature and concentration of present ions.<sup>16,36,37</sup> The same drastic dependency has been reported for bacterial growth rate that can be of great importance in both biology and in relation to food conservation.<sup>38,39</sup> As more specific cases, it has been reported that presence of some chaotropic anions like  $\text{SCN}^-$  and  $\text{ClO}_4^-$  interferes and decreases the iodide transport to infants via human breast milk, which may negatively affect thyroid-related functions.<sup>40,41</sup> Precipitation and formation of amyloid fibrils that is the suspected origin of Alzheimer disease has also been confirmed to be susceptible to variations in type and amount of dissolved ions.<sup>42,43</sup> With respects to all the cases enumerated above, it is confirmed that healthy biological functioning requires an almost fixed combination of the salts, and any variation in the ions types or concentrations can impose some unwanted side-effects. Knowing the key role of the ions mixtures in complex biological systems and based on what we simply explained here, studying the Hofmeister effect in solutions containing more ionic components or even different macromolecules can be the next step for future investigations.

## Acknowledgements

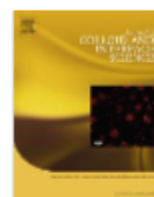
The authors acknowledge financial support from the Swedish Research Council, VR.

## Notes and references

- 1 F. Hofmeister, *Arch. Exp. Pathol. Pharmacol.*, 1888, **25**, 1–30.
- 2 P. Jungwirth and P. S. Cremer, *Nat. Chem.*, 2014, **6**, 261–263.
- 3 W. Xie, C. Liu, L. Yang and Y. Gao, *Sci. China: Chem.*, 2014, **57**, 36–47.
- 4 Y. Zhang and P. S. Cremer, *Annu. Rev. Phys. Chem.*, 2010, **61**, 63–83.
- 5 Y. Zhang and P. S. Cremer, *Curr. Opin. Chem. Biol.*, 2006, **10**, 658–663.
- 6 Y. Zhang, S. Furry, L. B. Sagie, Y. Cho, D. E. Bergbreiter and P. S. Cremer, *J. Phys. Chem. C*, 2007, **111**, 8916–8924.
- 7 E. Thormann, *RSC Adv.*, 2012, **2**, 8297–8305.
- 8 J. Heyda and J. Dzubiella, *J. Phys. Chem. B*, 2014, **118**, 10979–10988.
- 9 M. M. Bloksma, D. J. Bakker, C. Weber, R. Hoogenboom and U. S. Schubert, *Macromol. Rapid Commun.*, 2010, **31**, 724–728.
- 10 B. A. Deyerle and Y. Zhang, *Langmuir*, 2011, **27**, 9203–9210.
- 11 R. Freitag and F. Garret-Flaudy, *Langmuir*, 2002, **18**, 3434–3440.
- 12 W. Kunz, P. Lo Nostro and B. W. Ninham, *Curr. Opin. Colloid Interface Sci.*, 2004, **9**, 1–18.
- 13 P. Lo Nostro and B. W. Ninham, *Chem. Rev.*, 2012, **112**, 2286–2322.
- 14 Y. Okazaki, K. Ishizuki, S. Kawauchi, M. Satoh and J. Komiyama, *Macromolecules*, 1996, **29**, 8391–8397.
- 15 K. D. Collins, *Methods*, 2004, **34**, 300–311.
- 16 J.-Q. Lai, Z. Li, Y.-H. Lu and Z. Yang, *Green Chem.*, 2011, **13**, 1860–1868.
- 17 I. B. Ivanov, R. I. Slavchov, E. S. Basheva, D. Sidzhakova and S. I. Karakashev, *Adv. Colloid Interface Sci.*, 2011, **168**, 93–104.
- 18 A. Salis and B. W. Ninham, *Chem. Soc. Rev.*, 2014, **43**, 7358–7377.
- 19 W. Kunz, *Curr. Opin. Colloid Interface Sci.*, 2010, **15**, 34–39.
- 20 D. Roy, W. L. A. Brooks and B. S. Sumerlin, *Chem. Soc. Rev.*, 2013, **42**, 7214–7243.
- 21 S. Dai, P. Ravi and K. C. Tam, *Soft Matter*, 2009, **5**, 2513–2533.
- 22 E. Boucher and P. Hines, *J. Polym. Sci., Polym. Phys. Ed.*, 1976, **14**, 2241–2251.
- 23 E. Florin, R. Kjellander and J. C. Eriksson, *J. Chem. Soc., Faraday Trans. 1*, 1984, **80**, 2889–2910.
- 24 X. Chen, T. Yang, S. Kataoka and P. S. Cremer, *J. Am. Chem. Soc.*, 2007, **129**, 12272–12279.
- 25 Y. Cho, Y. Zhang, T. Christensen, L. B. Sagie, A. Chilkoti and P. S. Cremer, *J. Phys. Chem. B*, 2008, **112**, 13765–13771.
- 26 S. C. Flores, J. Kherb and P. S. Cremer, *J. Phys. Chem. C*, 2012, **116**, 14408–14413.
- 27 D. Parsons, M. Bostrom, T. Maceina, A. Salis and B. W. Ninham, *Langmuir*, 2009, **26**, 3323–3328.
- 28 Y. Zhang and P. S. Cremer, *Proc. Natl. Acad. Sci. U. S. A.*, 2009, **106**, 15249–15253.
- 29 A. Salis, F. Cugia, D. F. Parsons, B. W. Ninham and M. Monduzzi, *Phys. Chem. Chem. Phys.*, 2012, **14**, 4343–4346.
- 30 Y. Zhang, S. Furry, D. E. Bergbreiter and P. S. Cremer, *J. Am. Chem. Soc.*, 2005, **127**, 14505–14510.
- 31 K. B. Rembert, J. Paterová, J. Heyda, C. Hilty, P. Jungwirth and P. S. Cremer, *J. Am. Chem. Soc.*, 2012, **134**, 10039–10046.
- 32 L. M. Pegram and M. T. Record, *J. Phys. Chem. B*, 2007, **111**, 5411–5417.

- 33 M. T. Record, E. Guinn, L. Pegram and M. Capp, *Faraday Discuss.*, 2013, **160**, 9–44.
- 34 Y. Marcus, *Ion properties*, CRC Press, 1997.
- 35 Y. Marcus, *Chem. Rev.*, 2009, **109**, 1346–1370.
- 36 P. Bauduin, A. Renoncourt, D. Touraud, W. Kunz and B. W. Ninham, *Curr. Opin. Colloid Interface Sci.*, 2004, **9**, 43–47.
- 37 A. Kumar, A. Rani and P. Venkatesu, *New J. Chem.*, 2015, DOI: 10.1039/c4nj01596g.
- 38 P. Mester, M. Wagner and P. Rossmanith, *Ecotoxicol. Environ. Saf.*, 2015, **111**, 96–101.
- 39 P. Lo Nostro, B. W. Ninham, A. Lo Nostro, G. Pesavento, L. Fratoni and P. Baglioni, *Phys. Biol.*, 2005, **2**, 1–7.
- 40 P. K. Dasgupta, A. B. Kirk, J. V. Dyke and S.-I. Ohira, *Environ. Sci. Technol.*, 2008, **42**, 8115–8121.
- 41 A. B. Kirk, J. V. Dyke, C. F. Martin and P. K. Dasgupta, *Environ. Health Perspect.*, 2007, 182–186.
- 42 N. Debeljuh, C. J. Barrow and N. Byrne, *Phys. Chem. Chem. Phys.*, 2011, **13**, 16534–16536.
- 43 K. Klement, K. Wieligmann, J. Meinhardt, P. Hortschansky, W. Richter and M. Fändrich, *J. Mol. Biol.*, 2007, **373**, 1321–1333.

## **PAPER II**



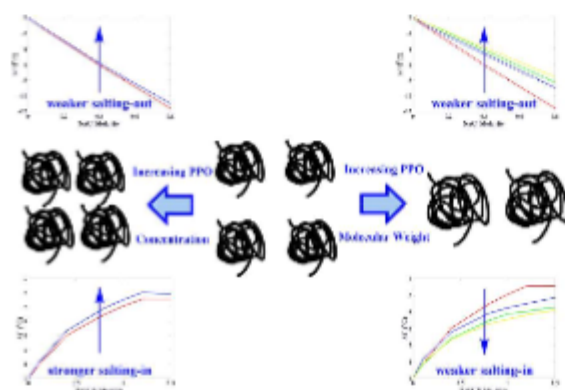
# Hofmeister effect on thermo-responsive poly(propylene oxide): Role of polymer molecular weight and concentration



Saeed Zajforoushan Moghaddam, Esben Thormann \*

Department of Chemistry, Technical University of Denmark, 2800 Kgs. Lyngby, Denmark

## GRAPHICAL ABSTRACT



Reprinted from DOI: 10.1016/j.jcis.2015.11.040 with permission from Elsevier.

## ARTICLE INFO

### Article history:

Received 3 September 2015

Revised 17 November 2015

Accepted 18 November 2015

Available online 28 November 2015

### Keywords:

Hofmeister effect

Poly(propylene oxide)

Lower critical solution temperature

Hydrophobic hydration

Differential scanning calorimetry

## ABSTRACT

Although a vast amount of research has been dedicated to investigate the Hofmeister effect on the stability of polymer solutions, a clear understanding of the role of polymer properties in this phenomenon is still missing. Here, the Hofmeister effect of NaCl (destabilizing) and NaSCN (stabilizing) salts on aqueous solutions of poly(propylene oxide) (PPO) is studied. Four different molecular weights of PPO were investigated, to determine how the variation in the polymer coil size affects the Hofmeister effect. The investigation was further conducted for different PPO concentrations, in order to understand the effect of inter-chain interactions on the response to addition of salt. The temperature-driven phase separation of the solutions was monitored by differential scanning calorimetry, which provides the precise value of the phase separation temperature, as well as the enthalpy change accompanied with the transition. It was observed that increasing the molecular weight weakens the effect of the both salts, which is interpreted in terms of a scaling law between the molecular weight and the accessible surface area of the polymers. Increasing the PPO concentration further diminished the NaCl effect, but amplified the NaSCN effect. This difference is attributed to an electrostatic stabilization mechanism in the case of NaSCN.

© 2015 Elsevier Inc. All rights reserved.

## 1. Introduction

Thermo-responsive polymers are macromolecules that display a sudden change in solubility and conformation in a well-defined temperature regime and their possible applications are multiple, ranging from viscosity control [1,2] to controlled wettability [3,4]

\* Corresponding author.

E-mail address: [esth@kemi.dtu.dk](mailto:esth@kemi.dtu.dk) (E. Thormann).



and are further of great importance in many biomedical applications [5,6]. Besides temperature-responsiveness, it has been demonstrated that the aqueous solution stability of such macromolecules can be tuned by addition of different salts, an effect generally recognized as the Hofmeister effect [7–11]. It was first postulated that destabilization (salting-out) by strongly hydrated ions and stabilization (salting-in) by poorly hydrated ions was due to their “water structure making” and “water structure breaking” effects, respectively [12–14]. Some anomalies from the order of ion hydration strengths compared to the Hofmeister series however indicated that information on how ions alter the water structure cannot solely elucidate such an intricate phenomenon, which is involved with the hydration of both ions and polymer chains, as well as direct interactions between the ions and the polymer backbone [15–19]. Hence in an approach toward understanding the Hofmeister effect on polymer solutions, one must consider that the mutual interactions of ion, water and polymer determine the solution stability [20–24].

In one description that takes the ion-polymer interplay into account, known as the solute partitioning model, Pegram and Record have suggested that the salting-out effect is a result of the exclusion of ions from the polymer hydration shell, while the salting-in effect is due to the favorable accumulation of ions at the polymer interface [25,26]. Accordingly, the partition coefficient, which is the ratio of the concentration of ions near the polymer surface to the concentration of ions in the bulk solution, determines both the strength and the direction of the Hofmeister effect of salts. The partition coefficient of a certain ion strongly depends on the chemistry of the surface, as different values have been reported for the partition coefficient of certain ions over hydrophobic surfaces and polar groups. Although this thermodynamic exclusion/accumulation picture can successfully explain why salts have different effects on polymer stability, it does not render a clear microscopic description for the stabilization and destabilization mechanisms.

In a more microscopic approach, Cremer and coworkers have focused on explaining the Hofmeister effect of different sodium salts on poly(*N*-isopropylacrylamide) (PNIPAM) aqueous solution [27,28]. For this system, they have suggested that the Hofmeister effect can be explained by a combination of three principal mechanisms. First, polarization of the water molecules around the strongly hydrated anions disturbs the hydration of polar amide bonds of PNIPAM, and so results in a salting-out effect. In more general term, this effect may be described as a competition for hydration water between the ions and the polar group. Such a competition will lead to destabilization of the polar group, due to the relatively stronger hydration strength of ions [29]. Second, the presence of ions can interfere with hydrophobic hydration of the polymer, by changing the surface tension between the (hydrophobic) polymer surface and water. This mechanism was formerly believed to have a relatively weak linear salting-out effect, but recently it has been suggested to cause either stabilization (by decreasing the surface tension) or destabilization (by increasing the surface tension), depending on chemistry and dielectric constant of the polymer [30,31]. For instance,  $\text{SCN}^-$  is reported to increase the surface tension of PNIPAM (less hydrophilic polymer, low dielectric constant), but decreases the surface tension of lysozyme (more hydrophilic polymer, high dielectric constant) in water [30]. Third, poorly hydrated anions can directly bind to the moieties on the polymer backbone with a partial positive charge, and then induce an electrostatic repulsion between the chains. Accordingly, the notable nonlinearity in salting-in effect of weakly hydrated ions like  $\text{SCN}^-$  is correlated to the limited number of binding sites on a polymer chain, and then follows the trend of the Langmuir isotherm binding model [32,33].

Irrespective of using a thermodynamic or a molecular description of the Hofmeister effect, it is expected that the effect should depend on the chemical structure and the accessible surface area of the polymer, as well as the possible inter-chain interaction between the polymer chains. With respect to the chemical structure, it has previously been observed that different polymers are not similarly affected by the presence of salts. For instance, poly(propylene oxide) (PPO) shows smaller changes in phase separation temperature in response to different salts, compared to poly(ethylene oxide) (PEO) [29,34]. Another interesting observation is that addition of NaSCN leads to a relatively small salting-in effect on PNIPAM with a maximum below 1M salt, where after it at higher salt concentrations shows a linear salting-out effect. In contrast, NaSCN has a relatively stronger salting-in effect on PPO, which does not seem to reach a maximum even at very high salt concentrations [35,36]. Although not often discussed in the literature on the Hofmeister effect, these differences due to different chemical structures are expected and can be rationalized from both the descriptions discussed above. Since most previous studies of the Hofmeister effect merely concerned with the effect of different ions and their interaction with a particular polymer, the questions regarding the effect of accessible surface area of the chains and inter-chain interaction have remained untouched. These parameters are related to the polymer chemistry, as well as the polymer molecular weight, the polymer concentration and the solvent quality. Hence, the “next stage” of studies on the Hofmeister effect should be focused on finding the role of the polymer properties in this phenomenon, and a better understanding of this can be gained by including the well-known descriptions and concepts from polymer physics.

In the present work, the Hofmeister effect of two sodium salts on aqueous solutions of PPO with different molecular weights and varying concentrations was investigated. As shown formerly in case of PPO solutions [29,35], NaCl and NaSCN show strong linear salting-out and non-linear salting-in effects, respectively. By changing the molecular weight of PPO from 1000, 2000, 2700 to 4000 g mol<sup>-1</sup>, we varied the hydrophilic/hydrophobic character of the polymer due to a relative decreasing influence of the end groups, as well as the accessible surface area due to a systematic change in the coil size. Solutions were further prepared at PPO concentrations of 0.5, 1 and 2 wt.%, which correspond to solutions of separated polymer coils in the diluted regime, but with different average coil-coil separation distance. To detect the phase separation of the solutions, differential scanning calorimetry (DSC) was employed. Hereon, we first investigate the phase separation of the different PPO samples in salt-free aqueous solution, then the effect of the two salts on the PPO solutions is studied.

## 2. Materials and methods

Poly(propylene oxide) with different molecular weights (1000, 2000, 2700 and 4000 g/mol) and pure analytical grades of NaCl (99.5%) and NaSCN (98.5%) salts were all supplied by Sigma-Aldrich. Solutions of PPO samples (concentrations of 0.5, 1 and 2 wt.%) in pure water and salt solutions were prepared by mixing for 24 h at 1 °C.

Measurements were conducted using a differential scanning calorimeter (Nano DSC, TA Instruments), with a constant heating rate of 0.4 °C/min, and under a pressure of 3 atm. All the salt and PPO solutions were degassed before the measurements to avoid bubble formation upon heating. The measured raw heat data were converted to molar heat capacity as explained formerly, and were used to obtain the phase separation temperature, enthalpy change and heat capacity change values (see more in [Supplementary Section S1](#)) [29]. Measurements were repeated 3 times for the salt-free



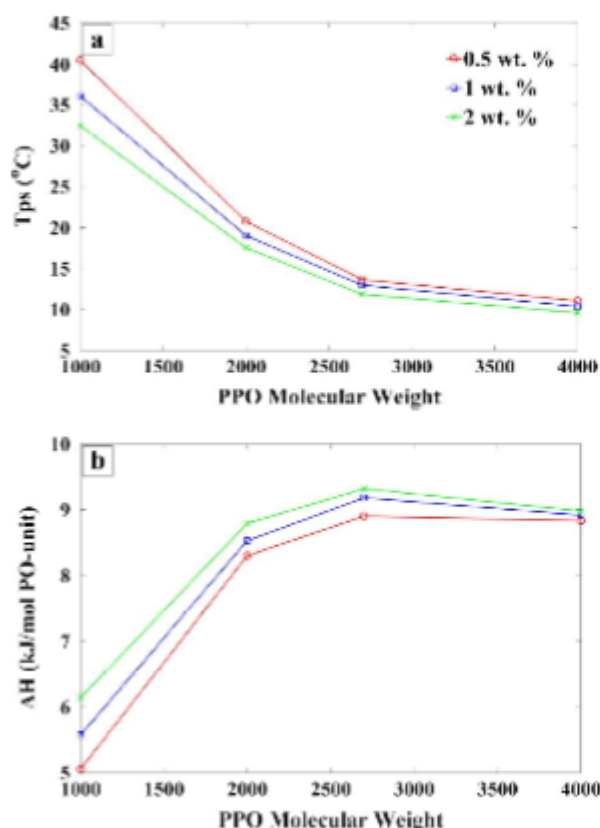


**Fig. 1.** Effect of PPO molecular weight and concentration on phase separation (a) temperature and (b) enthalpy change per mole of PO-unit.

solutions, which showed desirable reproducibility in the measured values with a standard deviation of  $\pm 0.07$  °C for the phase separation temperature and  $\pm 0.1$  kJ/mol PO-unit for the enthalpy change of transition.

### 3. Results and discussion

#### 3.1. Salt-free aqueous solution of PPO

First, we investigate how changing the molecular weight and concentration of polymer affects the phase separation of PPO in the salt-free solution. The phase separation temperature of PPO solutions at different molecular weights and concentrations is illustrated in Fig. 1a. The phase separation evidently occurs at

lower temperatures with an increase in either concentration or molecular weight, but the latter has a much more pronounced effect. Further, solutions of PPO with lower molecular weights are more susceptible to variation in polymer concentration, e.g. PPO1000 experiences a decline of 8 °C in phase separation temperature, while PPO4000 shows only a 1.4 °C decrement upon increasing the PPO concentration from 0.5 to 2 wt. %.

Fig. 1b shows the effect of molecular weight and concentration on the enthalpy change per PO-unit upon phase separation of the solutions. It is observed that going from PPO1000 to PPO2000 leads to a significant increase in enthalpy, while moving from PPO2000 to PPO2700 only shows a minor increment. In contrast, going from PPO2700 to PPO4000 leads to a slight decrease in the enthalpy. Increasing the concentration leads to a gain in the phase separation enthalpy, but with a relatively smaller extent. This effect becomes almost negligible for PPO4000. Generally, the lower molecular weight PPO samples show stronger dependency on concentration change, and more dilute solutions respond more strongly to molecular weight variation.

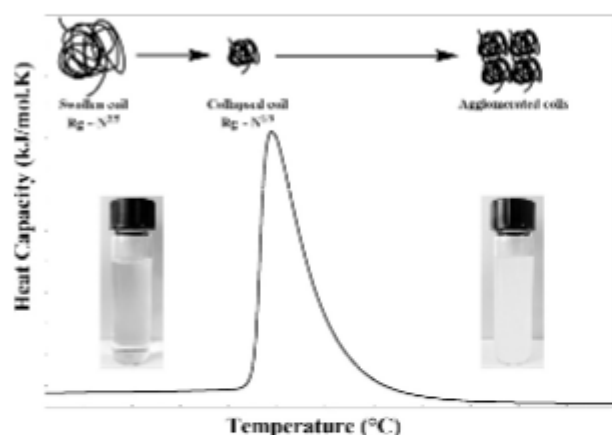
In order to understand these results, we have in Table 1 outlined some important parameters for the systems under investigation. A PPO chain consists of a number of partly hydrophobic PO-monomers and two hydrophilic hydroxyl end groups. As for any polymer, this chain should be found in a random-coiled conformation with a radius of gyration depending on both the molecular weight and the solvent quality [37–39]. In the case of thermo-responsive polymers, the solvent quality changes dramatically with the temperature. At low temperatures where water is considered as a good solvent for PPO, the polymer coil will be in a swollen state, with a radius of gyration approximately scaling with the number of monomers to the power of  $3/5$  [40,41]. However, close to the phase separation temperature, it is reasonable to assume the solvent quality to be poor, which will give rise to a collapsed globular conformation, with a radius of gyration approximately scaling with the number of monomers to the power of  $1/3$  [42,43]. Close to the phase separation temperature, it is further reasonable to assume that the hydrophilic end groups will be prone to be located on the surface of the coil, and thus in direct contact with the hydration water. This assumption is further supported by former reports, suggesting that hydrogen bonds between hydroxyl end groups and water molecules are even stronger than hydrogen bonds between water molecules [44,45]. Adopting this picture (Scheme 1), a PPO chain close to the phase separation temperature can be considered as a contracted polymer coil, with a surface consisting of partly hydrophobic PO-monomers and two hydroxyl groups.

Increasing the molecular weight (for a fixed PPO concentration by weight) thus has three effects with respect to the phase

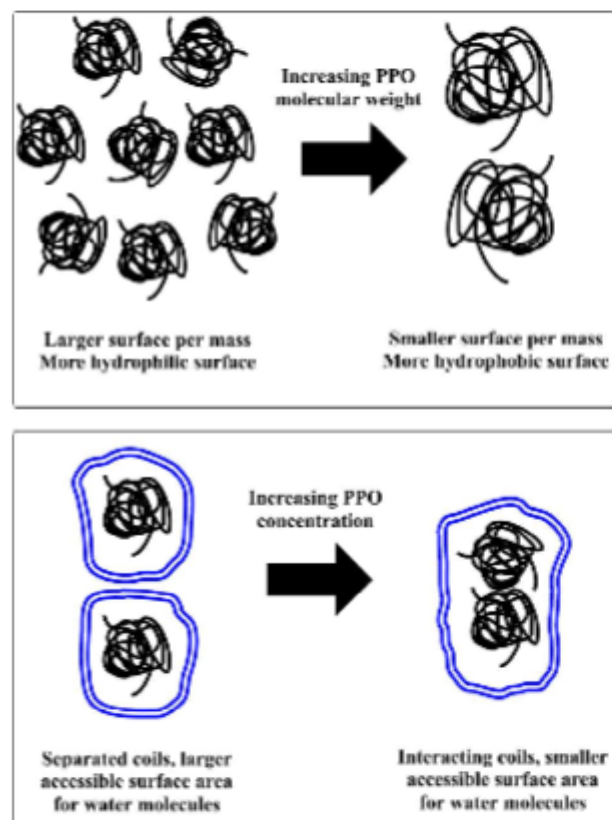
**Table 1**

Calculated average center-to-center-distance between the coils ( $d$ ), radius of gyration ( $R_g$ ) and  $C/C^*$  values for PPO solutions (see Supplementary Section S2).

MW (PO-units)	$C_{PPO}$ (wt.%)	$d$ (nm)	$R_g$ (nm) in good solvent	$R_g$ (nm) in bad solvent	Hydroxyl-to-coil surface ratio in bad solvent (%)	$C/C^*$ in good solvent	$C/C^*$ in bad solvent
1000 (17)	0.5	6.9	1.5	0.7	4.1	0.04	0.004
	1	5.5				0.08	0.008
	2	4.3				0.16	0.016
2000 (34)	0.5	8.7	2.2	0.9	2.5	0.07	0.004
	1	6.9				0.14	0.009
	2	5.5				0.28	0.018
2700 (46)	0.5	9.6	2.7	1	2	0.09	0.004
	1	7.6				0.18	0.009
	2	6.1				0.36	0.018
4000 (68)	0.5	11	3.3	1.1	1.6	0.12	0.004
	1	8.7				0.24	0.009
	2	6.9				0.48	0.018



**Scheme 1.** Typical DSC thermogram of aqueous PPO solution showing variation in the polymer coil size and stability upon increasing temperature.



**Scheme 2.** Illustration of the effect of increasing PPO molecular weight (top) and concentration (bottom).

separation (Scheme 2). First, it decreases the water-accessible surface area relative to the total polymer mass in the solution [46–49]. Under bad solvent condition, the accessible surface area per gram of the polymer is correlated to its molecular weight, according to the following scaling relation:

$$ASA(\text{\AA}^2/\text{g}) \sim M^\nu$$

The exponent ( $\nu$ ) varies approximately between  $-0.24$  to  $-0.34$ , depending on the system conditions. Assuming the state of having a fully collapsed polymer particle, the exponent should be  $-0.34$  according to the Flory theory, while the exponent for less collapsed conformations should have a lower numerical value [50–54].

Second, the effect of increasing the molecular weight is that the interface of the collapsed coil becomes more hydrophobic, since the number of the hydrophilic hydroxyl end groups is fixed to two, independently of the coil size. The effect of end groups can be better perceived by estimating the ratio of end group to coil surface areas. As shown in Table 1, going from PPO1000 to PPO4000, this ratio for the contracted coil decreases roughly from 4% to 1.5%.

Finally, looking at the entire system, another effect of changing the molecular weight (at a fixed concentration by weight) is that it changes the total number of coils, and thereby the average center-to-center-distance between two coils. Another way of addressing this effect is by estimating the  $C/C^*$  ratio, where  $C^*$  is defined as the concentration where the coils start to overlap (see more in Supplementary Section S2) [55]. Here we consider the average center-to-center-distance and the  $C/C^*$  ratio to be important parameters, since they work as indirect measures of the possible impact of inter-chain interactions.

In a similar way, a change in the polymer concentration will also lead to a change in the  $C/C^*$  ratio and the average center-to-center-distance between the coils [55]. An important difference between changing the concentration and the molecular weight is that the former only varies the average center-to-center-distance, but the latter also leads to a change in the hydrophilic/hydrophobic character of the coil. Therefore, their effects on inter-chain interaction might not be the same. According to Table 1, the estimated  $C/C^*$  ratio for all the solutions is slightly below unity at good solvent condition, and far below unity under bad solvent condition. This means that the PPO chains in all the cases are found as individual and separate coils, but the inter-chain interactions are still expected to play a role [55–57]. On a different level, one should notice that the entropy of mixing increases with the number of coils, which is why low molecular weight polymers are always more soluble than high molecular weight polymers [42].

Returning to the results presented in Fig. 1, we should now be able to interpret the observations. Looking at the effect of increasing the molecular weight, one observes a drop in phase separation temperature in apparent accordance with a lower entropy of mixing for the higher molecular weights. However, the significant difference between the phase separation temperatures of PPO1000 and PPO2000 compared to PPO2000 and PPO2700, together with huge variations in dehydration enthalpies (Fig. 1b), suggests that this is not the only effect. Considering the phase separation as dehydration of the coils and then aggregation of the collapsed polymer particles, increasing the molecular weight decreases the total accessible surface area and also makes the polymer interface more hydrophobic. The former effect should lead to a decrease in the absolute value of the enthalpy (less negative enthalpy), since the hydrophobic hydration scales with the exposed hydrophobic surface area [58–60]. For the same reason, the latter effect should increase the absolute value of the enthalpy (more negative enthalpy). Since the number of hydrophilic end groups is fixed to two independent of the molecular weight, the latter effect should dominate at lower molecular weights, while the former effect should dominate at higher molecular weights. Summing up these two effects, the absolute value of the enthalpy as a function of the molecular weight is expected to increase at lower molecular weights and decrease at higher molecular weight. This is exactly the observed trend in Fig. 1b, where the turnover is found around PPO2700. The significant effect of end groups on solubility behavior of PPO1000 and to some extent PPO2000 complies with the former studies of PEO aqueous solutions, which have reported that the effect of end groups are more pronounced for molecular weights below 3350 g/mol [44,45]. Regarding the more hydrophobic character of PPO compared to PEO, this criterion is then expected to shift to even lower molecular weights.



The second observation, that changing the polymer concentration has a relatively weaker effect, can be explained along the same lines. As the concentration is increased, the average center-to-center-distance is decreased and inter-chain interactions leading to solution destabilization will be more effective and thereby destabilize the solution (Scheme 2). To elucidate why this effect is weaker compared to the effect of molecular weight, one should again consider that changing the molecular weight varies the center-to-center distance and more importantly the hydrophilicity and accessible surface area of the PPO chains. Further, the strongest effect of changing the concentration is observed for PPO1000, where the number of coils and also surface-area-to-mass-ratio is the largest, then the strongest effect of inter-chain interaction is expected.

Our observations are also in agreement with the typical temperature-concentration phase diagrams reported for aqueous solutions of polymers with a lower critical solution temperature behavior [37,61,62]. Accordingly, increasing the molecular weight of the polymer shifts the critical point to lower concentrations, and makes the phase diagram broader and more flat in the proximity of the critical point. Employing the Flory Huggins theory as a simple thermodynamic description of polymer mixtures miscibility, this can be explained by the declining role of the solute's configurational entropy of mixing, resulted from increasing the polymer molecular weight [37]. Regarding the general relation between the concentration of critical point and the number of monomers ( $\phi_{cr} = 1/(1 + N^{0.5})$ ) [42], the critical point for PPO1000, 2000, 2700 and 4000 solutions are expected to be at concentrations around 20, 15, 13 and 11 wt.%, respectively. In the concentration regime that we are investigating (0.5–2 wt.%), PPO1000 has the largest offset from the critical point and is thus expected to show the strongest concentration-dependency. This can also be reasoned based on the concept of “cooperative dehydration”, which predicts a more flat miscibility diagram by increasing the molecular weight of the polymers, due to a more cooperative dehydration and collapse in the case of longer chains [63,64]. In this case, cooperativity and inter-molecular association in the phase separation of PPO solutions has been formerly reported, using a comparison of the calorimetrically obtained enthalpy of phase separation with the Van't Hoff enthalpy ( $\Delta H_{vH}$ ) that is calculated based on the assumption of having a two-state solubility model [65].

### 3.2. Solutions of PPO and salts

#### 3.2.1. Addition of NaCl: salting-out effect

Understanding the effect of molecular weight and concentration on the stability of pure PPO solutions, next we study the phase

separation of the same PPO solutions in presence of NaCl. Fig. 2 displays the shift in phase separation temperature,  $\Delta T = T_{ps}(\text{salt}) - T_{ps}(\text{no salt})$ , as a function of NaCl concentration. It is observed that NaCl has a strong linear salting-out effect on all the samples. However, the magnitude of the salting-out effect ( $\Delta T$ ) varies with the molecular weight and the concentration of PPO. By increasing the molecular weight, the salting-out effect considerably decreases, e.g. 0.5 wt.% solution of PPO1000 shows a 11.6 °C reduction in phase separation temperature, while 0.5 wt.% solution of PPO4000 experiences a 7.6 °C reduction in phase separation temperature when 0.8 M NaCl is added. With respect to the effect of increasing PPO concentration, a decrement in the salting-out effect is observed. This effect however appears to be much weaker than the effect of molecular weight. This effect becomes even less pronounced for the higher molecular weights, as we see almost no change in the salting-out effect on PPO2700 and PPO4000 by changing the polymer concentration.

To interpret the results, we will first discuss the expected effect of NaCl on PPO solution stability, and then apply the knowledge about the changes in accessible surface area and surface hydrophilicity/hydrophobicity to explain the correlation between the magnitude of the Hofmeister effect and the molecular weight and concentration of PPO. Based on the current understanding of the Hofmeister effect,  $\text{Cl}^-$  is expected to be effectively repelled from the hydration zone of the PPO chains. In the case of the hydrophobic part of PPO,  $\text{Cl}^-$  disfavors the hydrophobic hydration due to the increment in the surface tension, while in the case of the polar groups on PPO, it disturbs the hydration due to the strong polarization of the water molecules around the ions. It is generally considered that the salting-out effect on the polar groups (the polarization effect) is stronger than on the hydrophobic groups (the surface tension effect) [30,36].

Understanding the general Hofmeister effect of NaCl on PPO, we will now explain the observed differences in the Hofmeister effect of NaCl, resulted from changing the molecular weight and the concentration of PPO. As already mentioned, increasing the molecular weight leads to a decrease in the accessible surface area per mass of PPO, as well as in the total number of hydroxyl end groups. Less accessible surface area can be interpreted as less unfavorable ion-PPO interactions, and a weaker salting-out effect is thus expected. This interpretation is in direct agreement with the observations in Fig. 2, that the Hofmeister effect of NaCl is weaker on the higher molecular weights. Plotting the values of  $\Delta T$  versus the PPO molecular weight on a double log-scale interestingly gives straight lines with an approximate slope of  $-0.3$ . This seems to support the idea that the magnitude of the Hofmeister effect scales with the accessible surface area of the polymer, since the calculated slope is in good agreement with the exponent in the scaling law between the accessible surface area and the molecular weight of polymers (see more in Supplementary Section S3).

As discussed for the pure PPO solutions, another effect of varying the molecular weight is a change in the hydrophilic/hydrophobic ratio of the accessible surface area. As the salting-out effect on the hydroxyl end groups are supposed to be stronger than on the more hydrophobic PO-unit, this should strengthen the trend that the magnitude of the salting-out effect is larger on the more hydrophilic PPO1000, compared to the more hydrophobic PPO4000.

The reasoning for why the hydroxyl end groups should be found at the surface of the collapsed coils was based on the argument that these groups have a more favorable interaction with water. However, if the salting-out effect is stronger on these groups compared to the PO-unit, one could reversibly argue that these groups should be shielded inside the coils at temperatures close to the phase separation. This assumption is partly supported by the enthalpies measured for the phase separation of PPO in different concentrations of NaCl (Fig. 3). Here it is seen that increasing the

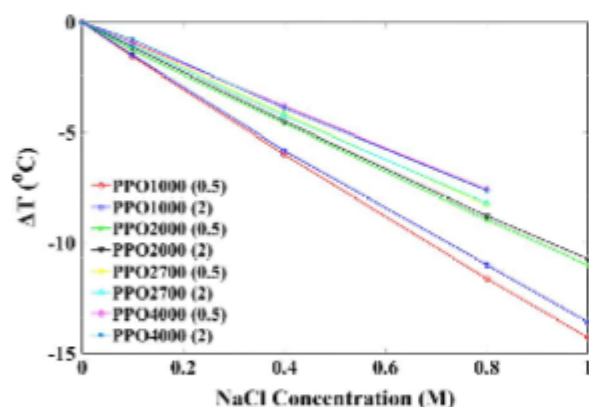
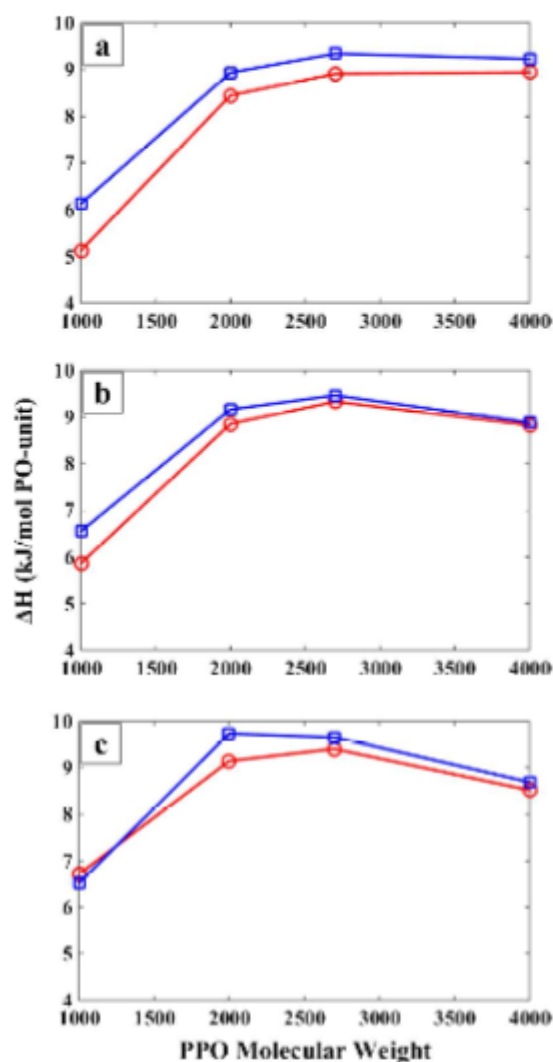


Fig. 2. Change in phase separation temperature ( $\Delta T = T_{ps}(\text{salt}) - T_{ps}(\text{no salt})$ ) of PPO aqueous solutions in presence of NaCl.



**Fig. 3.** Phase separation enthalpy change (per mol of PO-units) of 0.5 wt.% (circle) and 2 wt.% (square) PPO aqueous solutions in presence of NaCl salt; (a) 0.1 M (b) 0.4 M (c) 0.8 M.

NaCl concentration makes the presence of the turning point more prominent. This suggests that in presence of NaCl, the effect related to accessible surface area as a function of the molecular weight plays a more important role, and that the end groups play a smaller role compared to the case of salt-free system. It is also observed that increasing NaCl concentration leads to minor increment in enthalpy, which can be attributed to the fact that the phase separation in presence of NaCl occurs at relatively lower temperatures (see more in [Supplementary Section S4](#)).

To explain the minor decrease in the magnitude of the effect of NaCl by increasing the PPO concentration, we simply suggest that the effect is related to the fact that an increase in the polymer concentration brings the coils closer to each other, and then enhances the effect of the inter-chain interactions. Compared to a fully separated state, we expect two interacting PPO coils to expose relatively less accessible surface area to water molecules, which will result in a weaker salting-out effect (see [Scheme 2](#)). Since the  $C/C^*$  ratios for the chain in the collapsed state indicates relatively small changes in the inter-chain distances at the various concentrations, only a minor result on the magnitude of the Hofmeister effect can be expected.

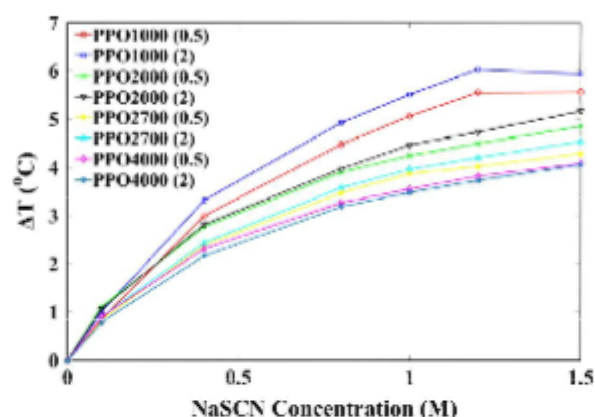


**Fig. 4.** Change in phase separation temperature ( $\Delta T = T_{ps}(\text{salt}) - T_{ps}(\text{no salt})$ ) of PPO aqueous solutions in presence of NaSCN.

### 3.2.2. Addition of NaSCN: salting-in effect

[Fig. 4](#) depicts changes in the phase separation temperature of the PPO solutions in presence of NaSCN. Addition of NaSCN leads to an increase in the phase separation temperature and shows a non-linear salting-in effect on all the samples. However, the magnitude of the salting-in effect,  $\Delta T = T_{ps}(\text{salt}) - T_{ps}(\text{no salt})$ , varies by changing the PPO molecular weight and concentration. Regarding the effect of molecular weight, the salting-in effect becomes considerably weaker upon increasing the PPO molecular weight, similar to what we observed in the case of NaCl. On the other hand, increasing the PPO concentration results in a stronger salting-in effect on PPO1000 and to some smaller extent on PPO2000 and PPO2700, while it seems to have a minor effect on PPO4000, if any at all.

To interpret the results, we will first discuss the expected Hofmeister effect of NaSCN on PPO, and then illustrate the effect of changing the PPO molecular weight and concentration. According to the current understanding of the Hofmeister effect, ions with a salting-in effect are favorably accumulated in the proximity of the polymer interface. The extent of the accumulation strongly depends on both the chemistry of the surface and on the type of ions. In our case,  $\text{SCN}^-$  has been reported to favorably interact with either hydrophobic surfaces or polar groups like esters and amides [\[10,12\]](#). We thus expect that  $\text{SCN}^-$  has a propensity to assemble around both the hydroxyl end groups and the partially hydrophobic surface of the PPO coils. Accordingly, the stabilizing effect of NaSCN can be assigned to a decrease in surface tension of the partially hydrophobic surface of PPO, as well as to an electrostatic repulsion between the partially-charged coils.

Pursuing this picture, we here argue that the magnitude of the salting-in effect by NaSCN is related to the accessible surface area and its hydrophilic/hydrophobic ratio. Accordingly, the salting-in effect is expected to become weaker by increasing the molecular weight, since less polymer surface is accessible for the ions to accumulate on. This argumentation is similar to what we employed to explain the effect of changing the PPO molecular weight on the salting-out effect of NaCl, however with an important distinction that NaCl affects the hydration shell of PPO, while NaSCN directly associates with the PPO backbone. Again, plotting the values of  $\Delta T$  versus the PPO molecular weight on a double log-scale provides straight lines with an approximate slope of  $-0.3$ , which reassures the correlation between the magnitude of the Hofmeister effect and the accessible surface area of PPO. In the case of the effect of NaSCN, it is however noticed that the exact value of the slope apparently depends on the polymer concentration (see more in [Supplementary Section S3](#)). We suggest that this illustrates that



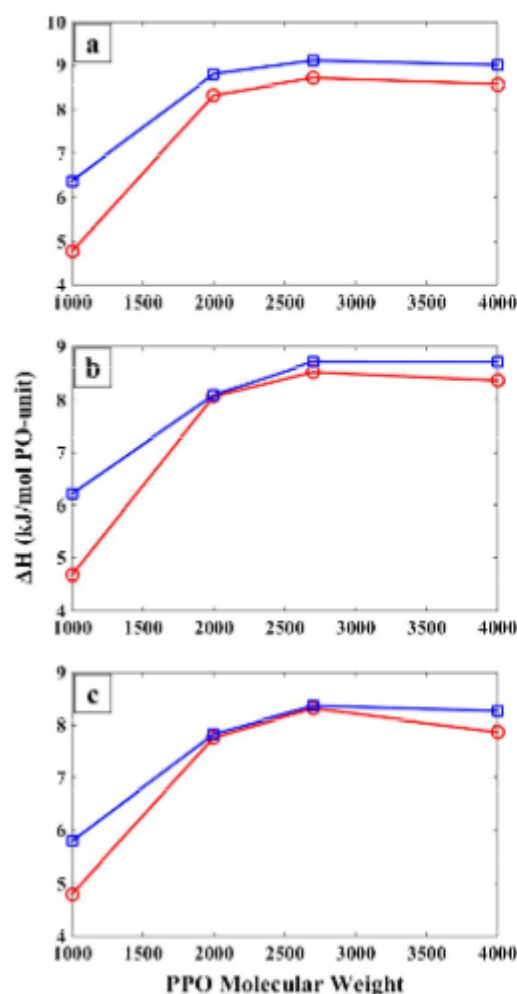


**Fig. 5.** Phase separation enthalpy change (per mol of PO-units) of 0.5 wt.% (circle) and 2 wt.% (square) PPO aqueous solutions in presence of NaSCN salt; (a) 0.1 M (b) 0.4 M (c) 0.8 M.

the magnitude of the Hofmeister effect of NaSCN is not solely related to the accessible surface area, but also to the electrostatic inter-chain repulsion discussed above.

Regarding the measured phase separation enthalpies (Fig. 5), the effect of NaSCN is different from the effect of NaCl. Firstly, the absolute values of the enthalpies diminish by increasing the salt concentration, which we suggest is mainly related to the fact that phase separation happens at relatively higher temperatures in presence of NaSCN (see more in [Supplementary Section S4](#)). Secondly, and more importantly, addition of NaSCN has almost no effect on the prominence of the turning point (compared to the effect of NaCl), suggesting that end groups here play a more important role for the hydration.

The effect of increasing the PPO concentration is different from what we observed in the case of NaCl salting-out effect. The larger salting-in effect observed by increasing the PPO concentration (particularly for PPO1000) may be explained by the different stabilization mechanism of NaSCN. One part of the stabilization was suggested to be a result of electrostatic repulsion between the partially-charged coils. Therefore, one can consider an additional stabilization effect on more concentrated PPO solutions, and this effect will obviously be stronger for closely-packed coils than for isolated coils, as well as for the coils with a relatively larger accessible surface area. This is also in agreement with the fact that inter-chain interactions have a more pronounced effect on solutions of

PPO with lower molecular weights, in the concentration regime that we are investigating.

#### 4. Conclusion

In the present study, the phase separation of PPO solutions of different molecular weights and concentrations in presence of NaCl and NaSCN salts was investigated. Generally, it was observed that the magnitude of the Hofmeister effect (either salting-out or salting-in) is strongly dependent on the molecular weight and the concentration of PPO. With respect to NaCl, it was shown that increasing the molecular weight of PPO leads to a considerable decrement in the salting-out effect, while increasing the PPO concentration has a similar but weaker effect. It was considered that  $\text{Cl}^-$  is effectively repelled from the PPO interface and that it can destabilize both hydrophilic end groups and the partially hydrophobic surface of the PPO coils. Since increasing either the molecular weight or the concentration decreases the accessible surface area of PPO in solution, the unfavorable interplay between ion and polymer is decreased and the magnitude of the salting-out is then attenuated.

With respect to NaSCN, increasing the molecular weight of PPO resulted in a pronounced decrease in the magnitude of the salting-in effect, while increasing the PPO concentration amplified the salting-in effect, specifically in the case of PPO1000. It was considered that  $\text{SCN}^-$  preferentially accumulates around the PPO coils, and stabilizes both the end groups and the partially hydrophobic surface of the coils. Since increasing the molecular weight leads to a decrease in the accessible surface area of PPO in solution, the magnitude of the salting-in effect becomes weaker. The larger salting-in effect on PPO1000 and to some extent PPO2000 and PPO2700 upon increasing the PPO concentration was explained by the stronger effect of electrostatic repulsions between closely-packed coils compared to more isolated coils.

Although not directly discussed in the literature, the key role of the macromolecule properties in the Hofmeister effect is irrefutable. The effect of polymer chemical structure can be inferred from previous studies showing that the Hofmeister effect on different macromolecules is not the same. In this case, we can enumerate several examples from the literature, where the authors addressed the important role of chemical structure of the polymer. Many reports can be found on the differences between the Hofmeister effect on proteins and nucleic acids, where the great difference in chemistry of the surface and conformation of the macromolecules has been suggested as the main reason [26,66,67]. Here, although the order of the Hofmeister series remains the same, the “null point” (ions that almost has no effect on polymer stability) is reported to shift, depending on base composition and conformation of the macromolecule. Comparison of the effect of ions on neutral and charged macromolecules also strengthens this idea. For instance, when Coulombic interactions also come into play, a reversal or amplification of the Hofmeister effect on polyelectrolytes has been reported [16,19,68]. Furthermore, several reports are available in the literature discussing the effect of size and molecular weight of PEG on its stabilizing/destabilizing effects on nucleic acid and protein solutions. Here it has been suggested that physical effects resulted from the size of cosolute, i.e. the excluded volume effect, have a strong influence on the Hofmeister effect [69–71]. Considering these examples, the chemical structure of the macromolecule seems to be the first and foremost parameter, which plays a role in the Hofmeister effect. Here we further demonstrated that not only the chemical structure but also the basic properties of a specific polymer like molecular weight and concentration can significantly influence the magnitude of the Hofmeister effect.

Our work suggests that investigating the role of polymer properties can be the “next stage” of studies on the Hofmeister effect. It seems that both the salting-in and salting-out effects are reasonably scaled with the accessible surface area of the polymer. Hence, obtaining universal scaling laws between the basic properties of the polymer in solution, i.e. solvent-accessible surface area, and the extent of Hofmeister effect can be one possible target for the future works. This can be accomplished by obtaining information on the dimensional and structural characteristics of the polymer in pure and saline solutions, using scattering techniques or molecular dynamics simulation studies. All in all, we should bear in mind that the prerequisite of understanding how a polymer responds to the salts is to first perceive how it behaves in the salt-free solution.

## Acknowledgement

The authors acknowledge financial support from the Swedish Research Council, VR.

## Appendix A. Supplementary material

Supplementary data associated with this article can be found, in the online version, at <http://dx.doi.org/10.1016/j.jcis.2015.11.040>.

## References

- [1] R.G. Ezell, C.L. McCormick, Electrolyte- and pH-responsive polyampholytes with potential as viscosity-control agents in enhanced petroleum recovery, *J. Appl. Polym. Sci.* 104 (2007) 2812–2821.
- [2] R. Bodvik, E. Thormann, L. Karlson, P.M. Claesson, Temperature responsive surface layers of modified celluloses, *Phys. Chem. Chem. Phys.* 13 (2011) 4260–4268.
- [3] A.E. Ivanov, J. Ekeröth, L. Nilsson, B. Mattiasson, B. Bergenstahl, L.Y. Galaev, Variations of wettability and protein adsorption on solid siliceous carriers grafted with poly(N-isopropylacrylamide), *J. Colloid Interface Sci.* 296 (2006) 538–544.
- [4] A. Dedinaite, E. Thormann, G. Olanya, P.M. Claesson, B. Nyström, A.-L. Kjøniksen, K. Zhu, Friction in aqueous media tuned by temperature-responsive polymer layers, *Soft Matter* 6 (2010) 2489–2498.
- [5] M.A. Ward, T.K. Georgiou, Thermoresponsive polymers for biomedical applications, *Polymers* 3 (2011) 1215–1242.
- [6] M.A.C. Stuart, W.T. Huck, J. Genzer, M. Müller, C. Ober, M. Stamm, G.B. Sukhorukov, I. Szleifer, V.V. Tsukruk, M. Urban, Emerging applications of stimuli-responsive polymer materials, *Nat. Mater.* 9 (2010) 101–113.
- [7] E. Florin, R. Kjellander, J.C. Eriksson, Salt effects on the cloud point of the poly(ethylene oxide)+ water system, *J. Chem. Soc., Faraday Trans. 1: Phys. Chem. Condensed Phases* 80 (1984) 2889–2910.
- [8] W. Kunz, Specific ion effects in colloidal and biological systems, *Curr. Opin. Colloid Interface Sci.* 15 (2010) 34–39.
- [9] Y. Zhang, P.S. Cremer, Chemistry of Hofmeister anions and osmolytes, *Annu. Rev. Phys. Chem.* 61 (2010) 63–83.
- [10] L.M. Pegram, M.T. Record Jr., Thermodynamic origin of Hofmeister ion effects, *J. Phys. Chem. B* 112 (2008) 9428–9436.
- [11] D.A. Garrec, I.T. Norton, Boundary lubrication by sodium salts: a Hofmeister series effect, *J. Colloid Interface Sci.* 379 (2012) 33–40.
- [12] M.T. Record, E. Guinn, L. Pegram, M. Capp, Introductory lecture: interpreting and predicting Hofmeister salt ion and solute effects on biopolymer and model processes using the solute partitioning model, *Faraday Discuss.* 160 (2013) 9–44.
- [13] A. Salis, B.W. Ninham, Models and mechanisms of Hofmeister effects in electrolyte solutions, and colloid and protein systems revisited, *Chem. Soc. Rev.* 43 (2014) 7358–7377.
- [14] B.W. Ninham, T.T. Duignan, D.F. Parsons, Approaches to hydration, old and new: insights through Hofmeister effects, *Curr. Opin. Colloid Interface Sci.* 16 (2011) 612–617.
- [15] M. Boström, F. Tavares, S. Finet, F. Skouri-Panet, A. Tardieu, B. Ninham, Why forces between proteins follow different Hofmeister series for pH above and below pI, *Biophys. Chem.* 117 (2005) 217–224.
- [16] D. Parsons, M. Boström, T. Maccina, A. Salis, B.W. Ninham, Why direct or reversed Hofmeister series? Interplay of hydration, non-electrostatic potentials, and ion size, *Langmuir* 26 (2009) 3323–3328.
- [17] D.F. Parsons, M. Boström, P.L. Nostro, B.W. Ninham, Hofmeister effects: interplay of hydration, nonelectrostatic potentials, and ion size, *Phys. Chem. Chem. Phys.* 13 (2011) 12352–12367.
- [18] J. Paterová, K.B. Rembert, J. Heyda, Y. Kurra, H.J. Okur, W.R. Liu, C. Hilty, P.S. Cremer, P. Jungwirth, Reversal of the Hofmeister series: specific ion effects on peptides, *J. Phys. Chem. B* 117 (2013) 8150–8158.
- [19] N. Schwierz, D. Horinek, R.R. Netz, Reversed anionic Hofmeister series: the interplay of surface charge and surface polarity, *Langmuir* 26 (2010) 7370–7379.
- [20] L. Pérez-Fuentes, C. Drummond, J. Faraudo, D. Bastos-González, Anions make the difference: insights from the interaction of big cations and anions with poly(N-isopropylacrylamide) chains and microgels, *Soft Matter* (2015). DOI.
- [21] T. López-León, J.L. Ortega-Vinuesa, D. Bastos-González, A. Elaissari, Thermally sensitive reversible microgels formed by poly(N-isopropylacrylamide) charged chains: a Hofmeister effect study, *J. Colloid Interface Sci.* 426 (2014) 300–307.
- [22] W.J. Xie, Y.Q. Gao, A simple theory for the Hofmeister series, *J. Phys. Chem. Lett.* 4 (2013) 4247–4252.
- [23] C. Yan, T. Mu, Molecular understanding of ion specificity at the peptide bond, *Phys. Chem. Chem. Phys.* 17 (2015) 3241–3249.
- [24] P.M. Reddy, P. Venkatesu, Influence of ionic liquids on the critical micellization temperature of a tri-block co-polymer in aqueous media, *J. Colloid Interface Sci.* 420 (2014) 166–173.
- [25] L.M. Pegram, M.T. Record, Hofmeister salt effects on surface tension arise from partitioning of anions and cations between bulk water and the air–water interface, *J. Phys. Chem. B* 111 (2007) 5411–5417.
- [26] L.M. Pegram, T. Wendorff, R. Erdmann, I. Shkel, D. Bellissimo, D.J. Felitsky, M.T. Record, Why Hofmeister effects of many salts favor protein folding but not DNA helix formation, *Proc. Natl. Acad. Sci.* 107 (2010) 7716–7721.
- [27] K.B. Rembert, H.L. Okur, C. Hilty, P.S. Cremer, An NH moiety is not required for anion binding to amides in aqueous solution, *Langmuir* (2015). DOI.
- [28] K.B. Rembert, J. Paterová, J. Heyda, C. Hilty, P. Jungwirth, P.S. Cremer, Molecular mechanisms of ion-specific effects on proteins, *J. Am. Chem. Soc.* 134 (2012) 10039–10046.
- [29] E. Thormann, On understanding of the Hofmeister effect: how addition of salt alters the stability of temperature responsive polymers in aqueous solutions, *Rsc Adv.* 2 (2012) 8297–8305.
- [30] B.A. Deyler, Y. Zhang, Effects of Hofmeister anions on the aggregation behavior of PEO–PPO–PEO triblock copolymers, *Langmuir* 27 (2011) 9203–9210.
- [31] Y. Zhang, S. Furry, D.E. Bergbreiter, P.S. Cremer, Specific ion effects on the water solubility of macromolecules: PNIPAM and the Hofmeister series, *J. Am. Chem. Soc.* 127 (2005) 14505–14510.
- [32] I. Shechter, O. Ramon, I. Portnaya, Y. Paz, Y.D. Livney, Microcalorimetric study of the effects of a chaotropic salt, KSCN, on the lower critical solution temperature (LCST) of aqueous poly(N-isopropylacrylamide) (PNIPAA) solutions, *Macromolecules* 43 (2009) 480–487.
- [33] M. Boncina, J. Lah, J. Reščič, V. Vlachy, Thermodynamics of the lysozyme – salt interaction from calorimetric titrations, *J. Phys. Chem. B* 114 (2010) 4313–4319.
- [34] M. Ataman, Properties of aqueous salt solutions of poly(ethylene oxide), *Cloud points, 0 temperatures*, *Colloid Polym. Sci.* 265 (1987) 19–25.
- [35] S.Z. Moghaddam, E. Thormann, Hofmeister effect of salt mixtures on thermoresponsive poly(propylene oxide), *Phys. Chem. Chem. Phys.* 17 (2015) 6359–6366.
- [36] Y. Zhang, S. Furry, L.B. Sagie, Y. Cho, D.E. Bergbreiter, P.S. Cremer, Effects of Hofmeister anions on the LCST of PNIPAM as a function of molecular weight, *J. Phys. Chem. C* 111 (2007) 8916–8924.
- [37] L.H. Sperling, *Introduction to Physical Polymer Science*, John Wiley & Sons, 2005.
- [38] T. Lodge, M. Muthukumar, Physical chemistry of polymers: entropy, interactions, and dynamics, *J. Phys. Chem.* 100 (1996) 13275–13292.
- [39] E. Thormann, D.R. Evans, V.S.J. Craig, Experimental studies of the dynamic mechanical response of a single polymer chain, *Macromolecules* 39 (2006) 6180–6185.
- [40] P.J. Flory, *Principles of Polymer Chemistry*, Cornell University Press, 1953.
- [41] K. Devanand, J. Selser, Asymptotic behavior and long-range interactions in aqueous solutions of poly(ethylene oxide), *Macromolecules* 24 (1991) 5943–5947.
- [42] P.J. Flory, Thermodynamics of high polymer solutions, *J. Chem. Phys.* 10 (1942) 51–61.
- [43] K. Kubota, S. Fujishige, I. Ando, Single-chain transition of poly(N-isopropylacrylamide) in water, *J. Phys. Chem.* 94 (1990) 5154–5158.
- [44] E.E. Dormidontova, Influence of end groups on phase behavior and properties of PEO in aqueous solutions, *Macromolecules* 37 (2004) 7747–7761.
- [45] E.E. Dormidontova, Role of competitive PEO–water and water–water hydrogen bonding in aqueous solution PEO behavior, *Macromolecules* 35 (2002) 987–1001.
- [46] T.V. Chalikian, R. Filfil, How large are the volume changes accompanying protein transitions and binding?, *Biophys. Chem.* 104 (2003) 489–499.
- [47] S. Miller, J. Janin, A.M. Lesk, C. Chothia, Interior and surface of monomeric proteins, *J. Mol. Biol.* 196 (1987) 641–656.
- [48] N. Tautier, T.V. Chalikian, Compressibility of protein transitions, *Biochim. Biophys. Acta (BBA) – Protein Struct. Mol. Enzymol.* 1595 (2002) 48–70.
- [49] T.V. Chalikian, M. Totrov, R. Abagyan, K.J. Breslauer, The hydration of globular proteins as derived from volume and compressibility measurements: cross correlating thermodynamic and structural data, *J. Mol. Biol.* 260 (1996) 588–603.
- [50] J. Janin, Surface and inside volumes in globular proteins, *Nature* 277 (1979) 491–492.
- [51] C. Chothia, The nature of the accessible and buried surfaces in proteins, *J. Mol. Biol.* 105 (1976) 1–12.
- [52] S. Miller, A.M. Lesk, J. Janin, C. Chothia, The accessible surface area and stability of oligomeric proteins, *Nature* 328 (1987) 834–836.



- [53] J. Janin, S. Miller, C. Chothia, Surface, subunit interfaces and interior of oligomeric proteins, *J. Mol. Biol.* 204 (1988) 155–164.
- [54] S. Jones, J.M. Thornton, Principles of protein–protein interactions, *Proc. Natl. Acad. Sci.* 93 (1996) 13–20.
- [55] M. Daoud, G. Jannink, Temperature-concentration diagram of polymer solutions, *J. Phys.* 37 (1976) 973–979.
- [56] J. Cotton, M. Nierlich, F. Boue, M. Daoud, B. Farnoux, G. Jannink, R. Duplessix, C. Picot, Experimental determination of the temperature–concentration diagram of flexible polymer solutions by neutron scattering, *J. Chem. Phys.* 65 (1976) 1101–1108.
- [57] L. Utracki, B. Favis, *Polymer Alloys and Blends*, Marcel Dekker, New York, 1989.
- [58] T. Inoue, K. Yamashita, Aggregation behavior of polypropylene oxide with electric charges at both ends in aqueous solution, *J. Colloid Interface Sci.* 300 (2006) 774–781.
- [59] H. Feil, Y.H. Bae, J. Feijen, S.W. Kim, Effect of comonomer hydrophilicity and ionization on the lower critical solution temperature of N-isopropylacrylamide copolymers, *Macromolecules* 26 (1993) 2496–2500.
- [60] S.K. Nixon, S. Hvidt, C. Booth, Micellization of block copolymer P94 in aqueous solution, *J. Colloid Interface Sci.* 280 (2004) 219–223.
- [61] S. Saeki, N. Kuwahara, M. Nakata, M. Kaneko, Upper and lower critical solution temperatures in poly(ethylene glycol) solutions, *Polymer* 17 (1976) 685–689.
- [62] G. Allen, C. Baker, Lower critical solution phenomena in polymer–solvent systems, *Polymer* 6 (1965) 181–191.
- [63] Y. Okada, F. Tanaka, Cooperative hydration, chain collapse, and flat LCST behavior in aqueous poly(N-isopropylacrylamide) solutions, *Macromolecules* 38 (2005) 4465–4471.
- [64] Y. Ono, T. Shikata, Hydration and dynamic behavior of poly(N-isopropylacrylamide)s in aqueous solution: a sharp phase transition at the lower critical solution temperature, *J. Am. Chem. Soc.* 128 (2006) 10030–10031.
- [65] J. Armstrong, B. Chowdhry, R. O'Brien, A. Beezer, J. Mitchell, S. Leharne, Scanning microcalorimetric investigations of phase transitions in dilute aqueous solutions of poly(oxypropylene), *J. Phys. Chem.* 99 (1995) 4590–4598.
- [66] E. Courtenay, M. Capp, R. Saecker, M. Record, Thermodynamic analysis of interactions between denaturants and protein surface exposed on unfolding: Interpretation of urea and guanidinium chloride m-values and their correlation with changes in accessible surface area (ASA) using preferential interaction coefficients and the local-bulk domain model, *Proteins: Struct. Funct. Bioinform.* 41 (2000) 72–85.
- [67] E.J. Guinn, L.M. Pegram, M.W. Capp, M.N. Pollock, M.T. Record, Quantifying why urea is a protein denaturant, whereas glycine betaine is a protein stabilizer, *Proc. Natl. Acad. Sci.* 108 (2011) 16932–16937.
- [68] Y. Zhang, P.S. Cremer, The inverse and direct Hofmeister series for lysozyme, *Proc. Natl. Acad. Sci.* 106 (2009) 15249–15253.
- [69] R. Bhat, S.N. Timasheff, Steric exclusion is the principal source of the preferential hydration of proteins in the presence of polyethylene glycols, *Protein Sci.* 1 (1992) 1133–1143.
- [70] C.H. Spink, J.B. Chaires, Effects of hydration, ion release, and excluded volume on the melting of triplex and duplex DNA, *Biochemistry* 38 (1999) 496–508.
- [71] R.M. Kramer, V.R. Shende, N. Motl, C.N. Pace, J.M. Scholtz, Toward a molecular understanding of protein solubility: increased negative surface charge correlates with increased solubility, *Biophys. J.* 102 (2012) 1907–1915.

## **Supporting Information**

### **Hofmeister Effect on Thermo-responsive Poly(propylene oxide): Role of Polymer Molecular Weight and Concentration**

Saeed Zajforoushan Moghaddam and Esben Thormann\*

Department of Chemistry, Technical University of Denmark, 2800 Kgs. Lyngby,  
Denmark

---

\* To whom correspondence should be addressed. E-mail: [esth@kemi.dtu.dk](mailto:esth@kemi.dtu.dk).

Telephone: (+45) 4525 2439



## S1. Thermodynamic analysis of DSC thermograms

Three basic thermodynamic parameters of phase separation process can be obtained from a DSC thermogram, namely phase separation temperature ( $T_{ps}$ ), enthalpy change of phase separation ( $\Delta H$ ), and change in heat capacity by phase separation ( $\Delta C_p$ ). Here, the phase separation temperature of the solution is considered to be the onset temperature ( $T_{onset}$ ) on DSC thermogram.  $\Delta H$  value can be obtained by calculating the area under the excess heat capacity function, which can be calculated from equation S1.  $\Delta C_p$  of the phase transition is defined as the difference between the pre- and post-transition baselines.

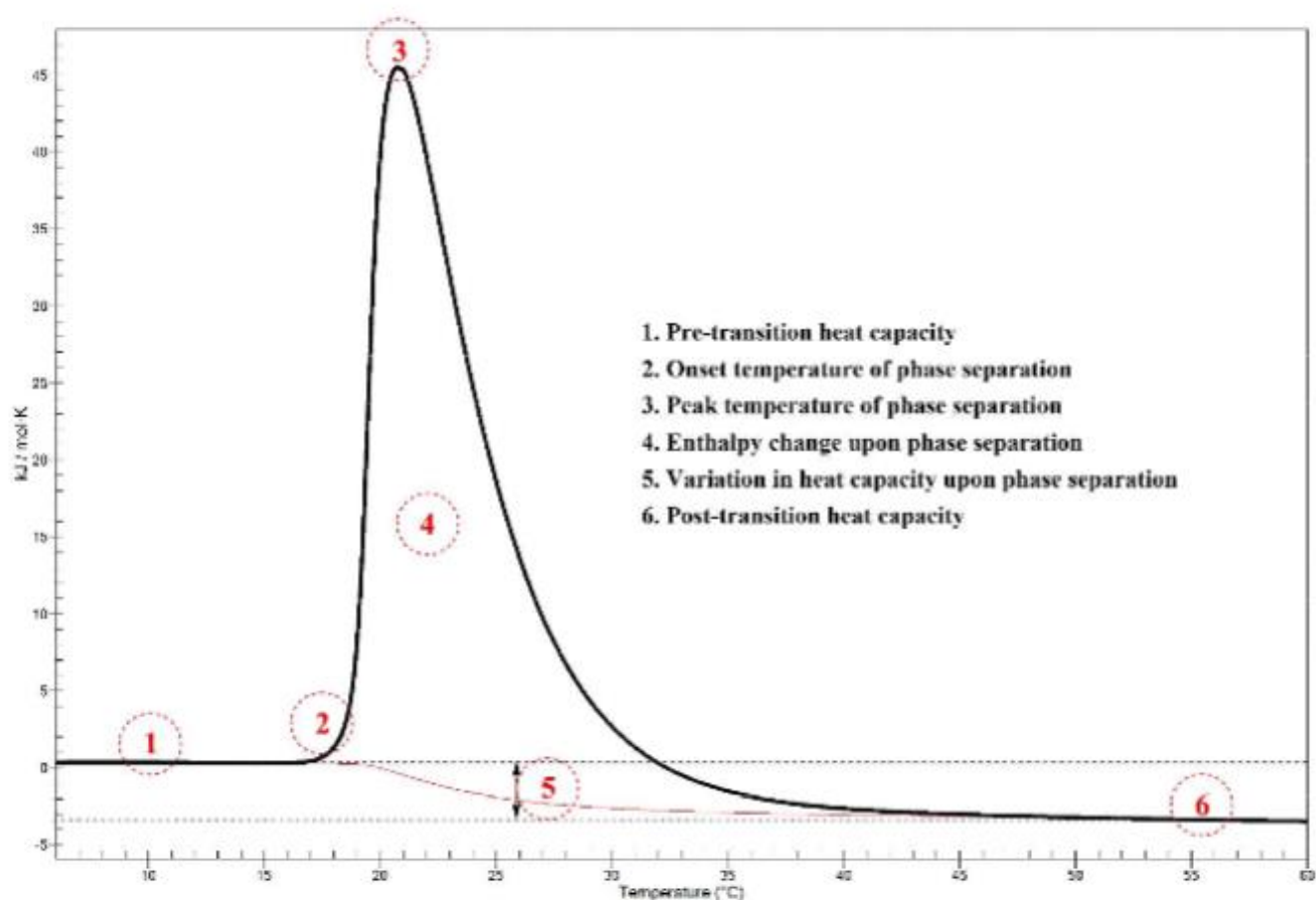


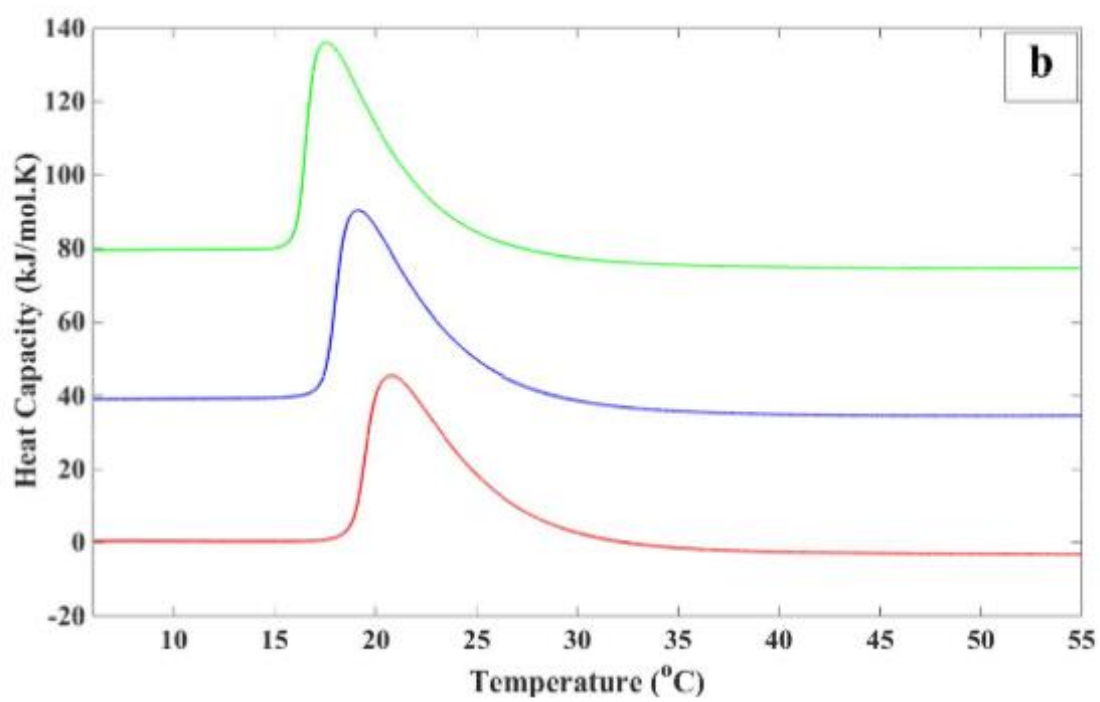
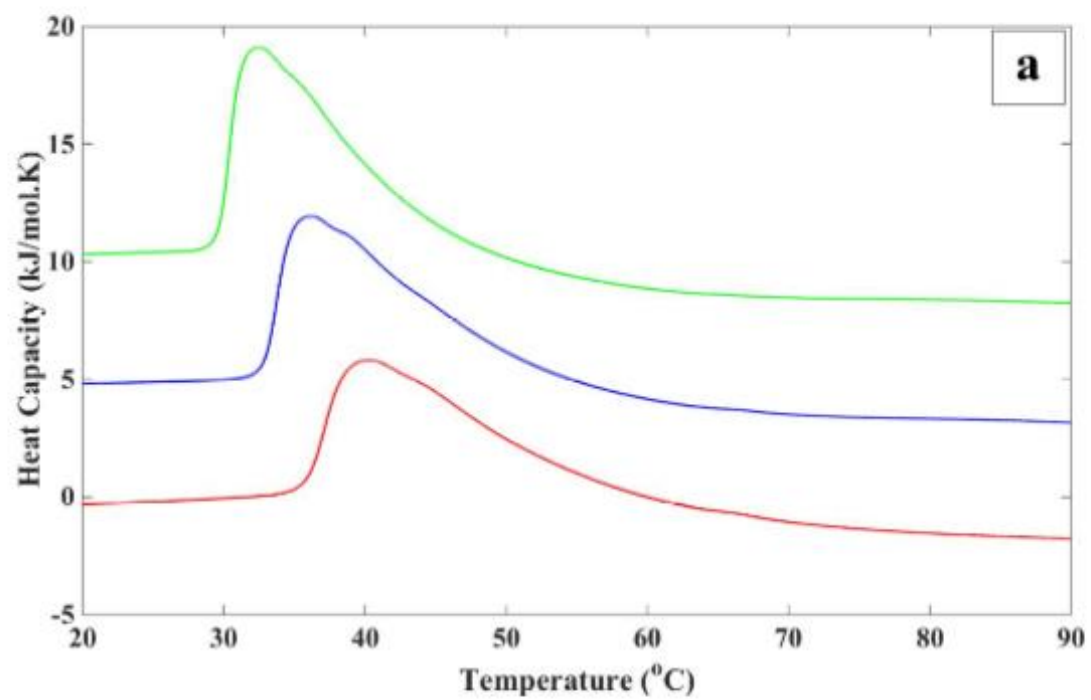
Fig. S1 Thermodynamic analysis of a typical DSC thermogram

$$\Delta H = \int_{T_0}^{T_f} C_{p,excess} dT \quad (S1)$$

The calculated  $\Delta H$  value is the total amount of heat exchange during phase separation of the solution. This can be attributed to breakage of water-polymer hydrogen bonds, as well as melting of the “ice-like” structure of water molecules around the hydrophobic surfaces of polymer. Regarding all the PPO solutions, a negative  $\Delta C_p$  value is observed, which can be attributed to liberation of the water molecules from the polymer hydration shell and also burial of the polymer hydrophobic surfaces.

From the obtained calorimetric data, one can also obtain the temperature dependence of the enthalpy change of phase separation, according to equation S2. Here, it is assumed that the heat capacity decrement is independent of temperature. Considering the effect of  $\Delta C_p$  in calculating  $\Delta H$  values is of great importance in cases where we want to compare the enthalpy change of the collapse processes that occur at different temperatures.

$$\Delta H(T) = \Delta H(T1) + \Delta C_p(T - T1) \quad (S2)$$



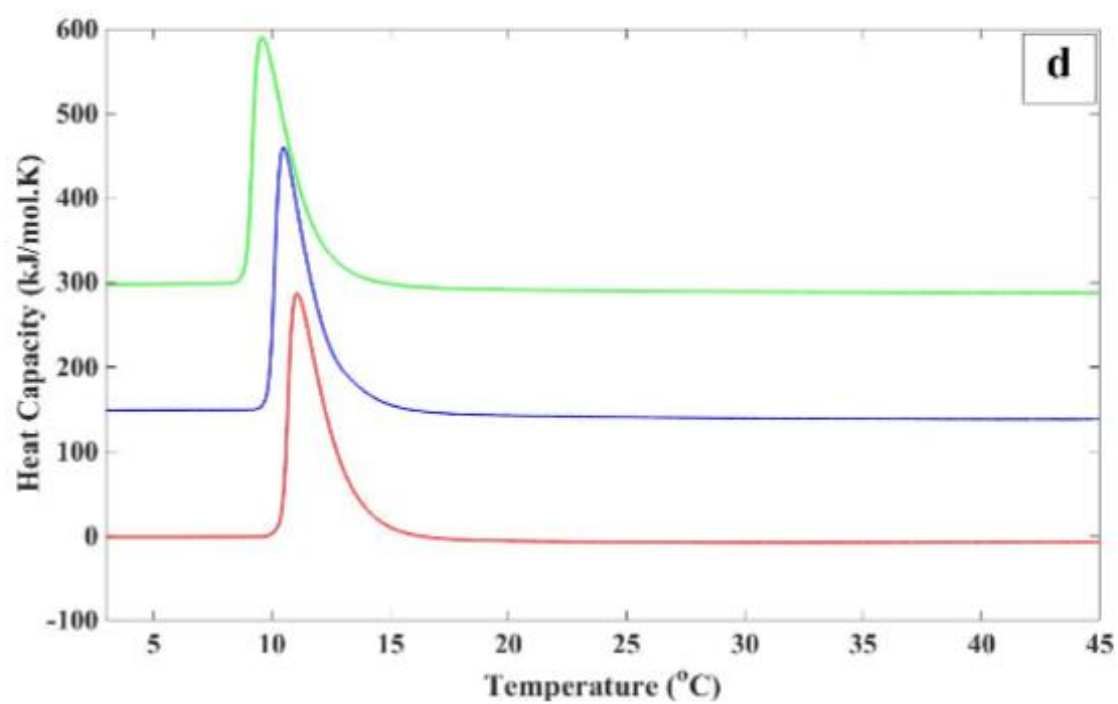
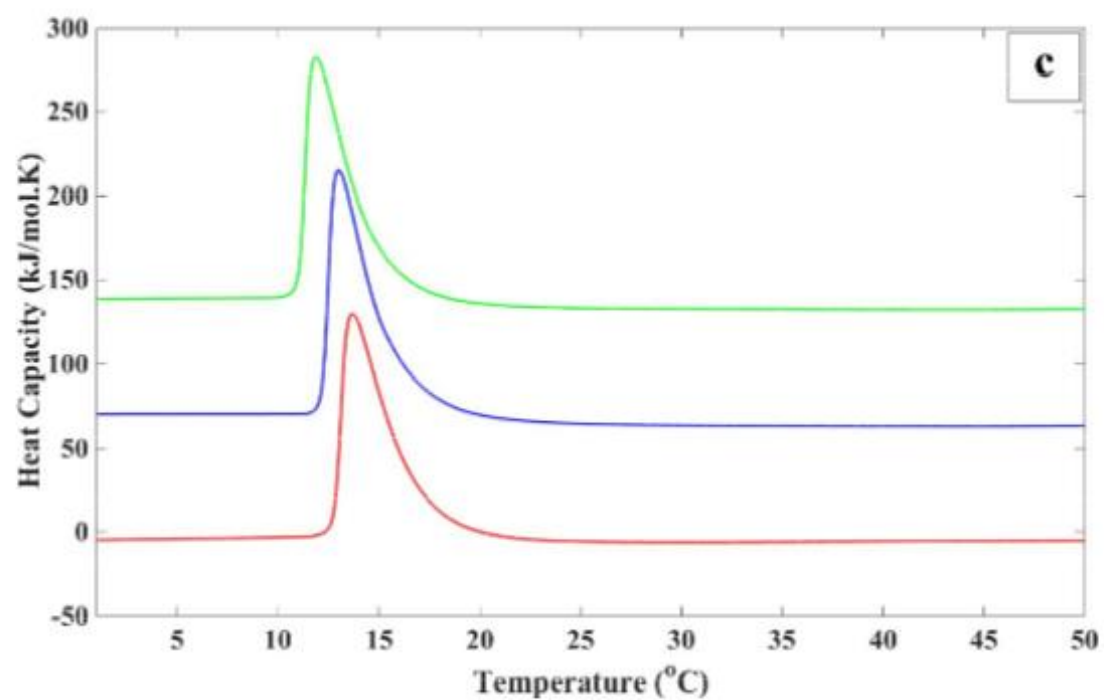


Fig S2 DSC thermograms of salt-free PPO solutions; (a) PPO1000 (b) PPO2000 (c) PPO2700 (d) PPO4000; (red) 0.5 wt.% (blue) 1 wt.% (green) 2 wt.%

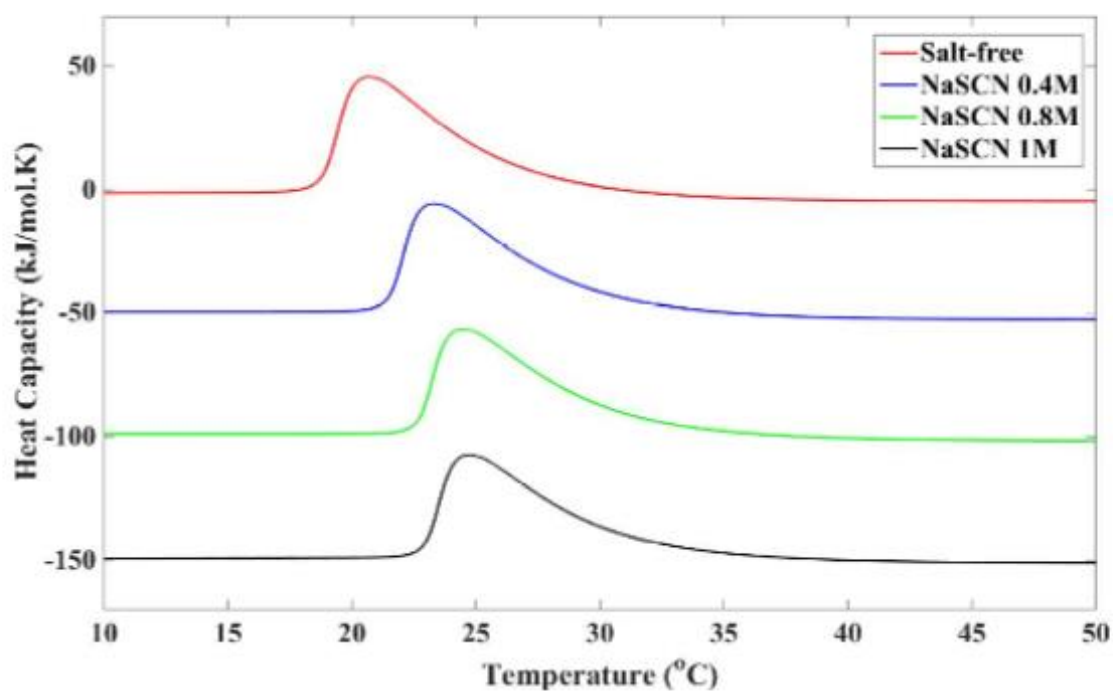
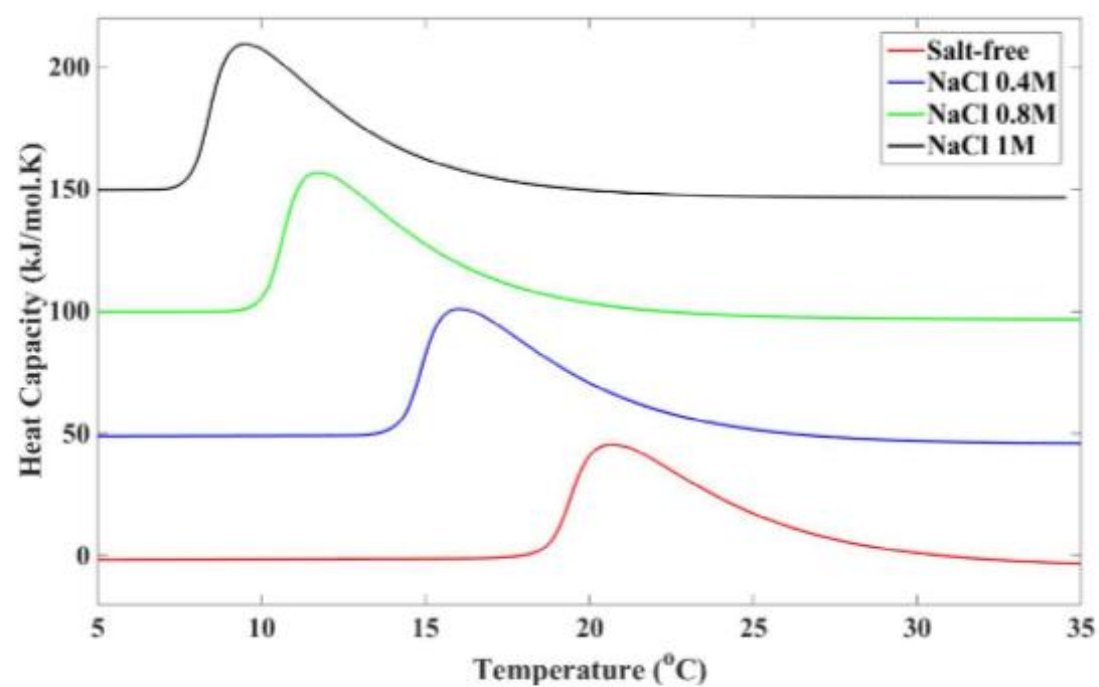


Fig S3 Typical DSC thermograms of PPO (PPO2000) solutions in presence of (top) NaCl (bottom) NaSCN

DSC thermograms of PPO solutions of different molecular weights and concentrations are presented in Fig. S2. With respect to the effect of increasing the molecular weight, the peak related to the phase separation becomes sharper and narrower. This observation supports the idea of a stronger effect of hydrophobic hydration in the case of higher molecular weight PPOs. This can also be explained based on the cooperative dehydration theory, suggesting a sharper and narrower phase separation upon increasing the polymer molecular weight.[1, 2] With respect to the effect of increasing PPO concentration, similar trend is observed, which can be explained in the same line as the effect of molecular weight was illustrated.

General effect of NaCl and NaSCN salts on the shape of DSC thermogram of PPO aqueous solution is illustrated in Fig. S3. Addition of NaCl makes the peak sharper and also diminishes the width of peak, while NaSCN makes the peak broader. These observations are in agreement with previous reports on the Hofmeister effect of salts on PNIPAM and PPO aqueous solutions[3, 4], and can be explained according to the effect of ions on the cooperative dehydration of the polymer coil.[1, 2] With respect to the effect of NaSCN, accumulation of ions near the polymer surface may interfere with the phase separation cooperativity or in other words makes the collapse process less cooperative, which then makes the phase separation peak broader and shorter. On the other hand, “water withdrawing” feature of strongly hydrated ions supposedly makes the hydrogen bonding between water-PPO weaker, and then results in stronger inter-molecular association and a more cooperative collapse.

## **S2. Calculation of center-to-center-distance, radius of gyration and overlap concentration**

The average center-to-center distance ( $d$ ) between the PPO coils was simply calculated by estimating the number of PPO chains per volume of the solution, and then calculating the approximate available volume for one PPO chain in the solution. Assuming a cubic packing geometry, the center-to-center distance is then the cube root of the calculated volume value as follows:

$$d = \sqrt[3]{\frac{M}{C \times \rho \times N_A}} \quad (\text{S3})$$

In where  $M$ ,  $C$ ,  $\rho$  and  $N_A$  are the PPO molecular weight, the PPO concentration (wt. %), the solution density and the Avogadro number, respectively.

The radius of gyration ( $R_g$ ) of a polymer random coil is related to the number of repeating units according to the Flory equation[5, 6]:

$$R_g = b \times N^v \quad (\text{S4})$$

Where  $b$  (characteristic length of the repeating unit) is a constant structural factor and  $v$  (the Flory exponent) varies from  $1/3$  (for a poor solvent) to  $3/5$  (for a good solvent). For our calculations, the  $b$

value was estimated to be around 0.28 nm, which has been previously reported for scattering measurements and molecular dynamic simulation studies on aqueous solution of poly(ethylene oxide).[7-9]

Having the values of  $R_g$  and average molecular weight of PPO samples, the approximate overlap concentration ( $C^*$ ) of the solutions was calculated, which can be defined as the mass density of a single polymer chain in its equal sphere of the radius of  $R_g$ . [6]

$$C^* = \frac{\frac{M}{N_A}}{\frac{4}{3} \times \pi \times R_g^3} \quad (S5)$$

Here,  $M$  is the average molecular weight of polymer and  $N_A$  is the Avogadro number. As believed, at concentrations below the  $C^*$  polymer coils are separated from each other, while at  $C^*$  they start to overlap with each other.



### S3. Scaling law between $\Delta T$ values of salts and the PPO molecular weight

It has been demonstrated that the accessible surface area of polymers in a bad solvent decreases by increasing their molecular weight, according to equation S6, where the exponent is reported to roughly vary between -0.24 to -0.34 for different systems.[10, 11]

$$ASA (\text{\AA}^2/g) \sim M^v \quad (\text{S6})$$

To check if there is a correlation between the magnitude of the Hofmeister effect and the accessible surface area of PPO,  $\log(\Delta T)$  values versus  $\log(M)$  values are plotted in Fig. S4 and S5. Regarding Fig. S4, the magnitude of the salting-out effect of NaCl roughly scales with the PPO molecular weight (for both 0.5wt. % and 2wt. % solutions) according to equation S7:

$$\Delta T \sim M^{-0.3} \quad (\text{S7})$$

By comparing this equation to equation S6, it can be inferred that the magnitude of the salting-out effect directly scales with the accessible surface area of PPO in solution. It should be noticed that changing the concentration of PPO from 0.5 to 2 wt. % has a minor effect on the power law equation and the exponent, suggesting that in both cases the accessible surface area plays the key role.

Regarding Fig. S5, the magnitude of the salting-in effect of NaSCN roughly scales with the PPO molecular weight (for 0.5 wt. % solution) according to equation S8:

$$\Delta T \sim M^{-0.27} \quad (\text{S8})$$

It should be noticed that increasing the PPO concentration from 0.5 to 2 wt. %, changes the power law relation, as the exponent changes approximately to -0.38. This difference supports the idea that stabilization mechanisms are not the same in case of 0.5 and 2 wt. % solutions.

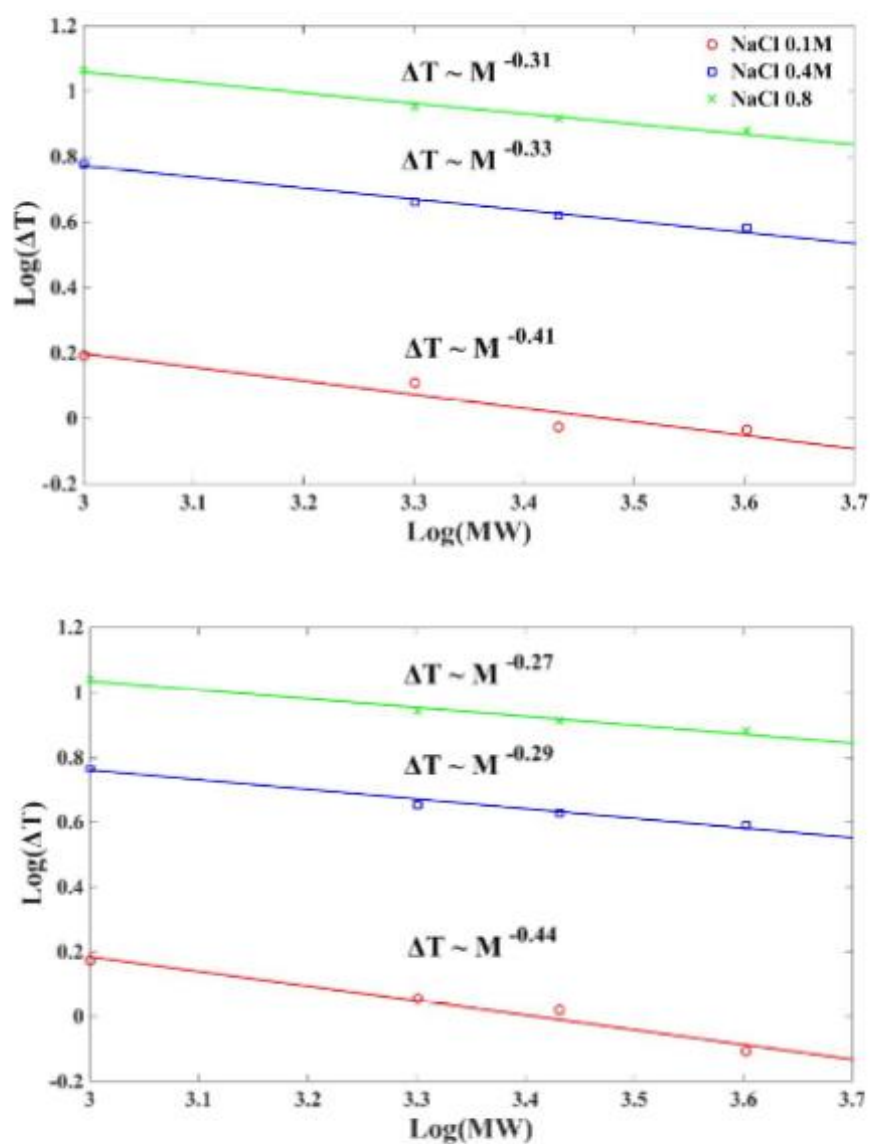


Fig. S4 Logarithmic plot of  $\Delta T$  values of NaCl versus the PPO molecular weight; (top) 0.5 wt. % and (bottom) 2wt. % PPO solutions

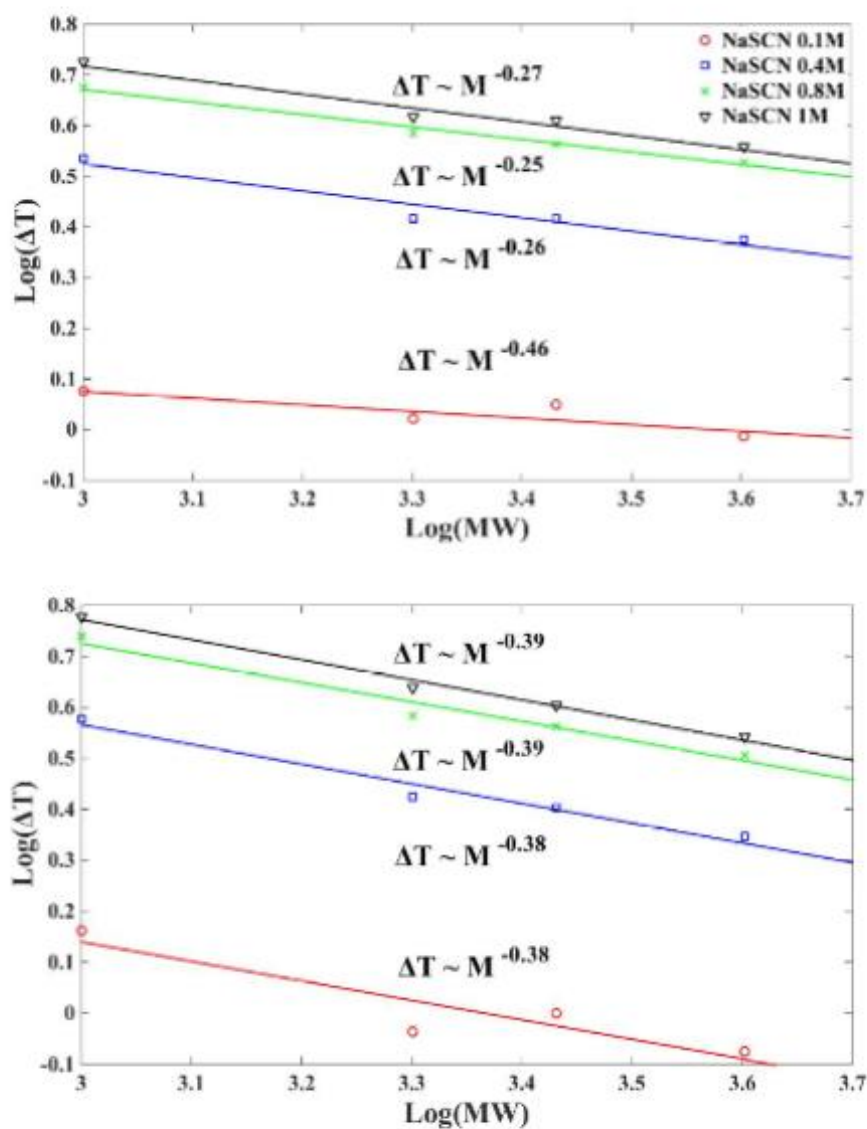


Fig. S5 Logarithmic plot of  $\Delta T$  values of NaSCN versus the PPO molecular weight; (top) 0.5 wt. % and (bottom) 2wt. % PPO solutions

#### S4. Calculating the effect of $\Delta C_p$ on $\Delta H$ of phase separation of the solutions

Addition of NaCl seems to partially increase the enthalpy of transition. But it must be considered that the phase separation of NaCl-containing solutions occurs at lower temperatures compared to the salt-free solution, which can itself increase the enthalpy. Similarly, phase separation of NaSCN-containing solutions happens at higher temperatures compared to the salt-free solution, which can lead to a decrease in the enthalpy. So in order to compare the enthalpy values, one should first subtract this effect by recalculating all the enthalpy values at one specific temperature. To do so, equation S2 together with  $\Delta C_p$  values of each PPO molecular weight and concentration were used, to obtain the corrected enthalpy values at an arbitrarily chosen temperature of 25 °C.

Table S1 Thermodynamic data and recalculated enthalpy of phase separation (at 25 °C) for the salt-free PPO solutions

PPO molecular weight (g/mol)	1000		2000		2700		4000	
PPO Concentration (wt. %)	0.5	2	0.5	2	0.5	2	0.5	2
$\Delta C_p$ (kJ/mol.K)	-1.6	-1.8	-3.9	-4.5	-5	-5.8	-6.6	-8.2
Phase transition temperature (°C)	35.78	29.54	18.73	16.06	12.83	11.12	10.31	9.10
Enthalpy at phase separation temperature (kJ/mol)	85.97	104.41	282.23	298.94	409.45	428.62	600.6	610.6
Recalculated enthalpy at 25 °C (kJ/mol)	103.21	112.582	257.77	258.71	348.6	347.422	503.64	481.01

The corrected enthalpy of salt-containing solutions can be recalculated in a similar way.

Table S2 Recalculated enthalpy of phase separation (at 25 °C) for salt-containing solutions of PPO (0.5 wt. % concentration)

PPO MW	Salt type	0.1M	0.4M	0.8M
1000	NaCl	84.75	90.294	96.76
	NaSCN	83.114	85.07	89.08
2000	NaCl	282.39	282.77	276.99
	NaSCN	287.34	284.36	279.135
2700	NaCl	402.47	408.28	392.42
	NaSCN	402.94	404.31	399.78
4000	NaCl	616.9	577.394	527.85
	NaSCN	588.60	584.46	556.798

Table S3 Recalculated enthalpy of phase separation (at 25 °C) for salt-containing solutions of PPO (2 wt. % concentration)

PPO MW	Salt type	0.1M	0.4M	0.8M
1000	NaCl	109.94	109.93	100.37
	NaSCN	118.44	119.85	115.76
2000	NaCl	258.68	251.25	252.175
	NaSCN	263.39	246.9	243.39
2700	NaCl	340.81	330.25	315.65
	NaSCN	343.3	333.9	308.29
4000	NaCl	500.44	438.35	397.11
	NaSCN	490.2	480.58	460.53

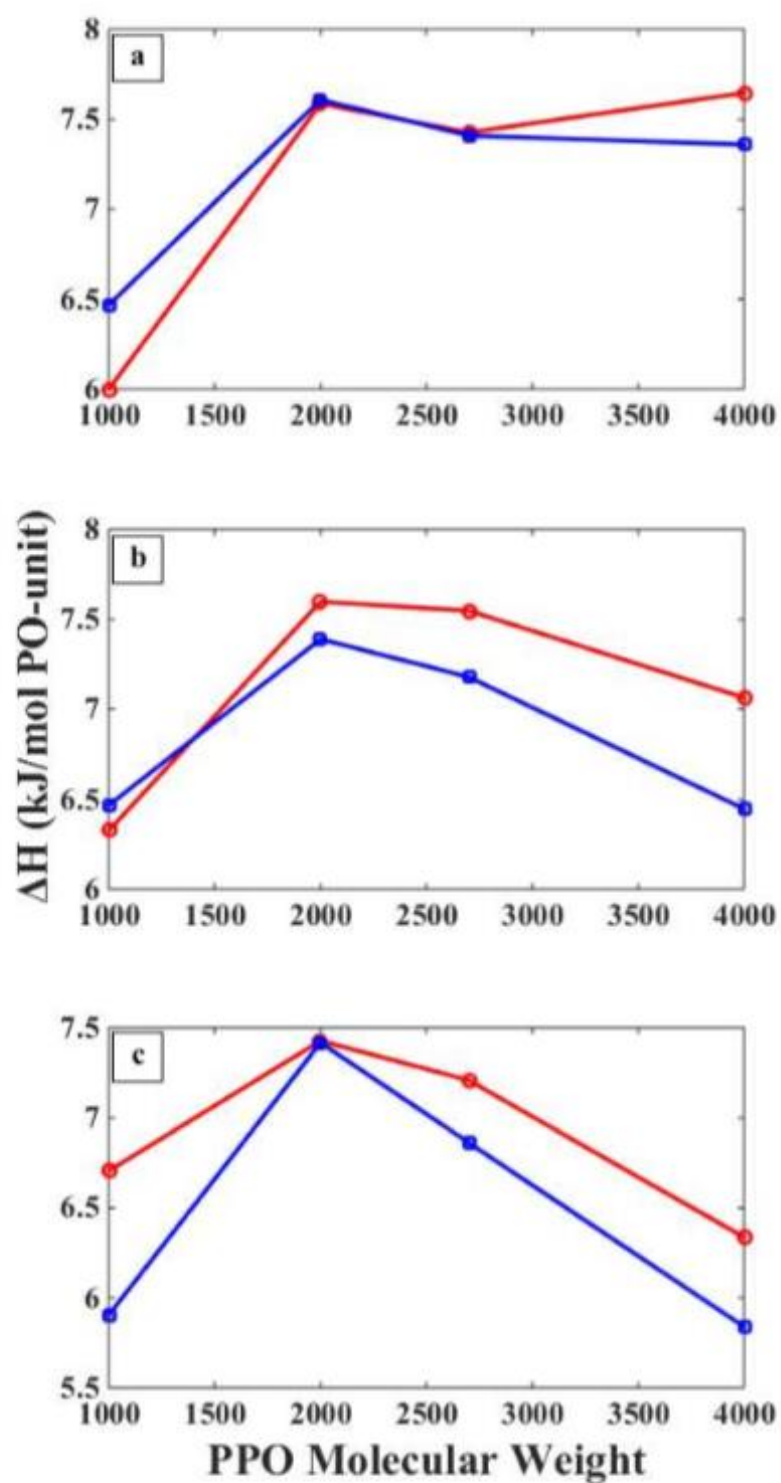


Fig S6 Recalculated enthalpy change (per mol of PO-unit) of 0.5 wt. % (circle) and 2 wt. % (square) PPO aqueous solutions in presence of NaCl salt; (a) 0.1 M (b) 0.4 M (c) 0.8 M.

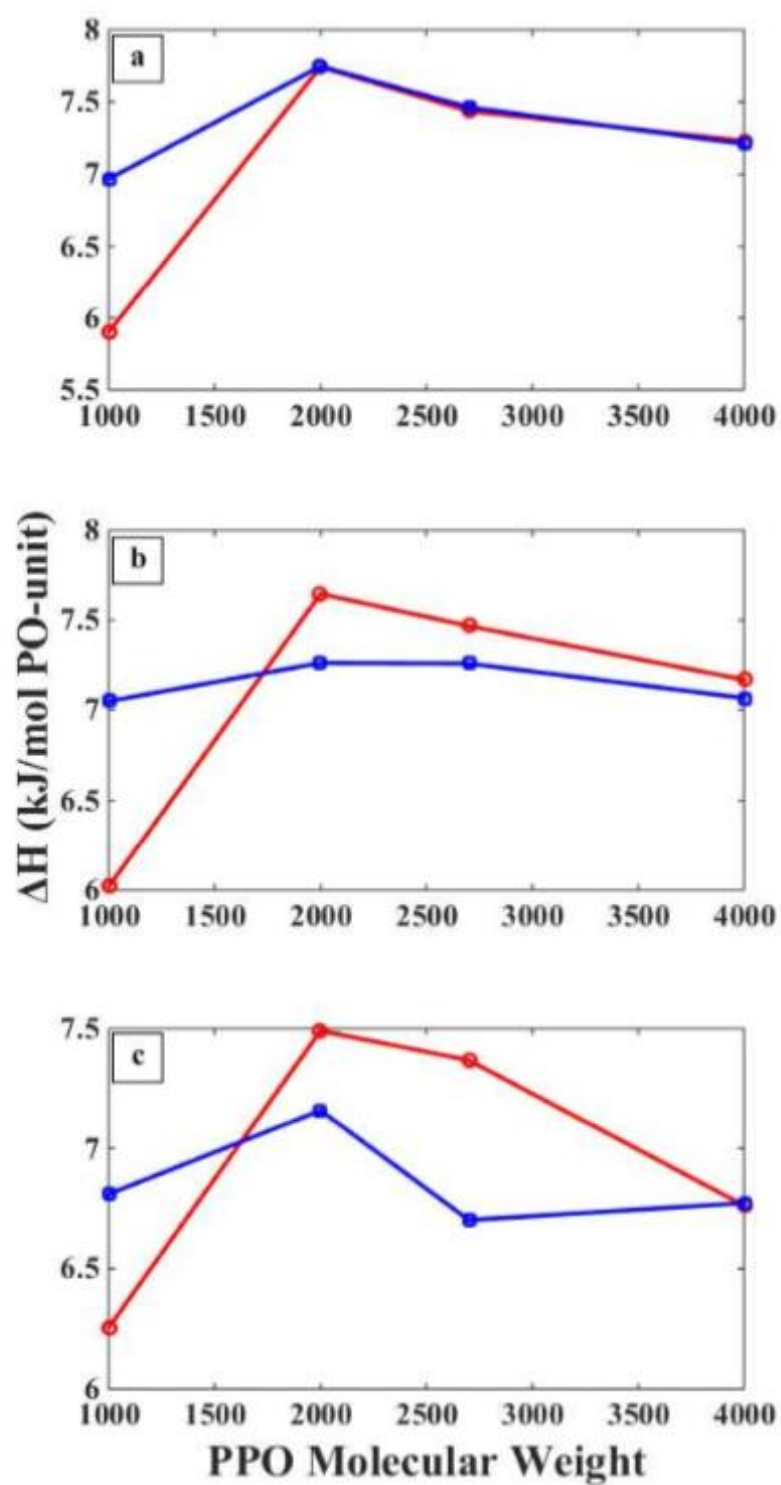


Fig S7 Recalculated enthalpy change (per mol of PO-unit) of 0.5 wt. % (circle) and 2 wt. % (square) PPO aqueous solutions in presence of NaSCN salt; (a) 0.1 M (b) 0.4 M (c) 0.8 M.



## REFERENCES

- [1] Y. Okada, F. Tanaka, Cooperative hydration, chain collapse, and flat LCST behavior in aqueous poly (N-isopropylacrylamide) solutions, *Macromolecules*, 38 (2005) 4465-4471.
- [2] Y. Ono, T. Shikata, Hydration and dynamic behavior of poly (N-isopropylacrylamide) s in aqueous solution: A sharp phase transition at the lower critical solution temperature, *Journal of the American Chemical Society*, 128 (2006) 10030-10031.
- [3] H.G. Schild, D.A. Tirrell, Microcalorimetric detection of lower critical solution temperatures in aqueous polymer solutions, *Journal of Physical Chemistry*, 94 (1990) 4352-4356.
- [4] I. Shechter, O. Ramon, I. Portnaya, Y. Paz, Y.D. Livney, Microcalorimetric study of the effects of a chaotropic salt, KSCN, on the lower critical solution temperature (LCST) of aqueous poly (N-isopropylacrylamide)(PNIPA) solutions, *Macromolecules*, 43 (2009) 480-487.
- [5] P.J. Flory, Thermodynamics of high polymer solutions, *The Journal of chemical physics*, 10 (1942) 51-61.
- [6] L.H. Sperling, *Introduction to physical polymer science*, John Wiley & Sons 2005.
- [7] H. Lee, A.H. de Vries, S.-J. Marrink, R.W. Pastor, A coarse-grained model for polyethylene oxide and polyethylene glycol: conformation and hydrodynamics, *The journal of physical chemistry B*, 113 (2009) 13186-13194.
- [8] H. Lee, R.M. Venable, A.D. MacKerell, R.W. Pastor, Molecular dynamics studies of polyethylene oxide and polyethylene glycol: hydrodynamic radius and shape anisotropy, *Biophysical Journal*, 95 (2008) 1590-1599.
- [9] Y. Hu, J. Jin, Y. Han, J. Yin, W. Jiang, H. Liang, Study of fibrinogen adsorption on poly (ethylene glycol)-modified surfaces using a quartz crystal microbalance with dissipation and a dual polarization interferometry, *Rsc Advances*, 4 (2014) 7716-7724.
- [10] T.V. Chalikian, M. Totrov, R. Abagyan, K.J. Breslauer, The hydration of globular proteins as derived from volume and compressibility measurements: cross correlating thermodynamic and structural data, *Journal of molecular biology*, 260 (1996) 588-603.
- [11] N. Taulier, T.V. Chalikian, Compressibility of protein transitions, *Biochimica et Biophysica Acta (BBA)- Protein Structure and Molecular Enzymology*, 1595 (2002) 48-70.

**PAPER III**



Cite this: *RSC Adv.*, 2016, 6, 27969

Received 29th January 2016  
Accepted 9th March 2016

DOI: 10.1039/c6ra02703b

www.rsc.org/advances

## Hofmeister effect on thermo-responsive poly(propylene oxide) in H<sub>2</sub>O and D<sub>2</sub>O

Saeed Zafjoroushan Moghaddam and Esben Thormann\*

The Hofmeister effect of NaSCN, NaCl and NaF on poly(propylene oxide) solutions in H<sub>2</sub>O and D<sub>2</sub>O is studied. The effect of the solvent substitution is shown to vary for different salts and we suggest that this is due to a change in the polymer accessible surface area and ion hydration.

### Introduction

Thermo-responsive polymers in aqueous solution undergo a coil-globule transition within a defined temperature range.<sup>1–3</sup> To this end, solvent isotope effect studies have provided important information about the polymer collapse process.<sup>4–6</sup> Due to the more restricted atomic vibrations, the hydrogen bonding strength in heavy water (D<sub>2</sub>O) is roughly 5% stronger compared to light water (H<sub>2</sub>O), simply meaning that D<sub>2</sub>O is a relatively more “structured” solvent.<sup>5–7</sup> This delicate difference makes D<sub>2</sub>O a suitable substitute for H<sub>2</sub>O for solvent perturbation experiments on polymer solutions, where it can be investigated how hydrogen bonding and the hydrophobic effect contribute to the polymer–water miscibility and the phase separation process.<sup>7–10</sup>

Polymers in aqueous solution are also selectively responsive to the presence of different ions, an effect, which is widely known as the Hofmeister effect.<sup>11–13</sup> Here, weakly-hydrated ions promote a swollen polymer conformation in solution (salting-in effect), while strongly-hydrated ions promote a globular conformation (salting-out effect).<sup>14,15</sup> With respect to the mechanisms,<sup>16–18</sup> it is currently believed that destabilizing ions are excluded from the polymer interface, and withdraw the water molecules from the hydration shell of the polymer. On the other hand, stabilizing ions favourably accumulate at the polymer surface, which induces an electrostatic repulsion between the polymer chains. To further examine these mechanisms, a series of investigations have been dedicated to

studying the effect of changing the polymer (solute) properties, *e.g.* the molecular weight of the polymer.<sup>19,20</sup> Further studies have dealt with addressing the effect of varying the properties of the co-solute, *e.g.* the composition of ions in solution.<sup>21–23</sup>

Here we suggest that studying the solvent isotope effect on polymer/salt aqueous solutions can indicate how a delicate variation in the solvent properties can change the Hofmeister effect, and thus can be a new approach towards further understanding the Hofmeister effect. To our knowledge, this is the first systematic report of how solvent isotope perturbation affects the Hofmeister effect. Herein, one should notice that isotope substitution affects the hydration of both the polymer and the ions. With respect to the polymer hydration, the interaction between the water molecules and the hydrogen bond acceptor groups on the polymer backbone as well as the hydrophobic effect on the non-polar regions of the polymer become stronger in D<sub>2</sub>O compared to in H<sub>2</sub>O.<sup>24–26</sup> While the stronger hydrogen bonding between the polymer and the water molecules enhances the polymer stability, the stronger hydrophobic effect will decrease the polymer stability. With respect to the ions hydration, it has been suggested that different ions are not similarly affected by the solvent isotope substitution. In general terms, hydration of structure-breaking (chaotrope) anions such as SCN<sup>−</sup> becomes less favourable in D<sub>2</sub>O, while strong structure-making (kosmotrope) anions such as F<sup>−</sup> are prone to stronger hydration in D<sub>2</sub>O compared to in H<sub>2</sub>O.<sup>27–30</sup> The combination of these different effects on polymer and ion hydration should determine whether the polymer stability increases or decreases when going from H<sub>2</sub>O to D<sub>2</sub>O.

In the present work, the Hofmeister effect on poly(propylene oxide) (PPO) solutions in H<sub>2</sub>O and D<sub>2</sub>O is studied using differential scanning calorimetry. PPO is composed of hydrophilic (ether and hydroxyl groups) and hydrophobic (backbone and methyl side-groups) regions, and the hydration of both these regions will be affected by the solvent isotope substitution. NaSCN, NaCl and NaF were chosen considering two criteria. First, their different Hofmeister effects on PPO, where it has been shown that NaSCN has a strong non-linear salting-in

Department of Chemistry, Technical University of Denmark, 2800 Kgs. Lyngby, Denmark. E-mail: esth@kemi.dtu.dk

effect, while NaCl and NaF have linear salting-out effects.<sup>31</sup> Second, their different change in hydration level when going from H<sub>2</sub>O to D<sub>2</sub>O, where SCN<sup>−</sup> and Cl<sup>−</sup> supposedly become more weakly hydrated and F<sup>−</sup> becomes more strongly hydrated in D<sub>2</sub>O compared to in H<sub>2</sub>O.<sup>27–30</sup>

## Experimental section

Poly(propylene oxide) with an average molecular weight of 2000 g mol<sup>−1</sup>, heavy water (D<sub>2</sub>O, 99.9 atom% D) and analytical pure grades of NaF (99%), NaCl (99.5%) and NaSCN (98.5%) salts were all supplied by Sigma-Aldrich. Ultra-pure H<sub>2</sub>O was obtained from a Milli-Q Integral 3 system, and filtered through a 0.2 μm Millipak filter. The resistivity of the purified water was 18.2 MΩ cm, and the organic content was less than 3 ppb. Solutions of PPO in H<sub>2</sub>O (0.55 wt%) and D<sub>2</sub>O (0.5 wt%) were prepared by mixing at 5 °C overnight. The PPO concentrations were chosen in a way where there are the same number of water molecules per mass of polymer in H<sub>2</sub>O and D<sub>2</sub>O.

The phase transition of the solutions was monitored using a differential scanning calorimeter (Nano DSC, TA Instruments). The samples were degassed before the experiments, and measurements were conducted at a constant heating rate of 0.4 °C min<sup>−1</sup> and under a pressure of 3 atm. For the salt-free solutions of PPO, cooling experiments were performed under the same conditions. The measured raw heat data were normalized by the polymer concentration to obtain the molar heat capacity, as previously reported.<sup>31</sup> The measurements were repeated five times for the salt-free solutions. Both the measured phase transition temperatures (the peak temperature) and enthalpies (the area under the peak) showed desirable reproducibility (standard deviation of ±0.05 °C for the phase transition temperature and ±3.0 kJ mol<sup>−1</sup> for the enthalpy). For each salt concentration, the measurements were repeated twice.

## Results and discussion

DSC thermograms of salt-free solutions of PPO in H<sub>2</sub>O and D<sub>2</sub>O are presented in Fig. 1. The phase separation upon heating occurs at a lower temperature in D<sub>2</sub>O, while the change in enthalpy ( $\Delta H$ ) is just slightly larger in H<sub>2</sub>O. Upon cooling, the transition from a 2-phase system to a 1-phase system happens at a much lower temperature in D<sub>2</sub>O, and the enthalpy is also considerably smaller compared to in H<sub>2</sub>O. Comparing the heating and cooling thermograms for each solvent, a pronounced hysteresis is observed for PPO solution in D<sub>2</sub>O, while almost no hysteresis is seen for PPO solution in H<sub>2</sub>O.

To be able to interpret the observations, we will first briefly introduce the system under investigation. PPO is a thermoresponsive polymer with a typical LCST phase behaviour, meaning that it becomes less stable in solution upon heating. Below the phase separation temperature, hydrogen bonding between water and polar groups of PPO make the polymer more stable in solution (favourable enthalpic term), while the non-polar regions of PPO are surrounded by “ice-like” structures formed due to the hydrophobic effect (unfavourable entropic term). Although the former effect favors expansion of the

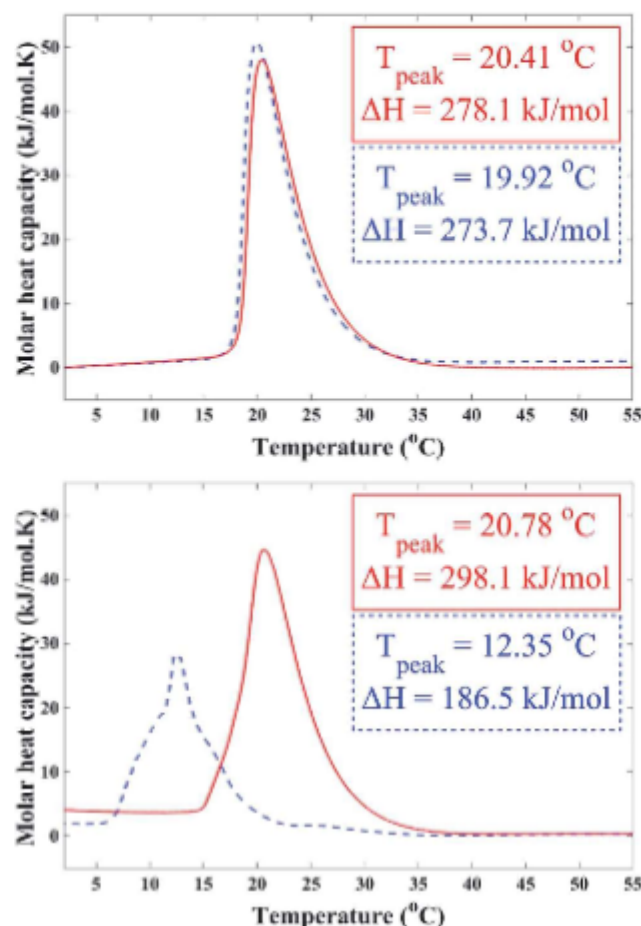


Fig. 1 DSC thermograms of salt-free PPO solutions in H<sub>2</sub>O (red line) and D<sub>2</sub>O (blue dashed line); (top) heating (bottom) cooling.

polymer coil (increment in solvent-accessible surface area), the latter effect promotes shrinkage of the polymer coil (decrement in solvent-accessible surface area) in order to compensate the entropic loss. At the phase separation temperature, the polymer is no longer miscible with water, and water-rich and polymer-rich phases will form. The phase separation upon heating is accompanied with (i) breakage of the hydrogen bonds between the water molecules and the polar groups of PPO, and (ii) liberation of water molecules from the hydrophobic hydration shell around the non-polar regions of PPO. The increment in the entropy associated with the latter effect is then the thermodynamic driving force of the phase separation. Now, changing the solvent from H<sub>2</sub>O to D<sub>2</sub>O affects both the enthalpic and entropic terms. Here, both hydrogen bonding between water and polar groups of PPO and the hydrophobic effect are expected to become stronger.<sup>24–26</sup>

Based on this knowledge, it can be inferred that PPO coils are more contracted and expose less accessible surface area in D<sub>2</sub>O compared to in H<sub>2</sub>O. In spite of the stronger hydrogen bonding between PPO and D<sub>2</sub>O, the larger hydrophobic effect in D<sub>2</sub>O appears to overcome the enthalpic term and make PPO less stable in D<sub>2</sub>O. This is seen by the lower phase separation temperature in D<sub>2</sub>O.



Regarding the measured enthalpies, it should be noticed that the main contribution to the change in enthalpy upon the phase separation originates from melting of the “ice-like” structures around the non-polar regions of the polymer. Thereby, the enthalpy change scales with the accessible surface area of the polymer, as well as with the strength of the hydrogen bonds between the water molecules.<sup>9,32</sup> Further, although the measured values for the change in heat capacity by the phase separations ( $\Delta C_p$ ) are minor, it is evident that the magnitude of  $\Delta C_p$  is relatively smaller in  $D_2O$ , which indicates a difference in the accessible surface area of the polymer in the two solvents.<sup>33–35</sup> Thus, although the strength of the hydrogen bonding is larger in  $D_2O$ , the exposed hydrophobic surface area of PPO is supposedly smaller. The combination of these two opposite effects may elucidate the minor difference between the measured enthalpies in  $H_2O$  and  $D_2O$ .

Based on previous reports,<sup>7–10</sup> it is further expected that inter-molecular interactions between PPO chains become enhanced in  $D_2O$ , and the results of the heating and cooling measurements strengthen this idea. The much smaller degree of hysteresis for the solution in  $H_2O$  shows that inter-chain interactions are not strong enough to interfere with single chain collapse. Therefore, the phase transition temperature and enthalpy values are almost identical for the heating and cooling measurements. The irreversible phase transition in  $D_2O$  can be explained conversely. Robust aggregates of PPO chains resulted from strong inter-chain interactions are more difficult to dissociate into individually-solvated chains, and the apparent phase transition therefore occurs at a much lower temperature upon cooling. The considerably smaller enthalpy observed in the cooling process also suggests that not all the PPO chains are liberated from the aggregates.

After discussing the solvent isotope effect on the stability of PPO in salt-free solutions, we next investigate how the isotope perturbation affects the Hofmeister effect. A comparison between the Hofmeister effect of NaSCN, NaCl and NaF on the stability of PPO solutions in  $H_2O$  and  $D_2O$  is provided in Fig. 2. NaSCN increases the phase separation temperature of PPO in the both solvents with a nonlinear trend, and this salting-in effect is approximately 10% stronger in  $D_2O$  compared to in  $H_2O$ . Addition of NaCl linearly decreases the phase separation temperature and the salting-out effect is roughly 5% weaker in  $D_2O$  compared to in  $H_2O$ . NaF has a relatively stronger linear salting-out effect, but only a minor difference, if any at all, is observed between the salting-out effects in  $H_2O$  and  $D_2O$ . To elucidate the observations, we first discuss the expected Hofmeister effect on PPO stability and then try to interpret the observed trends for the solvent isotope effect.

It is currently believed that anions with a salting-in effect tend to accumulate at the polymer interface, due to a combination of favourable interaction with the polymer and weak ion hydration. This bulk-to-interface migration of the ions has been suggested to induce an electrostatic repulsion between the polymer chains, leading to solution stabilization and an increment in the phase separation temperature.<sup>16–18</sup> On the other hand, anions with a salting-out effect are effectively repelled from the polymer interface, because of their strong and

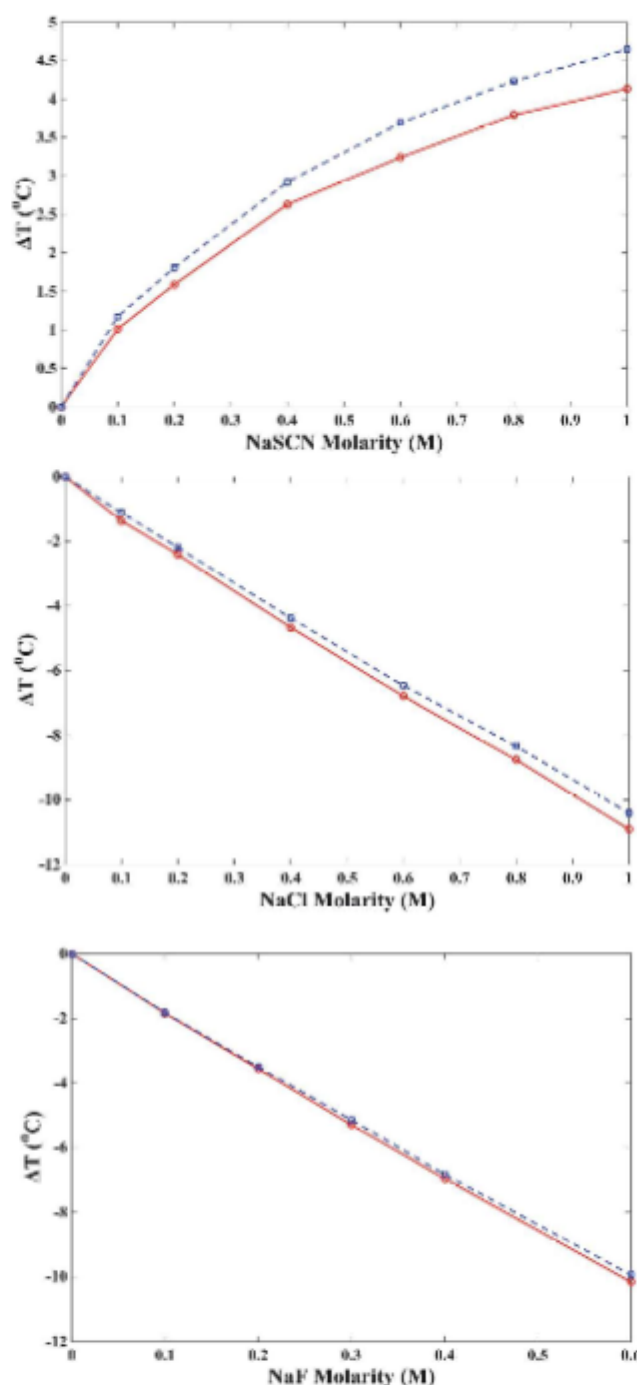


Fig. 2 Hofmeister effect of the salts in  $H_2O$  (red line) and  $D_2O$  (blue dashed line).

favourable hydration in the bulk solution. The excluded ions in the solution are capable of withdrawing the water molecules from the polymer hydration shell, and thereby destabilize the solution and decrease the phase separation temperature.<sup>16–18</sup>

The salting-in effect of NaSCN is thus considered to be a result of accumulation of weakly hydrated  $SCN^-$  at the PPO interface. By going from  $H_2O$  to  $D_2O$ , the interaction between  $SCN^-$  and water molecules is expected to become even more unfavourable.<sup>27–30,36–38</sup> This relatively weaker anion–water interaction in  $D_2O$  can lead to

a larger propensity of the ions to accumulate at the polymer interface. This can elucidate the considerably larger salting-in effect of NaSCN on PPO in D<sub>2</sub>O as shown in Fig. 2.

The salting-out effect of NaCl is attributed to the exclusion of Cl<sup>−</sup> from the PPO interface, and that the ions then will compete with the polymer chains for the hydration water. With respect to the solvent isotope effect, it has been reported that the hydration of Cl<sup>−</sup> becomes slightly weaker in D<sub>2</sub>O, but this effect is relatively smaller in extent compared to the isotope effect on the SCN<sup>−</sup> hydration.<sup>27–30,36–38</sup> Since NaCl still has a linear salting-out effect in D<sub>2</sub>O, it can be inferred that Cl<sup>−</sup> is repelled from the PPO interface, but has a relatively weaker ability to withdraw the water molecules from PPO in D<sub>2</sub>O. It is thus more difficult for Cl<sup>−</sup> to dehydrate the polar groups of PPO, and a decline in the salting-out effect is expected. We have further argued that the accessible surface area of PPO is expected to be smaller in D<sub>2</sub>O compared to in H<sub>2</sub>O. This decrement in the solvent-accessible surface area will also lead to a weaker salting-out effect, due to the less unfavourable ion–polymer interaction.

The large salting-out effect of NaF (compared to the effect of NaCl) can be attributed to the stronger hydration of F<sup>−</sup>, and thus the stronger ability of F<sup>−</sup> to compete with the polymer for the hydration water. Unlike most other anions, it has been suggested that F<sup>−</sup> becomes more strongly hydrated in D<sub>2</sub>O compared to in H<sub>2</sub>O.<sup>28–30</sup> Therefore, the water-withdrawing ability of F<sup>−</sup> and its effect on solution stability is expected to be stronger in D<sub>2</sub>O. On the other hand, considering that PPO exposes a relatively smaller accessible surface area in D<sub>2</sub>O, a weaker salting-out effect is expected. These two opposite effects apparently cancel each other, so that only a minor difference between the salting-out effects in H<sub>2</sub>O and D<sub>2</sub>O is obtained.

## Conclusions

It was shown that a minor solvent perturbation leads to an observable change in the magnitude of the Hofmeister effect. With respect to the effect of NaSCN, a considerable increment in the salting-in effect was observed in D<sub>2</sub>O compared to in H<sub>2</sub>O. In both solvents, SCN<sup>−</sup> is expected to be accumulated near the interface of the PPO chains. However, due to the relatively weaker hydration of SCN<sup>−</sup> in D<sub>2</sub>O compared to in H<sub>2</sub>O, we suggest that the SCN<sup>−</sup> ions are more strongly attracted to the PPO interface in D<sub>2</sub>O, which is thus leading to a stronger salting-in effect. With respect to the effect of NaCl, a decrement in the salting-out effect was observed in D<sub>2</sub>O compared to in H<sub>2</sub>O. This was explained by the solvent isotope effect on both the ion hydration and the polymer hydration. In D<sub>2</sub>O, the hydration of Cl<sup>−</sup> becomes slightly weaker and the polymer accessible surface area diminishes. These two effects both lead to a weaker salting-out effect in D<sub>2</sub>O compared to in H<sub>2</sub>O. With respect to the effect of NaF, it was observed that the salting-out effect is almost the same in both the solvents. This was explained by the opposite solvent isotope effects on the ion hydration and the polymer accessible surface area, which in this case are nearly cancelling each other.

Our results suggest that studying the solvent isotope effect is a relevant approach for examining the fundamental mechanisms of the Hofmeister effect. The fact that different ions are not similarly influenced by the solvent isotope effect, suggests that studying the Hofmeister effect of different ions in H<sub>2</sub>O and D<sub>2</sub>O can enhance our understanding of the role of both the ion hydration and the solvent-accessible surface area of the polymer in the Hofmeister effect.

## Acknowledgements

The authors acknowledge financial support from the Swedish Research Council, VR.

## Notes and references

- 1 N. Ishida and S. Biggs, *Langmuir*, 2007, **23**, 11083–11088.
- 2 K. Zhou, Y. Lu, J. Li, L. Shen, G. Zhang, Z. Xie and C. Wu, *Macromolecules*, 2008, **41**, 8927–8931.
- 3 S. Peng and B. Bhushan, *RSC Adv.*, 2012, **2**, 8557–8578.
- 4 P. Sasisanker, A. Oleinikova, H. Weingärtner, R. Ravindra and R. Winter, *Phys. Chem. Chem. Phys.*, 2004, **6**, 1899–1905.
- 5 Y. Efimova, S. Haemers, B. Wierczinski, W. Norde and A. Van Well, *Biopolymers*, 2007, **85**, 264–273.
- 6 S.-Y. Sheu, E. Schlag, H. Selzle and D.-Y. Yang, *J. Phys. Chem. A*, 2008, **112**, 797–802.
- 7 M. M. Lopez and G. I. Makhatadze, *Biophys. Chem.*, 1998, **74**, 117–125.
- 8 Y. Cho, L. B. Sagale, S. Iimura, Y. Zhang, J. Kherb, A. Chilkoti, J. M. Scholtz and P. S. Cremer, *J. Am. Chem. Soc.*, 2009, **131**, 15188–15193.
- 9 G. I. Makhatadze, G. M. Clore and A. M. Gronenborn, *Nat. Struct. Biol.*, 1995, **2**, 852–855.
- 10 Z. Shi, B. A. Krantz, N. Kallenbach and T. R. Sosnick, *Biochemistry*, 2002, **41**, 2120–2129.
- 11 F. Hofmeister, *Arch. Exp. Pathol. Pharmacol.*, 1888, **25**, 1–30.
- 12 A. Salis and B. W. Ninham, *Chem. Soc. Rev.*, 2014, **43**, 7358–7377.
- 13 L. Tomé, C. Sousa, J. Gomes, O. Ferreira, J. Coutinho and S. Pinho, *RSC Adv.*, 2015, **5**, 15024–15034.
- 14 P. Ball and J. E. Hallsworth, *Phys. Chem. Chem. Phys.*, 2015, **17**, 8297–8305.
- 15 K. D. Collins, *Biophys. Chem.*, 2012, **167**, 43–59.
- 16 Y. Zhang and P. S. Cremer, *Annu. Rev. Phys. Chem.*, 2010, **61**, 63–83.
- 17 L. M. Pegram and M. T. Record Jr, *J. Phys. Chem. B*, 2008, **112**, 9428–9436.
- 18 M. T. Record, E. Guinn, L. Pegram and M. Capp, *Faraday Discuss.*, 2013, **160**, 9–44.
- 19 Y. Zhang, S. Furry, L. B. Sagale, Y. Cho, D. E. Bergbreiter and P. S. Cremer, *J. Phys. Chem. C*, 2007, **111**, 8916–8924.
- 20 S. Z. Moghaddam and E. Thormann, *J. Colloid Interface Sci.*, 2016, **465**, 67–75.
- 21 S. Z. Moghaddam and E. Thormann, *Phys. Chem. Chem. Phys.*, 2015, **17**, 6359–6366.
- 22 Y. Xu and G. Liu, *J. Phys. Chem. B*, 2014, **118**, 7450–7456.

- 23 M. Bončina, J. Reščič and V. Vlady, *Biophys. J.*, 2008, **95**, 1285–1294.
- 24 B. Hammouda, D. Ho and S. Kline, *Macromolecules*, 2002, **35**, 8578–8585.
- 25 H. Shirota, N. Kuwabara, K. Ohkawa and K. Horie, *J. Phys. Chem. B*, 1999, **103**, 10400–10408.
- 26 G. Nemethy and H. A. Scheraga, *J. Chem. Phys.*, 1964, **41**, 680–689.
- 27 Y. Marcus, *Chem. Rev.*, 2009, **109**, 1346–1370.
- 28 R. Shearman and A. W. Menzies, *J. Am. Chem. Soc.*, 1937, **59**, 185–186.
- 29 C. G. Swain and R. F. Bader, *Tetrahedron*, 1960, **10**, 182–199.
- 30 R. D. Eddy and A. W. Menzies, *J. Phys. Chem.*, 1940, **44**, 207–235.
- 31 E. Thormann, *RSC Adv.*, 2012, **2**, 8297–8305.
- 32 H. Feil, Y. H. Bae, J. Feijen and S. W. Kim, *Macromolecules*, 1993, **26**, 2496–2500.
- 33 A. Cooper, C. M. Johnson, J. H. Lakey and M. Nöllmann, *Biophys. Chem.*, 2001, **93**, 215–230.
- 34 V. V. Loladze, D. N. Ermolenko and G. I. Makhatadze, *Protein Sci.*, 2001, **10**, 1343–1352.
- 35 V. Y. Grinberg, A. S. Dubovik, D. V. Kuznetsov, N. V. Grinberg, A. Y. Grosberg and T. Tanaka, *Macromolecules*, 2000, **33**, 8685–8692.
- 36 H. D. B. Jenkins and Y. Marcus, *Chem. Rev.*, 1995, **95**, 2695–2724.
- 37 Y. Marcus, *J. Solution Chem.*, 1994, **23**, 831–848.
- 38 Y. Marcus and A. Ben-Naim, *J. Chem. Phys.*, 1985, **83**, 4744–4759.

## **PAPER IV**



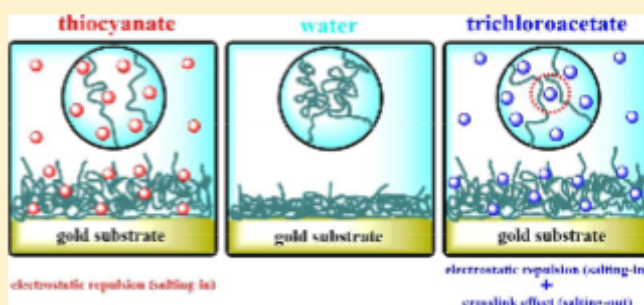
## Hofmeister Effect on PNIPAM in Bulk and at an Interface: Surface Partitioning of Weakly Hydrated Anions

Saeed Zajforoushan Moghaddam<sup>✉</sup> and Esben Thormann\*

Department of Chemistry, Technical University of Denmark, 2800 Kgs. Lyngby, Denmark

## Supporting Information

**ABSTRACT:** The effect of sodium fluoride, sodium trichloroacetate, and sodium thiocyanate on the stability and conformation of poly(*N*-isopropylacrylamide), in bulk solution and at the gold–aqueous interface, is investigated by differential scanning calorimetry, dynamic light scattering, quartz crystal microbalance, and atomic force microscopy. The results indicate a surface partitioning of the weakly hydrated anions, i.e., thiocyanate and trichloroacetate, and the findings are discussed in terms of anion-induced electrostatic stabilization. Although attractive polymer–ion interactions are suggested for thiocyanate and trichloroacetate, a salting-out effect is found for sodium trichloroacetate. This apparent contradiction is explained by a combination of previously suggested mechanisms for the salting-out effect by weakly hydrated anions.



## 1. INTRODUCTION

Stimuli-responsive polymers undergo a change in conformation and interaction in response to an external stimulus and are of great importance in numerous areas, such as biomedical engineering and the fabrication of smart surfaces.<sup>1–4</sup> Since the earliest report in 1967, poly(*N*-isopropylacrylamide) (PNIPAM) has drawn enormous attention because of its abrupt phase transition, which is reminiscent of protein folding and denaturation.<sup>5</sup> Furthermore, PNIPAM has a phase separation temperature in the proximity of human body temperature, rendering it a promising candidate for drug delivery and other biomedical applications.<sup>6–8</sup> Regarding thermoresponsiveness, PNIPAM shows lower critical solution temperature (LCST) phase behavior, meaning that water miscibility decreases with increasing temperature.<sup>9–11</sup> Below the phase separation temperature, PNIPAM adopts a swollen coil conformation, while a drastic decline in hydrophilicity and coil size occurs upon crossing the phase separation boundary.

The presence of ions, particularly anions, can also influence the stability of PNIPAM in aqueous solutions; this effect is widely known as the Hofmeister effect.<sup>12–15</sup> This phenomenon not only depends on the ionic strength of the solution but also relies on other ionic properties, such as size, polarizability, hydration energetics, and the partition coefficient. In other words, it is “ion-specific”.<sup>16–18</sup> The Hofmeister effect of anions on uncharged polymers, such as PNIPAM, can be divided into two distinct types:<sup>19–24</sup>

(i) Strongly hydrated anions, e.g., fluoride ( $F^-$ ), decrease the polymer stability in solution (a “salting-out” effect) and produce a linear drop in the phase separation temperature as a function of salt concentration. Such anions are effectively repelled from the polymer surface, and the LCST depression

mainly stems from their “water withdrawing power”, meaning that they can compete with the polymer for hydration water.<sup>25,26</sup>

(ii) Weakly hydrated and highly polarizable anions, e.g., thiocyanate ( $SCN^-$ ), promote polymer stability in solution (a “salting-in” effect) and raise the phase separation temperature in a nonlinear manner. The stabilization effect originates from preferential partitioning and accumulation of anions at the polymer surface because of the loose bulk hydration and favored interactions with the polymer surface.<sup>27–29</sup> The anion–polymer association can be of different natures, e.g., dispersion forces resulting from the high polarizability of the anions or Coulombic interactions with partially positive sites on the polymer backbone.<sup>30–32</sup> For many polymers, including PNIPAM, this salting-in effect is limited to relatively low salt concentrations, after which a linear salting-out effect is observed.<sup>20,33</sup>

In the present study, we target two important obscurities in the Hofmeister effect for weakly hydrated anions. First, the accumulation of anions to promote polymer stability is not yet fully understood, although an abundance of studies have been performed to determine why such anions have an affinity for the polymer surface. Previous studies suggested an electrostatic stabilization mechanism;<sup>34–36</sup> nevertheless, further experimental proof is still needed. Our objective is to ascertain the association of weakly hydrated anions with PNIPAM by studying the structural properties of PNIPAM in saline solutions. Second, we investigate the behavior of a PNIPAM

Received: March 20, 2017

Revised: April 25, 2017

Published: April 27, 2017



solution in a system where a salting-out effect is observed by a weakly hydrated anion to better understand the turning point (i.e., the salting-in to salting-out transition), which is another enigmatic aspect of the Hofmeister effect of weakly hydrated anions.

The Hofmeister effect of three sodium salts on the PNIPAM stability, in bulk and at an interface, is investigated. Sodium fluoride (NaF) and sodium thiocyanate (NaSCN) are selected because these salts have strong salting-out and salting-in effects, respectively. Sodium trichloroacetate (NaTCA) is chosen as the third salt. Trichloroacetate ( $\text{TCA}^-$ ) is a weakly hydrated bulky anion with a significant binding tendency toward proteins and hydrophobic entities.<sup>37–39</sup> The effect of the salts on the PNIPAM stability is inspected using four different techniques. Differential scanning calorimetry is performed to obtain the phase separation temperature of the solutions and the enthalpy and entropy of dehydration. Dynamic light scattering is employed to determine the effect of the salts on the hydrodynamic coil size of PNIPAM and aggregation temperature. A quartz crystal microbalance with dissipation is used to monitor the conformational changes of the PNIPAM film in the presence of the salts. Finally, atomic force microscopy colloidal probe measurements are conducted to scrutinize the interactions between the PNIPAM films in the salt solutions at various temperatures.

## 2. EXPERIMENTAL SECTION

**2.1. Materials.** PNIPAM (number-average molecular weight ( $M_n$ ) of 475 000 g/mol and polydispersity index ( $\text{PDI} = M_w/M_n$ ) of 1.3) and mono thiol-terminated poly(*N*-isopropylacrylamide) (PNIPAM-SH,  $M_n = 8000$  g/mol,  $\text{PDI} = 1.3$ ) were purchased from Polymer Source Inc. (Dorval, Canada) and used as received. NaF ( $\geq 99\%$ ), NaTCA ( $\geq 97\%$ ), NaSCN ( $\geq 98.5\%$ ), and gold-coated silicon wafer (99.999% Au, layer thickness of 1000 Å) were supplied by Sigma-Aldrich. Gold-coated barium titanate glass microspheres (coating thickness: around 20 nm) were purchased from Cospheric LLC (Santa Barbara, CA). Degassed ultrapure Milli-Q water with a resistivity of 18.2 M $\Omega$ -cm and organic content below 5 ppb was used. All PNIPAM solutions were prepared using a nutating mixer at 5 °C for 24 h.

**2.2. Methods. Differential Scanning Calorimetry (DSC).** To analyze the phase separation thermodynamics of the solutions, DSC (Nano DSC, TA Instruments, New Castle, DE) was employed. Measurements were carried out using 0.1 wt % solutions of PNIPAM in pure water and in 200 mM salt solutions. The solutions were thermally stabilized at 10 °C for 30 min and then heated from 10 to 50 °C at a heating rate of 0.2 °C/min. To avoid bubble formation, the measurements were conducted under a constant pressure of 3 bar. The endothermic peak maximum was considered to be the phase separation temperature ( $T_{ps}$ ). The raw heat data were normalized to the monomer molecular weight and concentration to obtain the molar heat capacities. The molar enthalpy of the phase separation ( $\Delta H$ ) was determined by integrating the area under the peak, and the molar entropy of the phase separation ( $\Delta S$ ) was calculated according to  $\Delta S = \Delta H/T_{ps}$ . Three measurements were conducted for each solution. (Analysis of the raw heat data is provided in the [Supporting Information](#), section S1.)

**Dynamic Light Scattering (DLS).** The apparent hydrodynamic diameter of PNIPAM in the salt-free and 200 mM saline solutions at various temperatures between 20 and 40 °C was determined using a DLS apparatus (Zetasizer Nano-ZS, Malvern Instruments, Worcester-shire, UK). In brief, this technique measures time-dependent fluctuations in the scattered light intensity resulting from Brownian motion of the polymer coils. By fitting the time correlation function to the measured intensity fluctuations, the diffusion coefficients of the polymer chains are found. The diffusion coefficient is inversely related to the coil size and can be converted into the hydrodynamic diameter using the Stokes–Einstein equation.<sup>40</sup> Measurements were performed

using 0.1 wt % dilute solutions of PNIPAM in pure water and 200 mM saline solutions. The PNIPAM concentration was optimized to minimize the overlap between the polymer coils in solution (well below the overlap concentration, which was estimated to be around 0.9 wt %), while a satisfactory scattering intensity was measured. Before starting the measurements, the solutions were thermally stabilized for 30 min at 20 °C. For each solution, the measurements were repeated once, and each experimental run consists of  $3 \times 12$  consecutive measurements. The standard analysis software of the instrument (Zetasizer software) was used for data analysis and obtaining the size distribution from the fitted autocorrelation function. The Z-average hydrodynamic diameter obtained from cumulants fit was used here.

**Quartz Crystal Microbalance with Dissipation (QCM-D).** The conformational change of the PNIPAM film in the salt solutions was monitored using QCM-D (Q-Sense E1, Biolin Scientific, Gothenburg, Sweden). A gold-coated sensor chip (fundamental frequency of 4.95 MHz) was repeatedly rinsed in acetone, washed with copious Milli-Q water, and ultimately plasma-cleaned (PDC-32G plasma cleaner, Harrick Plasma) for 5 min in air under a constant pressure of 500 mTorr. The sensor was immediately placed in the flow module of the apparatus, and the measurement was started at 20 °C under a 100  $\mu\text{L}/\text{min}$  steady flow of degassed Milli-Q water. After obtaining a stable baseline for all the harmonics (1st to 11th overtones), the bulk shifts of the frequency and dissipation values were measured for each salt solution at various temperatures. In brief, at each constant temperature, the buffer was changed from water to a 200 mM saline solution and then switched back to water. After obtaining the bulk shifts, a 0.1 wt % solution of PNIPAM was flowed over the bare sensor for 24 h at 20 °C to obtain a polymer layer formed by physically adsorbed PNIPAM chains on the gold surface. The cell was then rinsed with Milli-Q water to remove any loosely adsorbed polymer chains until a stable baseline for all the overtones was reached. The same experimental procedure as used for measuring the bulk shifts was applied on the polymer-coated sensor to study the effect of changing the solvent from water to the saline solutions at various temperatures. To obtain the polymer response, the measured bulk shifts were subtracted from the data. Herein, the third overtone data are used for the analysis and discussion. All measurements on the bare sensor and the polymer-coated sensor were repeated three times and showed very good reproducibility. It should be noted that the same experiments were performed on the thiol-terminated PNIPAM; nevertheless, the shifts in frequency and dissipation after bulk subtraction were not large enough to provide reliable trends. Accordingly, only the results of the high molecular weight PNIPAM sample are provided and discussed here. (QCM-D data of the low molecular weight sample are available in the [Supporting Information](#), section S2.1.)

**Atomic Force Microscopy (AFM).** To inspect the interactions between the PNIPAM layers in different salt solutions and at different temperatures, AFM colloidal probe measurements (NanoWizard 3, JPK Instruments AG, Berlin, Germany) were carried out. A tipless rectangular cantilever (HQ-CSC38/Cr-Au, MikroMasch) with an approximate length of 250  $\mu\text{m}$ , width of 32.5  $\mu\text{m}$ , thickness of 1  $\mu\text{m}$ , and normal spring constant of 0.09 N  $\text{m}^{-1}$  was used. The accurate normal spring constant of the cantilever (with no particle attached) was obtained using the thermal noise method.<sup>41</sup> A gold-coated spherical particle (Cospheric LLC, Santa Barbara, CA) with a diameter of  $20 \pm 0.1$   $\mu\text{m}$  (measured using a Nikon Eclipse LV100ND optical microscope and the Infinity Analyze image processing software) was glued to the end of the cantilever using a small amount of a two-component epoxy adhesive (Araldite 2000 Plus).<sup>42,43</sup> A gold-coated silicon wafer (root-mean-square roughness below 2.5 nm over a 1  $\mu\text{m} \times 1$   $\mu\text{m}$  area, obtained from AFM imaging) was used as the flat substrate. To ensure stability of the PNIPAM layers during the measurements, PNIPAM chains were chemically grafted at one end to the gold surface using gold–thiol chemistry.<sup>44</sup> The cantilever with the attached gold-coated particle and the substrate were plasma-cleaned for 5 min and then immersed in a 0.1 wt % solution of thiol-terminated PNIPAM for 2 h. After rinsing with copious water, the samples were immediately used for the measurements. During the force measure-



ments, the temperature of the solution was controlled with an accuracy of  $\pm 0.1$  °C using a BioCell (JPK Instruments). Two syringe pumps (Aladdin syringe pump, World Precision Instruments, Sarasota, FL) were used to exchange the solutions in the AFM BioCell. When exchanging the solution or changing the cell temperature, the system was subjected to 15 min of stabilization time. For each measurement condition, 25 force curves were collected at various surface positions, which were equally separated over an area of  $5\ \mu\text{m} \times 5\ \mu\text{m}$ . The force measurements were conducted with an approach and retraction velocity of 300 nm/s, where the contribution from hydrodynamic forces could be neglected.<sup>45</sup> The standard software of the instrument (JPKSPM Data Processing) was used to process the raw data and analyze the force curves, as described in detail elsewhere.<sup>46</sup>

### 3. RESULTS AND DISCUSSION

Before discussing our findings, a general prelude on some aspects of PNIPAM hydration and phase transition is useful.<sup>11,47,48</sup> Below the phase separation temperature, PNIPAM chains adopt a swollen random coil conformation and are highly hydrated, with a water content of around 90%.<sup>49,50</sup> Regarding the structure of water molecules surrounding the PNIPAM chains, two types of hydration structures were previously suggested: (i) water molecules that are hydrogen-bonded to the amide groups and (ii) water molecules neighboring the hydrophobic backbone and isopropyl side groups, generally referred to as “hydrophobic hydration”. Upon heating the solution to the phase separation temperature, the PNIPAM coils abruptly shrink and adopt a collapsed conformation, while tending to aggregate because of attractive interchain interactions. The hydrogen-bonded water molecules are almost unaffected by the phase transition, and a collapsed PNIPAM coil still contains nearly 60% water.<sup>10,51,52</sup> Accordingly, it is the hydrophobic effect that dominantly governs the phase separation of PNIPAM.<sup>10,11</sup> Compared to the bulk structure, water molecules in the hydrophobic hydration shell form stronger hydrogen bonds (favorable enthalpic term) but possess a lesser degree of freedom (unfavorable entropic term). The balance of these two contrary factors determines the stability of PNIPAM in water at different temperatures. Below the phase separation temperature, the favorable enthalpic term keeps PNIPAM in the solution. Upon passing the phase separation temperature, the entropic term prevails, and water molecules escape from the hydrophobic hydration cage to acquire a higher entropic state. Knowing the determining role of the hydrophobic effect, the next step is to assess it in the salt solutions.

Ions can influence the hydrophobic effect of water on small nonpolar solutes.<sup>53–56</sup> Considering the surface exclusion of strongly hydrated anions, such ions could affect the hydrophobic effect by changing the enthalpy and entropy values of hydrogen bond formation in the bulk. As mentioned above with respect to pure water, formation of hydrogen bonds at the hydrophobic surfaces is enthalpically favorable but entropically costly. The combination of these two factors provides a net positive contribution to the free energy. The situation is reversed in strongly hydrated salt solutions, where the ion–water interaction is relatively stronger than the water–water interaction. Accordingly, the formation of hydrogen bonds in the hydrophobic hydration layer in the saline solutions is enthalpically costly but entropically favored. However, the net contribution to the free energy is even more positive than that of pure water, providing a relatively stronger hydrophobic effect in such saline solutions. Regarding the surface affinity of weakly hydrated anions, the hydrophobic effect can be affected in two

manners. On the one hand, the anions can modify the hydrophobic effect by changing the energetics of hydrogen bond formation. On the other hand, the accumulation of the anions at the surface constrains the space for water molecules; therefore, the number of water molecules in the hydrophobic shell decreases (surface effect). After becoming acquainted with these principles, henceforth, we discuss our findings on the Hofmeister effect of salts.

**3.1. DSC Measurements in Bulk Solution.** The DSC data of 0.1 wt % PNIPAM in pure water and saline solutions are presented in Figure 1 and Table 1. In agreement with former

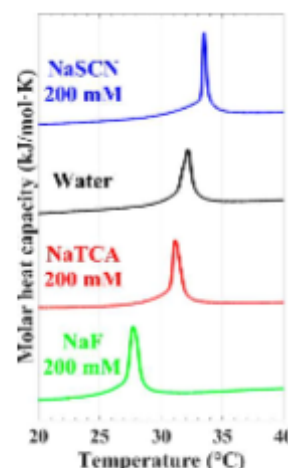


Figure 1. DSC thermograms of 0.1 wt % PNIPAM solutions.

Table 1. DSC Data of 0.1 wt % PNIPAM Salt-Free and Saline Solutions as Well as Enthalpy and Entropy Change per Monomer Unit

sample	$T_{\text{peak}}$ (°C)	$\Delta H$ (kJ/mol)	$\Delta S$ (J/(mol K))
NaSCN 200 mM	33.52 ( $\pm 0.06$ )	3.85 ( $\pm 0.08$ )	12.60 ( $\pm 0.25$ )
water	32.27 ( $\pm 0.01$ )	4.16 ( $\pm 0.10$ )	13.60 ( $\pm 0.35$ )
NaTCA 200 mM	31.06 ( $\pm 0.03$ )	4.11 ( $\pm 0.02$ )	13.50 ( $\pm 0.10$ )
NaF 200 mM	27.75 ( $\pm 0.01$ )	4.42 ( $\pm 0.07$ )	14.70 ( $\pm 0.25$ )

studies, PNIPAM undergoes a sharp endothermic phase separation in aqueous solutions at around 32 °C, which is accompanied by an increment in the system entropy. Considering hydrophobic dehydration as the primary driving force for phase separation, the enthalpy and entropy changes thus correspond to the transfer of water molecules from the hydrophobic hydration shell to the bulk solution.<sup>5,10</sup> The adsorbed heat resulting from the phase separation correlates to breakdown of the more strongly hydrogen-bonded water structures that surround the hydrophobic groups (which are often referred to as the “ice-like” structures). On the other hand, the observed positive entropy change of the phase separation indicates a higher degree of freedom for the water molecules that are transferred to the bulk solution.

With respect to the effects of the salts, 200 mM NaF lowers the phase separation temperature by 4.5 °C, whereas 200 mM NaSCN increases the phase separation temperature by 1.25 °C, in accordance with the hydration power of their constituent anions. Despite the poor hydration power of TCA<sup>−</sup>, 200 mM NaTCA shows a salting-out effect and leads to a decrement of the phase separation temperature by 1.2 °C. Besides the phase separation temperature, the salts also affect the enthalpy and entropy change of dehydration. Compared to the salt-free

solution, 200 mM NaF increases the enthalpy and entropy changes, while the values are relatively smaller in the NaSCN solution. The former observation supports the idea of having a stronger hydrophobic effect in the strongly hydrated salt solutions. On the other hand, the latter result implies that accumulation of the weakly hydrated anions at the polymer surface can interfere with hydrophobic hydration. Unlike the two other salts, 200 mM NaTCA has a negligible effect (i.e., within the range of the experimental uncertainties) on the phase separation energetics.

Regarding the strong affinity of  $\text{TCA}^-$  to accumulate at hydrophobic and polymer surfaces, attenuation of the hydrophobic hydration and then a decrement in the enthalpy and entropy values are anticipated, which are effects similar to those in the NaSCN solution. This may suggest an intensifying effect on the hydrophobic hydration to counterbalance the surface-related effect so that the enthalpy and entropy values remain almost the same. Thus, we will further investigate the idea of the strong association between  $\text{TCA}^-$  and PNIPAM in the following sections.

**3.2. DLS Measurements in Bulk Solution.** Figure 2 illustrates the effect of temperature and salts on the apparent hydrodynamic diameter of PNIPAM in solution. At temperatures well below the phase separation point, PNIPAM has a hydrodynamic diameter of  $\sim 41$  nm, which is in agreement with the previously suggested scaling law between the hydrodynamic diameter and the molecular weight of PNIPAM.<sup>59</sup> Within the experimental uncertainties, the salts generally appear to have an insignificant effect on the hydrodynamic coil size. Additionally, all of the samples show a considerable increment in the apparent hydrodynamic diameter near their phase separation temperatures. We suggest that this is not a real change in the coil size but is probably a result of stronger interchain interactions, and thus slower diffusion, when approaching the phase separation temperature. This speculation is further supported by additional DLS measurements conducted on solutions with lower and higher concentration of PNIPAM (see the Supporting Information, section S3). For the salt-free and all the saline solutions, there is a good correlation between the temperatures at which the apparent hydrodynamic size (from DLS) and the heat capacity (from DSC) begin to increase (compare Figures 1 and 2).

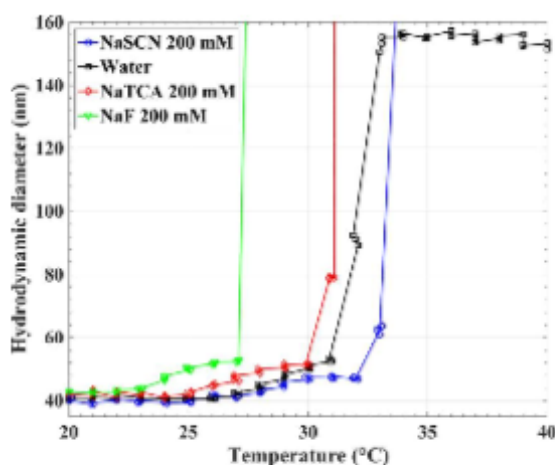


**Figure 2.** Hydrodynamic diameter (Z-average) of PNIPAM as a function of temperature in the saline and salt-free solutions.

Another interesting finding is the formation of nanosized PNIPAM mesoglobules after the phase separation temperature in water, whereas macroscopic segregation of the polymer-rich and water-rich phases occurs in all of the saline solutions. Although this topic is beyond the scope of our paper, it is worth a brief discussion. As reported, PNIPAM chains of specific molecular weights and at certain concentrations may form meso-stable, nano-sized globular aggregates after the collapse temperature.<sup>11,58</sup> There is still a disagreement about the stabilization mechanisms, but two explanations have gained more acceptance.<sup>59,60</sup> First, PNIPAM chains form aggregates to minimize their hydrophobic surface area, but the hydrated hydrophilic parts can stabilize the globules and hamper macroscopic flocculation. Second, the globules are partially charged, either because of the presence of an ionic initiator in the PNIPAM chain or ion adsorption from solution, and are thus electrostatically repelled from each other. To investigate if the PNIPAM mesoglobules in the salt-free solution are charged, zeta potential measurements were conducted as a function of temperature, in which an average zeta potential of around  $-12$  mV was obtained for the mesoglobules (see the Supporting Information, section S3). Accordingly, the observed cessation of mesoglobule formation in all of the saline solutions suggests that the electrostatic stabilization mechanism plays an important role in mesoglobule stability, even though the other mechanism can still contribute.

**3.3. QCM-D Study of a Physically Adsorbed PNIPAM Film on the Gold Surface.** Figure 3 depicts the dissipation and frequency shifts resulting from changing the solvent from water to the saline solutions at various temperatures. (The

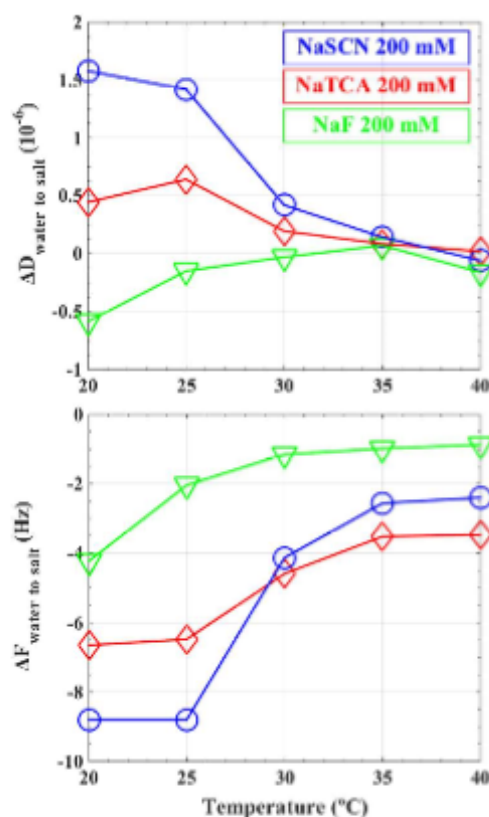


**Figure 3.** Subtracted dissipation ( $\Delta D_{\text{water to salt}}$ ) and frequency shifts ( $\Delta F_{\text{water to salt}}$ ) for changing the solvent from water to the saline solutions at various temperatures.



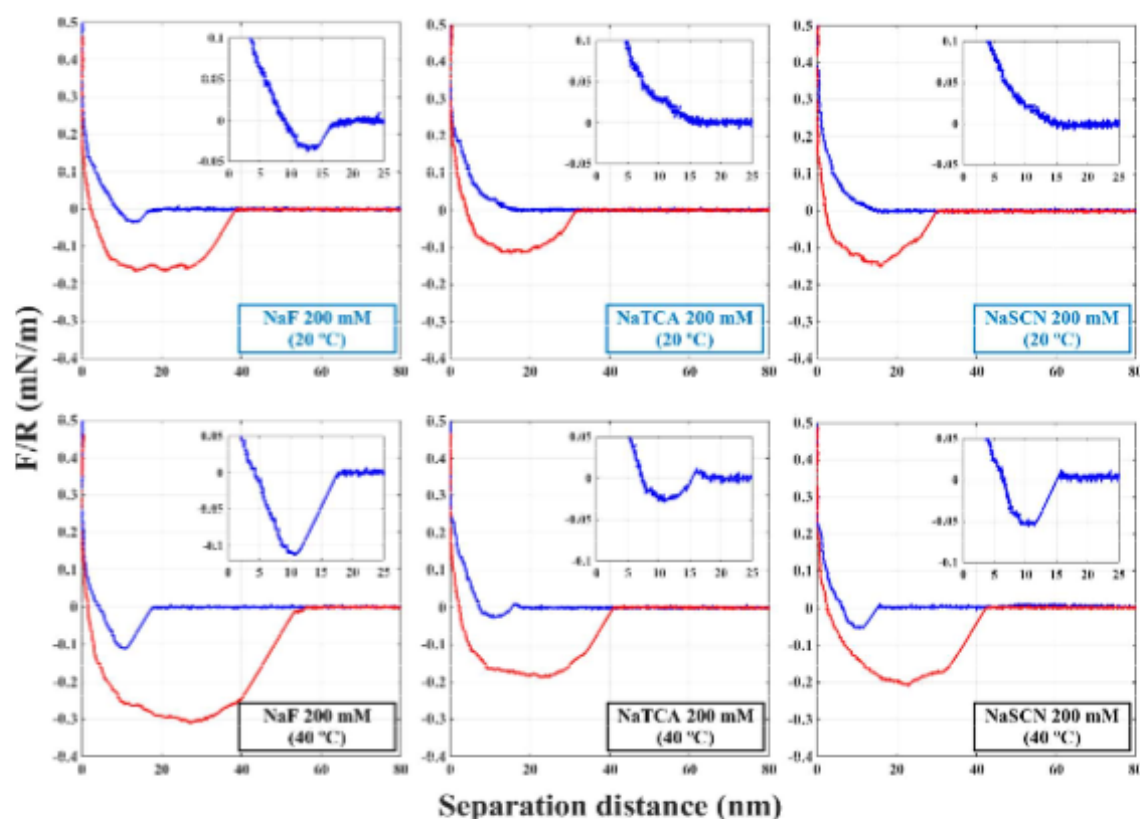


**Figure 4.** Approach (blue line) and retract (red line) force–distance curves between two PNIPAM layers in the salt solutions at 20 °C (top row, hydrated state) and 40 °C (bottom row, collapsed state); insets show the contact point in the approach step.

comprehensive analysis of PNIPAM physical adsorption on the gold surface and testing durability of the prepared film are available in the [Supporting Information](#), section S2.2.) During a QCM-D measurement, the drive generator output repeatedly ceases, and the subsequent decay of the sensor oscillation is monitored. Accordingly, the dissipation (damping) factor ( $D$ ) is determined as the energy dissipated per oscillation divided by the total energy stored in the system. A soft film attached to the sensor is deformed during oscillation and hence can provide a high dissipation value. In contrast, a rigid polymer layer follows the oscillation with no significant deformation and thus has a small damping factor. Accordingly, the dissipation value can provide semiquantitative structural and conformational information about the swelling and collapse of the polymer film.

The oscillation frequency ( $F$ ) is sensitive to the total mass coupled with the sensor, which in the present case includes the physically adsorbed PNIPAM chains, the associated water molecules (hydrodynamic water content), and the adsorbed and trapped ions. Considering the polymer chains to remain intact on the surface with no desorption, the subtracted frequency shift corresponds to variation in the solvent content of the PNIPAM layer as well as adsorption of the ions. With respect to the former, dehydration of PNIPAM chains gives rise to a positive frequency shift, and vice versa. Regarding the latter, adsorption of ions to the polymer surface or the bare gold surface can give rise to a negative frequency shift. In addition to the anion–polymer association, one can expect adsorption of sodium cations to the bare gold surface, regarding the partial negative charge present on the gold surface.<sup>61,62</sup>

First, we investigate how changing the solvent from water to a saline solution can alter the dissipation factor of the PNIPAM film at various temperatures. By doing so, a change in the

dissipation factor value ( $\Delta D_{\text{water to salt}}$ ) is detected, which can be either positive (the film becomes softer and more dissipative) or negative (the film becomes more rigid and less dissipative). As a general observation in [Figure 3](#), the PNIPAM film is more responsive to the addition of salts at low temperatures than at high temperatures. The salts provide almost no change in the dissipation factor ( $\Delta D \approx 0$ ) at 35 and 40 °C, indicating a fully collapsed state at these temperatures. In accordance with the DSC and DLS results, the collapse of the PNIPAM film commences at temperatures around 30 °C because the polymer film response to a change in the temperature or addition of the salts is notably weaker than that observed at 20 and 25 °C. This can also be seen from the subtracted dissipation shifts resulting from heating the PNIPAM film in the salt-free solution (see the [Supporting Information](#), section S2.2). It should be considered that polymers confined at the solid–liquid interface typically have a lower collapse temperature than that in bulk solution because of the entropic restriction imposed by the conformational confinement.<sup>63–65</sup> Regarding the effect of the salts at 20 and 25 °C, the observed trend of the Hofmeister series ( $\text{NaSCN} > \text{NaTCA} > \text{NaF}$ ) is similar to that of the DSC and DLS results, though with an important distinction. Changing the solvent from water to the NaF solution is accompanied by a negative  $\Delta D$ , meaning that the PNIPAM film becomes relatively rigid and partially collapses. In contrast, changing the solvent from water to either the NaTCA or NaSCN solutions provides a positive  $\Delta D$  value, which suggests swelling of the PNIPAM film from surface partitioning of the anions. Therefore, although 200 mM NaTCA produces a salting-out effect on the phase separation temperature of PNIPAM (inferred from the DSC and DLS measurements), our QCM-D findings imply the surface affinity of  $\text{TCA}^-$  and a swelling of

the polymer film. However, the  $\Delta D$  values are relatively smaller for NaTCA than NaSCN at all temperatures, and we suggest that this is another indication of an alternative destabilizing effect in the NaTCA solution.

The situation is more complicated in the case of the frequency shifts ( $\Delta F_{\text{water to salt}}$ ). According to Figure 3, changing the solvent from water to each of the saline solutions is associated with a negative frequency shift; however, the effect is evidently larger for the NaTCA and NaSCN solutions than the NaF solution. Moreover, it can be seen that the frequency shifts become considerably smaller by increasing the temperature, and a plateau is found for each saline solution at 35 and 40 °C, where the PNIPAM layer is in fully collapsed state. The observations can be discussed in terms of swelling/collapse of the PNIPAM layer as well as density of the solution within the layer.

With respect to the NaF solution, the dissipation data indicated partial conformational collapse of the PNIPAM layer; however, the salt solution within the layer has a relatively larger density than pure water and thus can give rise to a negative frequency shift. At 35 and 40 °C where the PNIPAM layer is fully collapsed, a smaller amount of the solvent is coupled with the layer, which can explain the relatively smaller frequency shifts. The notably larger frequency shifts found for the NaTCA and NaSCN solutions can be reasoned in the same manner. The dissipation data revealed that the PNIPAM film swells in both the solutions, meaning that more solvent is coupled with the oscillating sensor. The solution densities are also larger than pure water, which can contribute to a negative frequency shift. Furthermore, the preferential accumulation of the weakly hydrated anions within the PNIPAM layer can produce a negative frequency shift. The latter effect can be more clearly identified at high temperatures, i.e., 35 and 40 °C, where the PNIPAM layer is fully collapsed in all the salt solution, but the frequency shifts are considerably larger in the NaTCA and NaSCN solutions.

**3.4. Surface Forces between PNIPAM Layers.** The force curves measured between the grafted PNIPAM layers at 20 and 40 °C in the various salt solutions are provided in Figure 4 and Table 2. Before discussing the results in more detail, a brief

**Table 2. Statistical Data of the AFM Measurements**

solution	adhesion energy at 20 °C ( $10^{-17}$ J)	adhesion energy at 40 °C ( $10^{-17}$ J)
NaSCN 200 mM	2.55 ( $\pm 0.55$ )	6.70 ( $\pm 0.60$ )
NaTCA 200 mM	2.40 ( $\pm 0.41$ )	6.10 ( $\pm 0.81$ )
NaF 200 mM	4.55 ( $\pm 0.82$ )	12.45 ( $\pm 1.50$ )

recapitulation of the possible interactions between two polymer-coated surfaces in the aqueous solution would be appropriate.<sup>66</sup> When the surfaces are approaching each other, the dangling chains from one surface can begin to interact with the chains from the other surface and with the bare opposite surface (if the surfaces are not fully covered by the polymers). Depending on the surface affinity of the polymer, the surface coverage, and the solvent quality, these interactions will manifest themselves as either attractive bridging forces or steric repulsions.<sup>67–73</sup> On the basis of the QCM-D measurements, we know that PNIPAM has a strong affinity for the gold surface at all the investigated temperatures; hence, attractive chain–substrate bridging is likely in our system. With respect to PNIPAM chain–chain interactions, we postulate steric

repulsive forces at 20 °C, where PNIPAM is fully soluble in water, and attractive interchain interactions at 40 °C, where PNIPAM is partly dehydrated and insoluble in water.

After contact has been reached, a soft repulsive region corresponding to the compression of the polymer layers is predicted, regardless of whether the initial interactions were attractive or repulsive. The determining factor here is the solvent quality, which controls the polymer chain conformation. The more the polymer chains are swollen and stretched in the solution (good solvent condition), the more long-range this repulsive force will be. The repulsive double-layer forces—resulting from the ions adsorbed to the gold substrate or the polymers—can be present; nonetheless, such forces are extremely short-ranged because of the small Debye length (0.68 nm) in the 200 mM saline solutions. Moreover, the repulsive hydration force of the sodium cations at the gold surface is likely; however, it tends to be more short-ranged ( $\sim 1$ – $2$  nm) than repulsive compression of the polymer layers.<sup>74</sup> Ultimately, we do not expect van der Waals forces between the gold surfaces to be of significant magnitude, considering the roughness of the gold surfaces and the presence of a polymer layer.<sup>75</sup> With this in mind, we discuss the obtained force–distance profiles in each salt solution.

The approach force curve for 200 mM NaF at 20 °C exhibits an attractive jump-in, after which a repulsive force starts at surface separation of around 13 nm. This repulsion can be ascribed to the compression of the polymer layers. The retraction force curve also demonstrates a relatively strong adhesion between the two surfaces. Because PNIPAM is fully soluble in water at this temperature, the strong attractive forces observed in the approach and retrace curves are chiefly correlated to the PNIPAM–gold bridging forces. As mentioned above, the amount of the adsorbed polymer on the surface determines if the sum of bridging and steric forces is attractive or repulsive. Accordingly, a purely repulsive force profile is obtained at high surface coverage, whereas at low surface coverage only attractive force profile will exist. Herein, a rough estimation based on the QCM-D data can be made to assess the amount of PNIPAM grafted to the gold surface. According to the adsorption curve and by using the Sauerbrey equation (see the Supporting Information, section S2.1), the adsorbed hydrodynamic mass is estimated to be nearly 370 ng/cm<sup>2</sup>. As previously reported,<sup>76</sup> the water content of a PNIPAM film obtained by grafting-to method is approximately 70%. Accordingly, the grafting density of PNIPAM chains on the gold surface is estimated to be around 0.1 chain/nm<sup>2</sup>, which together with the estimated radius of gyration of the PNIPAM chain<sup>77</sup> suggests a relatively low grafting density and thus can explain the observed purely attractive bridging force. By increasing the solution temperature to 40 °C, the jump-in becomes even more pronounced, while the adhesion energy is almost tripled. Such an increment is mainly due to the presence of PNIPAM–PNIPAM interchain interactions at the collapsed state, which can be caused by either hydrophobic interactions or hydrogen bonding between the chains. Accordingly, both PNIPAM–gold and PNIPAM–PNIPAM bridging forces can contribute to the attractive jump-in and adhesion between the surfaces. One can also argue that the PNIPAM chains in bad solvent condition (above the phase separation temperature) are less swollen than in good solvent condition (below the phase separation temperature); thus, chain–surface bridging is more likely. The onset of repulsive compression region is decreased



to around 10 nm, which can be attributed to partial collapse and shrinkage of the polymer layer upon heating.

The force–distance curves in the 200 mM NaSCN differ greatly from those in the 200 mM NaF solution. At 20 °C, a purely repulsive force profile with no attractive jump-in is found at the separation distance of around 15 nm, and the adhesion energy is significantly smaller than in the NaF solution. Therefore, the PNIPAM–gold bridging forces are evidently weaker in the NaSCN solution, which can be explained in two ways. On the one hand, the QCM-D data indicated that 200 mM NaSCN promotes swelling of PNIPAM, which can hamper chain–substrate bridging. On the other hand, one can argue that accumulation of the anions within the layers can attenuate the attractive interactions through either electrostatic repulsive forces or weakening of the hydrophobic interactions. Heating the solution to 40 °C significantly changes the force–distance profile. An attractive jump-in is detected along with a notable gain in the adhesion energy. This again indicates the presence of PNIPAM–gold and PNIPAM–PNIPAM interactions. Nevertheless, the obtained adhesion energies are almost 50% smaller than that in the NaF solution, meaning that the chain–surface and chain–chain interactions are considerably weaker in the NaSCN solution. This observation affirms that even the collapsed PNIPAM layer is associated with the weakly hydrated SCN<sup>−</sup> anions, in accordance with the QCM-D findings. Moreover, the separation distance at which the repulsive force kicks in is decreased to around 10 nm upon heating, indicating vertical collapse of the PNIPAM layer.

The force profiles in 200 mM NaTCA appear quite similar to those in the NaSCN solution. The attractive jump-in is not observed at 20 °C; moreover, the adhesion energy and repulsion distance values are quite comparable to those in the NaSCN solution. The force curves at 40 °C also represent the similarity in the interactions. Thus, despite the observed salting-out effect by 200 mM NaTCA, the AFM measurements ascertain accumulation of TCA<sup>−</sup> within the PNIPAM layer, weak attractive PNIPAM–gold and PNIPAM–PNIPAM interactions, and PNIPAM film swelling in such a solution. Another intriguing observation in the NaTCA and NaSCN solutions at 40 °C is a weak repulsion force before the jump-in. While Figure 4 only illustrates a single representative force curve for each case, this is a notable observation. We observed this repulsive force in nearly all of the 25 force–distance measurements in NaTCA and almost half of the measurements in NaSCN (see the Supporting Information, Figure S13). Such a repulsive force can be considered as further evidence for surface partitioning of the weakly hydrated anions within the PNIPAM film and possible electrostatic repulsions between the PNIPAM films that result from the adsorbed anions. This repulsion could also occur at temperatures below the phase separation temperature, i.e., 20 °C, but not plainly distinguishable from the purely repulsive approach force curve.

Concisely, the observations from the AFM measurements affirm surface partitioning of the two weakly hydrated anions, both below and above the phase separation temperature. The relatively weak PNIPAM–gold and PNIPAM–PNIPAM interactions together with the observed repulsive force at 40 °C apparently stem from the inter- and intrachain electrostatic repulsions within the polymer film. The appreciably stronger attractive bridging forces in the NaF solution can be reasoned in two ways. On the one hand, the attractive forces between the two hydrophobic surfaces are relatively larger in strongly hydrated salt solutions. On the other hand, the chance of

polymer–substrate bridging will be larger for a less swollen PNIPAM film.

**3.5. Further Discussion of Results.** The first objective of this study was to ascertain the surface partitioning of the weakly hydrated anions and thereupon scrutinize the following effects on the properties of PNIPAM in solution. This was chiefly addressed by our AFM and QCM-D results, which demonstrated that the conformation and interaction of PNIPAM in the two weakly hydrated salt solutions are utterly distinguishable from those in the NaF solution. Accordingly, either of the poorly hydrated anions could adsorb to the PNIPAM surface and produce a stabilization effect, regardless of whether the overall Hofmeister effect is a salting-in or salting-out effect. With respect to the stabilization mechanism, the observed swelling of the PNIPAM film could indicate the presence of inter- and intrachain electrostatic repulsions within the polymer film. The relatively weak attractive PNIPAM–gold and PNIPAM–PNIPAM interactions further support this claim; nonetheless, it could also indicate the solvent-mediated attenuation of the hydrophobic interactions in such salt solutions. The weak repulsive force before the jump-in, observed at 40 °C in the NaSCN and NaTCA solutions, also strengthens the electrostatic stabilization hypothesis. To picture it more simply, the polymer film is in a hydrophobically collapsed state, but the weakly hydrated anions can be found within it, which could then produce electrostatic repulsions and some degree of swelling.

The second objective of the study was to address the salting-out effect by a weakly hydrated salt, i.e., a 200 mM NaTCA solution. In this instance, TCA<sup>−</sup> is strongly adsorbed to the PNIPAM surface and has a stabilizing facet, even though it has an overall salting-out effect. Now the following question arises: what is the origin of the salting-out effect? Several arguments can be advanced to rationalize it. First, the poorly hydrated anions cannot be further accommodated at the polymer surface above a certain salt concentration; in other words, the polymer–water interface becomes saturated. Henceforth, the anions in the bulk solution might compete with the polymer for the hydration water and thus produce a salting-out effect.<sup>20,21</sup> Although the idea of surface saturation seems rational, we strongly doubt that the observed difference between the phase separation temperatures in the 200 mM NaSCN and 200 mM NaTCA solutions is solely caused by this effect. Both the anions are poorly hydrated; therefore, there should not be a significant difference in their abilities to withdraw water molecules from the polymer. Second, TCA<sup>−</sup> may have a relatively strong salting-out effect at the PNIPAM hydrophobic surface.<sup>19,25</sup> This idea was partly discussed in the DSC results section, where we reasoned that the accumulation of TCA<sup>−</sup> at the PNIPAM surface should reduce the phase separation enthalpy and entropy values (surface effect), whereas the change in water hydrogen-bonding energetics may have a salting-out effect. Therefore, this might be the reason that the total enthalpy and entropy change values are almost the same as that in pure water. Such a destabilization mechanism has been formerly suggested in terms of the change in surface tension at the polymer/water interface.<sup>13,19,25</sup>

Finally, it has recently been discussed in some MD simulation studies that strongly attractive cosolutes, e.g., perchlorate and urea, could induce a compact and collapsed polymer network through collective binding and a following weak cross-linking effect.<sup>78–80</sup> As argued by the authors of those studies, such a partially collapsed state would have quite a

different structure and different properties from those of the collapsed state found for purely repulsive cosolutes (strongly hydrated ions) because the polymer coils are highly saturated by the attractive cosolutes. Regarding the weak hydration and considerably strong binding affinity of  $\text{TCA}^-$  to macromolecules, such a cross-linking-like effect could be the main source of the observed salting-out effect. The PNIPAM film showed identical properties in both the NaSCN and NaTCA solutions, all suggesting the accumulation of anions within the film and a subsequent stabilization effect. However, a notable difference in their corresponding phase separation temperatures was detected. Such a huge difference in the specific ion effect most likely originated from the suggested cross-linking effect, rather than the surface tension and saturation effects. Our argument regarding the accumulation of  $\text{TCA}^-$  in the PNIPAM film is in agreement with this view. Adopting this picture, we could also explain the relatively smaller dissipation values (relatively more rigid conformation) for the PNIPAM film in the NaTCA solution compared to that in the NaSCN solution, which was partially discussed in the QCM-D results section. Considering the PNIPAM chains are partially involved with each other through physically cross-linked sites, a relatively more rigid and less dissipative structure is expected, even though the layer is swollen.

#### 4. SUMMARY AND CONCLUSION

In the present work, we investigated the Hofmeister effect of three sodium salts on PNIPAM, both in bulk aqueous solution and at the gold–water interface. Addition of 200 mM NaF (strongly hydrated anion) demonstrated all the generic features of a merely destabilizing salt. For PNIPAM in the bulk phase, the addition of NaF led to a large decline in the phase separation temperature (salting-out effect) and a notable gain in the enthalpy and entropy changes of dehydration. While the former mainly correlates to the surface exclusion and water-withdrawing power of the anion, the latter is suggested to represent a stronger hydrophobic effect. QCM-D studies of the physically adsorbed PNIPAM layer on the gold surface confirmed conformational collapse and shrinkage in the NaF solution. AFM force measurements indicated considerably strong PNIPAM–gold and PNIPAM–PNIPAM attractive interactions. Addition of 200 mM NaSCN (weakly hydrated anion) represented all the characteristics of a stabilizing salt. In the bulk phase, the addition of NaSCN increased the phase separation temperature and reduced the enthalpy and entropy values. The former is attributed to the anion–polymer association, while the latter is most probably due to the spatial interference of the anions with water molecules in the hydrophobic hydration shell. QCM-D studies demonstrated swelling of the PNIPAM film in the NaSCN solution, which implies accumulation of the anions within the film. AFM based force–distance measurements revealed relatively weak attractive forces, which further reinforce the idea of having a polymer film saturated with the anions. Finally, studies of the effect of 200 mM NaTCA (weakly hydrated anion) revealed features of both a stabilizing and a destabilizing salt. In the bulk solution, a decrement in the phase separation temperature was found, whereas the enthalpy and entropy values remained essentially constant. Although the former implies a pure destabilization effect, the latter raised the suspicion of simultaneous salting-out and salting-in effects. This speculation was bolstered by the QCM-D and AFM measurements, which demonstrated a swollen film conformation in the NaTCA solution and weak

chain–substrate and chain–chain interactions, quite similar to the findings in the NaSCN solution. Therefore, the salting-in facet of NaTCA is evidently of the same nature as that in the NaSCN solution, resulting from the interplay between the polymer and anions.

#### ■ ASSOCIATED CONTENT

##### Supporting Information

The Supporting Information is available free of charge on the ACS Publications website at DOI: 10.1021/acs.langmuir.7b00953.

Analysis of the DSC data, QCM-D data of the PNIPAM physical adsorption to gold the surface together with the thiol-terminated sample, additional DLS and zeta potential measurements, AFM force curves, and the tapping mode images (PDF)

#### ■ AUTHOR INFORMATION

##### Corresponding Author

\*E-mail: [esth@kemi.dtu.dk](mailto:esth@kemi.dtu.dk); Tel (+45) 4525 2439.

##### ORCID

Saeed Zajfroushan Moghaddam: 0000-0002-6536-7490

##### Notes

The authors declare no competing financial interest.

#### ■ ACKNOWLEDGMENTS

We acknowledge the Swedish Research Council (VR) for financial support, which was transferred to the Technical University of Denmark via the EU initiative “Money Follow Researcher”.

#### ■ REFERENCES

- (1) Mendes, P. M. Stimuli-responsive surfaces for bio-applications. *Chem. Soc. Rev.* **2008**, 37 (11), 2512–2529.
- (2) Dedinaite, A.; Thormann, E.; Olanya, G.; Claesson, P. M.; Nyström, B.; Kjoniksen, A.-L.; Zhu, K. Friction in aqueous media tuned by temperature-responsive polymer layers. *Soft Matter* **2010**, 6 (11), 2489–2498.
- (3) Bodvik, R.; Thormann, E.; Karlson, L.; Claesson, P. M. Temperature responsive surface layers of modified celluloses. *Phys. Chem. Chem. Phys.* **2011**, 13 (10), 4260–4268.
- (4) Liu, C.; Thormann, E.; Claesson, P. M.; Tyrode, E. Surface grafted chitosan gels. Part II. Gel formation and characterization. *Langmuir* **2014**, 30 (29), 8878–8888.
- (5) Halperin, A.; Kröger, M.; Winnik, F. M. Poly (N-isopropylacrylamide) Phase Diagrams: Fifty Years of Research. *Angew. Chem., Int. Ed.* **2015**, 54 (S1), 15342–15367.
- (6) Guan, Y.; Zhang, Y. PNIPAM microgels for biomedical applications: from dispersed particles to 3D assemblies. *Soft Matter* **2011**, 7 (14), 6375–6384.
- (7) Ashraf, S.; Park, H.-K.; Park, H.; Lee, S.-H. Snapshot of phase transition in thermoresponsive hydrogel PNIPAM: Role in drug delivery and tissue engineering. *Macromol. Res.* **2016**, 24 (4), 297–304.
- (8) Ramos, J.; Imaz, A.; Forcada, J. Temperature-sensitive nanogels: poly (N-vinylcaprolactam) versus poly (N-isopropylacrylamide). *Polym. Chem.* **2012**, 3 (4), 852–856.
- (9) Okada, Y.; Tanaka, F. Cooperative hydration, chain collapse, and flat LCST behavior in aqueous poly (N-isopropylacrylamide) solutions. *Macromolecules* **2005**, 38 (10), 4465–4471.
- (10) Bischofberger, I.; Calzolari, D.; De Los Rios, P.; Jelezarov, I.; Trappe, V. Hydrophobic hydration of poly-N-isopropyl acrylamide: a matter of the mean energetic state of water. *Sci. Rep.* **2015**, 4, 4377.
- (11) Bischofberger, I.; Trappe, V. New aspects in the phase behaviour of poly-N-isopropyl acrylamide: systematic temperature dependent



shrinking of PNIPAM assemblies well beyond the LCST. *Sci. Rep.* **2015**, *5*, 15520.

(12) Hofmeister, F. Zur lehre von der wirkung der salze. *Naunyn-Schmiedeberg's Arch. Pharmacol.* **1888**, *25* (1), 1–30.

(13) Zhang, Y.; Foryk, S.; Bergbreiter, D. E.; Cremer, P. S. Specific ion effects on the water solubility of macromolecules: PNIPAM and the Hofmeister series. *J. Am. Chem. Soc.* **2005**, *127* (41), 14505–14510.

(14) Humphreys, B. A.; Willott, J. D.; Murdoch, T. J.; Webber, G. B.; Wanless, E. J. Specific ion modulated thermoresponse of poly (N-isopropylacrylamide) brushes. *Phys. Chem. Chem. Phys.* **2016**, *18* (8), 6037–6046.

(15) Murdoch, T. J.; Humphreys, B. A.; Willott, J. D.; Gregory, K. P.; Prescott, S. W.; Nelson, A.; Wanless, E. J.; Webber, G. B. Specific Anion Effects on the Internal Structure of a Poly (N-isopropylacrylamide) Brush. *Macromolecules* **2016**, *49* (16), 6050–6060.

(16) Song, J.; Kang, T. H.; Kim, M. W.; Han, S. Ion specific effects: decoupling ion–ion and ion–water interactions. *Phys. Chem. Chem. Phys.* **2015**, *17* (13), 8306–8322.

(17) Pollard, T. P.; Beck, T. L. Toward a quantitative theory of Hofmeister phenomena: From quantum effects to thermodynamics. *Curr. Opin. Colloid Interface Sci.* **2016**, *23*, 110–118.

(18) Marcus, Y. Specific ion effects on the surface tension and surface potential of aqueous electrolytes. *Curr. Opin. Colloid Interface Sci.* **2016**, *23*, 94–99.

(19) Zhang, Y.; Cremer, P. S. Chemistry of Hofmeister anions and osmolytes. *Annu. Rev. Phys. Chem.* **2010**, *61*, 63–83.

(20) Heyda, J.; Dzubiella, J. Thermodynamic description of Hofmeister effects on the LCST of thermosensitive polymers. *J. Phys. Chem. B* **2014**, *118* (37), 10979–10988.

(21) Record, M. T.; Guinn, E.; Pegram, L.; Capp, M. Introductory lecture: interpreting and predicting Hofmeister salt ion and solute effects on biopolymer and model processes using the solute partitioning model. *Faraday Discuss.* **2013**, *160*, 9–44.

(22) Thormann, E. On understanding of the Hofmeister effect: how addition of salt alters the stability of temperature responsive polymers in aqueous solutions. *RSC Adv.* **2012**, *2* (22), 8297–8305.

(23) Moghaddam, S. Z.; Thormann, E. Hofmeister effect on thermo-responsive poly (propylene oxide): Role of polymer molecular weight and concentration. *J. Colloid Interface Sci.* **2016**, *465*, 67–75.

(24) Moghaddam, S. Z.; Thormann, E. Hofmeister effect on thermo-responsive poly (propylene oxide) in H<sub>2</sub>O and D<sub>2</sub>O. *RSC Adv.* **2016**, *6* (33), 27969–27973.

(25) Zhang, Y.; Foryk, S.; Sagle, L. B.; Cho, Y.; Bergbreiter, D. E.; Cremer, P. S. Effects of Hofmeister anions on the LCST of PNIPAM as a function of molecular weight. *J. Phys. Chem. C* **2007**, *111* (25), 8916–8924.

(26) Kunz, W.; Lo Nostro, P.; Ninham, B. W. The present state of affairs with Hofmeister effects. *Curr. Opin. Colloid Interface Sci.* **2004**, *9* (1), 1–18.

(27) Pegram, L. M.; Record, M. T. Thermodynamic origin of Hofmeister ion effects. *J. Phys. Chem. B* **2008**, *112* (31), 9428–9436.

(28) Gokarn, Y. R.; Fesinmeyer, R. M.; Saluja, A.; Razinkov, V.; Chase, S. F.; Laue, T. M.; Brems, D. N. Effective charge measurements reveal selective and preferential accumulation of anions, but not cations, at the protein surface in dilute salt solutions. *Protein Sci.* **2011**, *20* (3), 580–587.

(29) Gibb, C. L.; Gibb, B. C. Anion binding to hydrophobic concavity is central to the salting-in effects of Hofmeister chaotropes. *J. Am. Chem. Soc.* **2011**, *133* (19), 7344–7347.

(30) Rembert, K. B.; Okur, H. I.; Hilty, C.; Cremer, P. S. An NH Moiety Is Not Required for Anion Binding to Amides in Aqueous Solution. *Langmuir* **2015**, *31* (11), 3459–3464.

(31) Kunz, W.; Belloni, L.; Bernard, O.; Ninham, B. W. Osmotic coefficients and surface tensions of aqueous electrolyte solutions: role of dispersion forces. *J. Phys. Chem. B* **2004**, *108* (7), 2398–2404.

(32) Lo Nostro, P.; Ninham, B. W. Hofmeister phenomena: an update on ion specificity in biology. *Chem. Rev.* **2012**, *112* (4), 2286–2322.

(33) Rembert, K. B.; Paterová, J.; Heyda, J.; Hilty, C.; Jungwirth, P.; Cremer, P. S. Molecular mechanisms of ion-specific effects on proteins. *J. Am. Chem. Soc.* **2012**, *134* (24), 10039–10046.

(34) Collins, K. D. Why continuum electrostatics theories cannot explain biological structure, polyelectrolytes or ionic strength effects in ion–protein interactions. *Biophys. Chem.* **2012**, *167*, 43–59.

(35) Kou, R.; Zhang, J.; Wang, T.; Liu, G. Interactions between Polyelectrolyte Brushes and Hofmeister Ions: Chaotropes versus Kosmotropes. *Langmuir* **2015**, *31* (38), 10461–10468.

(36) Irigoyen, J.; Moya, S.; Iturri, J.; Llerena, I.; Azzaroni, O.; Donath, E. Specific  $\zeta$ -potential response of layer-by-layer coated colloidal particles triggered by polyelectrolyte ion interactions. *Langmuir* **2009**, *25* (6), 3374–3380.

(37) Sokkalingam, P.; Shraberg, J.; Rick, S. W.; Gibb, B. C. Binding Hydrated Anions with Hydrophobic Pockets. *J. Am. Chem. Soc.* **2015**, *138* (1), 48–51.

(38) Oku, N.; MacDonald, R. C. Solubilization of phospholipids by chaotropic ion solutions. *J. Biol. Chem.* **1983**, *258* (14), 8733–8738.

(39) Hanstein, W. G. Chaotropic ions and their interactions with proteins. *Appl. Biochem. Biotechnol.* **1979**, *4* (3), 189–206.

(40) Hassan, P. A.; Rana, S.; Verma, G. Making sense of brownian motion: colloid characterization by dynamic light scattering. *Langmuir* **2014**, *31* (1), 3–12.

(41) Sader, J. E.; Chon, J. W.; Mulvaney, P. Calibration of rectangular atomic force microscope cantilevers. *Rev. Sci. Instrum.* **1999**, *70* (10), 3967–3969.

(42) Ducker, W. A.; Senden, T. J.; Pashley, R. M. Direct measurement of colloidal forces using an atomic force microscope, 1991.

(43) Ducker, W. A.; Senden, T. J.; Pashley, R. M. Measurement of forces in liquids using a force microscope. *Langmuir* **1992**, *8* (7), 1831–1836.

(44) Xue, Y.; Li, X.; Li, H.; Zhang, W. Quantifying thiol–gold interactions towards the efficient strength control. *Nat. Commun.* **2014**, *5*, 4348.

(45) Chan, D. Y.; Horn, R. The drainage of thin liquid films between solid surfaces. *J. Chem. Phys.* **1985**, *83* (10), 5311–5324.

(46) Thormann, E.; Pettersson, T.; Claesson, P. M. How to measure forces with atomic force microscopy without significant influence from nonlinear optical lever sensitivity. *Rev. Sci. Instrum.* **2009**, *80* (9), 093701.

(47) Deshmukh, S. A.; Sankaranarayanan, S. K.; Suthar, K.; Mancini, D. C. Role of solvation dynamics and local ordering of water in inducing conformational transitions in poly (N-isopropylacrylamide) oligomers through the LCST. *J. Phys. Chem. B* **2012**, *116* (9), 2651–2663.

(48) Philipp, M.; Kyriakos, K.; Silvi, L.; Lohstroh, W.; Petry, W.; Krüger, J. K.; Papadakis, C. M.; Müller-Buschbaum, P. From molecular dehydration to excess volumes of phase-separating PNIPAM solutions. *J. Phys. Chem. B* **2014**, *118* (15), 4253–4260.

(49) Schmidt, S.; Zeiser, M.; Hellweg, T.; Duschl, C.; Fery, A.; Möhlwald, H. Adhesion and mechanical properties of PNIPAM microgel films and their potential use as switchable cell culture substrates. *Adv. Funct. Mater.* **2010**, *20* (19), 3235–3243.

(50) Burmistrova, A.; Steitz, R.; von Klitzing, R. Temperature response of PNIPAM derivatives at planar surfaces: Comparison between polyelectrolyte multilayers and adsorbed microgels. *ChemPhysChem* **2010**, *11* (17), 3571–3579.

(51) Pelton, R. Poly(N-isopropylacrylamide) (PNIPAM) is never hydrophobic. *J. Colloid Interface Sci.* **2010**, *348* (2), 673–674.

(52) Heskins, M.; Guillet, J. E. Solution properties of poly(N-isopropylacrylamide). *J. Macromol. Sci., Chem.* **1968**, *2* (8), 1441–1455.

(53) Mancera, R. L. Influence of salt on hydrophobic effects: A molecular dynamics study using the modified hydration-shell hydrogen-bond model. *J. Phys. Chem. B* **1999**, *103* (18), 3774–3777.

(54) Athawale, M. V.; Sarupria, S.; Garde, S. Enthalpy-entropy contributions to salt and osmolyte effects on molecular-scale

- hydrophobic hydration and interactions. *J. Phys. Chem. B* **2008**, *112* (18), 5661–5670.
- (55) Zangi, R.; Hagen, M.; Berne, B. Effect of ions on the hydrophobic interaction between two plates. *J. Am. Chem. Soc.* **2007**, *129* (15), 4678–4686.
- (56) Smith, P. E. Computer simulation of cosolvent effects on hydrophobic hydration. *J. Phys. Chem. B* **1999**, *103* (3), 525–534.
- (57) Hamano, K. K.; Kuwahara, N.; Fujishige, S.; Ando, I. Characterization of poly (N-isopropylmethacrylamide) in water. *Polym. J.* **1990**, *22* (12), 1051–1057.
- (58) Kujawa, P.; Aseyev, V.; Tenhu, H.; Winnik, F. M. Temperature-sensitive properties of poly (N-isopropylacrylamide) mesoglobules formed in dilute aqueous solutions heated above their demixing point. *Macromolecules* **2006**, *39* (22), 7686–7693.
- (59) Zhang, G.; Wu, C. Folding and formation of mesoglobules in dilute copolymer solutions. In *Conformation-Dependent Design of Sequences in Copolymers I*; Springer: 2006; pp 101–176.
- (60) Aseyev, V.; Hietala, S.; Laukkanen, A.; Nuopponen, M.; Confortini, O.; Du Prez, F. E.; Tenhu, H. Mesoglobules of thermoresponsive polymers in dilute aqueous solutions above the LCST. *Polymer* **2005**, *46* (18), 7118–7131.
- (61) Plunkett, M. A.; Claesson, P. M.; Ernstsson, M.; Rutland, M. W. Comparison of the adsorption of different charge density polyelectrolytes: a quartz crystal microbalance and X-ray photoelectron spectroscopy study. *Langmuir* **2003**, *19* (11), 4673–4681.
- (62) Plunkett, M. A.; Claesson, P. M.; Rutland, M. W. Adsorption of a cationic polyelectrolyte followed by surfactant-induced swelling, studied with a quartz crystal microbalance. *Langmuir* **2002**, *18* (4), 1274–1280.
- (63) Ishida, N.; Biggs, S. Direct Observation of the Phase Transition for a Poly(N-isopropylacrylamide) Layer Grafted onto a Solid Surface by AFM and QCM-D. *Langmuir* **2007**, *23* (22), 11083–11088.
- (64) Annaka, M.; Yahiro, C.; Nagase, K.; Kikuchi, A.; Okano, T. Real-time observation of coil-to-globule transition in thermosensitive poly(N-isopropylacrylamide) brushes by quartz crystal microbalance. *Polymer* **2007**, *48* (19), 5713–5720.
- (65) Laloyaux, X.; Mathy, B.; Nysten, B.; Jonas, A. M. Surface and bulk collapse transitions of the thermoresponsive polymer brushes. *Langmuir* **2009**, *26* (2), 838–847.
- (66) Cappella, B. Physical Principles of Force–Distance Curves by Atomic Force Microscopy. In *Mechanical Properties of Polymers Measured through AFM Force-Distance Curves*; Springer: 2016; pp 3–66.
- (67) Goodman, D.; Kizhakkedathu, J. N.; Brooks, D. E. Attractive bridging interactions in dense polymer brushes in good solvent measured by atomic force microscopy. *Langmuir* **2004**, *20* (6), 2333–2340.
- (68) Sui, X.; Zapotoczny, S.; Benetti, E. M.; Schön, P.; Vancso, G. J. Characterization and molecular engineering of surface-grafted polymer brushes across the length scales by atomic force microscopy. *J. Mater. Chem.* **2010**, *20* (24), 4981–4993.
- (69) Malham, I. B.; Bureau, L. Density effects on collapse, compression, and adhesion of thermoresponsive polymer brushes. *Langmuir* **2010**, *26* (7), 4762–4768.
- (70) Thormann, E.; Simonsen, A. C.; Hansen, P. L.; Mouritsen, O. G. Interactions between a polystyrene particle and hydrophilic and hydrophobic surfaces in aqueous solutions. *Langmuir* **2008**, *24* (14), 7278–7284.
- (71) Olanya, G.; Thormann, E.; Varga, I.; Makuška, R.; Claesson, P. M. Protein interactions with bottle-brush polymer layers: Effect of side chain and charge density ratio probed by QCM-D and AFM. *J. Colloid Interface Sci.* **2010**, *349* (1), 265–274.
- (72) Thormann, E.; Bodvik, R.; Karlson, L.; Claesson, P. M. Surface forces and friction between non-polar surfaces coated by temperature-responsive methylcellulose. *Colloids Surf., A* **2014**, *441*, 701–708.
- (73) Fleer, G.; Stuart, M. C.; Scheutjens, J.; Cosgrove, T.; Vincent, B. *Polymers at Interfaces*; Springer Science & Business Media: 1993.
- (74) Butt, H.-J. Measuring electrostatic, van der Waals, and hydration forces in electrolyte solutions with an atomic force microscope. *Biophys. J.* **1991**, *60* (6), 1438–1444.
- (75) Thormann, E. Surface forces between rough and topographically structured interfaces. *Curr. Opin. Colloid Interface Sci.* **2017**, *27*, 18–24.
- (76) Furusawa, H.; Sekine, T.; Ozeki, T. Hydration and Viscoelastic Properties of High- and Low-Density Polymer Brushes Using a Quartz-Crystal Microbalance Based on Admittance Analysis (QCM-A). *Macromolecules* **2016**, *49* (9), 3463–3470.
- (77) Kubota, K.; Fujishige, S.; Ando, I. Solution properties of poly (N-isopropylacrylamide) in water. *Polym. J.* **1990**, *22* (1), 15–20.
- (78) Heyda, J.; Muzdalo, A.; Dzubiel, J. Rationalizing polymer swelling and collapse under attractive cosolvent conditions. *Macromolecules* **2013**, *46* (3), 1231–1238.
- (79) Crevenna, A. H.; Naredi-Rainer, N.; Lamb, D. C.; Wedlich-Söldner, R.; Dzubiel, J. Effects of Hofmeister ions on the  $\alpha$ -helical structure of proteins. *Biophys. J.* **2012**, *102* (4), 907–915.
- (80) Heyda, J.; Okur, H. I.; Hladíková, J.; Rembert, K. B.; Hunn, W.; Yang, T.; Dzubiel, J.; Jungwirth, P.; Cremer, P. S. Guanidinium can both Cause and Prevent the Hydrophobic Collapse of Biomacromolecules. *J. Am. Chem. Soc.* **2017**, *139* (2), 863–870.

**Supplementary information for**

**Hofmeister Effect on PNIPAM in Bulk and at Interfaces: Surface**

**Partitioning of Weakly Hydrated Anions**

Saeed Zajforoushan Moghaddam and Esben Thormann\*

Department of Chemistry, Technical University of Denmark, 2800 Kgs. Lyngby,  
Denmark

---

\* To whom correspondence should be addressed. E-mail: [esth@kemi.dtu.dk](mailto:esth@kemi.dtu.dk).  
Telephone: (+45) 4525 2439

## S1. Analysis of DSC Data:

The area under the phase separation peak corresponds to the molar enthalpy of dehydration ( $\Delta H$ ). To be able to calculate  $\Delta H$ , one should first convert the thermograms into molar heat capacity (MHC) scale. The measured raw heat data depends on the sample amount, so it must be normalized with respect to NIPAM molecular weight, concentration, and density of the solution, as follows:

$$c_p \left( \frac{kJ}{mol.K} \right) = C_p \left( \frac{kJ}{K} \right) \times \frac{M_{NIPAM}}{V_{cell} \times w_{NIPAM} \times \rho_{solution}}$$

Where  $c_p$  is the molar heat capacity,  $C_p$  is the raw measured heat data,  $M_{NIPAM}$  is the molecular weight of NIPAM monomer,  $V_{cell}$  is the volume of the instrument sample cell,  $w_{NIPAM}$  is the weight concentration of solution, and  $\rho_{solution}$  is the density of the solution. The density of the solutions was measured using a density meter (DMA 4100 M, Anton Paar):

Sample	Water	NaF 200mM	NaSCN 200mM	NaTCA 200mM
Density at 25 °C (g/ml)	0.9973	1.0061	1.0055	1.0096

After converting the raw data to molar heat capacity values, the area under the peak can be integrated, using a first order fitting for pre- and post-transition baselines.

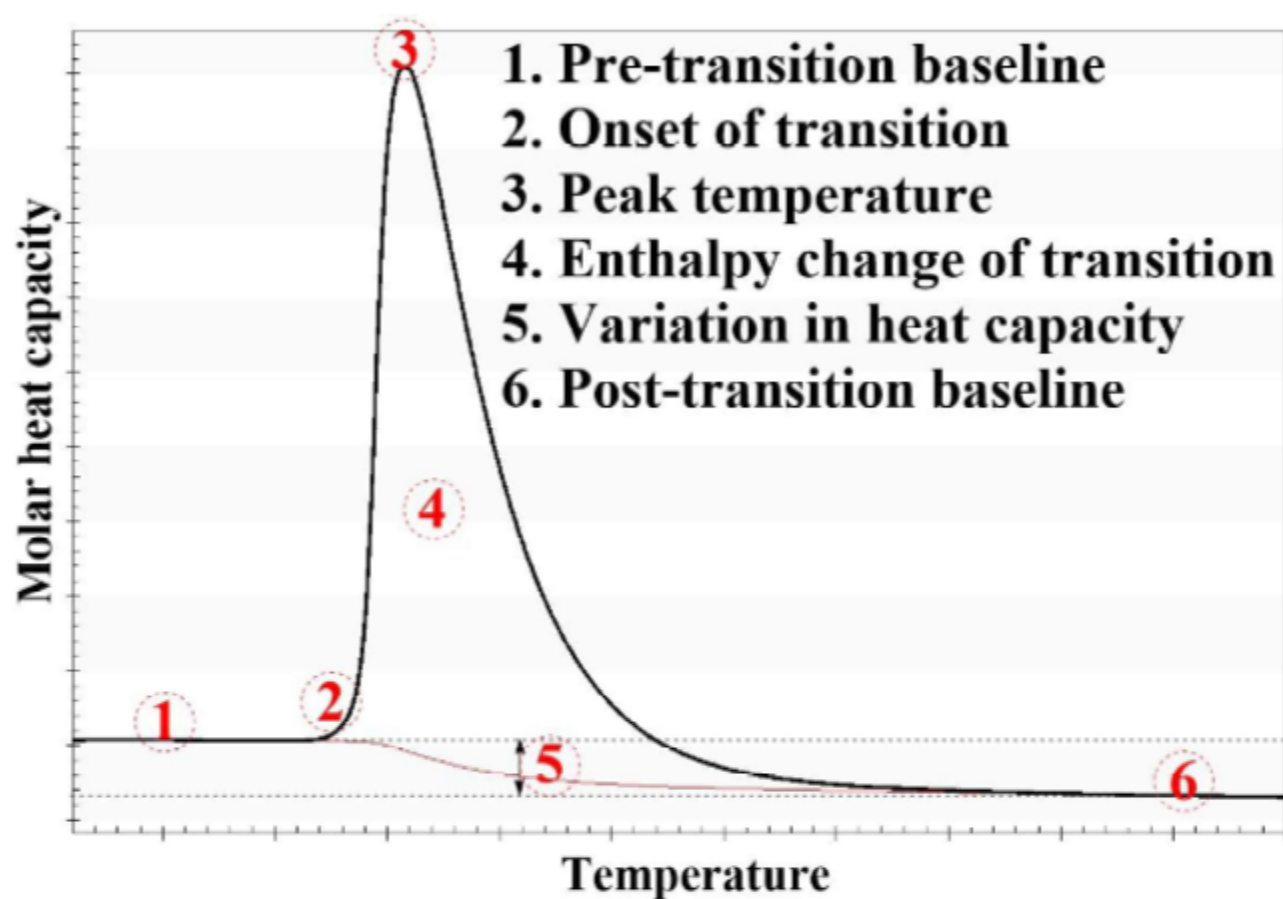


**Fig. S1** Typical DSC thermogram and corresponding thermodynamic data; the entropy change upon phase separation can be calculated by dividing the enthalpy change per peak temperature value.



## S2. Analysis of QCM measurements:

**S2.1 Adsorption using gold-thiol chemistry:** Adsorption of the thiol-terminated PNIPAM on the gold surface and the effects of the salts were initially studied. However, as shown in Fig. S4, the subtracted  $\Delta F_{\text{water to salt}}$  and  $\Delta D_{\text{water to salt}}$  values are relatively small in value; therefore, the observed trends are not reliable. Accordingly, a high molecular weight PNIPAM sample was used to obtain relatively larger QCM-D signals. However, the adsorption data together with the Sauerbrey equation are used to estimate the amount of PNIPAM grafted to the surface.

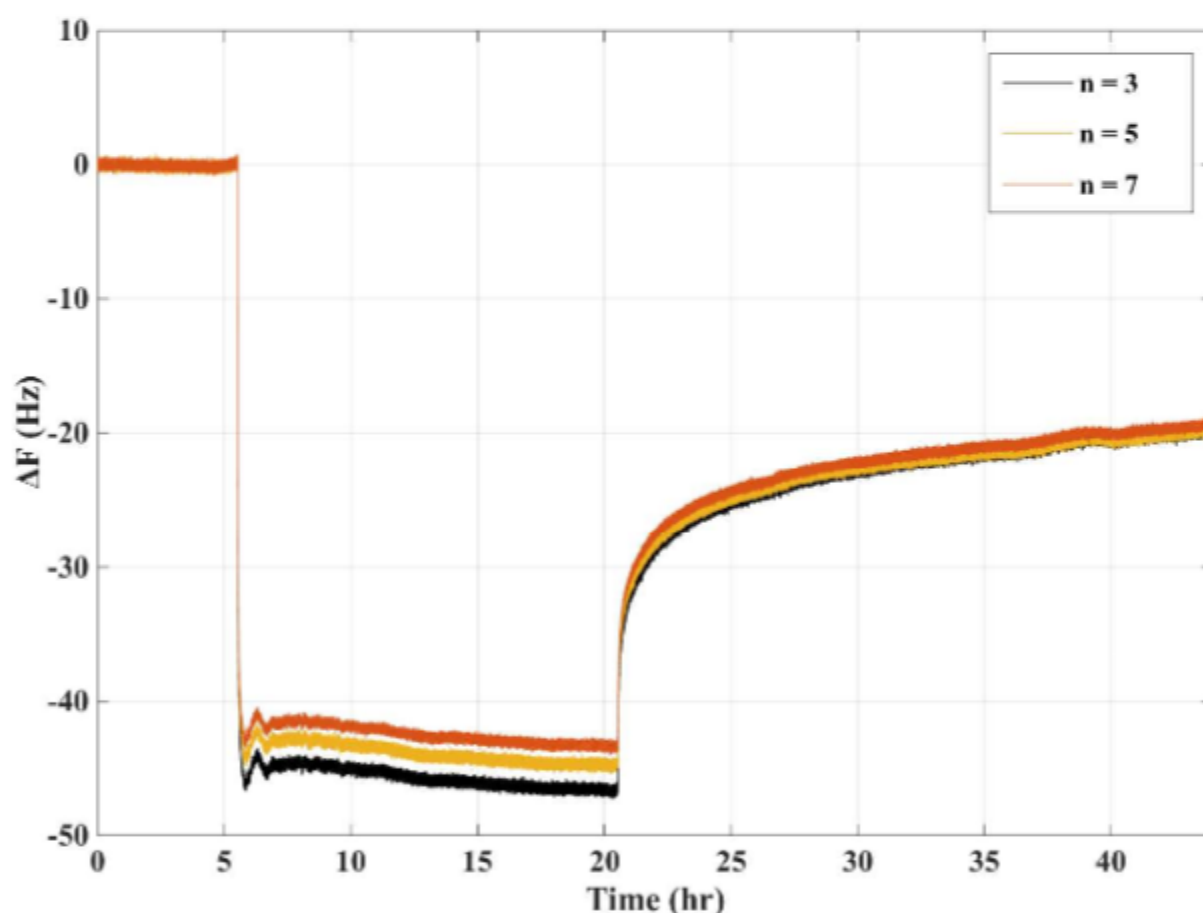
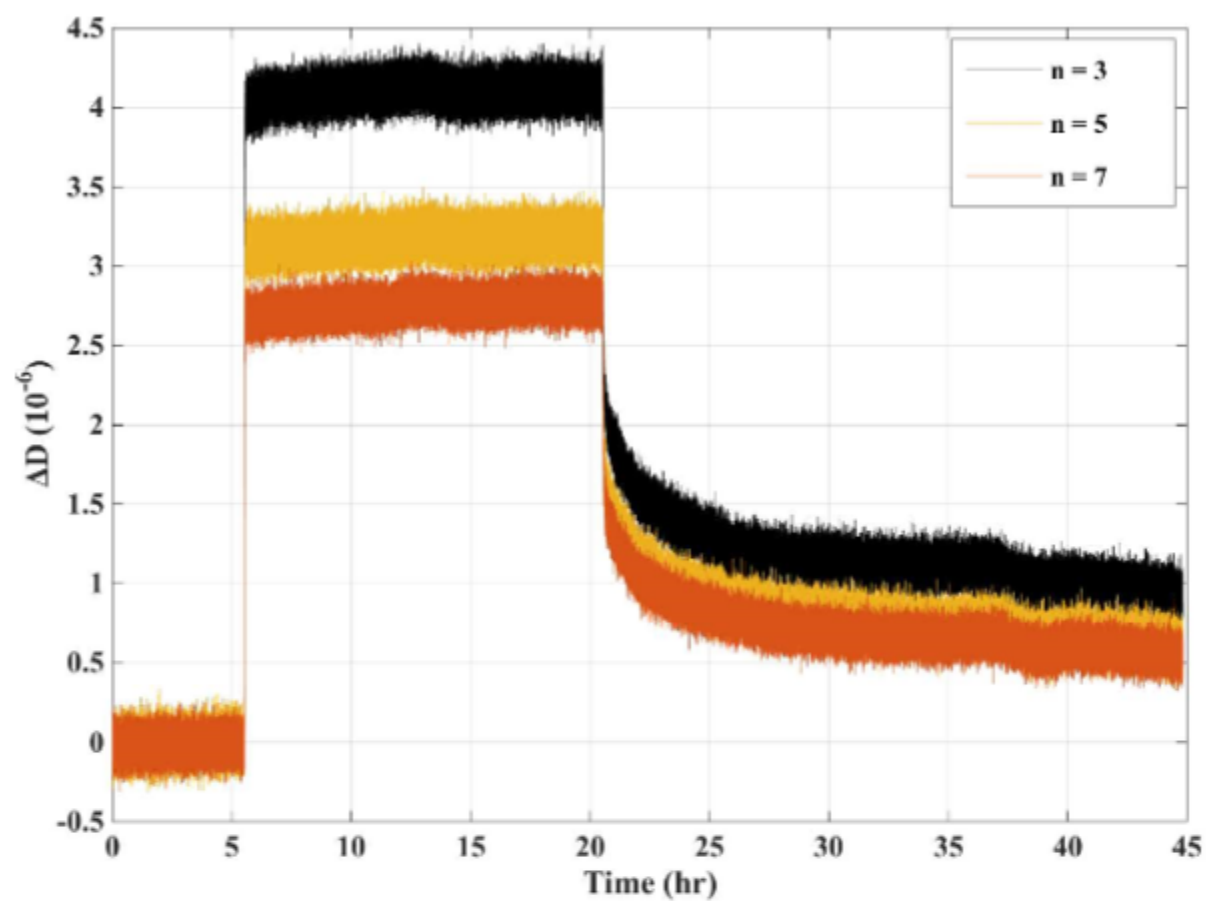
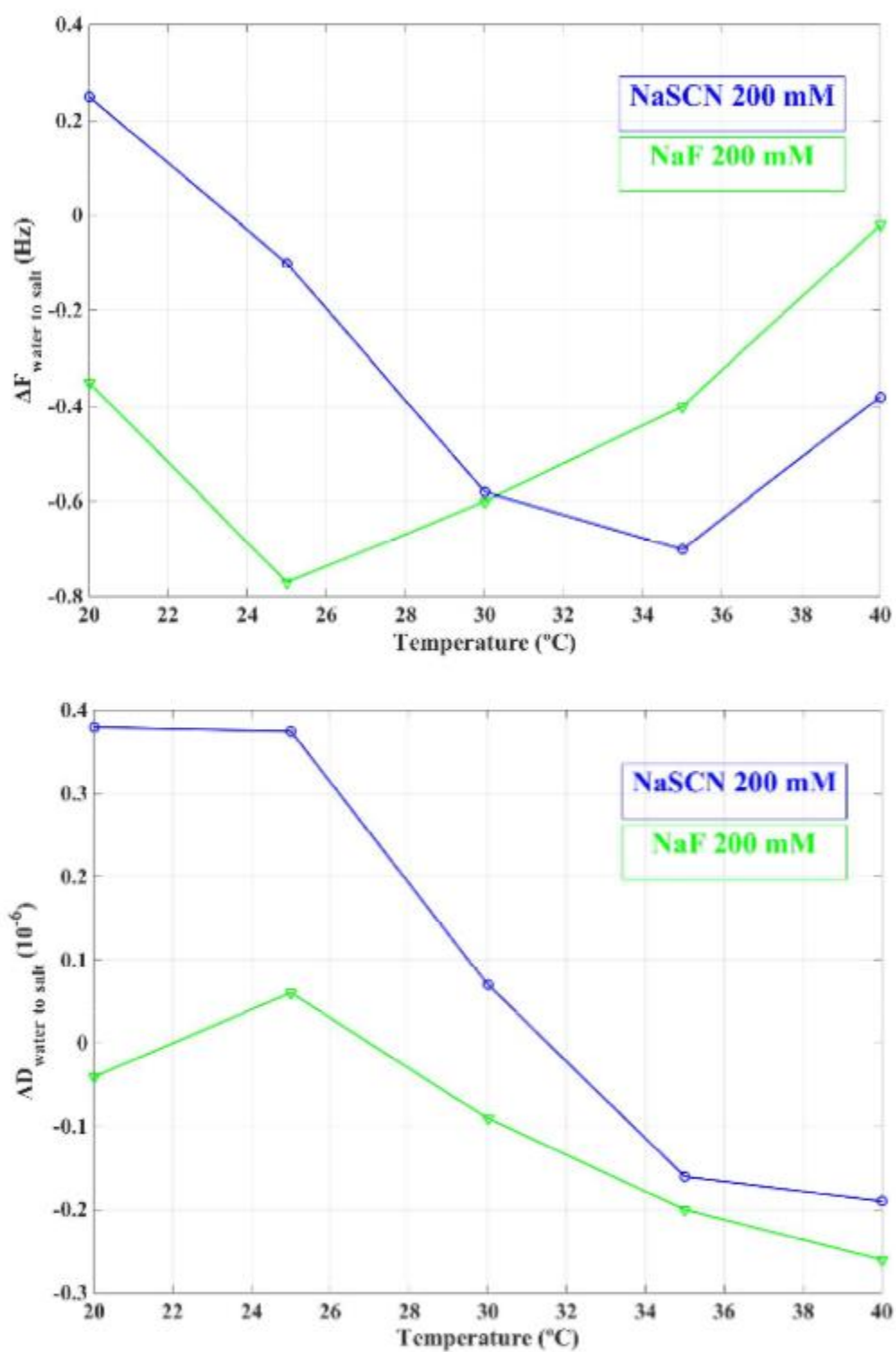


Fig. S2 Frequency shift resulting from adsorption of the thiol-terminated PNIPAM (0.1 wt% solution) on the gold sensor;



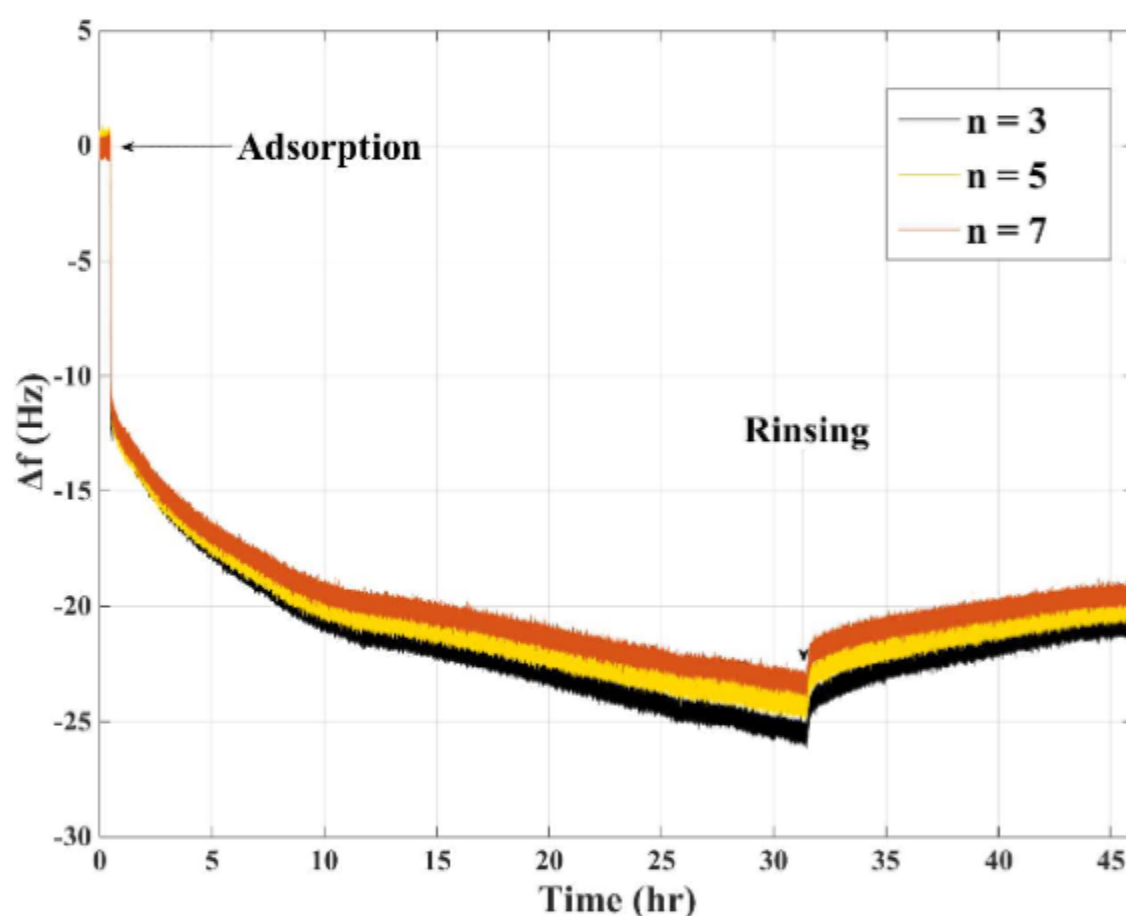
**Fig. S3** Dissipation shift resulting from adsorption of the thiol-terminated PNIPAM (0.1 wt% solution) on the gold sensor;



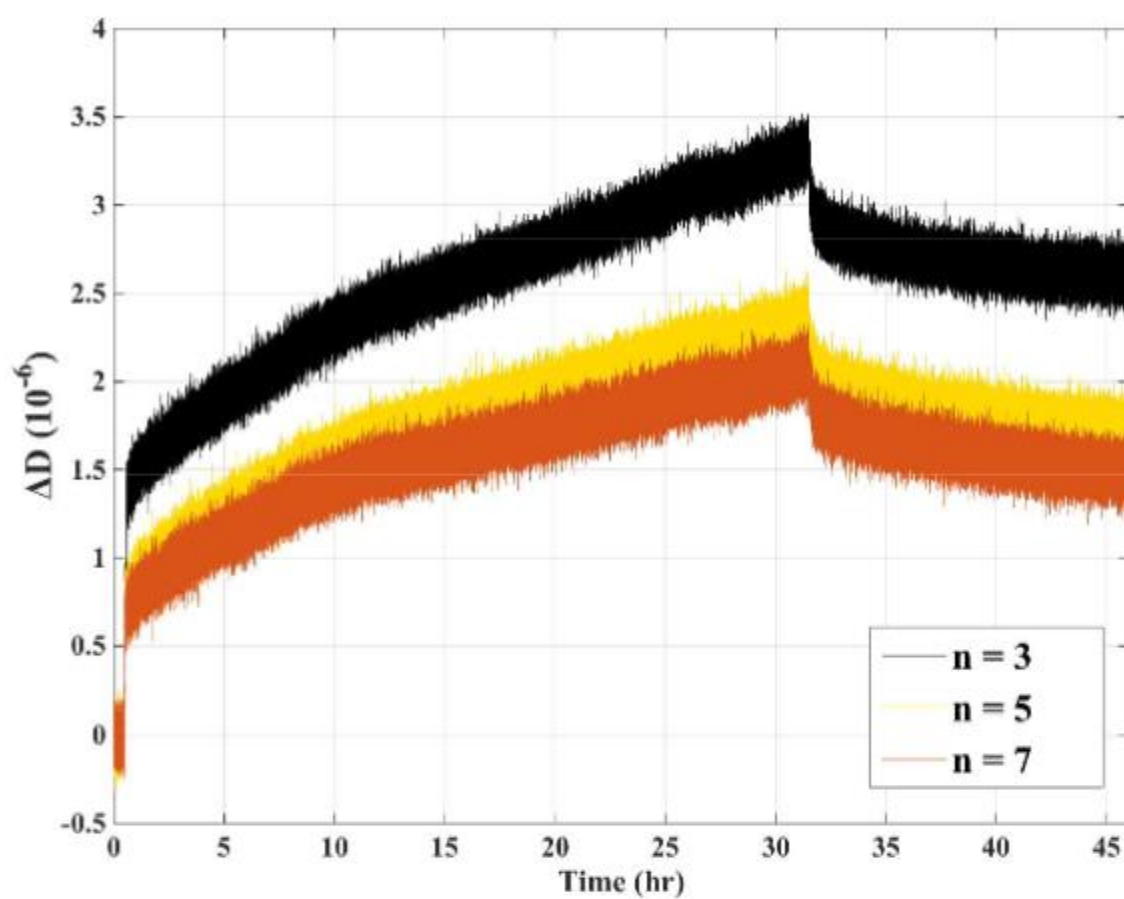
**Fig. S4** Subtracted frequency and dissipation shifts resulting from changing the solvent from water to the saline solutions. As shown, the subtracted values are quite close to zero making the trends difficult to interpret.



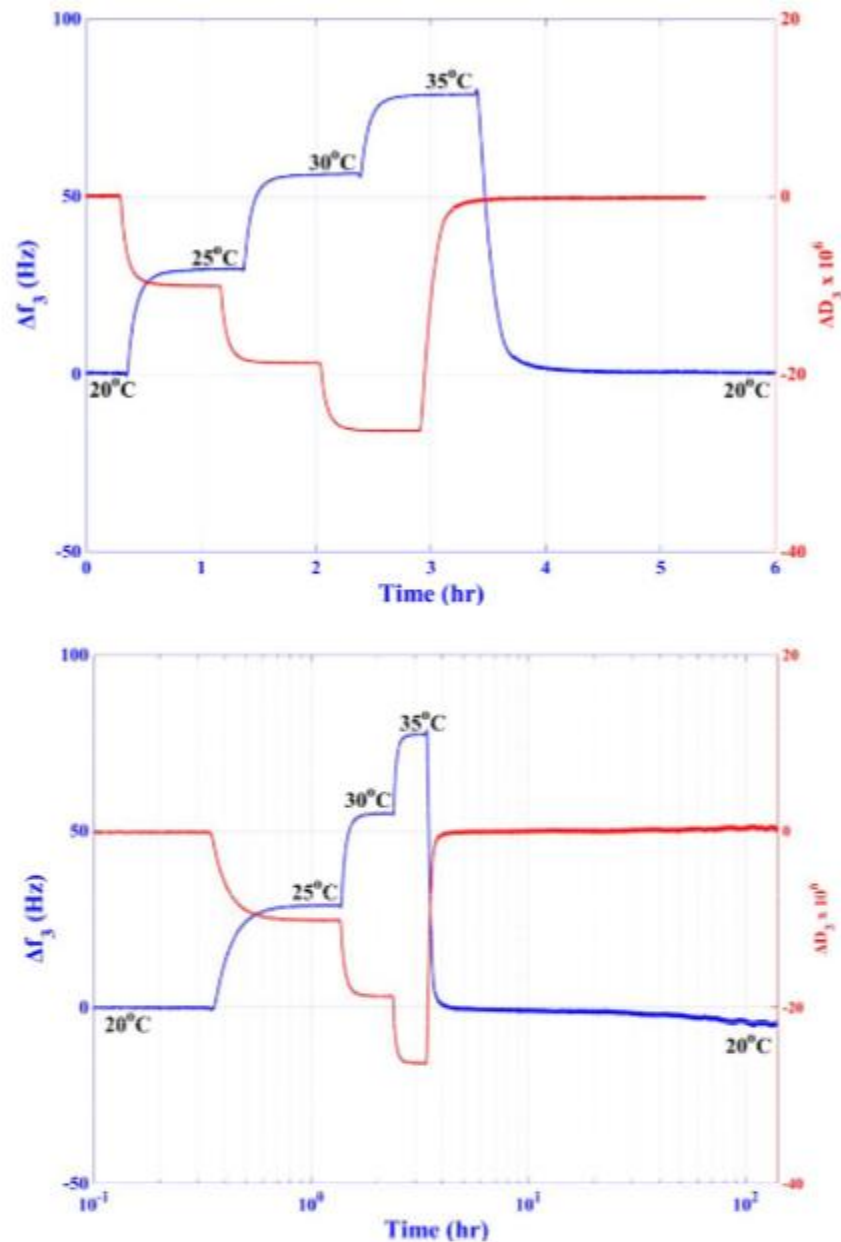
**S2.2 Physical adsorption on gold:** Due to strong hydrophobic interactions, PNIPAM can physically adsorb on the gold surface to produce a robust and stable polymer layer.<sup>1, 2</sup> Herein, to prepare the PNIPAM film for the QCM measurements, a dilute solution (0.1 wt%) of the high molecular weight PNIPAM was circulated in the QCM cell over the gold sensor for 30 hours at constant temperature of 20 °C. After rinsing the QCM cell with MQ water, the cell temperature was raised to 35 °C and then lowered back to 20 °C for two times and then left in flowing MQ water for 5 days.



**Fig. S5** Frequency shift resulting from physical adsorption of PNIPAM on the gold sensor; the negative shift in the oscillation frequency is attributed to the sensed mass over the sensor, which is indeed polymer plus its water content, known as the hydrodynamic polymer mass. Rinsing with water gives rise to an increment in the frequency, which is related to desorption of the loosely attached PNIPAM chains.

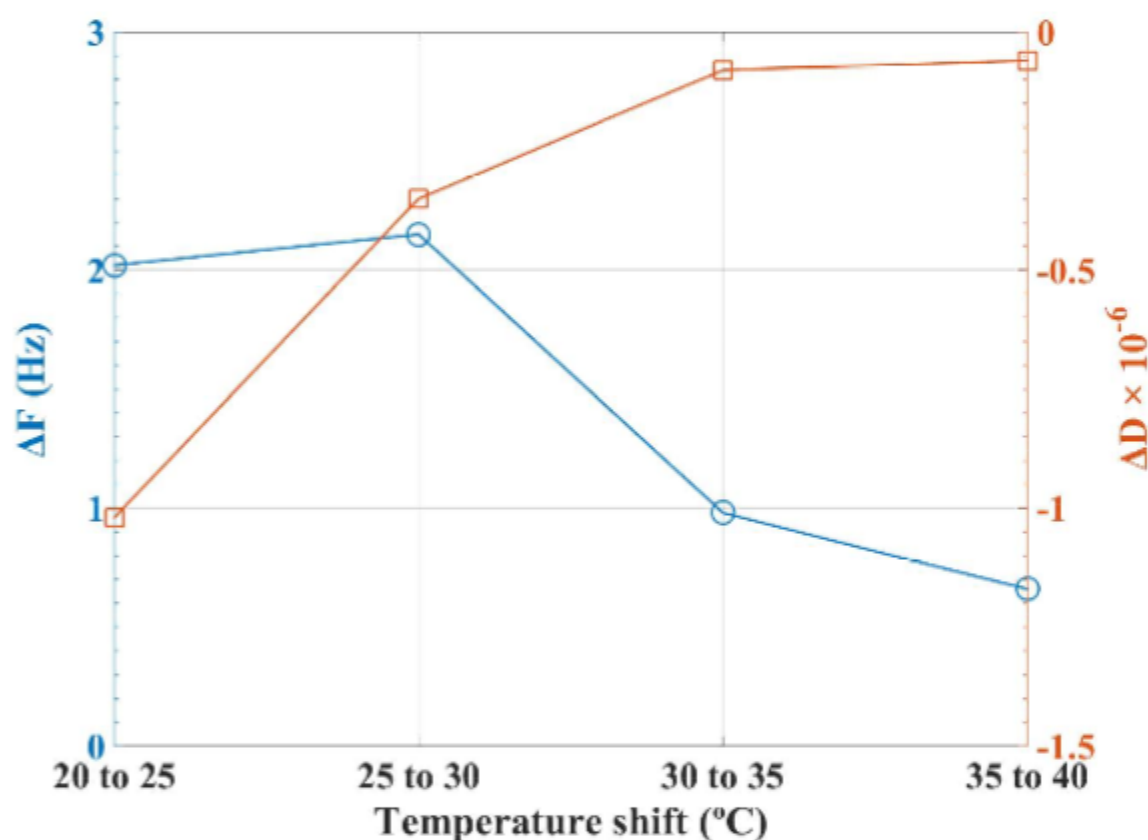


**Fig. S6** Dissipation shift resulting from physical adsorption of PNIPAM on the gold sensor; the positive shift in dissipation indicates formation of a viscoelastic polymer film on the sensor. The overtone-dependence of the dissipation shift further confirms viscoelasticity of the formed layer. Rinsing with water leads to a decrement in the dissipation factor, which can be assigned to desorption of the weakly attached PNIPAM chains.



**Fig. S7** (top) First heating and cooling cycle on the PNIPAM film (bottom) second heating and cooling cycle plus constant flow of MQ water at 20°C for 5 days. Both the experiments suggest robust film adsorption on the gold surface. By leaving the film in water for 5 days a slight decrement in frequency and increment in dissipation is observed, which is probably due to partial swelling of the film or instrumental drift, while still no trace of PNIPAM desorption and mass loss is found.

The effect of increasing temperature on the water content and conformation of the PNIPAM layer (in salt-free solution) is provided in Fig. S8. As shown, increasing the temperature is accompanied with a positive frequency shift and a negative dissipation shift. The former suggests dehydration of the PNIPAM layer and then a relatively smaller sensed mass, while the latter indicates conformational collapse of the PNIPAM layer. According to the figure, the phase transition is expected to occur at around 30 °C, considering the relatively small frequency and dissipation shifts at higher temperatures.



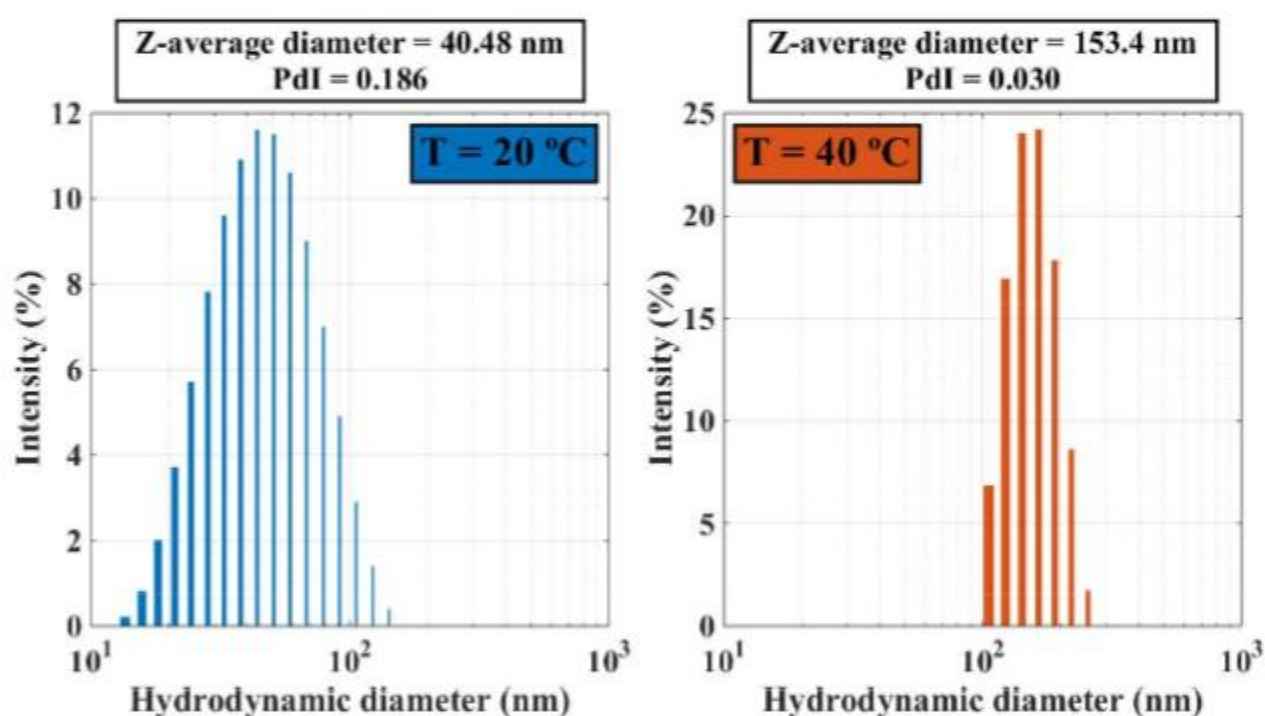
**Fig. S8** Subtracted frequency and dissipation shifts resulting from heating the PNIPAM layer from 20 to 40 °C. As illustrated, increasing the temperatures leads to an increment in oscillation frequency and a decrement in dissipation factor, suggesting dehydration and conformational collapse of the layer. Further, the frequency and dissipation shifts are relatively large for 20 → 25 and 25 → 30 steps, while drastically decrease at higher temperature steps. Hence, phase separation of the PNIPAM layer is expected to occur at around 30 °C. This is in accordance with the observation that the effect of salts is relatively small at 30 °C and higher temperatures.

Table S1 depicts dissipation shifts at 20, 30 and 40 °C, for changing the solution from water to the saline solutions on the bare and polymer-coated surface. The values in the parenthesis represent the dissipation shifts of changing the solvent from the saline solutions to water. As seen, when going from water to the saline solutions and then back to water, the dissipation shift values are similar, suggesting stability of the PNIPAM layer during the measurements. Thus, the subtracted values solely represent the changes in polymer layer conformation, and polymer desorption during the measurements is shown to be insignificant.

Table S1 Dissipation shift ( $10^{-6}$ )						
	Bare sensor			Polymer grafted sensor		
	NaTCA 200 mM	NaSCN 200 mM	NaF 200 mM	NaTCA 200 mM	NaSCN 200 mM	NaF 200 mM
20 °C	5.45 (-5.47)	1.62 (-1.58)	4.61 (-4.64)	5.92 (-5.95)	3.05 (-3.10)	3.98 (-4.05)
	5.47 (-5.46)	1.54 (-1.50)	4.58 (-4.60)	5.91 (-5.98)	3.09 (-3.08)	4.05 (-4.10)
	5.43 (-5.47)	1.54 (-1.52)	4.57 (-4.60)	5.94 (-5.98)	3.14 (-3.16)	3.99 (-4.02)
30 °C	4.03 (-4.05)	1.00 (-1.01)	3.55 (-3.60)	4.25 (-4.30)	1.42 (-1.39)	3.51 (-3.50)
	3.99 (-4.02)	1.01 (-0.99)	3.53 (-3.52)	4.29 (-4.30)	1.45 (-1.40)	3.55 (-3.52)
	4.01 (-4.02)	1.01 (-1.00)	3.58 (-3.55)	4.26 (-4.27)	1.44 (-1.42)	3.48 (-3.55)
40 °C	4.04 (-4.08)	1.72 (-1.70)	4.13 (-4.15)	4.12 (-4.05)	1.71 (-1.70)	3.97 (-4.03)
	4.06 (-4.05)	1.74 (-1.72)	4.15 (-4.10)	4.07 (-4.13)	1.69 (-1.75)	3.97 (-4.02)
	4.06 (-4.10)	1.72 (-1.71)	4.12 (-4.13)	4.03 (-4.10)	1.70 (-1.69)	3.99 (-4.02)

### S3. Additional DLS and zeta potential measurements:

As explained, the PNIPAM chains in the salt-free solution form stable mesoglobules upon crossing the phase separation temperature. The hydrodynamic diameter distribution profiles of PNIPAM below and above the phase transition temperature are provided in Fig. S9. At 20 °C, a relatively broad unimodal size distribution with an average diameter of around 40 nm (corresponding to single PNIPAM chains) is obtained. At 40 °C, the obtained size distribution is considerably narrower than 20 °C, and an average hydrodynamic diameter of around 150 nm is found (corresponding to nano-sized mesoglobules).



**Fig. S9** Hydrodynamic diameter distribution profiles (Intensity PSD) of 0.1 wt% PNIPAM in the salt-free solution at 20 and 40 °C. The Z-average diameter and PdI values obtained from the cumulants fitting are also provided for each condition.

It was argued that the hydrodynamic diameter of PNIPAM apparently increases at temperatures close to the phase transition, which was speculated to stem from relatively stronger PNIPAM-PNIPAM inter-chain interactions. To inquire this idea, additional DLS measurements on 0.05 and 0.2 wt% salt-free PNIPAM solutions were performed. As depicted in Fig. S10, almost no increment in the hydrodynamic size is observed below the phase transition temperature for the 0.05 wt% solution. In contrast, the 0.2 wt% solution demonstrates a more pronounced increment compared to the 0.1 wt% solution.

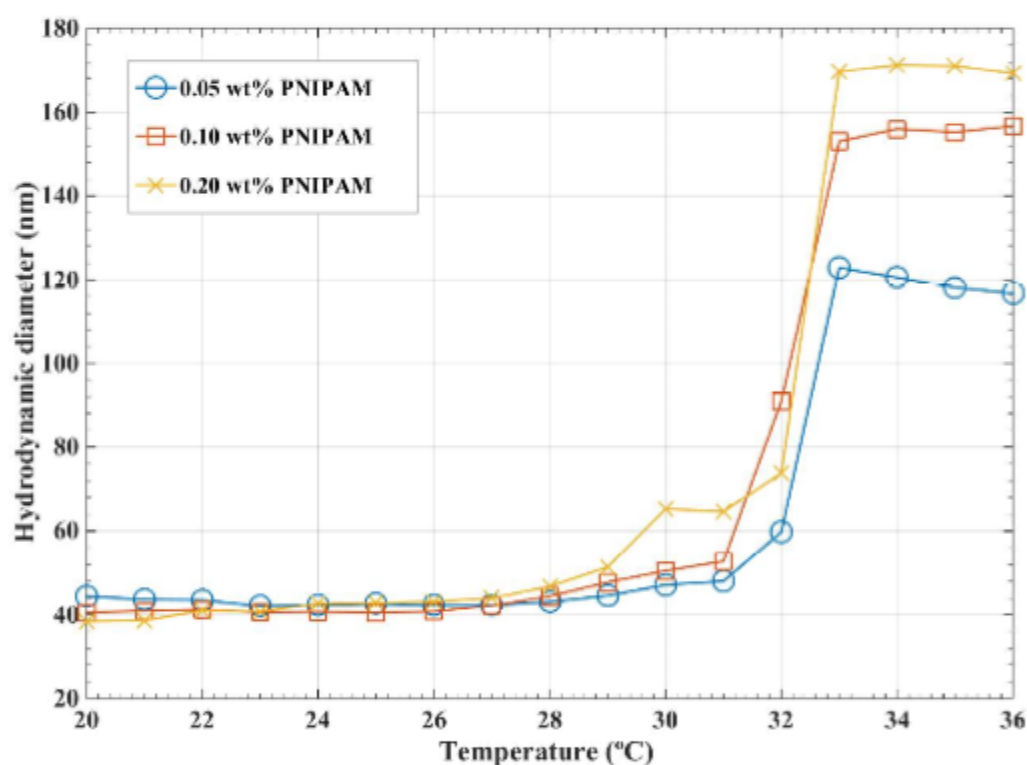


**Fig. S10** Z-average hydrodynamic diameter of 0.05, 0.10 and 0.20 wt% salt-free PNIPAM solutions. As shown, the increment in apparent hydrodynamic diameter below the phase transition temperature becomes more pronounced with increasing polymer concentration.



To inspect if the PNIPAM mesoglobules are electrostatically charged in the salt-free solution, zeta potential measurements were performed on a 0.05 wt% PNIPAM solution at various temperature between 20 and 40 °C. As indicated, a significant increment in zeta potential value is observed upon formation of mesoglobules; hence, the electrostatic repulsions can contribute to mesoglobule stability.

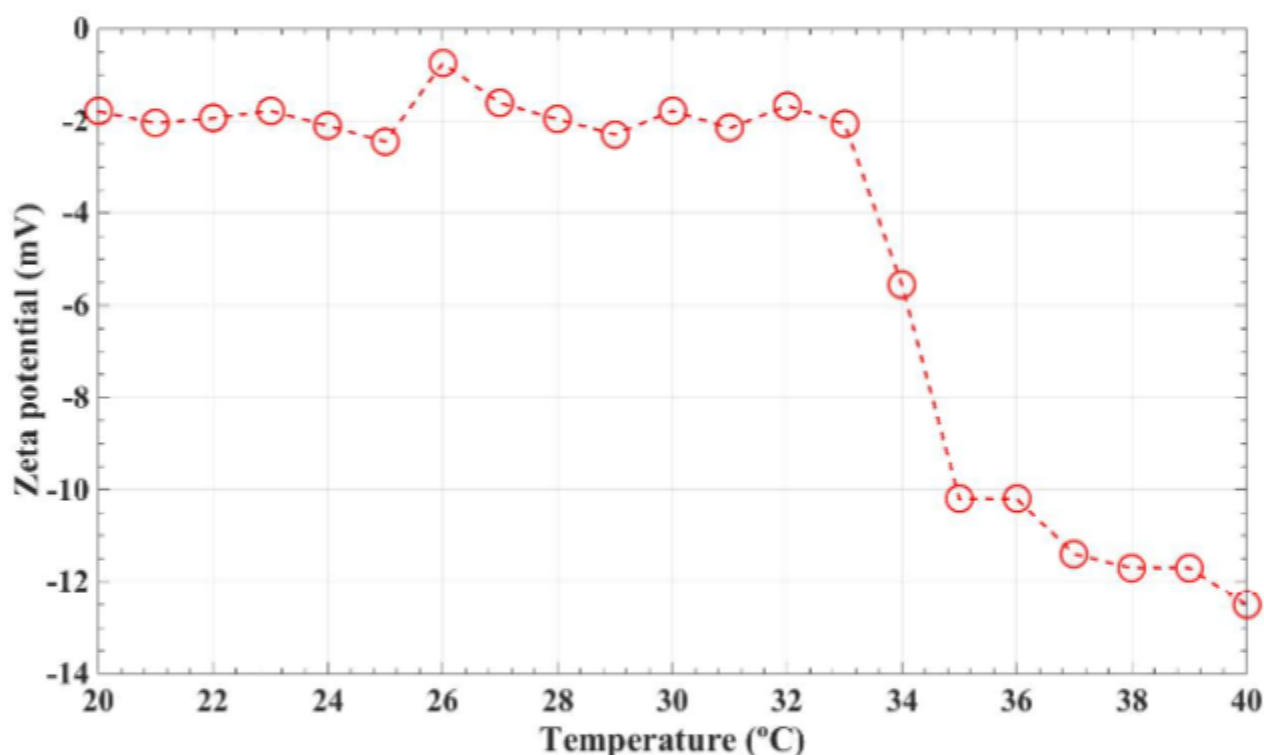


**Fig. S11** Surface zeta potential of 0.05 wt% salt-free PNIPAM solution as a function of temperature. As demonstrated, formation of mesoglobules is accompanied with a notable increment in the value of surface charge. This suggests that electrostatic stabilization is one of the mechanisms that can affect PNIPAM mesoglobules stability.

#### S4. Analysis of AFM measurements:

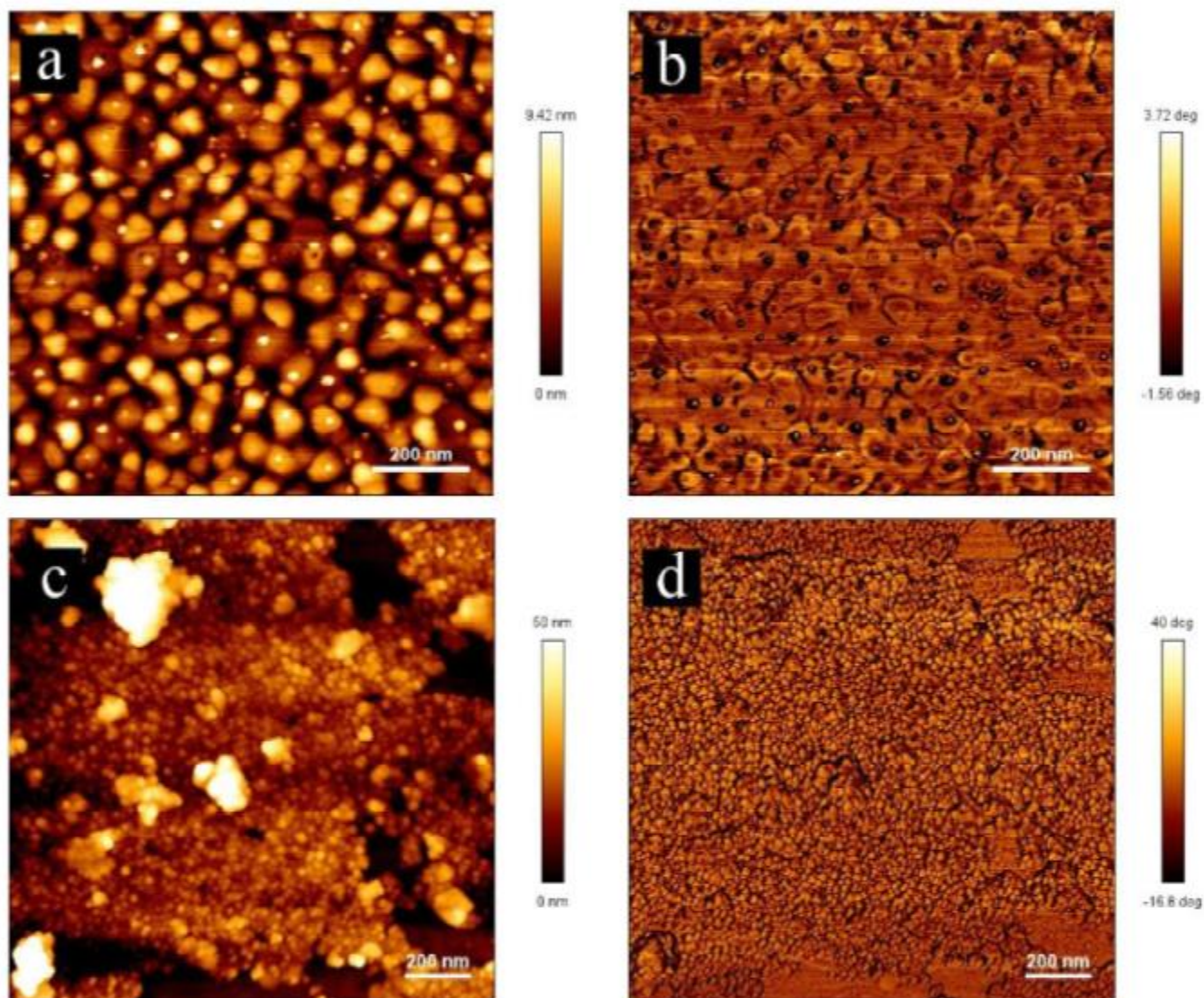


**Fig. S12** AFM tapping mode (a) height and (b) phase of gold coated wafer; (c) height and (d) phase of gold-coated particle. RMS roughness values of 2.125 nm and 10.490 nm were found for the gold-coated wafer (over  $1\mu\text{m} \times 1\mu\text{m}$  area) and the gold-coated particle (over  $1.5\mu\text{m} \times 1.5\mu\text{m}$  area), respectively.

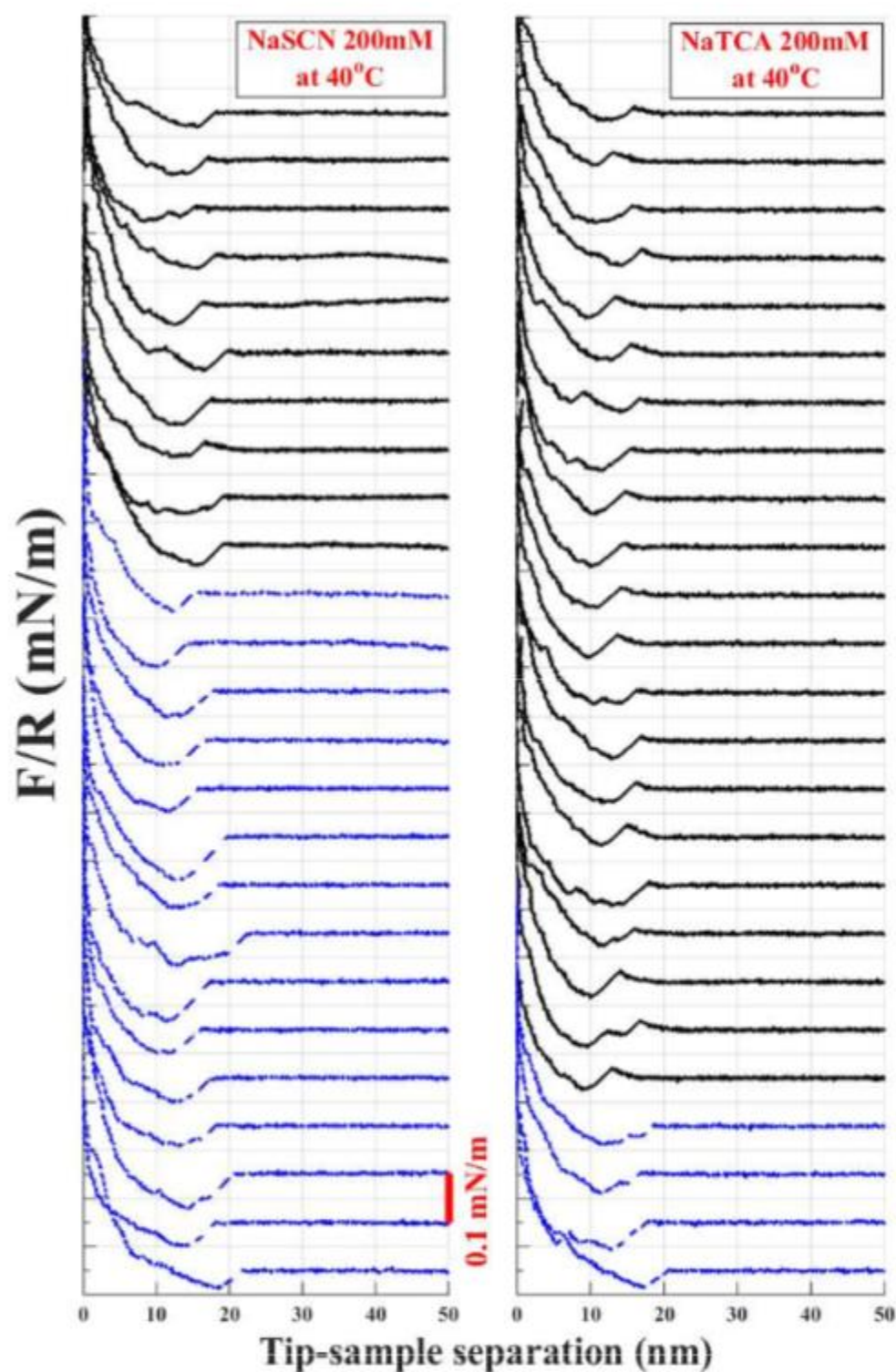


**Fig. S13** Approach force-distance curves between the PNIPAM layers in NaSCN 200mM and NaTCA 200mM at 40 °C. Black full lines represent measurements where a weak repulsion was observed before jump-in the surface. As shown, 21 out of 25 curves in NaTCA show initial repulsion, while it is 10 out of 25 curves in NaSCN.

## REFERENCES

1. M. A. Plunkett, Z. Wang, M. W. Rutland and D. Johannsmann, *Langmuir*, 2003, **19**, 6837-6844.
2. B. Wu, K. Wu, P. Wang and D.-M. Zhu, *The Journal of Physical Chemistry C*, 2007, **111**, 1131-1135.

## **PAPER V**

# **Thermo-responsive Diblock and Triblock Cationic Copolymers at the Silica/Aqueous Interface: A QCM-D and AFM study**

Saeed Zajforoushan Moghaddam <sup>a</sup>, Kaizheng Zhu <sup>b</sup>, Bo Nyström <sup>b</sup> and Esben

Thormann <sup>a\*</sup>

<sup>a</sup> *Department of Chemistry, Technical University of Denmark, 2800 Kgs. Lyngby,  
Denmark*

<sup>b</sup> *Department of Chemistry, University of Oslo, Blindern, P.O. Box 1033, Blindern,  
N-0315 Oslo, Norway, Norway*

---

\* To whom correspondence should be addressed. E-mail: [esth@kemi.dtu.dk](mailto:esth@kemi.dtu.dk).

Telephone: (+45) 4525 2439

**Abstract:** The properties of synthesized diblock poly(*N*-isopropylacrylamide)-poly((3-acrylamidopropyl)trimethylammonium chloride) and triblock methoxy-poly(ethylene glycol)-poly(*N*-isopropylacrylamide)-poly((3-acrylamidopropyl)trimethylammonium chloride) cationic copolymers at the silica/aqueous interface are investigated using quartz crystal microbalance with dissipation monitoring (QCM-D) and atomic force microscopy (AFM). Moreover, dynamic light scattering is employed to assess the copolymers in terms of the hydrodynamic size and micellization. Although viscoelastic Voigt modeling of the QCM-D data suggests a comparable layer thickness for the copolymers on the silica surface, the AFM imaging and colloidal probe measurements reveal significant differences in surface coverage and thickness of the layers, which are discussed and compared with respect to the stabilization effect by the hydrophilic PEG block.

**Keywords:** poly(*N*-isopropylacrylamide), poly(ethylene glycol), cationic copolymer, dynamic light scattering, quartz crystal microbalance with dissipation, atomic force microscopy



## 1. Introduction

Copolymers with novel structures have been the subject of interest during recent years, both from a fundamental and a practical point of view.[1-5] With respect to the fundamental point of view, studying such molecular systems can bolster our understanding of the stimuli-responsive materials, micellization, molecular self-assembly and interfacial phenomena.[6-12] From the practical standpoint, it can help us to develop various biotechnological applications, owing to the encapsulation capability of the copolymer and selective responsivity of the blocks to various external stimuli such as temperature and ions.[13-19]

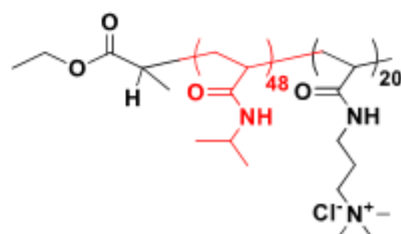
Poly(*N*-isopropylacrylamide) (PNIPAM) and poly(ethylene glycol) (PEG) are among the mostly investigated uncharged stimuli-responsive polymers.[20-22] Both of the polymers represent a lower critical solution temperature (LCST) phase behavior in aqueous solution; however, the molecular and thermodynamic mechanisms of the phase separation are indeed different. PNIPAM has a phase separation temperature of around 32 °C, at which undergoes an abrupt transition in interactions and conformation.[23-25] Below the phase separation temperature, PNIPAM chains adopt a swollen random coil conformation, with an approximate water content of 90%, including the water molecules forming hydrogen bonds with the amide groups and those in the hydrophobic hydration shell.[26, 27] Upon crossing the phase separation temperature in dilute solution, the swollen coils abruptly shrink to a collapsed globular structure with a water content of around 60%.[28, 29] This suggests that the phase separation mainly originates from hydrophobic dehydration, while the hydrogen-bonded water molecules almost remain intact. Such a sharp phase transition reminisces protein denaturation and folding, which renders PNIPAM a model thermo-responsive polymer for macromolecules with more complex structures.[30, 31] In addition, the phase separation temperature of PNIPAM is in the range of physiological temperature, making it a candidate

for drug delivery applications.[32-34] On the other hand, PEG exhibits a more hydrophilic character than PNIPAM, and thus generally has a phase separation temperature above 100 °C in salt-free solutions.[35, 36] In contrast to PNIPAM, the phase transition of PEG occurs over a relatively broad range of temperatures, which has been suggested to originate from gradual dehydration of the ether bonds.[37, 38] Regarding the conformation below the phase separation temperature, the PEG chains adopt a helical structure, which transform into collapsed disk-like structures at the fully collapsed state.[39, 40] Due to the stealth-like character toward human immune system, PEG has diverse usage in various biomedical applications such as gene-therapy and cell fusion.[41-43]

In the present study, a diblock poly(*N*-isopropylacrylamide)-poly((3-acrylamidopropyl)trimethylammonium chloride) (P(NIPAM)<sub>48</sub>-P(AMPTMA)<sub>20</sub>) and a triblock methoxy-poly(ethylene glycol)-poly(*N*-isopropylacrylamide)-poly((3-acrylamidopropyl)trimethylammonium chloride) (MP(EG)<sub>45</sub>-P(NIPAM)<sub>50</sub>-P(AMPTMA)<sub>20</sub>) copolymer are investigated. The PAMPTMA block of the copolymers is positively charged in aqueous solution, thus can electrostatically adsorb onto negatively charged surfaces such as silica.[44-46] This feature can be employed to produce stable polymer layers, which can be used in various practical applications, e.g., to prevent adhesion of biomolecules or conversely to promote specific attachment of cell types to surfaces.[47-49] Dynamic light scattering (DLS) is employed to inquire the thermo-responsive behavior and hydrodynamic size of the copolymers in bulk aqueous solution. The properties of the copolymers at the silica-aqueous interface are investigated by quartz crystal microbalance with dissipation monitoring (QCM-D) and atomic force microscopy (AFM) imaging and colloidal probe force-distance measurements. Using QCM-D, adsorption of the copolymers onto the silica surface is monitored, and then compared in terms of the amount of the adsorbed mass and the viscoelastic behavior of the layer. From AFM experiments, the topography of the adsorbed

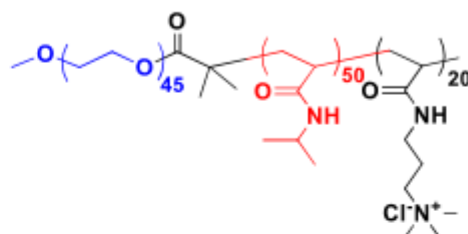
copolymers layers is assessed; moreover, the interactions between two copolymer-coated silica surfaces are investigated at various temperatures. The length of the cationic PAMPTMA and thermo-responsive PNIPAM blocks are identical between the diblock and triblock copolymers, giving us the opportunity to assess the effect of the hydrophilic PEG block on the interfacial properties of the copolymer. The objective of this work is to provide a fundamental knowledge of the copolymers interfacial and thermo-responsive behavior, as well as suggesting how tuning the structure of the copolymers can help us to obtain more uniform and homogenous polymer layers.

**Poly(N-isopropylacrylamide)-*block*-poly((3-acrylamidopropyl)trimethylammonium chloride) (P(NIPAM)<sub>48</sub>-*b*-P(AMPTMA)<sub>20</sub>)**



$M_w = 10\,800\text{ g/mol}$ ;  $M_w/M_n = 1.05$

**Methoxy-poly(ethylene glycol)-*block*-poly(N-isopropylacrylamide)-*block*-poly((3-acrylamidopropyl)trimethylammonium chloride) (MP(EG)<sub>45</sub>-*b*-P(NIPAM)<sub>50</sub>-*b*-P(AMPTMA)<sub>20</sub>)**



$M_w = 15\,000\text{ g/mol}$ ;  $M_w/M_n = 1.4$

**Scheme 1** Chemical structure, molecular weight and polydispersity of the cationic diblock copolymer (P(NIPAM)<sub>48</sub>-P(AMPTMA)<sub>20</sub>, top) and triblock copolymer (MP(EG)<sub>45</sub>-P(NIPAM)<sub>50</sub>-P(AMPTMA)<sub>20</sub>, bottom) studied here.

## 2. Experimental Section

**2.1. Materials:** The copolymers were synthesized according to a “one-pot” atom transfer radical polymerization (ATRP) procedure and the details on the synthesis and characterization were reported

in our previous publications.[50, 51] The chemical structures of the copolymers employed in this study are depicted in Scheme 1, together with their weight-average molecular weights and polydispersity index. PEG (Mn of 6000 g·mol<sup>-1</sup>, Sigma Aldrich) and PNIPAM (Mn of 5500 g·mol<sup>-1</sup>, Polymer Source Inc., Dorval, Canada) homopolymers were used as received. The solutions were all prepared in 10 mM NaCl buffer (Degassed Milli-Q water, resistivity of 18.2 MΩ·cm. organic content below 5 ppb, pH 5.6) using a nutating mixer for 24 hr.

**2.2. Dynamic light scattering (DLS):** DLS (Zetasizer Nano-ZS, Malvern Instruments, Worcestershire, UK) measurements were performed to assess the aggregation temperature and estimate the hydrodynamic size of the copolymers at temperatures between 20 and 45 °C. The measurements were conducted on 0.15 wt% dilute solutions of the copolymers in 10 mM NaCl buffer, which were passed through a 0.45 µm pore diameter filter. Prior to the measurements, the samples were thermally stabilized at 20 °C for 15 min. After each temperature step, the samples were given a 5 min stabilization time. The standard software of the instrument (Zetasizer software, Malvern Instruments) was used for fitting the correlation function data and obtain the hydrodynamic size from the Stokes-Einstein relationship.

**2.3. Quartz crystal microbalance with dissipation (QCM-D):** Adsorption of PNIPAM and PEG homopolymers and the copolymers on the silica surface was monitored using QCM-D (Q-Sense E1, Biolin Scientific, Gothenburg, Sweden). A silica-coated sensor (QX 303, Biolin Scientific) was repeatedly washed with acetone, rinsed with copious amount of Milli-Q water, and dried by a stream of nitrogen. The sensor was then plasma-cleaned (PDC-32G plasma cleaner, Harrick Plasma) for 5 min, using the high power level and 500 mTorr pressure of water vapor. The measurements were started at 20 °C under a 80 µl/min steady flow of degassed 10 mM NaCl buffer. After reaching stable baselines for all the harmonics (1<sup>st</sup> to 13<sup>th</sup> overtones), the polymer solution (0.15 wt.% for copolymers and 0.1 wt% for homopolymers) in 10 mM NaCl buffer was flowed into the cell for 1 h at 20 °C. To

remove the loosely adsorbed chains, the cell was afterwards rinsed with 10 mM NaCl solution, until stable baselines for all the overtones were found. The measurements were repeated twice for each polymer solution. The standard software of the instrument (Q-Sense Dfind, Biolin Scientific) was employed for data analysis and viscoelastic Voigt modelling.

**2.4. Atomic force microscopy (AFM):** To study the topography and interactions of the copolymers, AFM (NanoWizard 3, JPK Instruments AG, Berlin, Germany) measurements were carried out. Interactions between two copolymer-coated silica surfaces were evaluated by the AFM colloidal probe technique. A tipless rectangular cantilever (HQ:CSC38/Cr-Au, MikroMasch) with approximate length of 350  $\mu\text{m}$ , width of 32.5  $\mu\text{m}$ , thickness of 1  $\mu\text{m}$ , and normal spring constant of 0.03  $\text{N.m}^{-1}$  was used. The accurate normal spring constant of the tipless cantilever was obtained according to the thermal noise method.[52] Afterwards, a silica particle with a diameter of  $7.2 \pm 0.1 \mu\text{m}$  (measured by Nikon Eclipse LV100ND optical microscope) was glued to the end of the cantilever, using the two-component Araldite 2000 plus epoxy adhesive.[53] The cantilever and the silicon wafer (WaferNet Inc., San Jose, CA, USA) were plasma-cleaned for 5 min at the high power level and 500 mTorr pressure of water vapor, mounted in the instrument, and then immersed in a 0.15 wt% solution of the copolymer for 1 h at 20 °C. After rinsing with copious amount of water, the measurements were instantly conducted. The solution temperature was controlled with an accuracy of  $\pm 0.1$  °C using a BioCell (JPK Instruments). Two syringe pumps (Aladdin syringe pump, World Precision Instruments) were used to exchange the solutions in the BioCell. When changing the cell temperature, the system was given a 10 min of stabilization time. For each temperature, 65 force curves were obtained at various surface positions over a  $5\mu\text{m} \times 5\mu\text{m}$  area. To avoid the contribution from hydrodynamic forces, an approach and retraction velocity of 200 nm/s was employed. Topography of the copolymer-covered surfaces was inspected using the Qualitative Imaging (QI) mode. A rectangular cantilever (HQ:CSC38/Al BS, MikroMasch) with normal spring constant of 0.03  $\text{N.m}^{-1}$

and a conic probe of 8 nm radius was used. The set force value of 0.35 nN and a pixel resolution of 256×256 were employed for all the measurements. The standard software of the instrument (JPKSPM Data Processing) was used to analyze the images and the force curves.

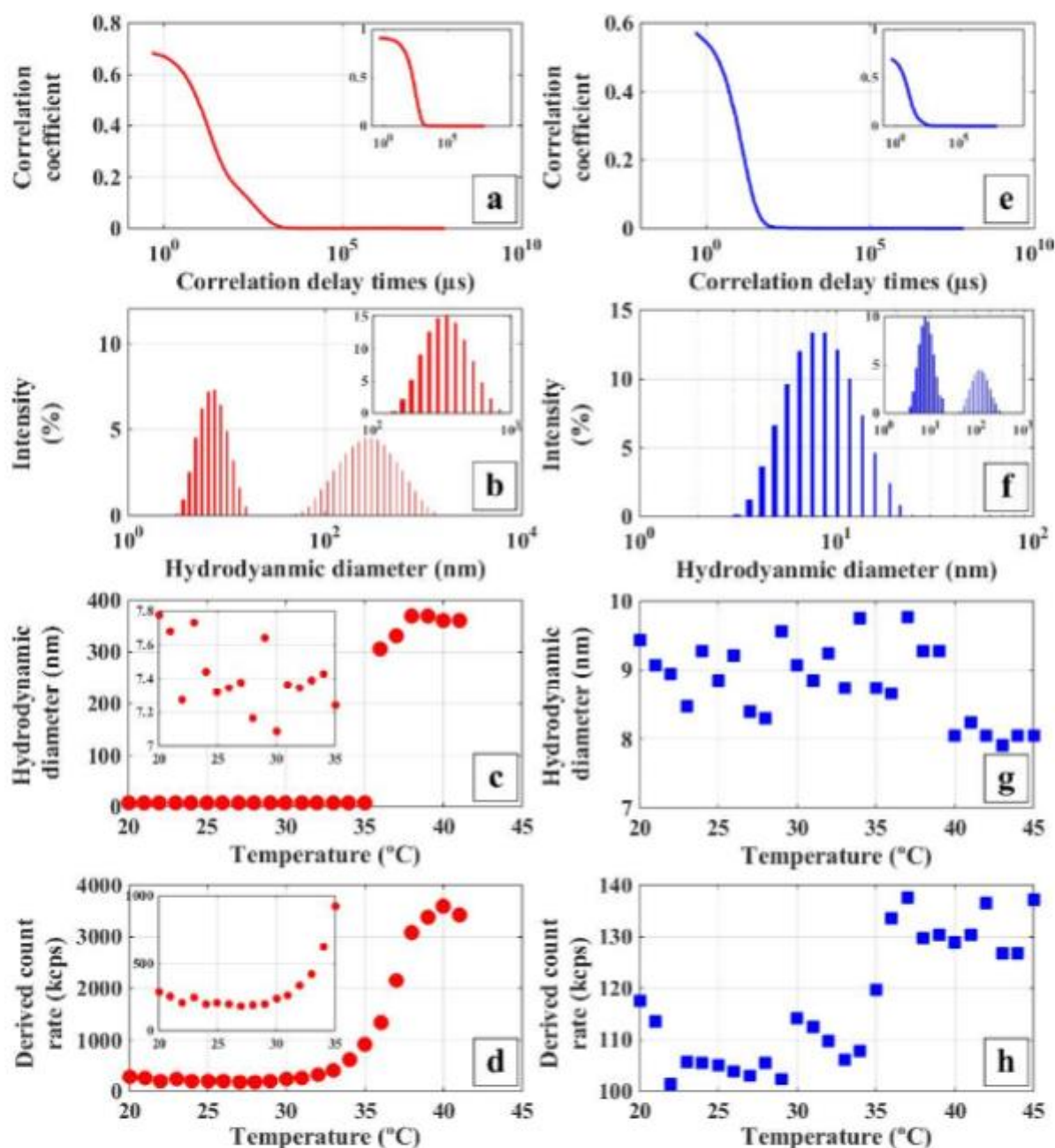


**Figure 1** DLS data of the diblock (Left panel, red figures) and the triblock (Right panel, blue figures) copolymer solutions (0.15 wt% copolymer, 10 mM NaCl buffer). (First row) correlation data at 20 °C (Inset shows the data at 40 °C), (Second row) hydrodynamic diameter distribution at 20 °C (Inset shows the data at 40 °C), (Third row) average hydrodynamic diameter as a function of temperature, (Last row) derived count rate as a function of temperature.

### 3. Results and Discussion

**3.1. DLS Measurements:** Before addressing the properties at the interface, we first evaluate the hydrodynamic size distribution and thermo-responsive behavior of the copolymers in bulk aqueous solution. Figure 1 depicts the hydrodynamic diameter and the derived count rate of the copolymer solutions at various temperatures between 20 and 45 °C, as well as the correlation data and hydrodynamic diameter distribution profiles at 20 and 40 °C. With respect to the diblock PNIPAM-PAMPTMA copolymer, the relatively slow decay of the correlation function and the observed shoulder imply polydispersity in size and presence of aggregates, respectively. Accordingly, a bimodal hydrodynamic diameter distribution is obtained at 20 °C, which represents a narrow peak at around 7.8 nm and a considerably broad peak at around 350 nm. While the former is attributed to the individual diblock chains, also known as the unimers, the latter reveals the presence of intermicellar complexes. Presence of such interchain aggregates has been previously investigated for different PNIPAM block lengths and salt concentrations.[50] It should be noted that the unimers are entirely dominant in number compared to the intermicellar structures.(Supplementary information, Section S1) By increasing the temperature up to 30 °C, both the peaks remain almost untouched in size and intensity, giving an average hydrodynamic diameter of 7.4 nm for the unimers. In the temperature range between 30 and 35 °C, the unimers peak continuously decays in intensity, while the second peak becomes progressively sharper, suggesting gradual formation and growth of the complexes at the expense of the unimers.[50] At 36 °C, the peak corresponding to the unimers completely disappears and the intermicellar structures peak is relatively narrower compared to at 20 °C. In the temperature range between 37 to 40 °C, the hydrodynamic diameter of the intermicellar structures remains constant around 350 nm, as well as the peak shape. The calculated hydrodynamic diameter is in the range of 1  $\mu$ m at 41 °C; however, poor quality of the correlation function indicates macroscopic phase separation of the solution; henceforth, the data at temperatures higher than 40 °C



are omitted. Regarding the derived count rate values, a similar trend is displayed. The temperature at which the count rate value rises is around 30 °C, in accordance with the temperature at which the unimers peak declines, supporting gradual transformation of the unimers into the intermicellar entities at the temperature range between 30 and 35 °C.

With respect to the MPEG-PNIPAM-PAMPTMA triblock copolymer, the correlation function shape represents a monodisperse system at 20 °C. Hereupon, a narrow unimodal size distribution with an average hydrodynamic diameter of around 9.4 nm is obtained, so merely unimers can be found in the solution. Moreover, the unimer average hydrodynamic diameter is relatively larger than that of the diblock copolymer, which can be attributed to the presence of the PEG chain. In general, increasing the temperature has no drastic effect on the average hydrodynamic diameter and the count rate values; henceforth, no significant aggregation occurs within the studied temperature range. However, at 40 °C, the average hydrodynamic diameter of the unimer entities slightly decreases (~ 8 nm), and a relatively weak and broad secondary peak corresponding to the intermicellar complexes appears. In the temperature range between 40 and 45 °C, the complexes peak becomes slightly stronger in intensity, but still the unimers are utterly dominant in population. (Supplementary information, Section S1) A similar trend is demonstrated for the count rate values, which show minor dependence on the temperature. All these observations together confirm that the hydrophilic PEG block stabilizes the unimer state and effectively prevents interchain aggregation throughout the studied temperature range. Knowing the behavior of the copolymers in the bulk solution, next step is to assess adsorption and self-assembly of the copolymers at the silica-aqueous interface.

**3.2. QCM-D Measurements:** Figure 2 represents the frequency and dissipation factor shifts resulting from adsorption of the homopolymers and the copolymers onto the silica surface. As a common observation, adsorption of the polymers is accompanied with a negative shift in the oscillation frequency ( $\Delta F < 0$ ), as well as a positive shift in the dissipation factor ( $\Delta D > 0$ ). The former is related

to the amount of the adsorbed mass over the sensor surface, which indeed includes the mass of the anchored polymer chains plus their water content, known as the “wet” polymer mass. The latter is attributed to the ability of the attached polymer chains to deform and dissipate some energy during each oscillation. Accordingly, a soft and swollen polymer film gives rise to a high dissipation value; whereas, a rigid and collapsed polymer film follows the sensor oscillation with no significant deformation, and thus is associated with a small damping factor.[54-56]

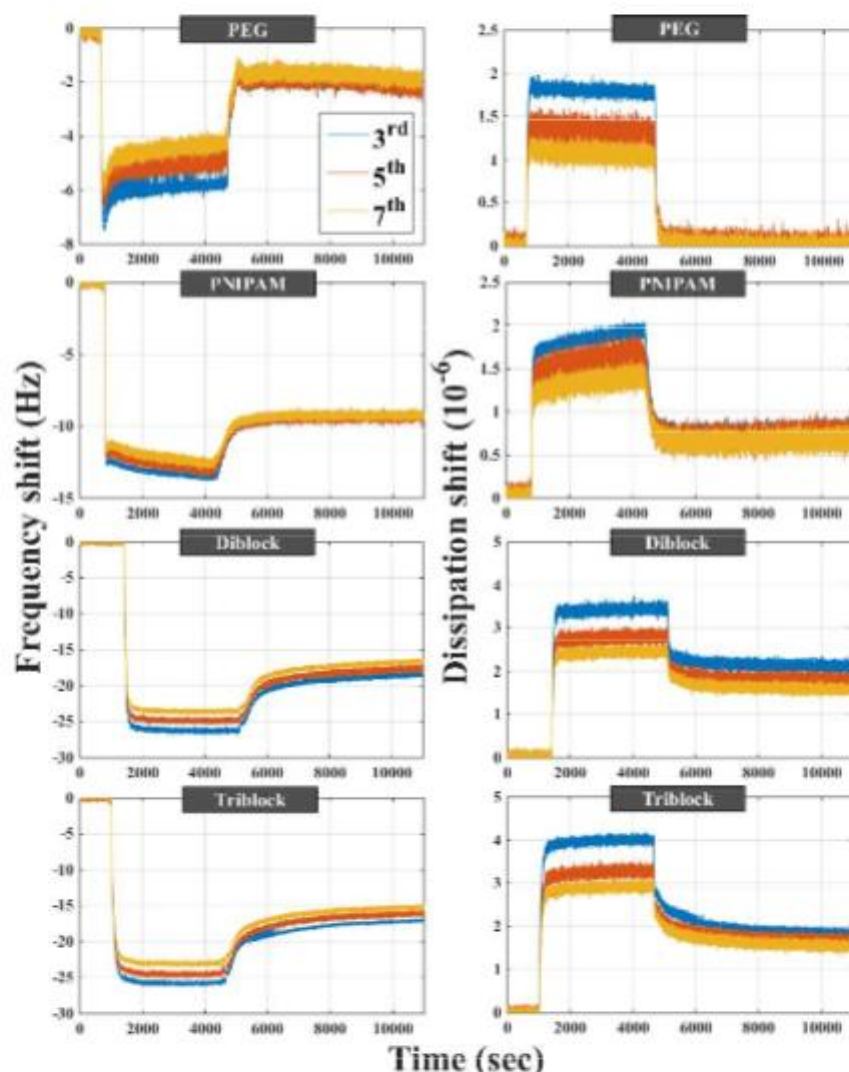


**Figure 2** QCM-D data of adsorption of the homopolymers and the copolymers on the silica surface; (left column) Frequency shift normalized by the overtone number (right column) Dissipation factor shift. The data of 3<sup>rd</sup>, 5<sup>th</sup> and 7<sup>th</sup> overtones are provided. In contrary to the homopolymers, notable overtone-dependence is found for the copolymers adsorption, suggesting formation of a soft and dissipative polymer layer.

In order to ascertain the affinity of the uncharged blocks for the silica surface, adsorption of PNIPAM and PEG homopolymers is first studied.[57, 58] It is demonstrated that PEG has a relatively weak segmental affinity towards the silica surface. The adsorption is accompanied with a 2 Hz decrement in the oscillation frequency and a negligible increment of 0.1 in the dissipation factor, for the third overtone. This observation indicates limited physical attractions between the ethylene glycol segments and the silica surface. Considering the notably small dissipation shifts alongside with minor overtone-dependence of the adsorption curve, the Sauerbrey equation can be used to estimate the adsorbed mass[59], giving an approximate value of 75 ng/cm<sup>2</sup>. On the other hand, PNIPAM homopolymer represents a relatively stronger physical interaction with the silica surface, which is evident from a 10 Hz decrement in the oscillation frequency and an increment of 0.7 in the damping factor. However, the adsorption curves render no significant overtone-dependence, suggesting a pancake conformation for the PNIPAM chains on the surface.[60, 61] Accordingly, the mass of the adsorbed PNIPAM layer is approximated using the Sauerbrey equation, giving an estimated value of 200 ng/cm<sup>2</sup>.

**Table 1** Viscoelastic modeling of the copolymer films (detailed description of modelling procedure is provided in the Supplementary information, Section S2)

Copolymer	Voigt thickness (nm)	Shear viscosity (mg/m·s)	Elastic modulus (Mg/m·s <sup>2</sup> )
PNIPAM-PAMPTMA	16.5	1080	5.0
PEG-PNIPAM-PAMPTMA	17.0	1040	3.5

Adsorption of the diblock PNIPAM-PAMPTMA copolymer gives rise to a frequency shift of −18.2 Hz and a dissipation shift of 2.1. The relatively large value of the dissipation factor

together with the apparent overtone-dependence of the adsorption curve imply formation of a soft and viscoelastic copolymer layer.(see the Supplementary information, Section S2) Therefore, the layer properties are estimated using the Voigt viscoelastic model[62-64], suggesting an average layer thickness of around 16.5 nm (Table 1). It is worth mentioning that the calculated thickness does not necessarily describe the real thickness of the prepared copolymer layer, but only provides the thickness of a homogenous and uniform layer that has the same viscoelastic behavior.[65, 66] With respect to adsorption of the triblock MPEG-PNIPAM-PAMPTMA copolymer, a frequency shift of  $-16.5$  Hz and dissipation shift of  $1.8$  is detected, as well as overtone-dependence of the adsorption curve, thus a swollen and soft layer conformation is expected. Using the viscoelastic modelling, a layer thickness of around  $17$  nm is found, which is indeed comparable with that of the diblock copolymer. Therefore, the QCM-D measurements exhibit similarity in the properties of the diblock and triblock copolymer layers. Nevertheless, as explained above, the viscoelastic modelling data can be misleading if the polymer layers are not homogeneous. Accordingly, the topography of the copolymer-covered surfaces will be further examined using AFM imaging.

**3.3. AFM imaging:** AFM topography images of the copolymer-covered silica surfaces in  $10$  mM NaCl at  $20$  °C are compared in Figure 3. In apparent contrast to the QCM-D modelling data, the thickness and topography of the copolymer-covered surfaces are shown to be significantly different. With respect to the diblock copolymer (Figure 3a,b), relatively large aggregates can be found on the surface, which can suggest adsorption of the intermicellar complexes from the solution. The clusters on the surface differ greatly in the planar dimension, relative height and shape. For the imaged entities, the typical planar dimension varies approximately from  $50$  to  $250$  nm, while the typical maximum relative height is roughly between  $20$ - $50$  nm.

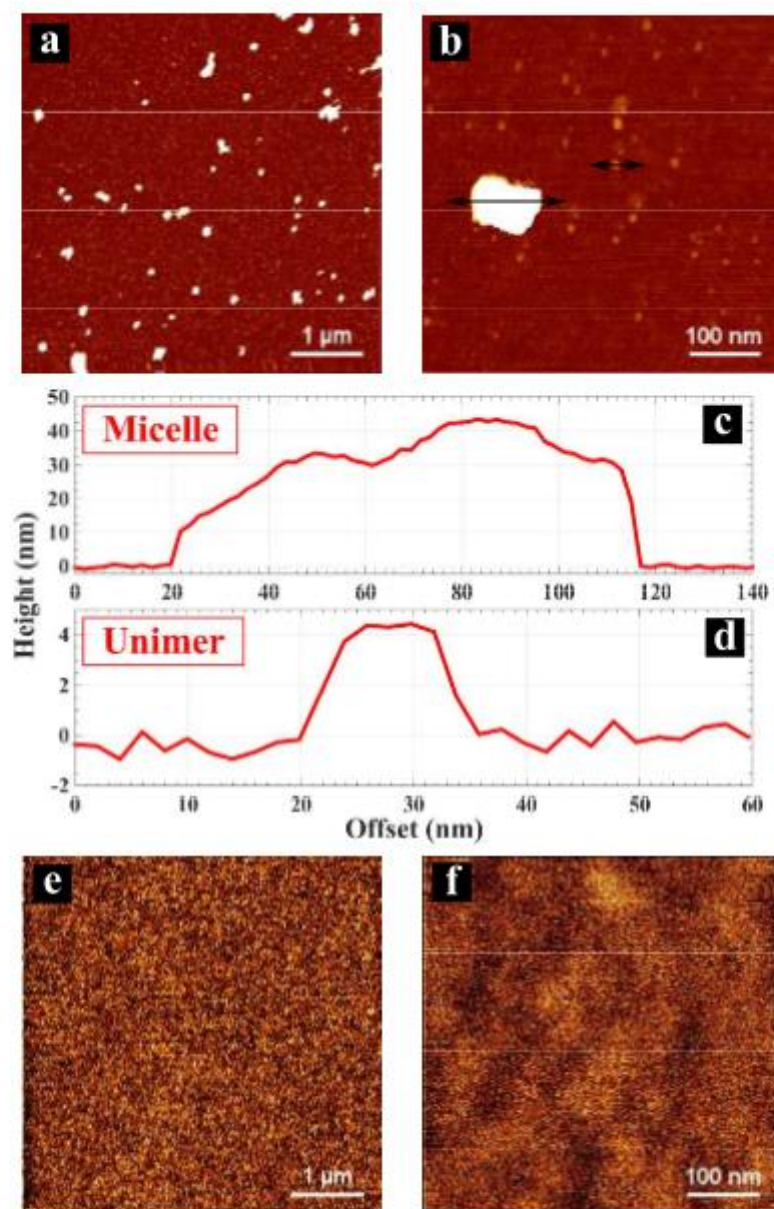


**Figure 3** Topography of the copolymers on the silica surface at 20 °C; (a)(b) Height images of PNIPAM-PAMPTMA diblock (c)(d) cross-section profiles of a micelle and an unimer, which are indicated on figure b. (e)(f) Height images of MPEG-PNIPAM-PAMPTMA triblock

This is in agreement with the fact that the complexes in solution are quite polydisperse in the hydrodynamic diameter (see Figure 1); moreover, the adsorbed complexes on the surface might merge to form relatively larger and asymmetrical clusters. In addition to the large aggregates, relatively smaller entities with an average planar dimension of around 10 nm and relative height of around 3 nm are apparently adsorbed on the surface. Since the dimension

values are comparable to the measured hydrodynamic dimeters of the unimers, we suggest such structures are the unimers that are heterogeneously adsorbed on the surface. With respect to either the aggregates or the unimers, the planar dimensions are apparently larger than the relative height values, which can be reasoned based on the relatively strong segmental affinity of the PNIPAM block to the silica surface (see Figure 2) that can favor a pancake-like conformation for the PNIPAM blocks. Besides, the cationic block is also expected to extend on the surface and adopt a flat conformation.

On the contrary, the triblock MPEG-PNIPAM-PAMPTMA copolymer (Figure 3e, f) evidently produces a more homogenous and uniform layer on the silica surface. There is no trace of large aggregates throughout the surface, which is in agreement with the DLS measurements in which only unimers were identified in the solution at 20 °C. Lack of large entities also indicates that the adsorbed unimers are unlikely to merge and form interchain aggregates at on the surface this temperature. Furthermore, one cannot observe distinguishable unimer entities even in small-scale images, which strengthens the idea of having a relatively dense and homogenous copolymer film, with a uniform surface coverage.

**3.4. AFM colloidal probe force-distance measurements:** The force-distance curves between two silica surfaces covered with the copolymers in a 10 mM NaCl solution at various temperatures are illustrated in Figure 4. It should be noted that the long-ranged electrostatic forces are effectively screened (Debye length of around 3 nm); hence, we can specifically study the polymer-related forces. Regarding the approach force curves between the surfaces covered with the diblock copolymer, a considerably long-ranged repulsive force is demonstrated. At 20 °C, the repulsive force starts at an average separation distance of around 95 nm. Such a long-ranged repulsion is indeed caused by the huge complexes present on the surfaces. Based on the images and force curves, the repulsive force that kicks in at the separation distance of around 95 nm can be attributed to compression of the



aggregates against each other or the opposite bare surface. However, since the layer is topographically non-uniform and heterogeneous, one cannot conclude a definite thickness from the AFM force measurement data. Increasing the temperature to 25 and 30 °C has no noticeable effect on the force-distance profile. By increasing the temperature to 35 °C, the repulsive force becomes slightly weaker and the contact point apparently decreases to nearly 90 nm.

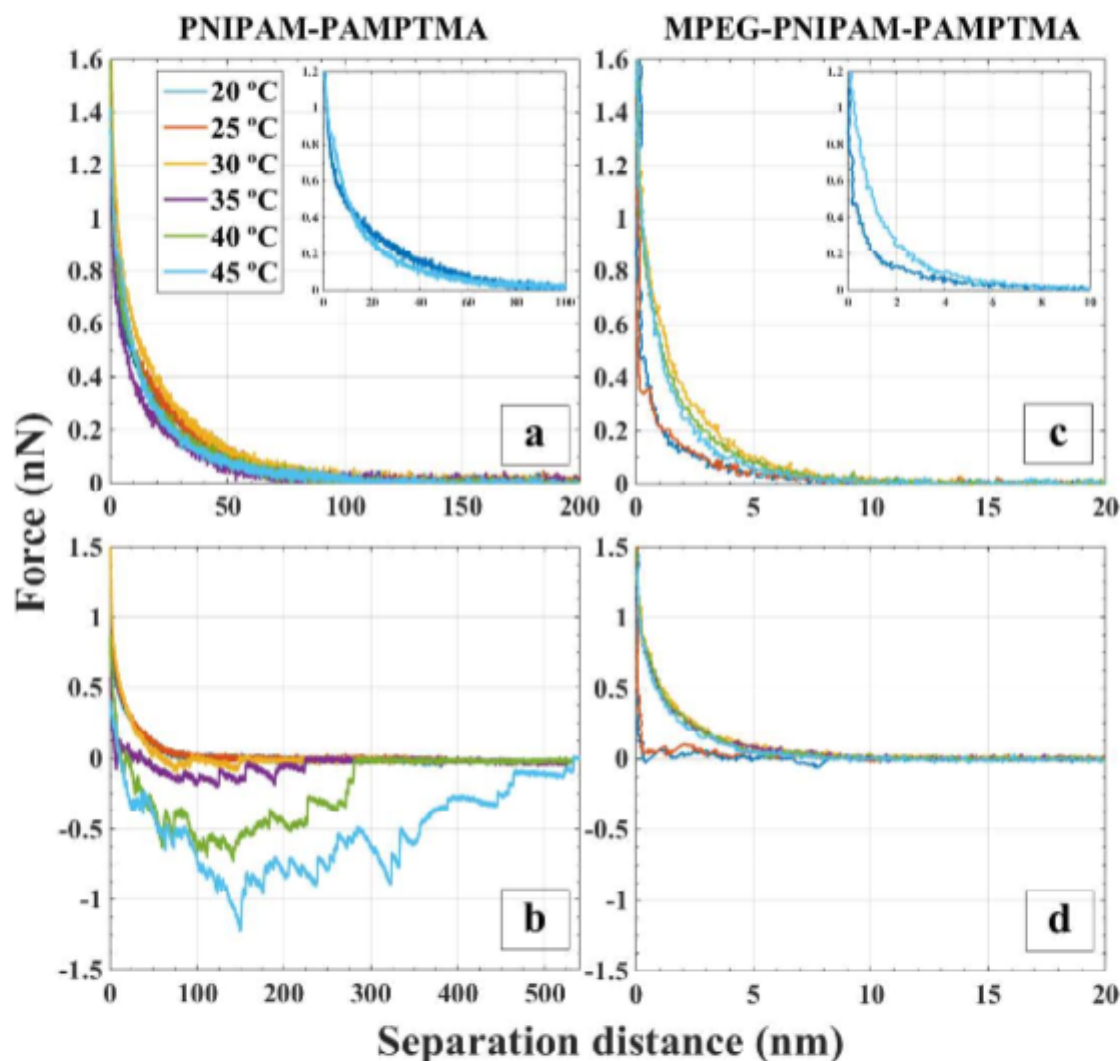


**Figure 4** Force-distance curves between two silica surfaces (silicon wafer and spherical silica probe) covered with the copolymer layers (left column) surfaces covered with the diblock copolymer (right column) surfaces covered with the triblock copolymer.

This change in the force profile may be attributed to the collapse of the PNIPAM blocks within the aggregates, at temperatures between 30 and 35 °C. However, it might also originate from



minor changes in the structure of the large domains, due to multiple compressions during the experiment. At 40 and 45 °C, the repulsive force profiles seem to become relatively stronger and are almost similar to the force curve at 20 °C. Compared to 20 °C, it seems that the repulsive forces are relatively weaker at distances larger than 15 nm; however, they are apparently relatively stronger at the shorter distances. Hence, although the maximum thickness of the aggregates is not notably affected by increasing the temperature, the internal layer structure of the micelles seems to be changed, which can be due to the collapsed and more compact conformation of the PNIPAM blocks, or again an experimental effect. With respect to the retract force-distance profiles, only a slight adhesion is found between the polymer-coated surfaces at 20 and 25 °C, indicating lack of strong inter-chain interactions. Increasing the temperature to 30 °C strengthens the adhesion and attractive forces, which can be attributed to presence of PNIPAM inter-chain interactions in the proximity of the collapse temperature. By further heating the solution, the adhesion energy becomes significantly stronger, and attraction between the surfaces is observed at separation distances up to around 500 nm, which can be correlated to the bridging aggregates.

Regarding the surfaces covered with the triblock copolymer, the approach force-distance profiles are evidently short-ranged. At 20 and 25 °C, the repulsive force starts at a separation distance of around 10 nm, which confirms the idea of having a homogenous layer, formed solely of the unimers. Since the layer was shown to be uniform and homogenous, the layer thickness then can be estimated from the force-distance profile to be around 5 nm, which is also comparable with the measured hydrodynamic diameter and the maximum relative height found from the AFM images. It should again be considered that the PNIPAM and PAMPTMA blocks could interact with the silica surface, and the adsorbed unimers are thus expected to flatten on the surface. Therefore, the film thickness is relatively smaller than the

hydrodynamic diameter of the unperturbed unimers in bulk solution. By increasing the temperature to 30 °C, the repulsive force becomes stronger, while the contact distance is apparently not significantly affected. This intensification of the repulsive force can be attributed to the collapse of the PNIPAM blocks, and thus a change in the layer internal structure and rigidity. One can argue that upon increasing the temperature, the PNIPAM-PNIPAM inter-chain interactions become notably stronger and the PNIPAM blocks tend to minimize their solvent-accessible surface area. Accordingly, a conformational transition from flat pancake to collapsed globule is expected, which could explain the relatively stronger repulsive force of layer compression. Further increment in temperature has no notable effect on the force-distance curves, suggesting a robust and stable layer structure up to 45 °C. Regarding the retract force profiles, a weak adhesion –in less than half of the measurements– between the surfaces is found at 20 and 25 °C, which can indicate relatively weak PNIPAM-PNIPAM interactions. Nevertheless, no adhesion is observed between the surfaces at 30 °C and higher temperatures, demonstrating an effective shielding effect by the PEG blocks that can be found on the outer surface of the copolymer layer, which can prevent adhesion between the collapsed PNIPAM blocks.

#### **4. Conclusions**

In the present work, the properties of diblock PNIPAM-PAMPTMA and triblock MPEG-PNIPAM-PAMPTMA copolymers at silica-aqueous interface were investigated. It was shown that presence of the PEG block drastically influences the behavior of the copolymer in bulk solution and when adsorbed to a silica surface. In the bulk state, it was indicated that the diblock copolymer solution is composed of unimers plus relatively large intermicellar structures, even below the collapse temperature of PNIPAM. On the other hand, the triblock

copolymer solution includes merely unimer entities below the collapse temperature of PNIPAM, while the intermicellar structures can form at relatively high temperatures, but are in minority. AFM topography images also revealed evident differences in the topography of the surfaces covered with the copolymers. While large aggregated domains and separated unimers were found for the diblock copolymer, the triblock copolymer was demonstrated to produce a uniform and homogenous layer in terms of thickness and surface coverage. Such a discrepancy in properties was not captured by the QCM-D measurements, in terms of the layer viscoelastic properties and thickness. The Voigt viscoelastic modeling data suggested comparable layer thicknesses and viscoelasticity for the both copolymer layers. The AFM colloidal probe force-distance measurements were in agreement with the height images, indicating long-ranged repulsive forces resulting from compression of the diblock copolymer clusters; on the other hand, a short-ranged repulsion in the range of unimers coil size was obtained for the triblock copolymer. Additionally, it was demonstrated that the diblock-covered surfaces render considerably strong adhesion above the PNIPAM phase separation temperature, while no adhesion was measured between the triblock-covered surfaces even at 45 °C. In conclusion, our work suggests how including a short hydrophilic block with minor tendency to the substrate into the copolymer backbone can efficiently tune the interfacial adsorption in order to produce polymer layers with a more homogeneous structure and uniform surface coverage. On the other hand, the observed shielding effect on adhesion forces mediated by the hydrophilic block in the outer region of the polymer film can be potentially employed for various applications, e.g. fabrication of antifouling surfaces against specific biomolecules, or more generally can be used to prepare surfaces with selective molecular recognition capabilities and interfacial properties.

## Acknowledgements

We would like to acknowledge the Swedish Research Council (VR) for the financial support, which was transferred to the Technical University of Denmark via the EU initiative “Money Follow Researcher”.

## References

- [1] E.G. Kelley, J.N. Albert, M.O. Sullivan, T.H. Epps III, Stimuli-responsive copolymer solution and surface assemblies for biomedical applications, *Chemical Society Reviews*, 42 (2013) 7057-7071.
- [2] X. Zhao, P. Liu, Reduction-responsive core-shell-corona micelles based on triblock copolymers: novel synthetic strategy, characterization, and application as a tumor microenvironment-responsive drug delivery system, *ACS applied materials & interfaces*, 7 (2014) 166-174.
- [3] J. Zhuang, M.R. Gordon, J. Ventura, L. Li, S. Thayumanavan, Multi-stimuli responsive macromolecules and their assemblies, *Chemical Society Reviews*, 42 (2013) 7421-7435.
- [4] E. Wischerhoff, K. Uhlig, A. Lankenau, H.G. Börner, A. Laschewsky, C. Duschl, J.F. Lutz, Controlled cell adhesion on PEG-based switchable surfaces, *Angewandte Chemie International Edition*, 47 (2008) 5666-5668.
- [5] M.-H. Cha, J. Choi, B.G. Choi, K. Park, I.H. Kim, B. Jeong, D.K. Han, Synthesis and characterization of novel thermo-responsive F68 block copolymers with cell-adhesive RGD peptide, *Journal of colloid and interface science*, 360 (2011) 78-85.
- [6] A.-L. Kjøniksen, K. Zhu, R. Pamies, B. Nyström, Temperature-induced formation and contraction of micelle-like aggregates in aqueous solutions of thermoresponsive short-chain copolymers, *The Journal of Physical Chemistry B*, 112 (2008) 3294-3299.
- [7] R. Rodríguez Schmidt, R. Pamies, A.-L. Kjøniksen, K. Zhu, J.G. Hernández Cifre, B. Nyström, J. García de la Torre, Single-molecule behavior of asymmetric thermoresponsive amphiphilic copolymers in dilute solution, *The Journal of Physical Chemistry B*, 114 (2010) 8887-8893.
- [8] S.K. Filippov, A. Bogomolova, L. Kabarov, N. Velychkivska, L. Starovoytova, Z. Cernochova, S.E. Rogers, W.M. Lau, V.V. Khutoryanskiy, M.T. Cook, Internal Nanoparticle Structure of Temperature-Responsive Self-Assembled PNIPAM-b-PEG-b-PNIPAM Triblock Copolymers in Aqueous Solutions: NMR, SANS, and Light Scattering Studies, *Langmuir*, 32 (2016) 5314-5323.
- [9] C. Zhang, H. Peng, S. Puttick, J. Reid, S. Bernardi, D.J. Searles, A.K. Whittaker, Conformation of Hydrophobically Modified Thermoresponsive Poly (OEGMA-co-TFEA) across the LCST Revealed by NMR and Molecular Dynamics Studies, *Macromolecules*, 48 (2015) 3310-3317.
- [10] I. Cobo, M. Li, B.S. Sumerlin, S. Perrier, Smart hybrid materials by conjugation of responsive polymers to biomacromolecules, *Nature materials*, 14 (2015) 143-159.
- [11] Y. Kotsuchibashi, K. Yamamoto, T. Aoyagi, Assembly behavior of double thermo-responsive block copolymers with controlled response temperature in aqueous solution, *Journal of colloid and interface science*, 336 (2009) 67-72.
- [12] S. Luo, C. Ling, X. Hu, X. Liu, S. Chen, M. Han, J. Xia, Thermoresponsive unimolecular micelles with a hydrophobic dendritic core and a double hydrophilic block copolymer shell, *Journal of colloid and interface science*, 353 (2011) 76-82.

- [13] M.T. Calejo, N. Hasirci, S. Bagherifam, R. Lund, B. Nyström, Stimuli-Responsive Structures from Cationic Polymers for Biomedical Applications, *Cationic Polymers in Regenerative Medicine*, Royal Society of Chemistry 2014, pp. 149-177.
- [14] X. Wu, Z. Wang, D. Zhu, S. Zong, L. Yang, Y. Zhong, Y. Cui, pH and thermo dual-stimuli-responsive drug carrier based on mesoporous silica nanoparticles encapsulated in a copolymer–lipid bilayer, *ACS applied materials & interfaces*, 5 (2013) 10895-10903.
- [15] S. Nowag, R. Haag, pH-responsive micro-and nanocarrier systems, *Angewandte Chemie International Edition*, 53 (2014) 49-51.
- [16] L. Li, K. Raghupathi, C. Song, P. Prasad, S. Thayumanavan, Self-assembly of random copolymers, *Chemical Communications*, 50 (2014) 13417-13432.
- [17] E. Thormann, P.M. Claesson, O.G. Mouritsen, Tuning structural forces between silica surfaces by temperature-induced micellization of responsive block copolymers, *Physical Chemistry Chemical Physics*, 12 (2010) 10730-10735.
- [18] X. Song, J.-I. Zhu, Y. Wen, F. Zhao, Z.-X. Zhang, J. Li, Thermoresponsive supramolecular micellar drug delivery system based on star-linear pseudo-block polymer consisting of  $\beta$ -cyclodextrin-poly (N-isopropylacrylamide) and adamantyl-poly (ethylene glycol), *Journal of colloid and interface science*, 490 (2017) 372-379.
- [19] N.S. Rejinold, M. Muthunarayanan, V. Divyarani, P. Sreerekha, K. Chennazhi, S. Nair, H. Tamura, R. Jayakumar, Curcumin-loaded biocompatible thermoresponsive polymeric nanoparticles for cancer drug delivery, *Journal of colloid and interface science*, 360 (2011) 39-51.
- [20] S. Strandman, X. Zhu, Thermo-responsive block copolymers with multiple phase transition temperatures in aqueous solutions, *Progress In Polymer Science*, 42 (2015) 154-176.
- [21] D. Roy, W.L. Brooks, B.S. Sumerlin, New directions in thermoresponsive polymers, *Chemical Society Reviews*, 42 (2013) 7214-7243.
- [22] S. Hocine, M.-H. Li, Thermoresponsive self-assembled polymer colloids in water, *Soft Matter*, 9 (2013) 5839-5861.
- [23] I. Bischofberger, V. Trappe, New aspects in the phase behaviour of poly-N-isopropyl acrylamide: systematic temperature dependent shrinking of PNIPAM assemblies well beyond the LCST, *Scientific reports*, 5 (2015) 15520.
- [24] R. Pamies, K. Zhu, A.-L. Kjøniksen, B. Nyström, Thermal response of low molecular weight poly-(N-isopropylacrylamide) polymers in aqueous solution, *Polymer bulletin*, 62 (2009) 487-502.
- [25] S. Zajforoushan Moghaddam, E. Thormann, Hofmeister Effect on PNIPAM in Bulk and at an Interface: Surface Partitioning of Weakly Hydrated Anions, *Langmuir*, DOI (2017).
- [26] I. Bischofberger, D. Calzolari, P. De Los Rios, I. Jelezarov, V. Trappe, Hydrophobic hydration of poly-N-isopropyl acrylamide: a matter of the mean energetic state of water, *Scientific reports*, 4 (2014) 4377.
- [27] J.J.I. Ramos, S.E. Moya, Water content of hydrated polymer brushes measured by an in situ combination of a quartz crystal microbalance with dissipation monitoring and spectroscopic ellipsometry, *Macromolecular rapid communications*, 32 (2011) 1972-1978.
- [28] R. Pelton, Poly (N-isopropylacrylamide)(PNIPAM) is never hydrophobic, *Journal of colloid and interface science*, 348 (2010) 673-674.
- [29] P. Kujawa, V. Aseyev, H. Tenhu, F.M. Winnik, Temperature-sensitive properties of poly (N-isopropylacrylamide) mesoglobules formed in dilute aqueous solutions heated above their demixing point, *Macromolecules*, 39 (2006) 7686-7693.
- [30] A. Halperin, M. Kröger, F.M. Winnik, Poly (N-isopropylacrylamide) Phase Diagrams: Fifty Years of Research, *Angewandte Chemie International Edition*, 54 (2015) 15342-15367.
- [31] R. Umapathi, P.M. Reddy, A. Kumar, P. Venkatesu, C.-J. Chang, The biological stimuli for governing the phase transition temperature of the “smart” polymer PNIPAM in water, *Colloids and Surfaces B: Biointerfaces*, 135 (2015) 588-595.

- [32] Y. Zhan, M. Gonçalves, P. Yi, D. Capelo, Y. Zhang, J. Rodrigues, C. Liu, H. Tomás, Y. Li, P. He, Thermo/redox/pH-triple sensitive poly (N-isopropylacrylamide-co-acrylic acid) nanogels for anticancer drug delivery, *Journal of Materials Chemistry B*, 3 (2015) 4221-4230.
- [33] Y. Pan, H. Bao, N.G. Sahoo, T. Wu, L. Li, Water-soluble poly (N-isopropylacrylamide)-graphene sheets synthesized via click chemistry for drug delivery, *Advanced Functional Materials*, 21 (2011) 2754-2763.
- [34] B. Sung, C. Kim, M.-H. Kim, Biodegradable colloidal microgels with tunable thermosensitive volume phase transitions for controllable drug delivery, *Journal of colloid and interface science*, 450 (2015) 26-33.
- [35] S. Saeki, N. Kuwahara, M. Nakata, M. Kaneko, Phase separation of poly (ethylene glycol)-water-salt systems, *Polymer*, 18 (1977) 1027-1031.
- [36] H.S. Ashbaugh, M.E. Paulaitis, Monomer hydrophobicity as a mechanism for the LCST behavior of poly (ethylene oxide) in water, *Industrial & engineering chemistry research*, 45 (2006) 5531-5537.
- [37] T. Shikata, M. Okuzono, N. Sugimoto, Temperature-dependent hydration/dehydration behavior of poly (ethylene oxide) s in aqueous solution, *Macromolecules*, 46 (2013) 1956-1961.
- [38] A. Matsuyama, F. Tanaka, Theory of solvation-induced reentrant phase separation in polymer solutions, *Physical review letters*, 65 (1990) 341.
- [39] J. Shen, C. Chen, W. Fu, L. Shi, Z. Li, Conformation-specific self-assembly of thermo-responsive poly (ethylene glycol)-b-polypeptide diblock copolymer, *Langmuir*, 29 (2013) 6271-6278.
- [40] G.D. Smith, D. Bedrov, O. Borodin, Conformations and chain dimensions of poly (ethylene oxide) in aqueous solution: a molecular dynamics simulation study, *Journal of the American Chemical Society*, 122 (2000) 9548-9549.
- [41] J.M. Harris, *Poly (ethylene glycol) chemistry: biotechnical and biomedical applications*, Springer Science & Business Media 2013.
- [42] Y. Inada, M. Furukawa, H. Sasaki, Y. Kodera, M. Hiroto, H. Nishimura, A. Matsushima, Biomedical and biotechnological applications of PEG-and PM-modified proteins, *Trends in biotechnology*, 13 (1995) 86-91.
- [43] A. Sousa-Herves, R. Riguer, E. Fernandez-Megia, PEG-dendritic block copolymers for biomedical applications, *New Journal of Chemistry*, 36 (2012) 205-210.
- [44] A. Dedinaite, E. Thormann, G. Olanya, P.M. Claesson, B. Nyström, A.-L. Kjøniksen, K. Zhu, Friction in aqueous media tuned by temperature-responsive polymer layers, *Soft Matter*, 6 (2010) 2489-2498.
- [45] A. Shovskiy, S. Knoch, A. Dedinaite, K. Zhu, A.-L. Kjøniksen, B. Nyström, P. Linse, P.M. Claesson, Cationic Poly (N-isopropylacrylamide) Block Copolymer Adsorption Investigated by Dual Polarization Interferometry and Lattice Mean-Field Theory, *Langmuir*, 28 (2012) 14028-14038.
- [46] J. An, A. Dédinaite, F.M. Winnik, X.-P. Qiu, P.M. Claesson, Temperature-dependent adsorption and adsorption hysteresis of a thermoresponsive diblock copolymer, *Langmuir*, 30 (2014) 4333-4341.
- [47] G. Olanya, E. Thormann, I. Varga, R. Makuška, P.M. Claesson, Protein interactions with bottle-brush polymer layers: Effect of side chain and charge density ratio probed by QCM-D and AFM, *Journal of colloid and interface science*, 349 (2010) 265-274.
- [48] X. Liu, A. Dedinaite, M. Rutland, E. Thormann, C. Visnevskij, R. Makuska, P.M. Claesson, Electrostatically anchored branched brush layers, *Langmuir*, 28 (2012) 15537-15547.
- [49] X. Liu, E. Thormann, A. Dedinaite, M. Rutland, C. Visnevskij, R. Makuska, P.M. Claesson, Low friction and high load bearing capacity layers formed by cationic-block-non-ionic bottle-brush copolymers in aqueous media, *Soft Matter*, 9 (2013) 5361-5371.
- [50] S. Bayati, K. Zhu, L.T. Trinh, A.-L. Kjøniksen, B. Nyström, Effects of temperature and salt addition on the association behavior of charged amphiphilic diblock copolymers in aqueous solution, *The Journal of Physical Chemistry B*, 116 (2012) 11386-11395.
- [51] M.A. Behrens, M. Lopez, A.-L. Kjøniksen, K. Zhu, B. Nyström, J.S. Pedersen, Structure and interactions of charged triblock copolymers studied by small-angle X-ray scattering: Dependence on temperature and charge screening, *Langmuir*, 28 (2011) 1105-1114.
- [52] J.E. Sader, J.W. Chon, P. Mulvaney, Calibration of rectangular atomic force microscope cantilevers, *Review of Scientific Instruments*, 70 (1999) 3967-3969.

- [53] W.A. Ducker, T.J. Senden, R.M. Pashley, Direct measurement of colloidal forces using an atomic force microscope, *nature*, 353 (1991) 239.
- [54] G. Dunér, E. Thormann, A. Dédinaité, Quartz Crystal Microbalance with Dissipation (QCM-D) studies of the viscoelastic response from a continuously growing grafted polyelectrolyte layer, *Journal of colloid and interface science*, 408 (2013) 229-234.
- [55] I. Reviakine, D. Johannsmann, R.P. Richter, *Hearing what you cannot see and visualizing what you hear: interpreting quartz crystal microbalance data from solvated interfaces*, ACS Publications, 2011.
- [56] F. Höök, B. Kasemo, T. Nylander, C. Fant, K. Sott, H. Elwing, Variations in coupled water, viscoelastic properties, and film thickness of a Mefp-1 protein film during adsorption and cross-linking: a quartz crystal microbalance with dissipation monitoring, ellipsometry, and surface plasmon resonance study, *Analytical chemistry*, 73 (2001) 5796-5804.
- [57] H. Xu, F. Yan, E.E. Monson, R. Kopelman, Room-temperature preparation and characterization of poly (ethylene glycol)-coated silica nanoparticles for biomedical applications, *Journal of Biomedical Materials Research Part A*, 66 (2003) 870-879.
- [58] M. Schönhoff, A. Larsson, P.B. Welzel, D. Kuckling, Thermoreversible polymers adsorbed to colloidal silica: a <sup>1</sup>H NMR and DSC study of the phase transition in confined geometry, *The Journal of Physical Chemistry B*, 106 (2002) 7800-7808.
- [59] G. Sauerbrey, Verwendung von Schwingquarzen zur Wägung dünner Schichten und zur Mikrowägung, *Zeitschrift für physik*, 155 (1959) 206-222.
- [60] M.R. Nejadnik, A.L. Olsson, P.K. Sharma, H.C. van der Mei, W. Norde, H.J. Busscher, Adsorption of pluronic F-127 on surfaces with different hydrophobicities probed by quartz crystal microbalance with dissipation, *Langmuir*, 25 (2009) 6245-6249.
- [61] G. Liu, H. Cheng, L. Yan, G. Zhang, Study of the Kinetics of the Pancake-to-Brush Transition of Poly (N-isopropylacrylamide) Chains, *The Journal of Physical Chemistry B*, 109 (2005) 22603-22607.
- [62] B.D. Vogt, E.K. Lin, W.-I. Wu, C.C. White, Effect of film thickness on the validity of the Sauerbrey equation for hydrated polyelectrolyte films, *The Journal of Physical Chemistry B*, 108 (2004) 12685-12690.
- [63] T.P. McNamara, C.F. Blanford, A sensitivity metric and software to guide the analysis of soft films measured by a quartz crystal microbalance, *Analyst*, 141 (2016) 2911-2919.
- [64] A.K. Dutta, G. Belfort, Adsorbed gels versus brushes: viscoelastic differences, *Langmuir*, 23 (2007) 3088-3094.
- [65] D. Johannsmann, I. Reviakine, E. Rojas, M. Gallego, Effect of sample heterogeneity on the interpretation of QCM (-D) data: comparison of combined quartz crystal microbalance/atomic force microscopy measurements with finite element method modeling, *Analytical chemistry*, 80 (2008) 8891-8899.
- [66] E. Rojas, M. Gallego, I. Reviakine, Effect of sample heterogeneity on the interpretation of quartz crystal microbalance data: impurity effects, *Analytical chemistry*, 80 (2008) 8982-8990.



**Supporting information for**

**Thermo-responsive Diblock and Triblock Cationic Copolymers at the**

**Silica/Aqueous Interface: A QCM-D and AFM study**

Saeed Zajforoushan Moghaddam <sup>a</sup>, Kaizheng Zhu <sup>b</sup>, Bo Nyström <sup>b</sup> and Esben  
Thormann <sup>a\*</sup>

<sup>a</sup> *Department of Chemistry, Technical University of Denmark, 2800 Kgs. Lyngby,*  
*Denmark*

<sup>b</sup> *Department of Chemistry, University of Oslo, Blindern, P.O. Box 1033, Blindern,*  
*N-0315 Oslo, Norway, Norway*

---

\* To whom correspondence should be addressed. E-mail: [esth@kemi.dtu.dk](mailto:esth@kemi.dtu.dk).

Telephone: (+45) 4525 2439

## S1. Additional DLS data

As explained, the diblock copolymer solution represents a bimodal hydrodynamic size distribution at 20 °C, where the first peak corresponds to the unimers and the other indicates the intermicellar complexes. However, regarding the population of the two species, the unimers are entirely dominant. This can be seen from the Number PSD figure, where only a unimodal size distribution corresponding to the unimers is found. For the triblock copolymer, it was explained that at 40 °C a bimodal size distribution is obtained, meaning that some intermicellar complexes form in the solution. However, it can be seen that still the unimers are dominant in number.

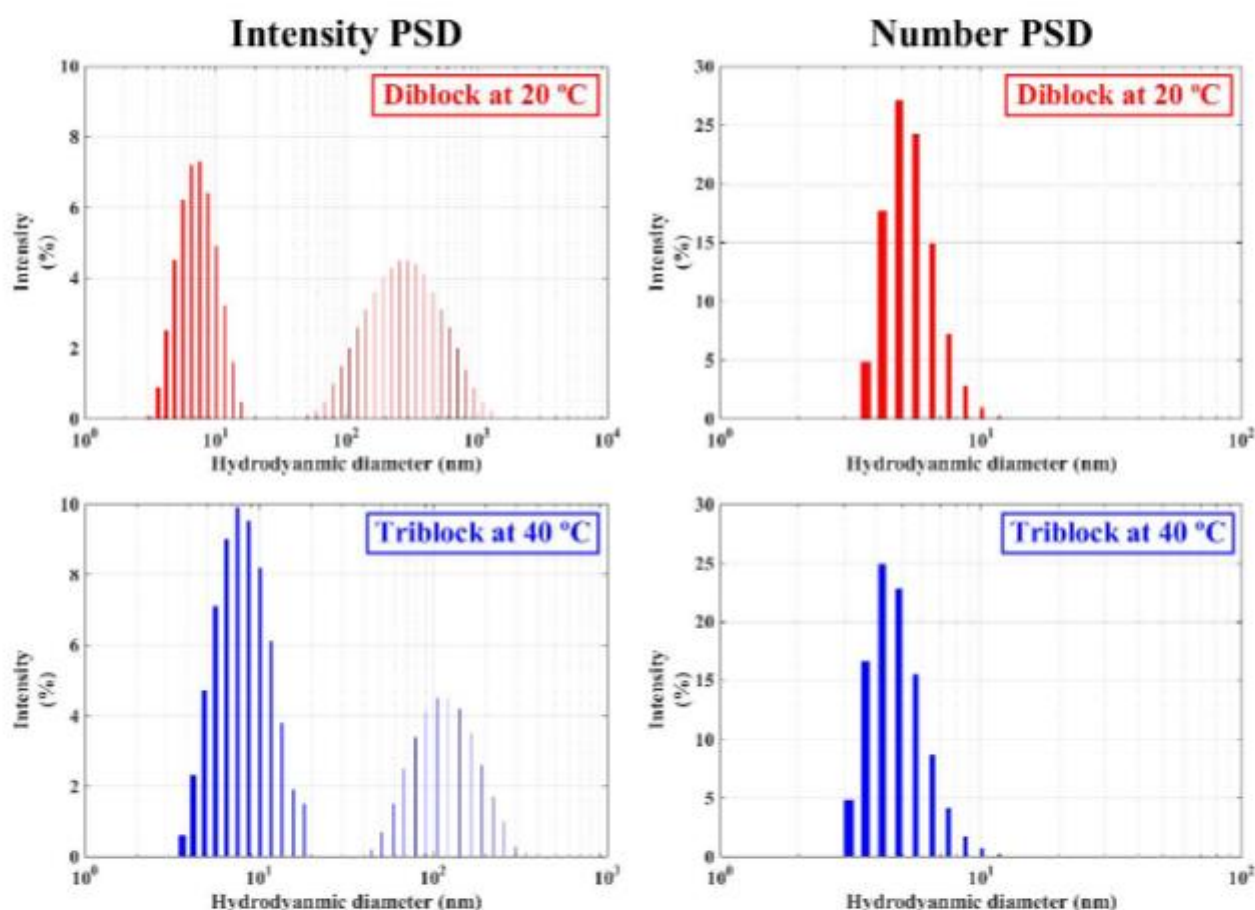


**Figure S1** Intensity PSD and Number PSD hydrodynamic size distribution profiles of (top row) the diblock copolymer at 20 °C, and (bottom row) the triblock copolymer at 40 °C

## S2. Viscoelastic modeling of the QCM-D data:

To assess the properties of the copolymer layers adsorbed on the silica sensor, the Sauerbrey equation and viscoelastic Voigt modeling were employed, using the standard software of the instrument (Q-Sense Dfind beta version, Biolin Scientific AB). By using the Sauerbrey equation, one can estimate the amount of adsorbed mass on the sensor. The attached mass onto the sensor is proportional to the frequency shift according to the following equation; where  $n$  is the harmonic number, and  $C$  a proportional constant that depends on fundamental frequency, thickness and density of the quartz crystal.[1]

$$\Delta m = -nC\Delta f$$

It should be considered that the Sauerbrey estimation is only valid if the added mass is small compared to the crystal mass, rigidly adsorbed with no slip or deformation imposed by the oscillating surface, and evenly distributed. With respect to the adsorption curve, the Sauerbrey estimation can be used when there are no significant dissipation shifts ( $\Delta D < 1$ ) and frequency shifts do not spread between the harmonics (no overtone-dependence).

For viscoelastic films, the linearity between  $\Delta f$  and  $\Delta m$  no longer holds and the Sauerbrey equation underestimates the coupled mass. This can be seen from adsorption curves that represent significant dissipation shifts ( $\Delta D > 1$ ) and well-separated frequency shifts for the different harmonics (overtone-dependence). According to the viscoelastic Voigt modeling, the adhered film is represented by a layer of homogenous thickness and density with elastic and viscous components.[2] Accordingly, the frequency and dissipation shifts can be found from the imaginary and real parts of the  $\beta$  function:

$$\Delta f = \frac{Im(\beta)}{2\pi t\rho}$$

$$\Delta D = \frac{Re(\beta)}{\pi f t \rho}$$

Where  $t$  and  $\rho$  are thickness and density of the quartz crystal, respectively. The  $\beta$  function represents shear viscosity  $\eta$  and shear elasticity  $\mu$ , and in the case of a single viscoelastic film (1) covered with a Newtonian liquid (2) can be obtained from the following equation[3]:

$$\beta = \frac{\xi_1 \omega \eta_1 - i \mu_1}{\omega} \frac{1 - \alpha^2 \xi_1 h_1}{1 + \alpha^2 \xi_1 h_1}$$

$$\omega = 2\pi f$$

$$\alpha = \frac{\frac{\xi_1 \omega \eta_1 - i \mu_1}{\xi_2 \omega \eta_2} + 1}{\frac{\xi_1 \omega \eta_1 - i \mu_1}{\xi_2 \omega \eta_2} - 1}$$

$$\xi_1 = \sqrt{-\frac{\omega^2 \rho_1}{\mu_1 + i \omega \eta_1}}$$

$$\xi_2 = \sqrt{i \frac{\omega \rho_2}{\eta_2}}$$

By fitting the viscoelastic Voigt model to the measured  $\Delta f$  and  $\Delta D$  data, one can obtain information on the density ( $\rho_1$ ), thickness ( $h_1$ ), shear viscosity ( $\eta_1$ ) and elasticity ( $\mu_1$ ) of the adhered layer. It should be considered that the film viscosity and density cannot be obtained together; thus, typically the density of the layer is independently determined or assumed. Using the instrument software, one has to provide densities of the solvent and polymer layer. Typically, the software suggests two solutions, where one would be a thin and rigid layer, and the other is a thicker and soft layer. The solution with a better fitting quality is used in this work. Density and viscosity of water at 20 °C was used for the solvent. An estimated average polymer layer density of 1050 kg/m<sup>3</sup> was used for fitting the data of

both diblock and triblock copolymers. In each case, the effect of changing the layer density from 1000 to 1200 kg/m<sup>3</sup>[4-6] on the obtained layer thickness and viscoelastic data was checked, but no significant effect on the fitting results was found.

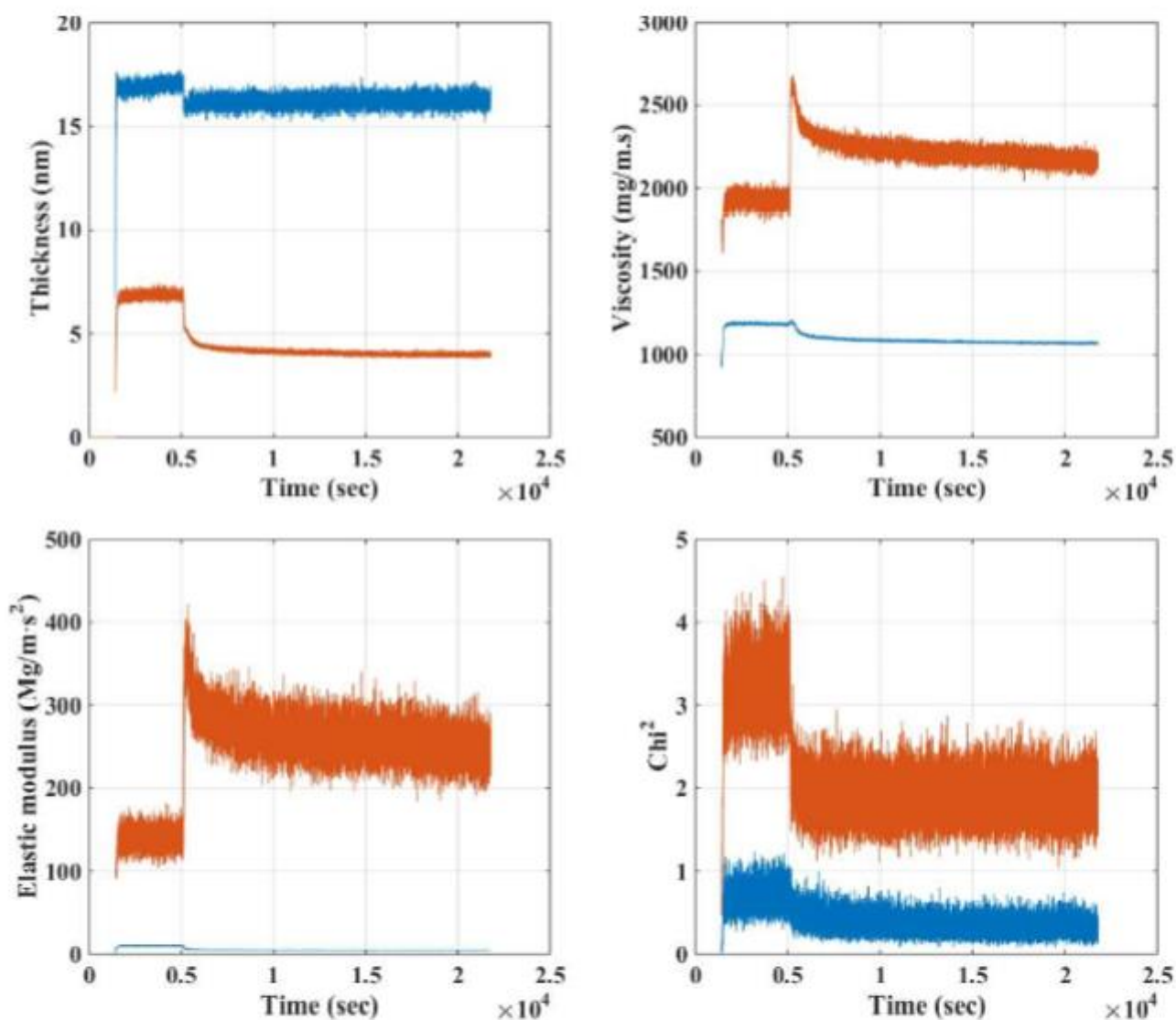


**Figure S2** Viscoelastic modelling data of the diblock copolymer

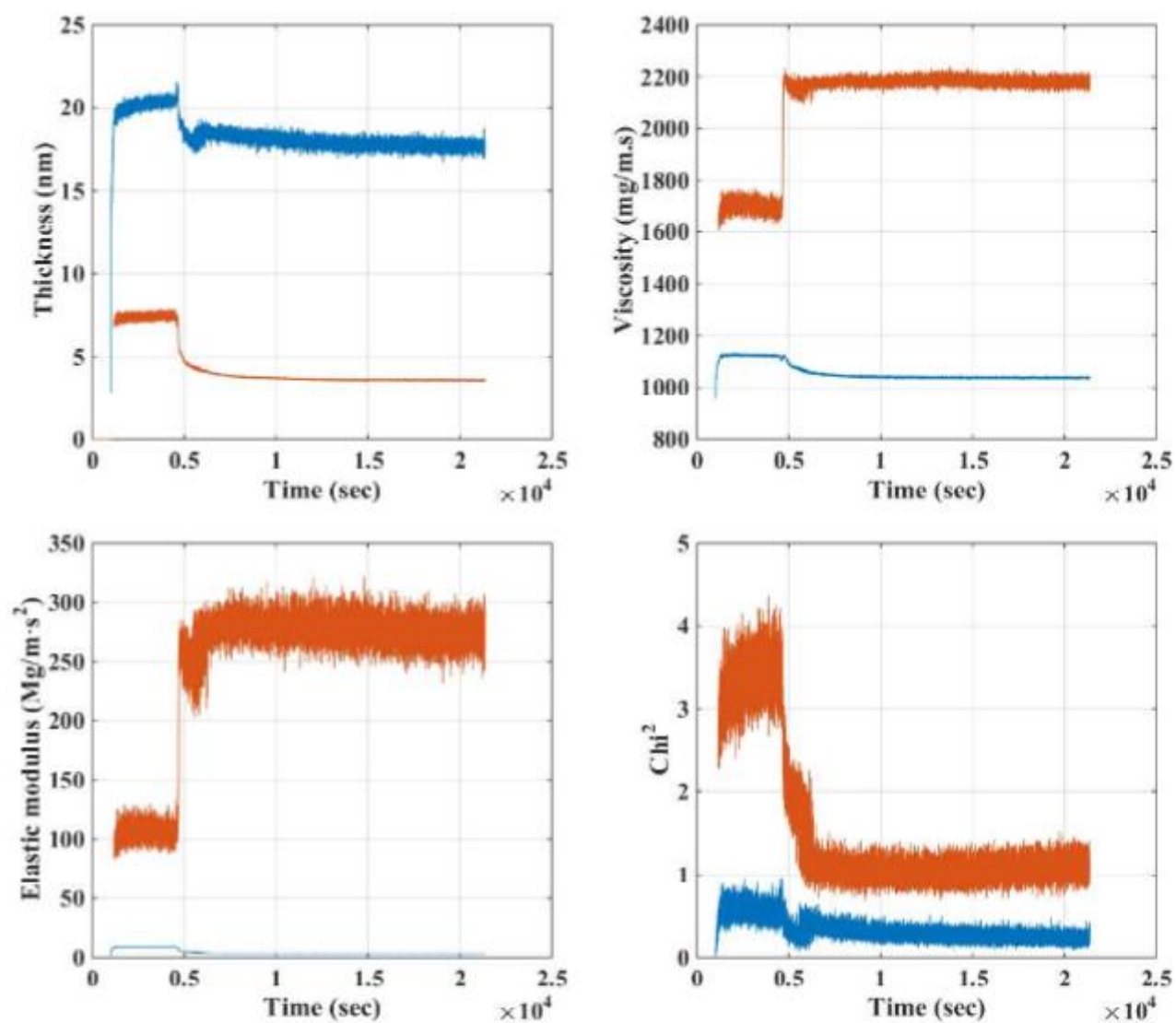


**Figure S3** Viscoelastic modelling data of the triblock copolymer

### S3. AFM images and force curves

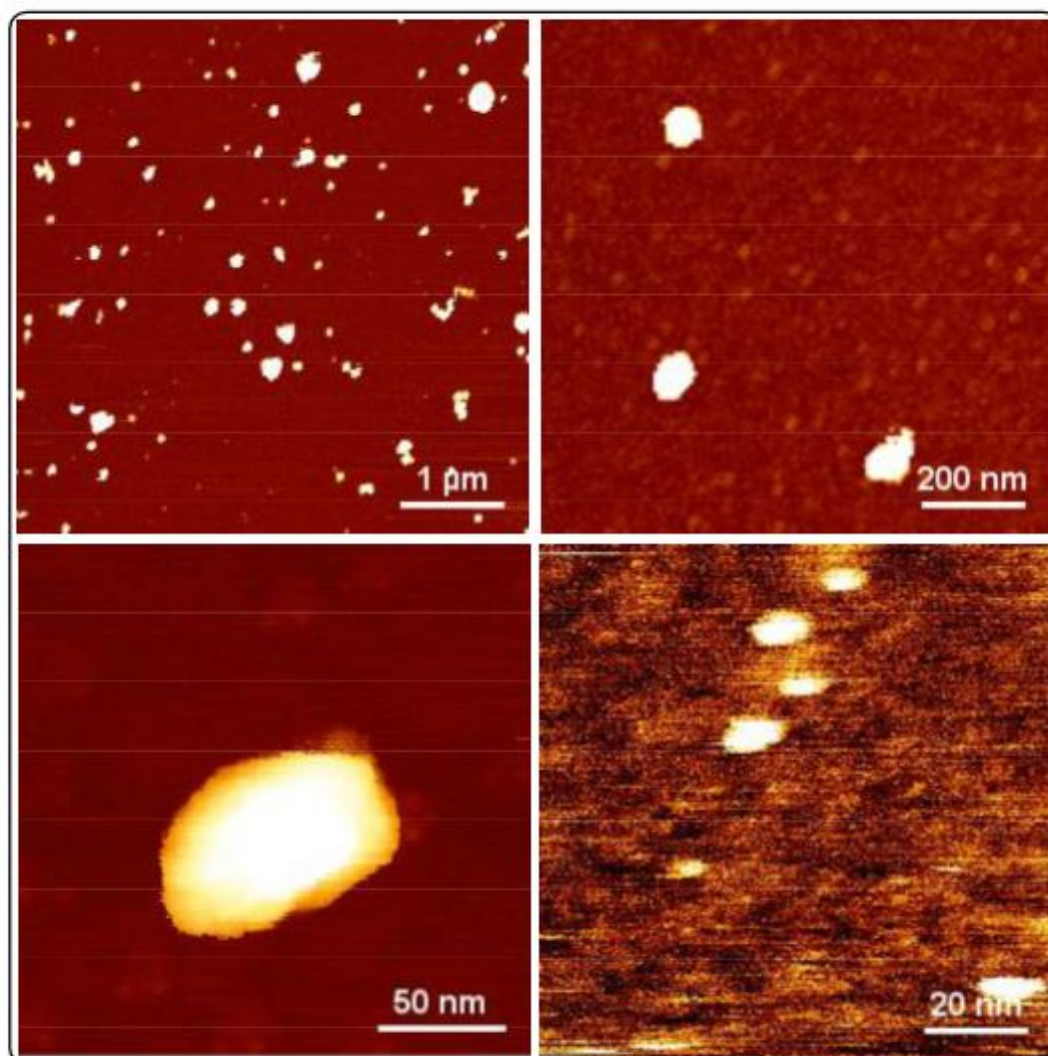
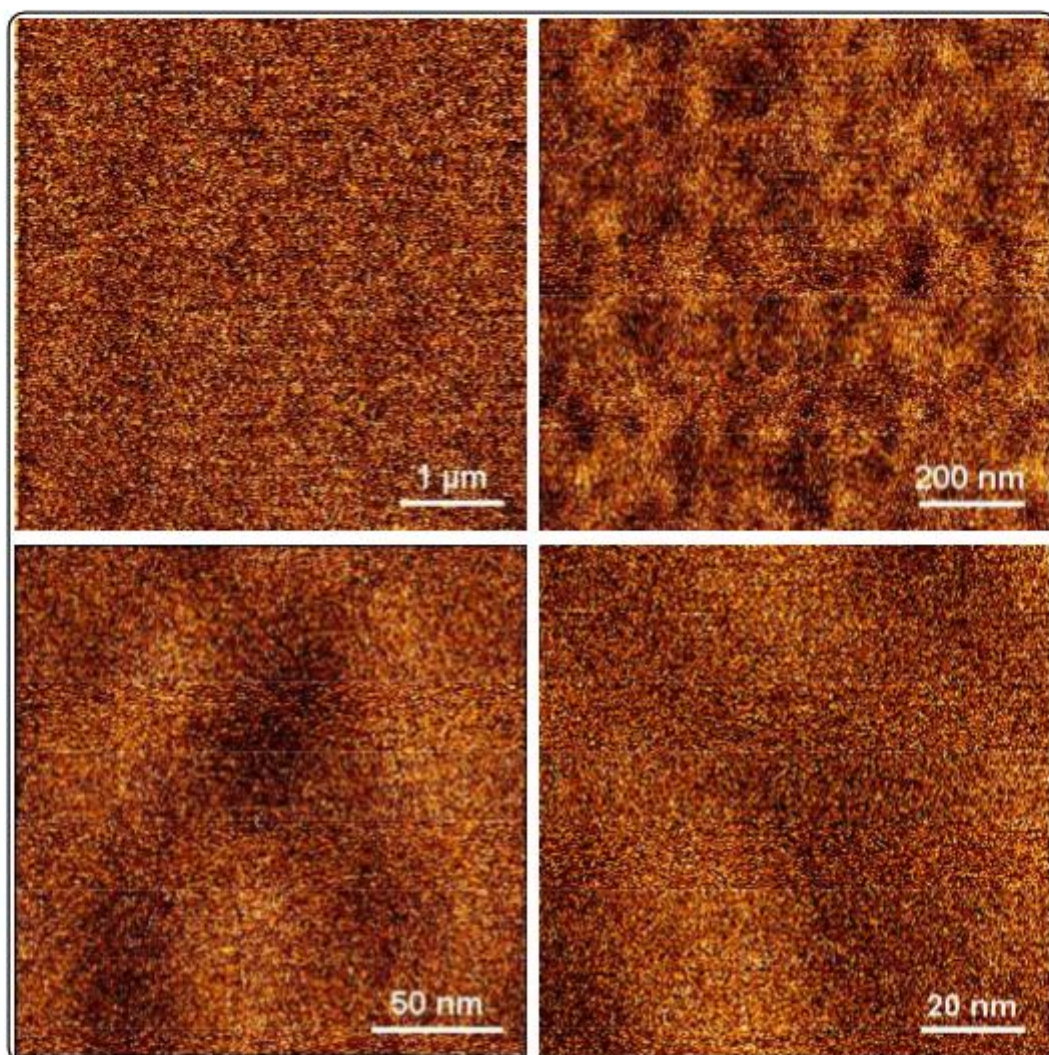
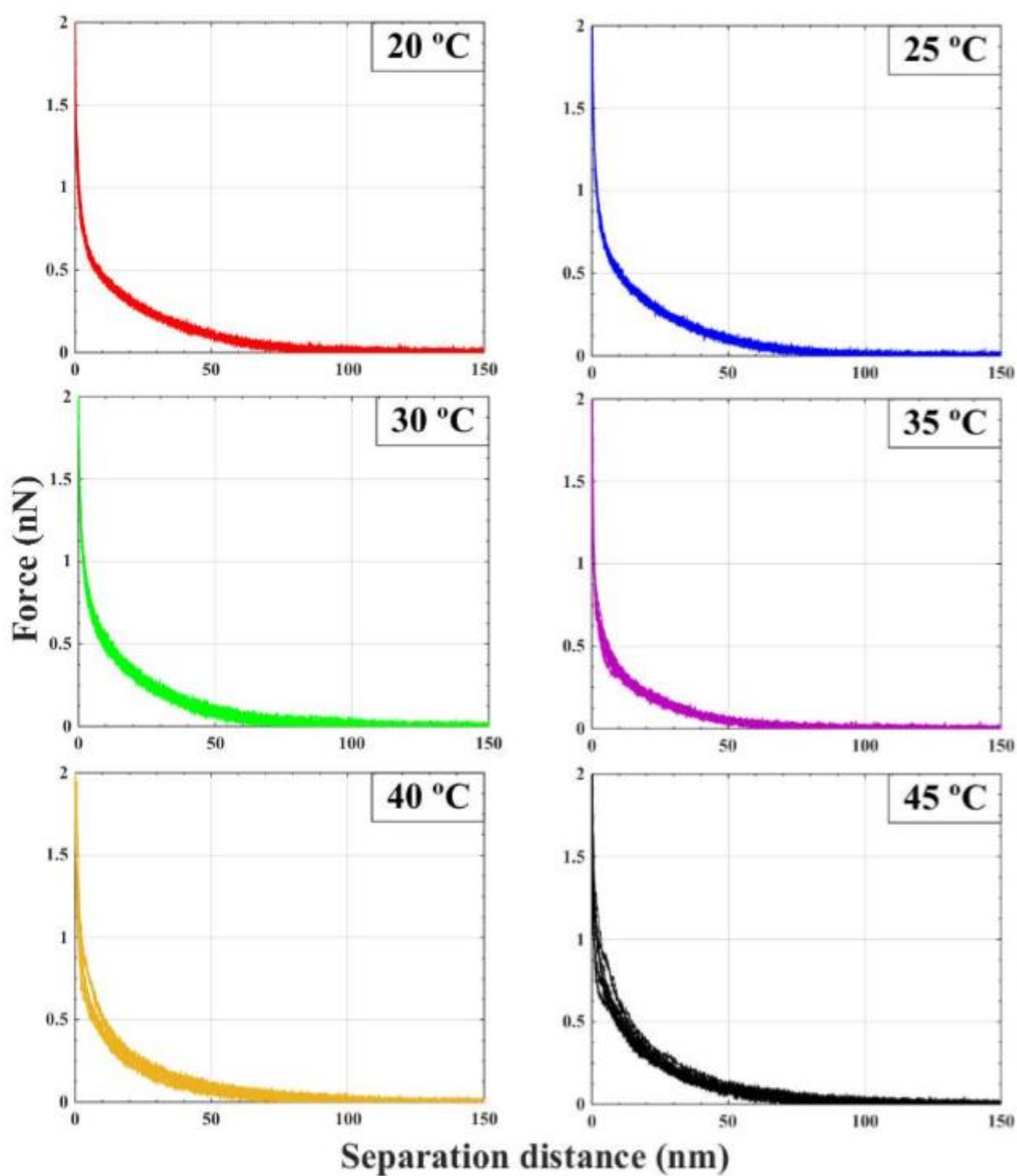


Figure S4 Additional AFM images of diblock copolymer





**Figure S5** Additional AFM images of triblock copolymer



**Figure S6** AFM force-distance curves between diblock-covered silica surfaces at various temperatures; each figure includes 10 force curves.

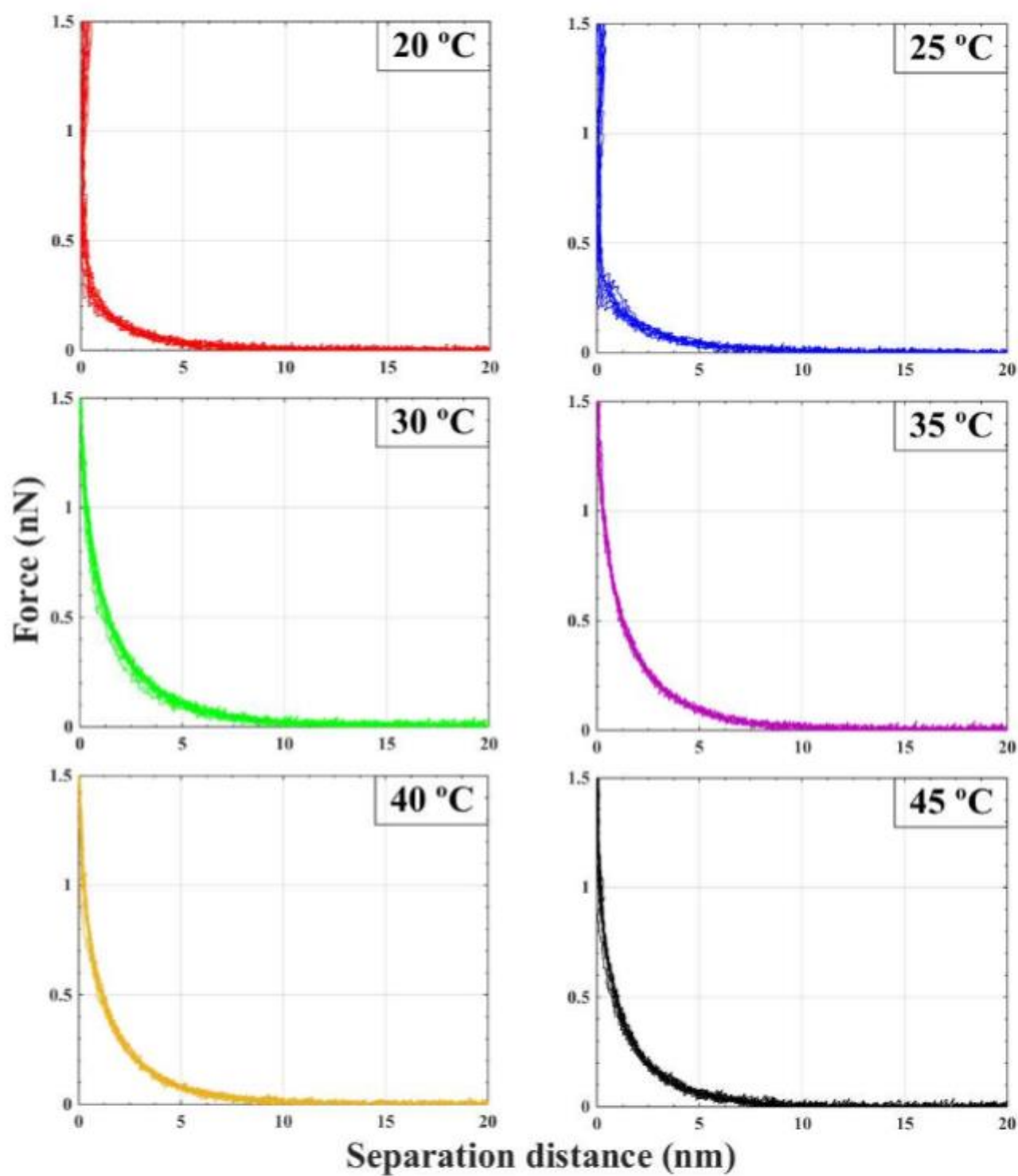


**Figure S7** AFM force-distance curves between triblock-covered silica surfaces at various temperatures; each figure includes 10 force curves.

## REFERENCES

- [1] G. Sauerbrey, Verwendung von Schwingquarzen zur Wägung dünner Schichten und zur Mikrowägung, *Zeitschrift für physik*, 155 (1959) 206-222.
- [2] G. Dunér, E. Thormann, A. Dédinaïté, Quartz Crystal Microbalance with Dissipation (QCM-D) studies of the viscoelastic response from a continuously growing grafted polyelectrolyte layer, *Journal of colloid and interface science*, 408 (2013) 229-234.
- [3] M. Rodahl, F. Höök, C. Fredriksson, C.A. Keller, A. Krozer, P. Brzezinski, M. Voinova, B. Kasemo, Simultaneous frequency and dissipation factor QCM measurements of biomolecular adsorption and cell adhesion, *Faraday Discussions*, 107 (1997) 229-246.
- [4] J. Malmström, H. Agheli, P. Kingshott, D.S. Sutherland, Viscoelastic modeling of highly hydrated laminin layers at homogeneous and nanostructured surfaces: quantification of protein layer properties using QCM-D and SPR, *Langmuir*, 23 (2007) 9760-9768.
- [5] S.M. Notley, M. Eriksson, L. Wågberg, Visco-elastic and adhesive properties of adsorbed polyelectrolyte multilayers determined in situ with QCM-D and AFM measurements, *Journal of colloid and interface science*, 292 (2005) 29-37.
- [6] J. Iruthayaraj, G. Olanya, P.M. Claesson, Viscoelastic Properties of Adsorbed Bottle-brush Polymer Layers Studied by Quartz Crystal Microbalance • Dissipation Measurements, *The Journal of Physical Chemistry C*, 112 (2008) 15028-15036.

## **PAPER VI**

# **Hofmeister Effect in Aqueous Polymer Solutions: Where We Are and Where We Should Go**

Saeed Zajforoushan Moghaddam and Esben Thormann\*

*Department of Chemistry, Technical University of Denmark, 2800 Kgs. Lyngby,  
Denmark*

---

\* To whom correspondence should be addressed. E-mail: [esth@kemi.dtu.dk](mailto:esth@kemi.dtu.dk).

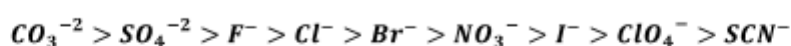
Telephone: (+45) 4525 2439

**Abstract.** Specific ion effects in aqueous polymer solutions has been under active investigation since the pioneering report by Franz Hofmeister. The current state-of-the-art research is mainly concerned with understanding the mechanisms and molecular origins of ion-specific effects on macromolecular solution stability, which is of twofold importance. First, it can bolster our knowledge of biological systems where the proper functioning depends on the presence of ions and their interaction with biomacromolecules. Moreover, getting to know how various ions affect the polymer stability, we can more effectively tune the behavior of stimuli-responsive polymers required for multiple applications. In this review paper, we first present the current opinion on the sources of ion-specificity and enumerate the previously reported mechanisms that have gained attention in the literature. Next, we will address the future research issues and bring up some less explored areas of study where further scrutiny is necessary.



## 1. Introduction to the Hofmeister Effect

It has been over a century since Franz Hofmeister, the Czech protein scientist, reported that various salts could differently affect the stability of the egg yolk protein in water.[1, 2] He proposed a ranking for anions and cations with respect to their ability to precipitate the investigated protein, which is now widely recognized as the *Hofmeister series*. The work by Hofmeister was then followed with another appreciable report by Green[3], which provided an empirical equation to quantify the effect of various salts on the proteins solubility in water, and accordingly obtained *salting-out* constants of different salts. It was soon revealed that the Hofmeister series is much more than a particular observation, as the *ion-specific* effects on the solubility of various molecules including polymers in water were ascertained[4-10], as well as on numerous physiochemical phenomenon in the aqueous and even non-aqueous medium such as bubble coalescence[11, 12] and enzymatic activity[13, 14]. In the proposed Hofmeister series (shown below), the anions to the right enhance the solubility of the polymers in water, an effect that is referred to as the *salting-in* effect. On the other hand, the more we go to the left in the series the ions become stronger in decreasing the polymer solubility and have a *salting-out* effect.



Although the Hofmeister series itself has been settled as a robust observation, the debate on the exact mechanisms of ion-specificity is still ongoing. In the early attempts, researchers attributed this effect merely to the specific interactions between ions and water molecules, and the following impact on the hydrogen-bonding network of water. By that time, it was already affirmed that ions in water can no more be considered as simple charged points, because the ions size, shape, and type (cation or anion) could strongly affect the ionic hydration strength and the properties of water.[15-20] To address the ion-specificity on water structure, the ions have been classified as being

*kosmotropic* or *chaotropic*, with respect to their hydration power and their effect on the adjacent water molecules structure.[21-26] The former term represents the behavior of the ions with small size and high charge density, which are strongly hydrated and make their adjacent water molecules more ordered compared to bulk water, thus are also known as *water structure makers*. The latter term describes the effect by large bulky ions with low surface charge density and with a subsequent weak hydration power, which indeed disrupt the water structure and promote *disorderness* in the hydrogen-bonding network, so are referred to as *water structure breakers*. Numerous validations for the specific ion effects on water structure have been proposed, such as the Jones-Dole viscosity coefficients[18], the electrochemical mobility of ions[27], activity coefficients[13, 28] and ion pairing.[29, 30] As one of the most important demonstrations of ion-specificity in water, Collins proposed the so-called *volcano plot* (Figure 1) in which the tendency of different anions and cations to form contact pairs in water is assessed.[24] According to this empirical theory, kosmotropes favorably pair with kosmotropes and chaotropes prefer association with chaotropes. Accordingly, a kosmotrope plus a chaotrope salt readily dissociates in water owing to the stronger kosmotrope-water interaction in solution compared to the kosmotrope-chaotrope interaction in the salt crystal. On the other hand, two kosmotropes in paired state tend to stick to each other in the crystal, thus dissociating the strong kosmotrope-kosmotrope interaction costs energy. Moreover, the relatively stronger water-water interactions will keep the chaotrope and chaotrope ion pairs together, thus dissociation is energy-costly due to strong water-water interactions.

Even though classification of ions into water structure makers and breakers could render a rather general justification for the Hofmeister series, it surely fails to enclose all facets of the Hofmeister effect, e.g. reversal of the Hofmeister series in some systems.[31-34] Such observations have revealed that besides specificity in interaction of ions with their hydration water, the ions have specific interactions with surfaces.[35-37] During recent years, it has been confirmed that

chaotropic ions preferentially accumulate at the non-polar surfaces such as the air/water interfacial region, an ion-specific effect that has been attributed to the polarizability of the ions and the contribution of dispersion forces, which were totally neglected in the classic electrostatic models.[37, 38]

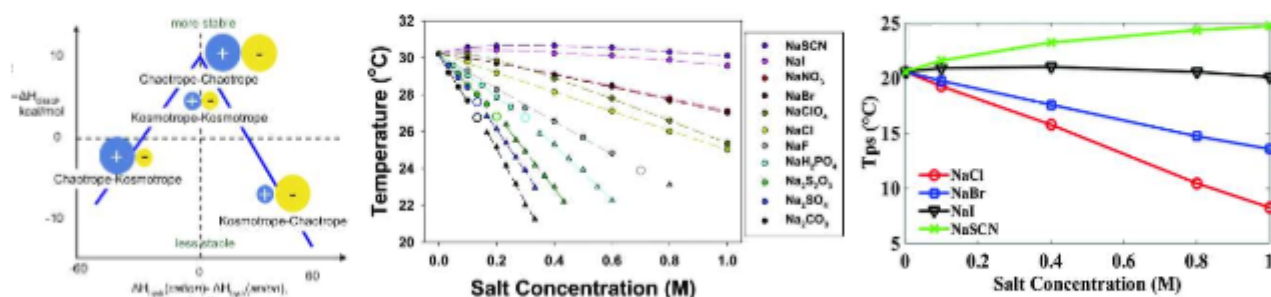


**Figure 1** (Left) schematic illustration of the Volcano plot, i.e., the standard enthalpy of solution of salts vs the difference between the enthalpies of hydration of the constituent gaseous anion and cation. The enthalpy of solution of chaotrope–chaotrope and kosmotrope–kosmotrope salts is positive, but the salt with a kosmotropic and a chaotropic ion have a negative enthalpy of solution (Reproduced from [24] with permission from Elsevier). (Middle) the Hofmeister series on the phase separation temperature of PNIPAM (Reproduced with permission from [39], Copyright (2017) American Chemical Society). (Right) the Hofmeister series on the phase separation temperature of PPO.

When it comes to the ion specific effect on macromolecular stability in water, one has to be aware that we are dealing with a mixture of water molecules, polymer chains, and ions, where each component can effectively interact with the others. Therefore, it seems rather naive to expect such a system to be solely governed by the ions hydration and their corresponding effects on the water structure. This has led to the recent generation of the studies in which one should inevitably take into account the interplay between all the components of the system, i.e., ion-water, ion-polymer, ion-ion, and polymer-water interactions. The dissection is yet not complete, as there is still much more complication. The polymer itself is basically composed of polar groups and apolar surfaces, each with distinctive interactions with water and hydration layer properties.[40, 41] Accordingly,

the way the ions interact with the polymer chain and its hydration water can be quite different, depending on the polymer interface properties, i.e., hydrophilic or hydrophobic, charged or uncharged. Dissecting the polymer into pieces, studying the effect of ions on each, now the final challenge is to combine all these to find out the overall effect on polymer stability, which indeed leads to distinguishable effects by the Hofmeister salts on the polymer stability as exemplified in Figure 1 for PNIPAM and PPO:

- Linear salting-out effect, e.g., NaF on PNIPAM and PPO
- Non-linear salting-out effect, e.g., NaBr on PNIPAM
- Salting-in effect with a turnover at low concentrations, e.g., NaI on PNIPAM and PPO
- Salting-in effect with no clear turnover: NaSCN on PPO

Based on the above narration, what we aim for in this review paper is twofold. The first objective is to enumerate the previously reported mechanisms for the ion-specificity in polymer solutions, and to underline the agreements and contradictions between them. We begin with the triple mechanisms suggested by Cremer and coworkers, which can be considered as a framework for the other theories as well. Then, the *solute partitioning model* suggested by Pegram and Record will be propounded, which is a quantification of the accumulation (exclusion) of different ions at (from) non-polar and polar surfaces. To understand the possible mechanisms that can drive the ions to surfaces, the *law of matching water affinities* by Collins and the theory of dispersion interactions by Ninham and coworkers will be introduced. Finally, the recently suggested thermodynamic description of the Hofmeister salts by Dzubiella and Heyda will be reviewed. After being acquainted with the present knowledge about the ion-specificity mechanisms, we will point out some of the missing pieces of the Hofmeister puzzle, which in our opinion should be particularly investigated in the future studies.

## 2. The Mechanisms

**2.1. The Triple Effects: Polarization, Surface Tension and Binding:** Cremer and coworkers have published a series of papers going back to 2004[42, 43], in which they investigated the specific ion effects on PNIPAM[44-48], lysozyme[49], elastin-like peptides[50, 51], negatively charged hydrophilic surfaces[52], proteins stability[53-56], and water structure[57, 58]. In their initial work[44], they have proposed three principal mechanisms through which different anions can affect the stability of PNIPAM (as well as other macromolecules), which are depicted in Figure 2.

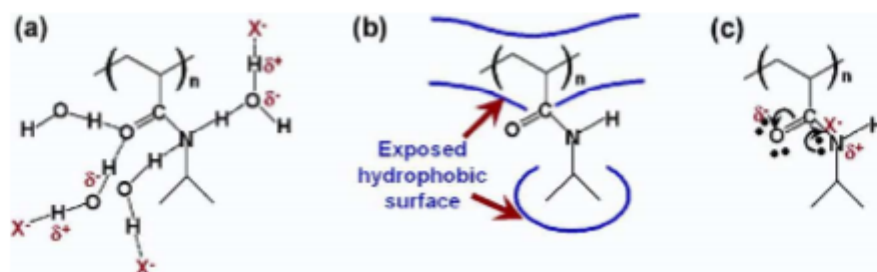


**Figure 2** Anions interaction with PNIPAM hydration water and PNIPAM surface. (a) Polarization effect through which the anions interact with the polymer hydration shell (b) The surface tension effect through which the anions affect the hydrophobic hydration (c) Direct binding of the anions to the polymer chain. (Reproduced with permission from [44] Copyright (2017) American Chemical Society).

The first suggested mechanism was the polarization of the water molecules that are hydrogen bonded to the amide groups of PNIPAM. Through this mechanism, strongly hydrated anions can interact with the hydration shell of the polymer, which indeed can facilitate dehydration of the amide groups and a salting-out effect is found. As argued, the anions power to polarize the water molecules -the salting-out power- is in direct correlation with their entropy of hydration. In other words, the higher the hydration capacity the stronger the polarization effect will be. With respect to the second mechanism, anions could interfere with the hydrophobic hydration of the polymer by increasing the surface tension of the cavity surrounding the backbone and the isopropyl side chains.

This could make the hydrophobic hydration more entropically costly and thus destabilize the polymer in solution. Such a destabilization mechanism was considered for all the anions in the beginning; nevertheless, the authors in their later publication[46] and another relevant report[59] have claimed that depending on the polymer surface chemistry, weakly hydrated anions might decrease the surface tension and favor the hydrophobic polymer hydration through this mechanism. Finally, the weakly hydrated anions can directly bind to the amide groups of PNIPAM to stabilize the polymer. The third mechanism was further discussed by the authors [48, 51, 60], suggesting how and where the ions could bind to the PNIPAM chain. Accordingly, while in their initial report the authors mainly described binding of anions to the amide moiety, later they have proposed other possible binding sites where the atoms bear a partial positive charge due to a relatively large dipole moment. In an attempt to quantify all these effects together on the phase separation temperature of the PNIPAM, the following empirical equation (Figure 1) was suggested:

$$T = T_0 + c[M] + \frac{B_{max}K_A[M]}{1 + K_A[M]}$$

Where  $T$  is the phase separation temperature of PNIPAM in the saline solution,  $T_0$  is the phase separation temperature in salt-free solution, and  $[M]$  is the molarity of the salt. The parameter  $c$  is the slope of the linear part (Figure 1), which represents the strength of the first and second mechanisms, so accounts for the salting-out power. For anions with very strong hydration capacity such as sulfate, two slopes were found at low and high salt concentrations, where the latter was mainly attributed to the surface tension effect. The last term on the right, which is reminiscent of the Langmuir isotherm binding, is responsible for the non-linear salting-in effect by the weakly hydrated anions.  $K_A$  is the binding constant of the anion to the polymer, and  $B_{max}$  is the maximum increase in the phase separation temperature (saturation point).

**2.2. Solute partitioning model:** Pegram and record have discussed the Hofmeister effect of salts (and osmolytes such as urea) on the air/water surface tension[61, 62] together with polymers and proteins stability[63-68], in terms of the *partition coefficient* of the ions at the non-polar and polar surfaces and the corresponding change in the *solvent-accessible surface area (ASA)* of the polymer chains. In the initial report[61], the effect of different salts on the surface tension of water was investigated, and accordingly preferential accumulation (exclusion) of the ions at (from) the air/water hydrophobic interfacial region was inferred, in accordance with the *direct* Hofmeister series. This means that weakly hydrated anions are preferentially accumulated at the air-water interface, while the strongly anions are effectively repelled from the interfacial region. To quantify this effect, they have calculated the partition coefficient values ( $K_p$ ) for the anions and cations at the air/water interface. It is defined as the ratio of the ions at the surface to the bulk solution, thus indicates the extent of surface accumulation and exclusion. Accordingly, a  $K_p$  value larger than unity shows surface accumulation, while a  $K_p$  smaller than unity describes surface exclusion.

To quantify ion-specificity at surfaces, the authors introduced the *solute partitioning model*, which examines the Hofmeister effect in terms of the surface hydration (number of water molecules per surface area) and the solute partition coefficient  $K_p$  of the ions. Similar two the two-state model that has been employed to assess the proteins folding/unfolding [69-72], two primary thermodynamic states can be envisaged for the polymer chain, i.e., the collapsed globule and the swollen coil states. The conformational stability and transition between these two states is characterized according to the equilibrium constant ( $K$ ) that can provide the standard free energy change:

$$K = \frac{k_s}{k_g} = \frac{[s]}{[g]}$$

$$\Delta G^\circ = -RT \ln K$$



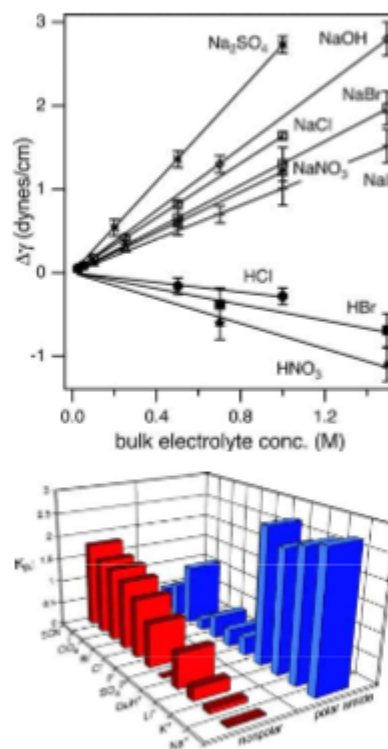


**Figure 3** (Top) effect of various salts on the surface tension of water. The  $m$ -value for each salt can be obtained from the slope of the figure.(reproduced with permission from [61] Copyright (2017) American Chemical Society) (Bottom) single ion partition coefficients for Hofmeister cations and anions at nonpolar and polar amide surfaces.(reproduced with permission from [63] Copyright (2017) American Chemical Society)

Where  $k_s$  and  $k_g$  are the rate constants for swelling and collapse reactions. Accordingly, the equilibrium constant is expressed in terms of the equilibrium concentrations of the products and reactants. The effect of salts on aqueous processes is then quantified using the typical  $m$ -values, which are defined as derivatives of the standard free energy change for the conformational stability with respect to the salt concentration:

$$m - value = \frac{d\Delta G^0}{dm_{salt}} = -RT \frac{d\ln K}{dm_{salt}}$$

Besides conformational transition of macromolecules, the  $m$ -value can be used to quantify the effect of salts for any aqueous process that is associated with a change in the exposed surface to water. For instance, it can be transferring the water molecules from the bulk solution to the air/water non-polar

interface (Figure 3). For this process, the standard free energy change per unit area is the surface tension and thus the m-value represents the *surface tension increment (STI)* in a salt solution, compared to pure water.[61] As shown in Figure 3, the surface tension increment is linearly proportional to the salt concentration, thus m-value can be obtained from the slope of the line for each salt, which is found to be independent from salt concentration over a wide range. In case of dissolving a model hydrophobic compound in water,  $K$  is the solubility of the compound and m-value is then proportional to the Setschenow coefficient.[73, 74] Considering both processes (as model processes that expose an uncharged non-polar surface to water), the authors demonstrated that the effect of different salts on the surface tension increment and solubility of the hydrophobic solute follows the same order as the Hofmeister series for the polymers.

The obtained m-values can also be interpreted in terms of the chemical potential derivatives of the polymer with respect to the salt concentration. Interaction of the salt with the polymer affects the activity coefficient of the polymer ( $f_{polymer}$ ) in solution, which gives rise to activity coefficient derivatives. The activity coefficient derivatives are almost equal to the reduced chemical potential derivatives, which can be determined from osmometry measurements. Accordingly, the m-values can be determined from the dependence of polymer activity coefficient on salt concentration or the reduced chemical potential:

$$m - value = -RT \frac{d \ln K}{dm_{salt}} = RT \Delta \frac{d \ln f_{polymer}}{dm_{salt}} = \Delta \frac{d \mu_{polymer}}{dm_{salt}} = \Delta \mu$$

The m-value is then interpreted as the value of reduced chemical potential for interaction of the salt with the change in the accessible surface area ( $\Delta ASA$ ) during the process. According to the *SPM* model for a polymer in solution, the chemical potential derivative is related to the accessible surface area change of the polymer through the proportionality constant ( $\alpha$ ). It includes a term for number of water molecules per molecular surface area ( $b$ ), as well as a microscopic partition coefficient ( $K_p$ )

term that quantifies the local competition between water and ions for the molecular surface. The former represents the average hydration, while the latter is the average solute partitioning coefficient:

$$\frac{m - value}{RT} = \frac{\Delta\mu}{RT} = \alpha\Delta ASA = \frac{-(v_+K_{p,+} + v_-K_{p,-} - v)b_1(1 + \varepsilon_{\pm})}{55.5}\Delta ASA$$

Where  $\varepsilon$  is the self-nonideality correction term for the salt, i.e., derivatives of activity coefficient of the salt with respect to its concentration, and  $v$  is the number of ions per formula. The interaction potential ( $\alpha$ ) quantifies the strength and direction of preferential interaction of salt with polymer surface, which is almost independent of the change in accessible surface area and salt concentration. For a salt where both anion and cation are excluded from the molecular surface, the partition coefficient values are equal to zero thus the average hydration value can be obtained. Accordingly, the authors obtained single partitioning coefficient of different anions and cations at model non-polar and polar amide groups that are provided in Figure 3.

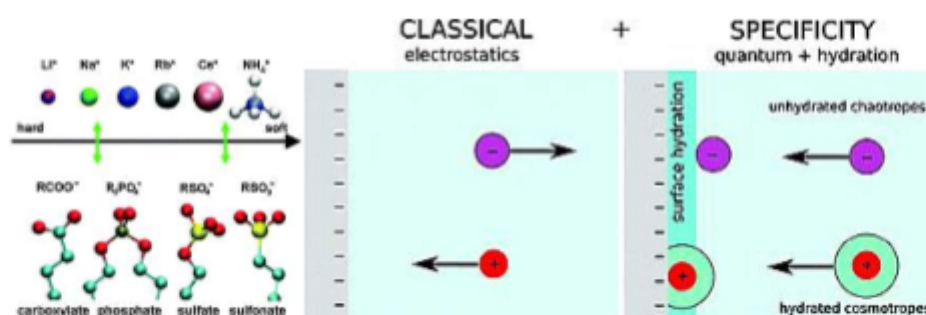


**Figure 4** (Left) ion-headgroup binding according to the law of matching water affinities.(reproduced from [81] with permission from Elsevier) (Right) the role of dispersion and hydration forces in ion-surface interaction by Ninham and coworkers.(reproduced from [38] with permission from the Royal Society of Chemistry)

**2.3. The law of matching water affinities:** The law of matching water affinities was proposed by Collins, which can be considered as a rather empirical rule to address the ion-ion and ion-charged site interactions.[23, 24, 75-80] Accordingly, the classic kosmotropic and chaotropic classification

of ions is employed to distinguish the small and strongly hydrated ions from the large and weakly hydrated ions. As mentioned above, the tendency of various anions and cations to form ion pairs has been illustrated by the Volcano plot (Figure 1), which simply says “*like seeks like*”. On the basis of this framework, Kunz[81, 82] has suggested a qualitative explanation for the affinity of various counter ions to bind to the charged head groups, which has been used to qualitatively explain the observed Hofmeister series for counter ion binding tendency to the charged residues of the proteins (Figure 4). It must be considered that the Law of matching water affinities is not actually a theory, but rather an empirical rule based on the observations. It does not clearly illustrate why the hydration properties of the ions at infinite dilution should correlate with ion pairing or ion-site binding. The other important drawback is that only the interaction of the ions with the charged groups of the polymers are considered; nevertheless, as mentioned before, ions can strongly interact with the hydrophobic and uncharged surfaces.

**2.4. Ion quantum (dispersion) interactions:** Ninham and coworkers have proposed quantum dispersion interactions as another source of ion-specificity.[83-103] As mentioned above, electrostatic interaction and hydration contributions cannot solely capture all the aspects of ion specificity, e.g., accumulation of ions at the neutral surfaces. While ionic charge and concentration are identical for all 1:1 electrolytes, ionic hydration and radius are quite different, which thus suggests inclusion of ion-specific dispersion interactions. Accordingly, ions experience a dispersion potential at any aqueous interface, which can be quantified by the Lifshitz theory. A simple implementation of this approach can be done by considering a colloidal particle interacting in an electrolyte solution. Besides the contribution from electrostatic forces, the role of the dispersion forces should be taken into account by including an additional mean field term ( $U_x^{\text{dispersion}}$ ) in the mean field Poisson-Boltzmann equation:

$$\rho_x = \rho_0 e^{-(ze\psi_x + U_x^{\text{dispersion}})/kT}$$

The dispersion potential includes the image forces, many body dipole-dipole, dipole-induced dipole, and induced dipole-induced dipole forces, which strongly depend on the nature of the participating entities. The dispersion potential itself is given as:

$$U_{\pm}(x) = \frac{1}{x^3} \int_0^{\infty} \frac{\alpha(i\omega)}{\varepsilon_w(i\omega)} \left( \frac{\varepsilon_w(i\omega) - \varepsilon_s(i\omega)}{\varepsilon_w(i\omega) + \varepsilon_s(i\omega)} \right) d\omega$$

Where  $x$  is the distance between the ions,  $\alpha$  represents the polarizability and  $\varepsilon$  refers to the dielectric constant. The integral is sum over frequencies, thus frequency dependence of the dielectric function of the substrate determines the sign of the dispersion potential. Hence, besides the electrostatic interaction with the neighbors, any ion will also experience an additional dispersion potential, which can either enhance or decrease the electrostatic potential. The dispersion potential can be estimated from the static polarizability of the ions and single adsorption frequency, which can be written as:

$$U_x^{dispersion} = \frac{B}{x^3}$$

$$B = \frac{\alpha^*(0)h\omega}{16\pi} (n_w^2 - n_s^2)$$

Where  $n$  represents the refractive index,  $h\omega$  indicates the ionization potential of the ions, and  $\alpha^*(0)$  is the static polarizability of the ion. As an important notion, the difference between the refractive index of water and the substrate determines the sign of the dispersion potential, i.e., if the refractive index of the substrate is larger the dispersion potential will be positive and vice versa. Moreover, the higher the polarizability, the stronger the dispersion force will be. In an attempt to include the ion hydration into the dispersion potential, Parsons and coworkers calculated the frequency dependent dynamic polarizability of the ions, calculating the dispersion potential as:

$$U_x^{dispersion} = \frac{B}{x^3} f(x)$$

$$B = \frac{kT}{2} \sum_n \frac{\alpha^*(i\omega_n)}{\varepsilon_w(i\omega_n)} \left( \frac{\varepsilon_w(i\omega) - \varepsilon_s(i\omega)}{\varepsilon_w(i\omega) + \varepsilon_s(i\omega)} \right)$$

Herein,  $f(x)$  is the form factor that accounts for the finite size of the ion and hydration. The  $\omega_n$  is equal to  $2\pi kTn/h$ ,  $\varepsilon(i\omega)$  represent the dielectric functions, and  $\alpha^*(i\omega)$  is the excess dynamic polarizability. It should be considered that ion size and polarizability have opposite effects on the dispersion potential. Polarizability increases with size, thus enhancing the dispersion forces. On the other hand, the increased size weakens the dispersion forces. Furthermore, ions being hydrated in the solution have a different effective size, which can also affect the dispersion forces. The outcome is thus a balance between all these effects, addressing the ion-specificity in the interactions ion-ion and ion-surface interactions. This in turn reveals the difference between the law of matching water affinities and the quantum approach. While the former concerns with binding of ions to specific binding sites, the latter discusses ion-surface interaction in terms of a uniform substrate with a dielectric constant.

## 2.5. Thermodynamic description:

Dzubiella and coworkers have published a series of computer simulation studies, in which they assessed the Hofmeister effect on the polymers and proteins from a thermodynamic point of view. [104-110] They have established an equation based on the second-order expansion of the two-state free energy in concentration and temperature space, assuming the polymer phase separation as a transition between extended coil and collapsed globule states:

$$\Delta T(c) \simeq - \frac{mc + \frac{1}{2}m'c^2}{\Delta S_0 + \Delta S'_0 c}$$

Herein,  $m$  is known as the m-value that has also been discussed by Pegram and Record, and quantifies the concentration dependence of the free energy function for the two state model.  $\Delta S_0$  represents the entropy of phase separation in salt-free solution, which is a constant for a particular

polymer. The derivative terms accounts for the concentration-dependence of  $m$  and  $\Delta S_0$ , and are responsible for the nonlinearity in Hofmeister effect. The  $m$ -values were calculated from the solute portioning model (*SPM*) and by using the chemical potential derivatives and solvent-accessible surface area values. To do so, the PNIPAM was divided into two sections, i.e., aliphatic nonpolar surfaces and the polar amide surfaces. By fitting the obtained equation to the experimentally obtained data for the Hofmeister effect of salts on PNIPAM phase separation temperature, they extracted the corresponding thermodynamic parameters for each salt. Furthermore, the obtained thermodynamic model was rearranged to reminisce the empirical equation suggested by Cremer et al.:

$$\Delta T(c) = \frac{(a + B_{max}K_A)c + aK_Ac^2}{1 + K_Ac}$$

Two different scenarios for the Hofmeister effect on polymer solutions was suggested in this work. For strongly hydrated anions, it was suggested that the ions act as simple hard spheres with specific excluded volumes, meaning that the transfer of the monomer from the interior globule to the solvent is accompanied with a change of the salt-inaccessible volume. For the weakly hydrated anions, it was argued that the ions preferentially adsorb to the coil state over the globular state at low salt concentrations, while preferentially adsorb on the globule over the coil at high salt concentrations. The authors also argued on the possible reason for the strong curvature in the Hofmeister effect of weakly hydrated anions such as  $\text{NaClO}_4^-$ , based on their previous work.[106]

Herein, the collapse and swelling behavior of a generic polymer was inspected for varying interaction strengths between the polymer and the cosolute. This systematic investigation has revealed that polymer swelling is maximal if both monomer–monomer and monomer–cosolute interactions are weakly attractive. In the most swollen state, the cosolute density inside the coil is remarkably bulk-like and homogeneous. On the other hand, highly attractive monomer–cosolute



interactions are found to induce a collapsed state, which, in contrast to the collapsed conformation induced by purely repulsive cosolvents, exhibits a considerably enhanced cosolute density within the globule. Thus, collapsed states, although appearing similar on a first glance, may result from very different mechanisms with distinct final structural and thermodynamic properties.

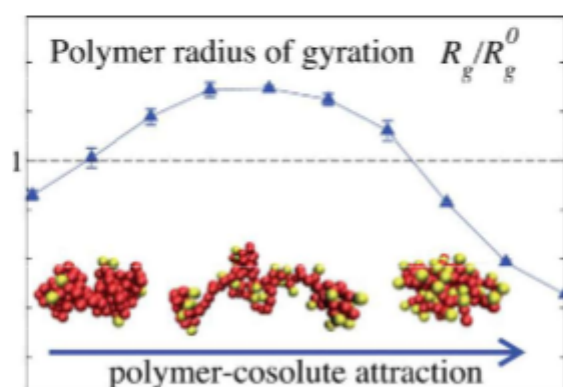


**Figure 5** Schematic illustration of a homopolymer coil size as a function of polymer-cosolute attraction. (reproduced with permission from [106], Copyright (2017) American Chemical Society) When the cosolute is repelled from the polymer chain, a collapsed conformation is found. By increasing the attraction between the polymer and cosolute, a swollen chain conformation enriched with cosolutes is observed. Further increment in the polymer-cosolute attraction gives rise to collapse of the coil while the cosolute is effectively accumulate at the polymer surface.

### 3. The Missing Points and Future Prospects

#### 3.1. Anions accumulate at the polymer interface. What next?

By now, we have discussed five essential mechanisms or approaches that inquire the ion-specificity in polymer solutions. As can be seen, all the provided mechanisms almost agree on the same concept, i.e., the accumulation of weakly hydrated anions at the polymer surface and the exclusion of strongly hydrated ions from the polymer surface. The principal difference between the mechanisms mainly originates from the suggested driving force for ions adsorption to the polymer surface, where some authors have suggested binding of the ions to specific binding sites on the polymer chain, i.e., the charged groups or partially charged atoms. On the other hand, the idea of

having an always-existing dispersion interaction between the ions and surfaces predicts ions accumulation at the charged and uncharged homogenous surfaces. This interpretation thus forms the underlying framework for understanding the source of ion-specificity in polymer solutions and corresponding effect on polymer stability. Nevertheless, various facets of this phenomenon that have not been yet clearly addressed in the previous research.

While the idea of having weakly hydrated ions at the surface is fairly accepted by now, the critical question is on the stabilization mechanism. Although there have been an enormous amount of research on quantifying ions accumulation or exclusion at or from the polymer surface, the fact that how ions at the polymer can stabilize the polymer seemingly have been forgotten. The first mechanism that comes into mind is the electrostatic stabilization; however, this requires further experimentation in the polymer solutions. There are several reports in which the stability of colloidal [111-115] and macromolecular systems [116-119] have been studied in the salt solutions, where the authors argued the effect of adsorbed ions on the stability of the species through electrostatic contribution. Herein, we would like to bring up two notable works in which important traces of electrostatic repulsions were detected.

Schwierz and coworkers have performed molecular dynamic simulation studies combined with AFM colloidal probe measurements [31, 35, 120, 121], and came up with a phase diagram for the Hofmeister series order depending on the surface charge and surface hydrophilicity. According to their findings, the direct or reversed Hofmeister series at the surfaces is a result of the ions specific adsorption to the surfaces and the following effect on the average surface charge density; hence; suggesting the ability of the accumulated ions to modulate the surface charge density of the host surface and the subsequent electrostatic interactions.

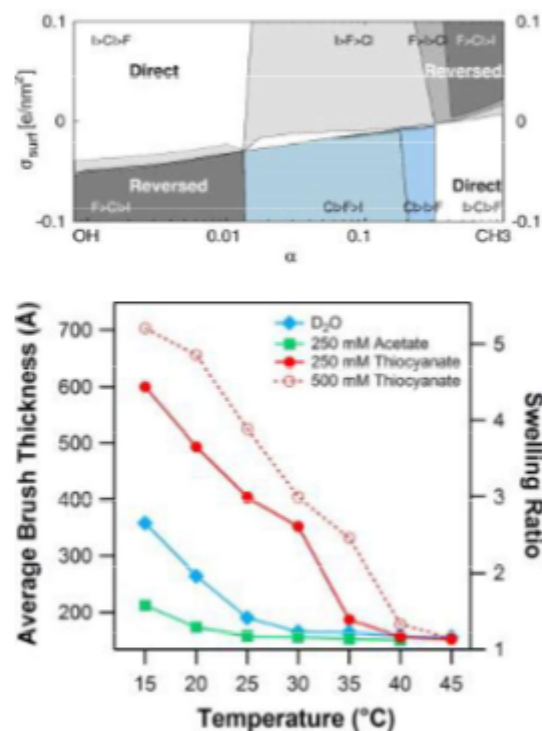


**Figure 6** (Top) the Hofmeister phase diagram suggested by Schwierz et al.(reprinted with permission from [120], Copyright (2017) American Chemical Society) (Bottom) expansion of polymer brush layer in a weakly hydrated salt solution.(reprinted with permission from [122], Copyright (2017) American Chemical Society)

In another notable work, Humphreys and coworkers have investigated the Hofmeister effect on neutral[122-124] and charged[125] brush polymer layers, mostly in terms of the polymer layer thickness and interaction. Based on the ellipsometry and QCM-D measurements, the authors suggested that the polymer layer thickness increases in a weakly hydrated salt solution, i.e. NaSCN, indicating the swelling of the polymer layer, which has been attributed to the inter- and intra-chain repulsive electrostatic interactions. For the studied polycationic brush layer, a reversed effect was expectedly observed, due to the surface charge compensation by the adsorbed anions.

Although the conducted research have successfully captured some traces of electrostatic stabilization, one has to consider that presence of ions at the polymer surface can impose more complex effects on the polymer interaction. One possibility is through affecting the surface tension, hydration and hydrophobic effect at different regions of the polymer surface, which is not settled

yet. Regarding the electrostatic mechanism, it is also important to understand if the stabilization effect is mostly affecting the single chain collapse or the aggregation process. The salting-in effect on the polymer phase separation temperature is typically observed at concentrations ( $\sim 100$  mM) where the electrostatic repulsions are effectively screened, which can be a robust indication that other stabilizing mechanisms persist.

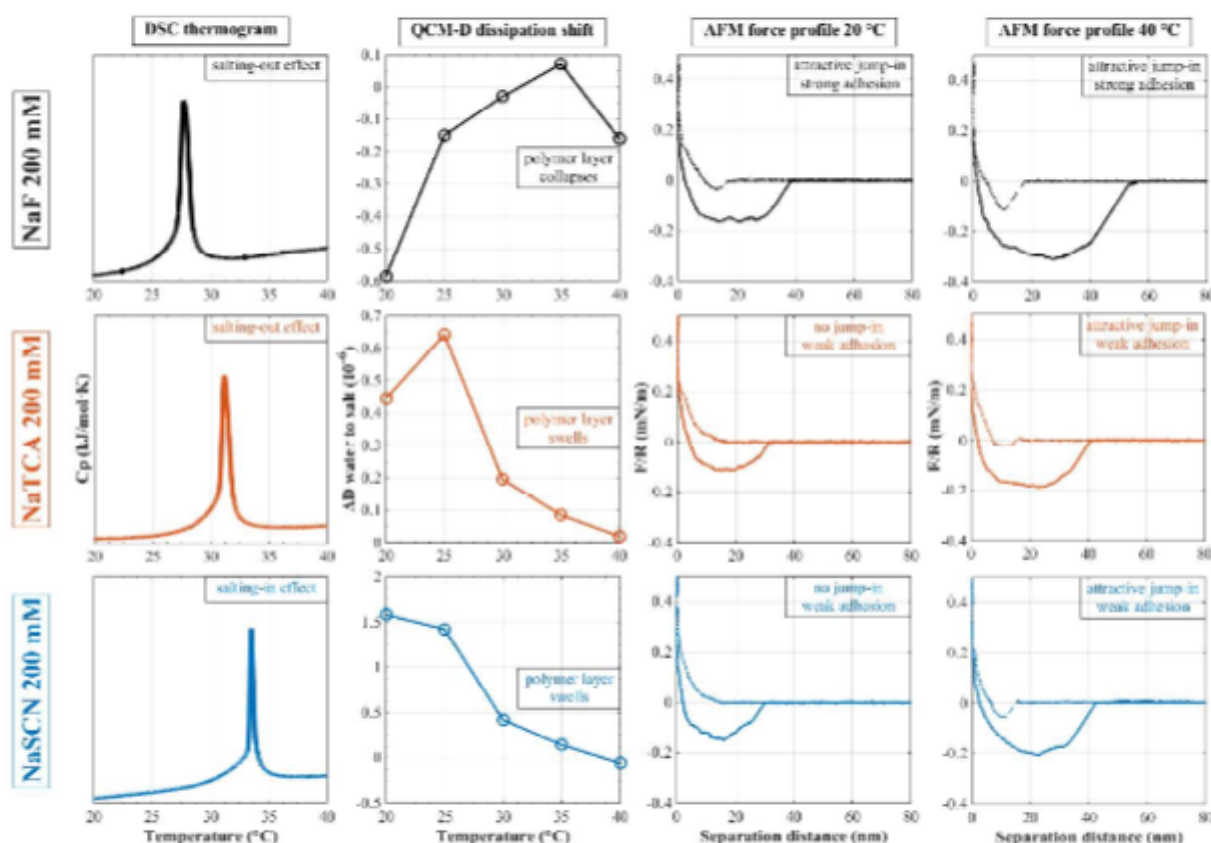


**Figure 7** Effect of NaF, NaTCA and NaSCN salts on PNIPAM: (first column) DSC thermograms, (second column) QCM-D dissipation shifts for a PNIPAM layer adsorbed to the gold surface when changing the solvent from water to saline solutions, (third and fourth column) AFM force-distance curves for between two PNIPAM-coated gold surfaces in the salt solutions at 20 and 40 °C.

### 3.2. Transition from salting-in to salting-out

Another ambiguous observation regarding the Hofmeister effect of weakly hydrated salts is the transition from the salting-in (at relatively low salt concentrations) to the salting-out (at relatively

high salt concentrations). Such an effect has been reported for weakly hydrated anions such as bromide, iodide and thiocyanate. The extremely important consideration regarding this effect is that it strongly depends on the studied polymer. For instance, thiocyanate has a salting-in effect on PNIPAM only up to concentrations of around 0.2 M, at which a turnover is observed and then a salting-out effect is shown. The same salt however has a pure salting-in effect on PPO and PEO even at relatively high concentrations up to 1 M no trace of salting-out effect is found. This suggests that adsorption of the anions at the polymer surface can have both stabilizing and destabilizing effects depending on the type of ion and the polymer. We have very recently studied this behavior by investigating the Hofmeister effect of three different sodium salts, i.e., sodium fluoride, sodium thiocyanate and sodium trichloroacetate, on the PNIPAM properties in bulk and at the gold/aqueous interface (Figure 7).[126]

From DSC measurements, it was concluded that NaTCA has a salting-out effect on the PNIPAM phase separation temperature, even though the anion is weakly hydrated. Our QCM-D measurements however suggested that the PNIPAM layer swells in the NaTCA solution just like in the NaSCN solution. This idea was further supported by the AFM colloidal probe measurements in which the attractive PNIPAM-PNIPAM and PNIPAM-gold interactions were effectively attenuated in the NaSCN and NaTCA solutions, compared to in the NaF solution. Therefore, the conclusion was that TCA anion strongly associates with the PNIPAM chains and can have an electrostatic stabilization effect, even though it has a salting-out effect. Regarding the destabilizing mechanism, different explanations have been suggested each seem applicable under some circumstances. First, the poorly hydrated anions cannot be further accommodated at the polymer surface above a certain salt concentration; in other words, the polymer-water interface becomes saturated. Henceforth, the anions in the bulk solution might compete with the polymer for the hydration water and thus produce a salting-out effect. Although the idea of surface saturation seems rational, we strongly

doubt that the observed difference between the phase separation temperatures in the NaSCN and NaTCA solutions is solely caused by this effect. Both the anions are poorly hydrated; therefore, there should not be a significant difference in their abilities to withdraw water molecules from the polymer. Second, TCA<sup>-</sup> may have a relatively strong salting-out effect at the PNIPAM hydrophobic surface, which has been formerly suggested in terms of the change in surface tension at the polymer/water hydrophobic interface. Finally, the above-discussed theory by Dzubiel and Heyda might explain this observation, where highly attractive cosolutes could induce a compact and collapsed polymer network through collective binding and a following weak cross-linking effect, and thus a salting-out effect is produced, even though presence of anions in the polymer coil induces electrostatic repulsions.

### **3.3. Salt mixtures: competitive hydration, competitive binding**

In spite of the numerous investigations on the Hofmeister effect, it is still unclear to what extent the effect has a role in nature and the biological processes, where a mixture of different ions is present. For instance, it has been reported that presence of some chaotropic anions such as thiocyanate interferes and decreases the iodide transport, which may negatively affect thyroid-related functions.[127-129] Moreover, precipitation and formation of amyloid fibrils that is the suspected origin of Alzheimer disease has also been confirmed to be susceptible to variations in type and amount of dissolved ions.[130-132] Nevertheless, most research on the Hofmeister effect in macromolecular solutions have focused on the effect of single salt species. Accordingly, understanding the Hofmeister effect originating from the salt mixtures can be an important step towards understanding the relevance of the Hofmeister effect in biological systems. Furthermore, comparing the effect of salt mixtures with their constituent's solutions can also be utilized to develop our understanding of the molecular mechanisms behind the Hofmeister effect.

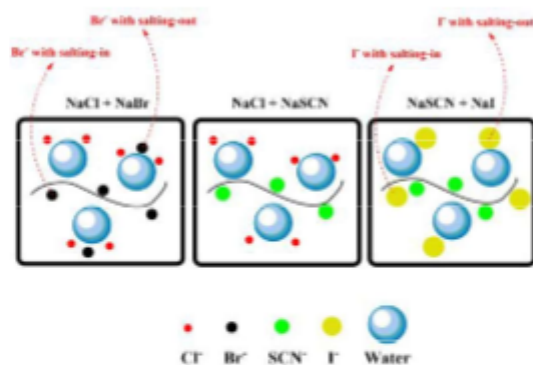


**Figure 8.** Schematic illustration of the Hofmeister effect by salt mixtures. (reproduced from [133] with permission from the Royal Society of Chemistry). Mixture of two salts with a salting-out effect gives rise to competition for polymer hydration shell, while mixture of two salts with a salting-in effect leads to competition for polymer surface area. Mixing two salts with salting-in and salting-out effects represents additive Hofmeister effect.

There are very few reports addressing the Hofmeister effect of more than one salt.[134-136] In one of our works, we have partly investigated the Hofmeister effect of three basic salt mixtures on the phase transition temperature of PPO, which were explainable by the current opinion about ion-specificity mechanisms. The mixture of two salts with considerable differences in nature (one salting-in and other salting-out) resulted in linear additive Hofmeister effects, which can support the idea that each anion applies its own specific effect on macromolecule stability, regardless of presence or absence of the other ion. In the case of mixing two salts with a salting-in effect, the stronger component (the one with higher propensity toward accumulating at the polymer/water interface) was shown to dominate the overall salting-in behavior of the mixture, while the other component is less favored to accumulate at the polymer/water interface, thus can have a relative salting-out effect. Analogously with respect to mixing two salts with a salting-out effect, the overall salting-out behavior of the mixture is also surmounted by the stronger component (the one with higher hydration capacity), while the other component may tend to directly associate with the polymer backbone and have a relative salting-in effect.



### **3.4. The role of polymer properties and solvent perturbation**

Another topic that has not been thoroughly addressed is the role of the polymer properties such as molecular weight, concentration, as well as structural characteristics such as tacticity and branching, which all were shown to affect the polymer stability in salt-free solutions.[137-140] Irrespective of using a thermodynamic or a molecular description of the Hofmeister effect, it is expected that the effect should depend on the chemical structure and the accessible surface area of the polymer, as well as the possible inter-chain interaction between the polymer chains. With respect to the chemical structure, it has previously been observed that different polymers are not similarly affected by the presence of salts. For instance, poly(propylene oxide) (PPO) shows smaller changes in phase separation temperature in response to different salts, compared to poly(ethylene oxide) (PEO). Since most previous studies of the Hofmeister effect merely concerned with the effect of different ions and their interaction with a particular polymer, the questions regarding the effect of accessible surface area of the chains and inter-chain interaction have remained untouched. These parameters are related to the polymer chemistry, as well as the polymer molecular weight, the polymer concentration and the solvent quality. Hence, the next stage of studies on the Hofmeister effect should be focused on finding the role of the polymer properties in this phenomenon, and a better understanding of this can be gained by including the well-known descriptions and concepts from polymer physics.

Although not directly discussed in the literature, the key role of the macromolecule properties in the Hofmeister effect is irrefutable. The effect of polymer chemical structure can be inferred from previous studies showing that the Hofmeister effect on different macromolecules is not the same. In this case, we can enumerate several examples from the literature, where the authors addressed the important role of chemical structure of the polymer. Many reports can be found on the differences between the Hofmeister effect on proteins and nucleic acids, where the great difference in chemistry

of the surface and conformation of the macromolecules has been suggested as the main reason.[66, 69] Comparison of the effect of ions on neutral and charged macromolecules also strengthens this idea. Furthermore, several reports are available in the literature discussing the effect of size and molecular weight of PEG on its stabilizing/destabilizing effects on nucleic acid and protein solutions, where the excluded volume effect on the Hofmeister effect have been suggested.[141, 142] It has been also shown in some studies that polymer molecular weight and concentration can significantly affect both the salting-in and salting-out effects, suggesting the correlation between the ions effect and solvent-accessible surface area.[46, 143] All these together imply the essential role of polymer properties in the Hofmeister effect, in other words the way the polymer is affected by the ions. Another intriguing approach to investigate the fundamentals of the Hofmeister can be through solvent perturbation studies. We have recently found out that such a delicate variation in the solvent properties can change the Hofmeister effect in a specific way[144], which then can be considered as a new approach towards further understanding the Hofmeister effect and addressing role of ion hydration and water withdrawing power is in the Hofmeister effect.

#### **4. Summary and Conclusion**

What we have presented in this review paper consisted of an overview of the previous work and the future research perspective. Considering the Hofmeister series as a fixed universal trend, the important question concerns with the origins of ion-specificity, which can be concisely divided as ion-polymer surface and ion-polymer hydration shell interactions. Although this picture has been successfully applied to many systems, we are still far away from having a universal explanation for the ion-specific effects in polymer solution systems.

## References

- [1] F. Hofmeister, Zur lehre von der wirkung der salze, Naunyn-Schmiedeberg's Archives of Pharmacology, 25 (1888) 1-30.
- [2] W. Kunz, J. Henle, B.W. Ninham, 'Zur Lehre von der Wirkung der Salze'(about the science of the effect of salts): Franz Hofmeister's historical papers, Current opinion in colloid & interface science, 9 (2004) 19-37.
- [3] A.A. Green, Studies in the physical chemistry of the proteins X. The solubility of hemoglobin in solutions of chlorides and sulfates of varying concentration, Journal of Biological Chemistry, 95 (1932) 47-66.
- [4] C. MacArthur, Solubility of oxygen in salt solutions and the hydrates of these salts, The Journal of Physical Chemistry, 20 (1916) 495-502.
- [5] L.A. Reber, W.W. McNabb, W.W. Lucasse, The Effect of Salts on the Mutual Miscibility of Normal Butyl Alcohol and Water, The Journal of Physical Chemistry, 46 (1942) 500-515.
- [6] R. Lundberg, F. Bailey, R. Callard, Interactions of inorganic salts with poly (ethylene oxide), Journal of Polymer Science Part A-1: Polymer Chemistry, 4 (1966) 1563-1577.
- [7] S. Saito, Salt effect on polymer solutions, Journal of Polymer Science Part A-1: Polymer Chemistry, 7 (1969) 1789-1802.
- [8] C. Mangels, C. Bailey, Relation of Concentration to Action of Gelatinizing Agents on Starch1, Journal of the American Chemical Society, 55 (1933) 1981-1988.
- [9] D. Napper, Steric stabilization and the Hofmeister series, Journal of colloid and interface science, 33 (1970) 384-392.
- [10] E. Heymann, H. Bleakley, A. Docking, Studies on the lyotropic series. I: The adsorption of salts on methylcellulose, The Journal of Physical Chemistry, 42 (1938) 353-368.
- [11] V.S. Craig, Bubble coalescence and specific-ion effects, Current opinion in colloid & interface science, 9 (2004) 178-184.
- [12] C.L. Henry, C.N. Dalton, L. Scruton, V.S. Craig, Ion-specific coalescence of bubbles in mixed electrolyte solutions, The Journal of Physical Chemistry C, 111 (2007) 1015-1023.
- [13] A. Salis, D. Bilanicova, B.W. Ninham, M. Monduzzi, Hofmeister effects in enzymatic activity: weak and strong electrolyte influences on the activity of Candida rugosa lipase, The Journal of Physical Chemistry B, 111 (2007) 1149-1156.
- [14] D. Bilanicová, A. Salis, B.W. Ninham, M. Monduzzi, Specific anion effects on enzymatic activity in nonaqueous media, The Journal of Physical Chemistry B, 112 (2008) 12066-12072.
- [15] J. Johnston, THE CHANGE OF THE EQUIVALENT CONDUCTANCE OF IONS WITH THE TEMPERATURE, Journal of the American Chemical Society, 31 (1909) 1010-1020.
- [16] M.P. Applebey, CCXI.—The viscosity of salt solutions, Journal of the Chemical Society, Transactions, 97 (1910) 2000-2025.
- [17] D.W. Smith, Ionic hydration enthalpies, J. Chem. Educ, 54 (1977) 540.
- [18] G. Jones, M. Dole, The viscosity of aqueous solutions of strong electrolytes with special reference to barium chloride, Journal of the American Chemical Society, 51 (1929) 2950-2964.
- [19] E.W. Washburn, THE HYDRATION OF IONS DETERMINED BY TRANSFERENCE EXPERIMENTS IN THE PRESENCE OF A NON-ELECTROLYTE, Journal of the American Chemical Society, 31 (1909) 322-355.
- [20] M. Randall, F.D. Rossini, Heat capacities in aqueous salt solutions, Journal of the American Chemical Society, 51 (1929) 323-345.
- [21] B. Hribar, N.T. Southall, V. Vlachy, K.A. Dill, How ions affect the structure of water, Journal of the American Chemical Society, 124 (2002) 12302-12311.
- [22] Y. Marcus, Effect of ions on the structure of water: structure making and breaking, Chemical reviews, 109 (2009) 1346-1370.
- [23] K.D. Collins, M.W. Washabaugh, The Hofmeister effect and the behaviour of water at interfaces, Quarterly reviews of biophysics, 18 (1985) 323-422.
- [24] K.D. Collins, Charge density-dependent strength of hydration and biological structure, Biophysical journal, 72 (1997) 65-76.
- [25] A.W. Omta, M.F. Kropman, S. Woutersen, H.J. Bakker, Negligible effect of ions on the hydrogen-bond structure in liquid water, Science, 301 (2003) 347-349.
- [26] H.S. Frank, W.-Y. Wen, Ion-solvent interaction. Structural aspects of ion-solvent interaction in aqueous solutions: a suggested picture of water structure, Discussions of the Faraday Society, 24 (1957) 133-140.
- [27] J.C. Ghosh, XXXVIII.—The abnormality of strong electrolytes. Part I. Electrical conductivity of aqueous salt solutions, Journal of the Chemical Society, Transactions, 113 (1918) 449-458.

- [28] C.W. Davies, 397. The extent of dissociation of salts in water. Part VIII. An equation for the mean ionic activity coefficient of an electrolyte in water, and a revision of the dissociation constants of some sulphates, *Journal of the Chemical Society (Resumed)*, DOI (1938) 2093-2098.
- [29] Y. Marcus, G. Hefter, Ion pairing, *Chemical reviews*, 106 (2006) 4585-4621.
- [30] C.J. Fennell, A. Bizjak, V. Vlatchy, K.A. Dill, Ion pairing in molecular simulations of aqueous alkali halide solutions, *The Journal of Physical Chemistry B*, 113 (2009) 6782-6791.
- [31] N. Schwierz, D. Horinek, R.R. Netz, Reversed anionic Hofmeister series: the interplay of surface charge and surface polarity, *Langmuir*, 26 (2010) 7370-7379.
- [32] J. Morag, M. Dishon, U. Sivan, The governing role of surface hydration in ion specific adsorption to silica: An AFM-based account of the Hofmeister universality and its reversal, *Langmuir*, 29 (2013) 6317-6322.
- [33] S. Finet, F. Skouri-Panet, M. Casselyn, F. Bonnete, A. Tardieu, The Hofmeister effect as seen by SAXS in protein solutions, *Current opinion in colloid & interface science*, 9 (2004) 112-116.
- [34] R.A. Robinson, R.H. Stokes, *Electrolyte solutions*, Courier Corporation 2002.
- [35] N. Schwierz, D. Horinek, U. Sivan, R.R. Netz, Reversed Hofmeister series—The rule rather than the exception, *Current opinion in colloid & interface science*, 23 (2016) 10-18.
- [36] D. Parsons, M. Bostrom, T. Maceina, A. Salis, B.W. Ninham, Why direct or reversed Hofmeister series? Interplay of hydration, non-electrostatic potentials, and ion size, *Langmuir*, 26 (2009) 3323-3328.
- [37] A. Salis, B.W. Ninham, Models and mechanisms of Hofmeister effects in electrolyte solutions, and colloid and protein systems revisited, *Chemical Society Reviews*, 43 (2014) 7358-7377.
- [38] D.F. Parsons, M. Boström, P.L. Nostro, B.W. Ninham, Hofmeister effects: interplay of hydration, nonelectrostatic potentials, and ion size, *Physical Chemistry Chemical Physics*, 13 (2011) 12352-12367.
- [39] Y. Zhang, P.S. Cremer, Chemistry of Hofmeister anions and osmolytes, *Annual review of physical chemistry*, 61 (2010) 63-83.
- [40] A. Lendlein, V.P. Shastri, Stimuli-Sensitive Polymers, *Advanced Materials*, 22 (2010) 3344-3347.
- [41] D. Roy, W.L. Brooks, B.S. Sumerlin, New directions in thermoresponsive polymers, *Chemical Society Reviews*, 42 (2013) 7214-7243.
- [42] M.C. Gurau, S.-M. Lim, E.T. Castellana, F. Albertorio, S. Kataoka, P.S. Cremer, On the mechanism of the Hofmeister effect, *Journal of the American Chemical Society*, 126 (2004) 10522-10523.
- [43] H. Mao, C. Li, Y. Zhang, S. Furryk, P.S. Cremer, D.E. Bergbreiter, High-throughput studies of the effects of polymer structure and solution components on the phase separation of thermoresponsive polymers, *Macromolecules*, 37 (2004) 1031-1036.
- [44] Y. Zhang, S. Furryk, D.E. Bergbreiter, P.S. Cremer, Specific ion effects on the water solubility of macromolecules: PNIPAM and the Hofmeister series, *Journal of the American Chemical Society*, 127 (2005) 14505-14510.
- [45] Y. Zhang, P.S. Cremer, Interactions between macromolecules and ions: the Hofmeister series, *Current opinion in chemical biology*, 10 (2006) 658-663.
- [46] Y. Zhang, S. Furryk, L.B. Sagle, Y. Cho, D.E. Bergbreiter, P.S. Cremer, Effects of Hofmeister anions on the LCST of PNIPAM as a function of molecular weight, *The journal of physical chemistry. C, Nanomaterials and interfaces*, 111 (2007) 8916.
- [47] X. Chen, T. Yang, S. Kataoka, P.S. Cremer, Specific ion effects on interfacial water structure near macromolecules, *Journal of the American Chemical Society*, 129 (2007) 12272-12279.
- [48] K.B. Rembert, H.I. Okur, C. Hilty, P.S. Cremer, An NH moiety is not required for anion binding to amides in aqueous solution, *Langmuir*, 31 (2015) 3459-3464.
- [49] Y. Zhang, P.S. Cremer, The inverse and direct Hofmeister series for lysozyme, *Proceedings of the National Academy of Sciences*, 106 (2009) 15249-15253.
- [50] Y. Cho, Y. Zhang, T. Christensen, L.B. Sagle, A. Chilkoti, P.S. Cremer, Effects of Hofmeister anions on the phase transition temperature of elastin-like polypeptides, *The journal of physical chemistry. B*, 112 (2008) 13765.
- [51] J. Kherb, S.C. Flores, P.S. Cremer, Role of carboxylate side chains in the cation Hofmeister series, *The Journal of Physical Chemistry B*, 116 (2012) 7389-7397.
- [52] S.C. Flores, J. Kherb, N. Konelick, X. Chen, P.S. Cremer, The effects of Hofmeister cations at negatively charged hydrophilic surfaces, *The Journal of Physical Chemistry C*, 116 (2012) 5730-5734.
- [53] X. Chen, S.C. Flores, S.-M. Lim, Y. Zhang, T. Yang, J. Kherb, P.S. Cremer, Specific anion effects on water structure adjacent to protein monolayers, *Langmuir*, 26 (2010) 16447-16454.
- [54] K.B. Rembert, J. Paterová, J. Heyda, C. Hilty, P. Jungwirth, P.S. Cremer, Molecular mechanisms of ion-specific effects on proteins, *Journal of the American Chemical Society*, 134 (2012) 10039-10046.
- [55] J. Paterová, K.B. Rembert, J. Heyda, Y. Kurra, H.I. Okur, W.R. Liu, C. Hilty, P.S. Cremer, P. Jungwirth, Reversal of the Hofmeister series: specific ion effects on peptides, *The Journal of Physical Chemistry B*, 117 (2013) 8150-8158.

- [56] H.I. Okur, J. Hladíková, K.B. Rembert, Y. Cho, J. Heyda, J. Dzubiella, P.S. Cremer, P. Jungwirth, Beyond the Hofmeister Series: Ion-Specific Effects on Proteins and Their Biological Functions, *The Journal of Physical Chemistry B*, 121 (2017) 1997-2014.
- [57] S.C. Flores, J. Kherb, P.S. Cremer, Direct and reverse Hofmeister effects on interfacial water structure, *The Journal of Physical Chemistry C*, 116 (2012) 14408-14413.
- [58] Y. Chen, H.I. Okur, N. Gomopoulos, C. Macias-Romero, P.S. Cremer, P.B. Petersen, G. Tocci, D.M. Wilkins, C. Liang, M. Ceriotti, Electrolytes induce long-range orientational order and free energy changes in the H-bond network of bulk water, *Science advances*, 2 (2016) e1501891.
- [59] B.A. Deyerle, Y. Zhang, Effects of Hofmeister anions on the aggregation behavior of PEO-PPO-PEO triblock copolymers, *Langmuir*, 27 (2011) 9203-9210.
- [60] H.I. Okur, J. Kherb, P.S. Cremer, Cations bind only weakly to amides in aqueous solutions, *Journal of the American Chemical Society*, 135 (2013) 5062-5067.
- [61] L.M. Pegram, M.T. Record, Hofmeister salt effects on surface tension arise from partitioning of anions and cations between bulk water and the air-water interface, *The Journal of Physical Chemistry B*, 111 (2007) 5411-5417.
- [62] L. Pegram, M. Record, Quantifying accumulation or exclusion of H<sup>+</sup>, HO<sup>-</sup>, and Hofmeister salt ions near interfaces, *Chemical physics letters*, 467 (2008) 1-8.
- [63] L.M. Pegram, M.T. Record Jr, The thermodynamic origin of hofmeister ion effects, *The journal of physical chemistry. B*, 112 (2008) 9428.
- [64] L.M. Pegram, M.T. Record, Quantifying the roles of water and solutes (denaturants, osmolytes, and Hofmeister salts) in protein and model processes using the solute partitioning model, *Protein Structure, Stability, and Interactions*, DOI (2009) 179-193.
- [65] L.M. Pegram, T. Wendorff, R. Erdmann, I. Shkel, D. Bellissimo, D.J. Felitsky, M.T. Record, Why Hofmeister effects of many salts favor protein folding but not DNA helix formation, *Proceedings of the National Academy of Sciences*, 107 (2010) 7716-7721.
- [66] E.J. Guinn, L.M. Pegram, M.W. Capp, M.N. Pollock, M.T. Record, Quantifying why urea is a protein denaturant, whereas glycine betaine is a protein stabilizer, *Proceedings of the National Academy of Sciences*, 108 (2011) 16932-16937.
- [67] M.T. Record, E. Guinn, L. Pegram, M. Capp, Introductory lecture: Interpreting and predicting Hofmeister salt ion and solute effects on biopolymer and model processes using the solute partitioning model, *Faraday discussions*, 160 (2013) 9-44.
- [68] M.T. Record Jr, E. Guinn, L. Pegram, M. Capp, Faraday Discussion 160 Introductory Lecture: Interpreting and Predicting Hofmeister Salt Ion and Solute Effects on Biopolymer and Model Processes Using the Solute Partitioning Model, *Faraday discussions*, 160 (2013) 9.
- [69] E. Courtenay, M. Capp, R. Saecker, M. Record, Thermodynamic analysis of interactions between denaturants and protein surface exposed on unfolding: Interpretation of urea and guanidinium chloride m-values and their correlation with changes in accessible surface area (ASA) using preferential interaction coefficients and the local-bulk domain model, *Proteins: Structure, Function, and Bioinformatics*, 41 (2000) 72-85.
- [70] E.S. Courtenay, M.W. Capp, M.T. Record, Thermodynamics of interactions of urea and guanidinium salts with protein surface: Relationship between solute effects on protein processes and changes in water-accessible surface area, *Protein Science*, 10 (2001) 2485-2497.
- [71] D.J. Felitsky, M.T. Record, Application of the local-bulk partitioning and competitive binding models to interpret preferential interactions of glycine betaine and urea with protein surface, *Biochemistry*, 43 (2004) 9276-9288.
- [72] L. Ma, L. Pegram, M. Record Jr, Q. Cui, Preferential interactions between small solutes and the protein backbone: a computational analysis, *Biochemistry*, 49 (2010) 1954-1962.
- [73] J. Setschenow, Über die konstitution der salzlösungen auf grund ihres verhaltens zu kohlenensäure, *Zeitschrift für Physikalische Chemie*, 4 (1889) 117-125.
- [74] W.L. Masterton, T.P. Lee, Salting coefficients from scaled particle theory, *The Journal of Physical Chemistry*, 74 (1970) 1776-1782.
- [75] K.D. Collins, Sticky ions in biological systems, *Proceedings of the National Academy of Sciences*, 92 (1995) 5553-5557.
- [76] K.D. Collins, Ions from the Hofmeister series and osmolytes: effects on proteins in solution and in the crystallization process, *Methods*, 34 (2004) 300-311.
- [77] K.D. Collins, Ion hydration: Implications for cellular function, polyelectrolytes, and protein crystallization, *Biophysical chemistry*, 119 (2006) 271-281.
- [78] K.D. Collins, G.W. Neilson, J.E. Enderby, Ions in water: characterizing the forces that control chemical processes and biological structure, *Biophysical chemistry*, 128 (2007) 95-104.
- [79] K.D. Collins, Why continuum electrostatics theories cannot explain biological structure, polyelectrolytes or ionic strength effects in ion-protein interactions, *Biophysical chemistry*, 167 (2012) 43-59.

- [80] T.T. Duignan, D.F. Parsons, B.W. Ninham, Collins's rule, Hofmeister effects and ionic dispersion interactions, *Chemical physics letters*, 608 (2014) 55-59.
- [81] N. Vlachy, B. Jagoda-Cwiklik, R. Vácha, D. Touraud, P. Jungwirth, W. Kunz, Hofmeister series and specific interactions of charged headgroups with aqueous ions, *Advances in colloid and interface science*, 146 (2009) 42-47.
- [82] W. Kunz, Specific ion effects in colloidal and biological systems, *Current opinion in colloid & interface science*, 15 (2010) 34-39.
- [83] S.J. Miklavic, B.W. Ninham, Competition for adsorption sites by hydrated ions, *Journal of colloid and interface science*, 134 (1990) 305-311.
- [84] B.W. Ninham, V. Yaminsky, Ion binding and ion specificity: the Hofmeister effect and Onsager and Lifshitz theories, *Langmuir*, 13 (1997) 2097-2108.
- [85] M. Boström, D. Williams, B. Ninham, Specific ion effects: why DLVO theory fails for biology and colloid systems, *Physical Review Letters*, 87 (2001) 168103.
- [86] M. Boström, D.R. Williams, B.W. Ninham, Ion specificity of micelles explained by ionic dispersion forces, *Langmuir*, 18 (2002) 6010-6014.
- [87] M. Boström, D. Williams, B.W. Ninham, Specific ion effects: why the properties of lysozyme in salt solutions follow a Hofmeister series, *Biophysical journal*, 85 (2003) 686-694.
- [88] P. Bauduin, A. Renoncourt, D. Touraud, W. Kunz, B.W. Ninham, Hofmeister effect on enzymatic catalysis and colloidal structures, *Current opinion in colloid & interface science*, 9 (2004) 43-47.
- [89] M. Boström, D. Williams, B. Ninham, Why the properties of proteins in salt solutions follow a Hofmeister series, *Current opinion in colloid & interface science*, 9 (2004) 48-52.
- [90] M. Bostrom, B. Ninham, Dispersion self-free energies and interaction free energies of finite-sized ions in salt solutions, *Langmuir*, 20 (2004) 7569-7574.
- [91] M. Boström, D. Williams, B. Ninham, Specific ion effects: why colloid science has failed to contribute to biology, *Trends in Colloid and Interface Science XVI*, DOI (2004) 110-113.
- [92] M. Boström, F.W. Tavares, S. Finet, F. Skouri-Panet, A. Tardieu, B. Ninham, Why forces between proteins follow different Hofmeister series for pH above and below pI, *Biophysical chemistry*, 117 (2005) 217-224.
- [93] M. Boström, W. Kunz, B.W. Ninham, Hofmeister effects in surface tension of aqueous electrolyte solution, *Langmuir*, 21 (2005) 2619-2623.
- [94] P.L. Nostro, B.W. Ninham, S. Milani, A.L. Nostro, G. Pesavento, P. Baglioni, Hofmeister effects in supramolecular and biological systems, *Biophysical chemistry*, 124 (2006) 208-213.
- [95] D.F. Parsons, B.W. Ninham, Importance of accurate dynamic polarizabilities for the ionic dispersion interactions of alkali halides, *Langmuir*, 26 (2009) 1816-1823.
- [96] M. Boström, D.F. Parsons, A. Salis, B.W. Ninham, M. Monduzzi, Possible origin of the inverse and direct Hofmeister series for lysozyme at low and high salt concentrations, *Langmuir*, 27 (2011) 9504-9511.
- [97] D.F. Parsons, B.W. Ninham, Surface charge reversal and hydration forces explained by ionic dispersion forces and surface hydration, *Colloids and Surfaces A: Physicochemical and Engineering Aspects*, 383 (2011) 2-9.
- [98] J. BORAH, N. SARMA, S. MAHIUDDIN, D. PERSONS, N. BARRY, Specific ion effects in adsorption at the solid/electrolyte interface: A probe into the concentration limit, *Langmuir*, 47 (2011) 8710-8717.
- [99] P. Lo Nostro, B.W. Ninham, Hofmeister phenomena: an update on ion specificity in biology, *Chemical reviews*, 112 (2012) 2286-2322.
- [100] A. Salis, F. Cugia, D.F. Parsons, B.W. Ninham, M. Monduzzi, Hofmeister series reversal for lysozyme by change in pH and salt concentration: insights from electrophoretic mobility measurements, *Physical Chemistry Chemical Physics*, 14 (2012) 4343-4346.
- [101] T.T. Duignan, D.F. Parsons, B.W. Ninham, A continuum model of solvation energies including electrostatic, dispersion, and cavity contributions, *The Journal of Physical Chemistry B*, 117 (2013) 9421-9429.
- [102] T.T. Duignan, D.F. Parsons, B.W. Ninham, Ion interactions with the air-water interface using a continuum solvent model, *The Journal of Physical Chemistry B*, 118 (2014) 8700-8710.
- [103] T.T. Duignan, D.F. Parsons, B.W. Ninham, A continuum solvent model of ion-ion interactions in water, *Physical Chemistry Chemical Physics*, 16 (2014) 22014-22027.
- [104] J. Heyda, J.C. Vincent, D.J. Tobias, J. Dzubiella, P. Jungwirth, Ion specificity at the peptide bond: Molecular dynamics simulations of N-methylacetamide in aqueous salt solutions, *The Journal of Physical Chemistry B*, 114 (2009) 1213-1220.
- [105] A. Muzdalo, J. Heyda, J. Dzubiella, Rationalizing polymer swelling and collapse under repulsive to highly attractive cosolvent conditions, *arXiv preprint arXiv:1211.0851*, DOI (2012).
- [106] J. Heyda, A. Muzdalo, J. Dzubiella, Rationalizing polymer swelling and collapse under attractive cosolvent conditions, *Macromolecules*, 46 (2013) 1231-1238.
- [107] J. Heyda, S. Soll, J. Yuan, J. Dzubiella, Thermodynamic description of the LCST of charged thermoresponsive copolymers, *arXiv preprint arXiv:1311.2784*, DOI (2013).

- [108] J. Heyda, J. Dzubiella, Thermodynamic description of Hofmeister effects on the LCST of thermosensitive polymers, *The Journal of Physical Chemistry B*, 118 (2014) 10979-10988.
- [109] J. Heyda, H.I. Okur, J. Hladíková, K.B. Rembert, W. Hunn, T. Yang, J. Dzubiella, P. Jungwirth, P.S. Cremer, Guanidinium can both Cause and Prevent the Hydrophobic Collapse of Biomacromolecules, *Journal of the American Chemical Society*, DOI (2017).
- [110] J. Heyda, J. Dzubiella, Ion-specific counterion condensation on charged peptides: Poisson-Boltzmann vs. atomistic simulations, *Soft Matter*, 8 (2012) 9338-9344.
- [111] F.J. Montes Ruiz-Cabello, G. Trefalt, T. Oncsik, I. Szilagyi, P. Maroni, M. Borkovec, Interaction forces and aggregation rates of colloidal latex particles in the presence of monovalent counterions, *The Journal of Physical Chemistry B*, 119 (2015) 8184-8193.
- [112] T. Oncsik, G. Trefalt, M. Borkovec, I. Szilagyi, Specific ion effects on particle aggregation induced by monovalent salts within the Hofmeister series, *Langmuir*, 31 (2015) 3799-3807.
- [113] V. Merk, C. Rehbock, F. Becker, U. Hagemann, H. Nienhaus, S. Barcikowski, In situ non-DLVO stabilization of surfactant-free, plasmonic gold nanoparticles: Effect of Hofmeister's anions, *Langmuir*, 30 (2014) 4213-4222.
- [114] J. Irigoyen, S. Moya, J. Iturri, I. Llaena, O. Azzaroni, E. Donath, Specific  $\zeta$ -potential response of layer-by-layer coated colloidal particles triggered by polyelectrolyte ion interactions, *Langmuir*, 25 (2009) 3374-3380.
- [115] C. Schneider, M. Hanisch, B. Wedel, A. Jusufi, M. Ballauff, Experimental study of electrostatically stabilized colloidal particles: Colloidal stability and charge reversal, *Journal of colloid and interface science*, 358 (2011) 62-67.
- [116] S. Fanaian, N. Al-Manasir, K. Zhu, A.-L. Kjoniksen, B. Nyström, Effects of Hofmeister anions on the flocculation behavior of temperature-responsive poly (N-isopropylacrylamide) microgels, *Colloid and Polymer Science*, 290 (2012) 1609-1616.
- [117] M. Kowacz, A. Mukhopadhyay, A.L. Carvalho, J.M. Esperança, M.J. Romão, L.P.N. Rebelo, Hofmeister effects of ionic liquids in protein crystallization: Direct and water-mediated interactions, *CrystEngComm*, 14 (2012) 4912-4921.
- [118] L.M. Gloss, B.J. Placek, The Effect of Salts on the Stability of the H2A– H2B Histone Dimer, *Biochemistry*, 41 (2002) 14951-14959.
- [119] C. Park, R.T. Raines, Quantitative analysis of the effect of salt concentration on enzymatic catalysis, *Journal of the American Chemical Society*, 123 (2001) 11472-11479.
- [120] N. Schwierz, D. Horinek, R.R. Netz, Anionic and cationic Hofmeister effects on hydrophobic and hydrophilic surfaces, *Langmuir*, 29 (2013) 2602-2614.
- [121] N. Schwierz, D. Horinek, R.R. Netz, Specific ion binding to carboxylic surface groups and the pH dependence of the hofmeister series, *Langmuir*, 31 (2014) 215-225.
- [122] T.J. Murdoch, B.A. Humphreys, J.D. Willott, S.W. Prescott, A. Nelson, G.B. Webber, E.J. Wanless, Enhanced specific ion effects in ethylene glycol-based thermoresponsive polymer brushes, *Journal of colloid and interface science*, 490 (2017) 869-878.
- [123] B.A. Humphreys, J.D. Willott, T.J. Murdoch, G.B. Webber, E.J. Wanless, Specific ion modulated thermoresponse of poly (N-isopropylacrylamide) brushes, *Physical Chemistry Chemical Physics*, 18 (2016) 6037-6046.
- [124] T.J. Murdoch, B.A. Humphreys, J.D. Willott, K.P. Gregory, S.W. Prescott, A. Nelson, E.J. Wanless, G.B. Webber, Specific Anion Effects on the Internal Structure of a Poly (N-isopropylacrylamide) Brush, *Macromolecules*, 49 (2016) 6050-6060.
- [125] J.D. Willott, T.J. Murdoch, B.A. Humphreys, S. Edmondson, E.J. Wanless, G.B. Webber, Anion-specific effects on the behavior of pH-sensitive polybasic brushes, *Langmuir*, 31 (2015) 3707-3717.
- [126] S. Zafjoroushan Moghaddam, E. Thormann, Hofmeister Effect on PNIPAM in Bulk and at an Interface: Surface Partitioning of Weakly Hydrated Anions, *Langmuir*, DOI (2017).
- [127] M.F. Erdoğan, Thiocyanate overload and thyroid disease, *Biofactors*, 19 (2003) 107-111.
- [128] P.-A. Dahlberg, A. Bergmark, M. Eltom, L. Björck, O. Claesson, Effect of thiocyanate levels in milk on thyroid function in iodine deficient subjects, *The American journal of clinical nutrition*, 41 (1985) 1010-1014.
- [129] C. Steinmaus, M.D. Miller, L. Cushing, B.C. Blount, A.H. Smith, Combined effects of perchlorate, thiocyanate, and iodine on thyroid function in the National Health and Nutrition Examination Survey 2007–08, *Environmental research*, 123 (2013) 17-24.
- [130] V. Yeh, J.M. Broering, A. Romanyuk, B. Chen, Y.O. Chernoff, A.S. Bommaris, The Hofmeister effect on amyloid formation using yeast prion protein, *Protein Science*, 19 (2010) 47-56.
- [131] P.J. Marek, V. Patsalo, D.F. Green, D.P. Raleigh, Ionic strength effects on amyloid formation by amylin are a complicated interplay among Debye screening, ion selectivity, and Hofmeister effects, *Biochemistry*, 51 (2012) 8478-8490.
- [132] G.B. Irvine, O.M. El-Agnaf, G.M. Shankar, D.M. Walsh, Protein aggregation in the brain: the molecular basis for Alzheimer's and Parkinson's diseases, *MOLECULAR MEDICINE-CAMBRIDGE MA THEN NEW YORK-*, 14 (2008) 451.



- [133] S.Z. Moghaddam, E. Thormann, Hofmeister effect of salt mixtures on thermo-responsive poly (propylene oxide), *Physical Chemistry Chemical Physics*, 17 (2015) 6359-6366.
- [134] J.A. Loughlin, L.S. Romsted, A new method for estimating counter-ion selectivity of a cationic association colloid: trapping of interfacial chloride and bromide counter-ions by reaction with micellar bound aryl diazonium salts, *Colloids and Surfaces*, 48 (1990) 123-137.
- [135] D.T. Bowron, K.J. Edler, Decyltrimethylammonium bromide micelles in acidic solutions: counterion binding, water structuring and micelle shape, *Langmuir*, DOI (2016).
- [136] P.E. Mason, C.E. Dempsey, L. Vrbka, J. Heyda, J.W. Brady, P. Jungwirth, Specificity of Ion- Protein Interactions: Complementary and Competitive Effects of Tetrapropylammonium, Guanidinium, Sulfate, and Chloride Ions, *The Journal of Physical Chemistry B*, 113 (2009) 3227-3234.
- [137] S. Foryk, Y. Zhang, D. Ortiz-Acosta, P.S. Cremer, D.E. Bergbreiter, Effects of end group polarity and molecular weight on the lower critical solution temperature of poly (N-isopropylacrylamide), *Journal of Polymer Science Part A: Polymer Chemistry*, 44 (2006) 1492-1501.
- [138] Y. Katsumoto, N. Kubosaki, Tacticity effects on the phase diagram for poly (N-isopropylacrylamide) in water, *Macromolecules*, 41 (2008) 5955-5956.
- [139] Y. Xia, N.A. Burke, H.D. Stöver, End group effect on the thermal response of narrow-disperse poly (N-isopropylacrylamide) prepared by atom transfer radical polymerization, *Macromolecules*, 39 (2006) 2275-2283.
- [140] R.G. de Azevedo, L. Rebelo, A. Ramos, J. Szydlowski, H. De Sousa, J. Klein, Phase behavior of (polyacrylamides+ water) solutions: concentration, pressure and isotope effects, *Fluid Phase Equilibria*, 185 (2001) 189-198.
- [141] R. Bhat, S.N. Timasheff, Steric exclusion is the principal source of the preferential hydration of proteins in the presence of polyethylene glycols, *Protein Science*, 1 (1992) 1133-1143.
- [142] C.H. Spink, J.B. Chaires, Effects of hydration, ion release, and excluded volume on the melting of triplex and duplex DNA, *Biochemistry*, 38 (1999) 496-508.
- [143] S.Z. Moghaddam, E. Thormann, Hofmeister effect on thermo-responsive poly (propylene oxide): Role of polymer molecular weight and concentration, *Journal of colloid and interface science*, 465 (2016) 67-75.
- [144] S.Z. Moghaddam, E. Thormann, Hofmeister effect on thermo-responsive poly (propylene oxide) in H<sub>2</sub>O and D<sub>2</sub>O, *Rsc Advances*, 6 (2016) 27969-27973.